

The development of novel biocatalytic routes for the synthesis of  
enantiomerically-pure chiral amines

A thesis submitted to the University of Manchester for the degree of Doctor of  
Philosophy (PhD) in the Faculty of Science and Engineering

2017

Shahed Hussain

School of Chemistry

## Contents

Chapter 1: Introduction .....	11
1.1 Chirality and chiral amines.....	11
1.2 Strategies for the production of chiral amines .....	12
1.2.1 Resolution.....	12
1.2.2 Asymmetric synthesis .....	15
1.2.3 Chemical imine reduction as a means to access chiral amines .....	15
1.3 Background on the evolution of biocatalysis .....	21
1.4 Reduction reactions – imine reduction .....	22
1.4.1 Artificial metalloenzymes for the reduction of imines .....	22
1.4.2 Imine reductases.....	23
1.5 Reduction reactions – carboxylic acid reduction .....	33
1.6 Biocatalytic asymmetric synthesis - $\omega$ -transaminases .....	34
1.7 Biocatalytic asymmetric synthesis – phenylalanine ammonia lyase .....	38
1.8 Biocatalytic asymmetric synthesis - amine dehydrogenase.....	40
1.9 Deracemisation of racemic amines .....	40
1.9.1 Chemical deracemisation methods.....	40
1.9.2 Amine oxidases for the biocatalytic deracemisation of amines .....	42
1.10 Research project aims .....	45
Chapter 2: Characterisation of the ( <i>R</i> )-imine reductase from <i>Streptomyces</i> sp. GF3587 and comparison of the enzyme with the ( <i>S</i> )-imine reductase from <i>Streptomyces</i> sp. GF3546 ...	46
2.1. Overview.....	46
2.1.1 Brief background on imine reductases as biocatalysts .....	46
2.1.2 Aims.....	46
2.2 Characterisation of the ( <i>R</i> )-imine reductase from <i>Streptomyces</i> sp. GF3587 .....	47
2.2.1 Previously reported substrate scope and synthesis of screening compounds .....	47
2.2.2 Biotransformation results with ( <i>R</i> )-IRED and characterisation of the enzyme substrate scope .....	53
2.2.3 Comparison of ( <i>R</i> )-IRED substrate scope with ( <i>S</i> )-IRED.....	59
2.2.4 Establishing substrate-enzyme kinetic parameters .....	62
2.2.5 Enzyme mechanistic study – mutagenesis of the ( <i>R</i> )-imine reductase .....	64
2.3 Conclusions and outlook.....	68
Chapter 3: One-pot enzymatic cascade reactions combining imine reductase (IRED) with amine transaminase (ATA) and carboxylic acid reductase (CAR) enzymes.....	73
3.1 Overview of enzymatic cascade reactions .....	73
3.1.1 Existing strategies for enzymatic cascade reactions .....	73
3.1.2 Aims.....	76
3.2 $\omega$ -transaminase/imine reductase cascade (ATA/IRED cascade) .....	78

3.2.1 Principle and synthesis of screening compounds.....	78
3.2.2 One-pot two-step enzymatic cascade for the production of 2,6-disubstituted piperidines.....	80
3.2.3 One-pot two-step enzymatic cascade for the production of 2,5-disubstituted pyrrolidines .....	88
3.3 Carboxylic acid reductase/ $\omega$ -transaminase/imine reductase cascade .....	89
3.3.1 Principle and synthesis of screening compounds.....	89
3.3.2 One-pot multi-enzyme cascade for the production of 3-phenylmorpholine 19 and 3-phenylthiomorpholine 22 .....	90
3.4 Conclusions and outlook.....	93
Chapter 4: Amine oxidase-catalysed redox deracemisation reactions of 2-substituted cyclic amines, tetrahydroquinolines and indolines.....	97
4.1 Overview of deracemisation strategies .....	97
4.1.1 Existing strategies for enzymatic deracemisation of amines.....	97
4.1.2 Aims.....	98
4.2 Amine oxidase/imine reductase catalysed deracemisation of 2-substituted cyclic amines.....	99
4.2.1 Optimisation of the biocatalytic deracemisation of amines with 6-HDNO and ( <i>R</i> )-IRED .....	99
4.2.2 Deracemisation of racemic cyclic amine 2-phenylpiperidine 6c with 6-HDNO/( <i>R</i> )-IRED cascade .....	101
4.3 Amine oxidase-catalysed deracemisation of tetrahydroquinolines .....	104
4.3.1 Current strategies for the deracemisation of tetrahydroquinolines .....	104
4.3.2 Synthesis of tetrahydroquinoline compounds.....	105
4.3.3 Establishing an autoinduction protocol for the expression and growth of CHAO .....	108
4.3.4 Biocatalytic deracemisation/kinetic resolution of tetrahydroquinolines – with AO/IRED combination .....	115
4.4 Deracemisation of indolines .....	117
4.4.1 Brief background on chiral indolines and synthesis of indolines .....	117
4.4.2 Kinetic resolution of indolines .....	119
4.5 Conclusions and outlook.....	128
Chapter 5: ( <i>R</i> )-IRED-catalysed bioreduction reaction in continuous flow .....	133
5.1 Brief introduction to reactions in flow and current strategies.....	133
5.2 Imine reductase reaction in flow using the Freactor modular flow reactor units – principle.....	135
5.3 ( <i>R</i> )-imine reductase reaction in flow – results .....	138
5.4 Conclusions and further work .....	140
Chapter 6: Conclusions and outlook.....	142
6.1 Conclusions .....	142

6.2 Outlook .....	143
Chapter 7: Methods and experimental .....	146
7.1 Materials, equipment and general analysis procedures .....	146
7.1.1 Chemicals .....	146
7.1.2 Equipment and general analysis procedures .....	146
7.2 Media, buffers and stock solutions .....	147
7.2.1 Growth media .....	147
7.2.2 Buffers .....	149
7.2.3 Antibiotics and IPTG stock solutions .....	149
7.3 Synthesis of substrates and analytical standards .....	150
7.3.1 Synthesis of 2-substituted cyclic imines and amines.....	150
7.3.2 Synthesis of 2-substituted cyclic amines.....	168
7.3.3 General procedure for the preparation of 1,5-diketones 11a – 11d .....	176
7.3.3 General procedure for the preparation of 1,5-diketone 11e .....	177
7.3.5 Procedure for the preparation of ketoacids 17 and 20.....	179
7.3.6 General procedure for the preparation of 2-substituted tetrahydroquinolines...	181
7.3.7 General procedure for the preparation of 2-substituted indolines.....	185
7.4 Growth and expression of biocatalysts .....	187
7.4.1 Amino acid sequences for proteins used in this report .....	187
7.4.2 Growth and expression of imine reductases .....	191
7.4.3 Growth and expression of CHAO .....	192
7.4.4 Growth and expression of 6-HDNO .....	193
7.4.5 Growth and expression of MAO-N D5, D9 and D11 .....	194
7.4.6 Growth and expression of MCAR .....	194
7.5 Biotransformation conditions .....	194
7.5.1 Procedure for imine reductase biotransformations .....	194
7.5.2 General procedure for carboxylic acid reductase, $\omega$ -transaminase and imine reductase cascade biotransformations .....	195
7.5.3 Procedure for amine oxidase-catalysed chemo-enzymatic redox biotransformations .....	196
7.5.4 Procedures for preparative-scale biotransformations.....	197
7.6 Protocols for the purification of the ( <i>R</i> )-IRED and glucose dehydrogenase (GDH-II)200	
7.6.1 Protocol for HisTag purification of ( <i>R</i> )-IRED and GDH-II .....	200
7.6.2 Gel filtration of isolated ( <i>R</i> )-IRED protein and de-salting of GDH-II.....	200
7.7 Isolated enzyme biotransformations with the ( <i>R</i> )-IRED .....	202
7.7.1 General procedure for pure enzyme biotransformations .....	202
7.7.2 Procedure for the continuous flow biotransformation of 2-( <i>n</i> -propyl)-1-piperidine.HCl 5i with purified ( <i>R</i> )-IRED enzyme.....	203

7.8 Spectrophotometric assay for the determination of kinetic constants with ( <i>R</i> )-imine reductase.....	203
7.9 Mutagenesis of the ( <i>R</i> )-IRED and general biotransformation procedure using ( <i>R</i> )-IRED D172A and ( <i>R</i> )-IRED D172L variants .....	209
7.9.1. Mutagenesis of wild-type ( <i>R</i> )-IRED to produce mutants D172A and D172L ....	209
7.9.2 General procedure for pure enzyme biotransformations with ( <i>R</i> )-IRED mutants .....	210
7.10 Methods and conditions used for biotransformation analysis .....	210
7.10.1 Chiral HPLC .....	210
7.10.2 Chiral GC-FID analysis .....	213
7.11 Determination of the absolute configuration of piperidines 6a – 6m .....	218
Chapter 8: References .....	220

Word count: 61,475

The University of Manchester

Shahed Hussain

Doctor of Philosophy

The Development of Novel Biocatalytic Routes for the Synthesis of Enantiomerically-Pure Chiral Amines

May 2017

## Abstract

Chiral amines represent a pervasive structural motif found in various natural products, pharmaceuticals, agrochemicals and fine chemicals. Their preparation in single-enantiomer form continues to attract significant research attention and although many advances have been made in the area of synthetic organic chemistry to increase the scope of the routes to these moieties, there remains an ever-growing need of general strategies for the assembly of structurally-diverse amines which also conform to the efficiency and environmental requirements of modern manufacturing processes. This report investigates biocatalytic routes as a means for constructing chiral amine scaffolds, which offer a more environmentally benign approach when compared with traditional chemocatalysed processes. Probing the catalysts available in the biocatalytic toolbox of enzymes, several routes were examined in more detail.

Imine reductases (IREDs) represent a recent addition to the toolbox, enzymes which by definition are able to reduce pre-formed imines to their corresponding amines with high selectivity. This report analyses the (*R*)-imine reductase [(*R*)-IREd] from *Streptomyces* sp. GF3587, one of the first imine reductases identified for its biocatalytic potential, in greater depth. The enzyme was found to catalyse the reduction of a broad range of cyclic imines while displaying high levels of activity and selectivity, thereby offering a direct route of access to chiral secondary and tertiary amines. Substrate kinetic parameters were established for the enzyme in order to understand its substrate preferences and the enzyme's catalytic mechanism was probed through the generation of mutant (*R*)-IREdS.

Owing to their operation under physiological conditions as well as the orthogonal nature of their reactions, it is possible to combine multiple enzyme reactions to enable cascades. This report examines a multi-enzyme reaction combining  $\omega$ -transaminases (ATAs) with imine reductases, for the synthesis of chiral disubstituted piperidines from simple diketone substrates. The cascade was then taken a step further by the inclusion of the carboxylic acid reductase (CAR) enzyme, for the synthesis of the nitrogen-containing heterocycles morpholine and thiomorpholine from ketoacid compounds. Finally, the well-established deracemisation technique, employing a selective amine oxidase (AO) with either a non-selective chemical reducing agent or a biocatalytic reductant (IREd), was explored in more detail by encompassing new substrate motifs.

As biocatalysis becomes more readily accepted as a general technique in the synthetic chemist's repertoire, the concept of carrying out enzymatic reactions in constant flow was explored as a means for applying this methodology with increased production and decreased processing rates.

## **Declaration**

I declare that no portion of the work referred to in the thesis has been submitted in support of an application for another degree or qualification of this or any other university or other institute of learning.

## **Copyright**

**i.** The author of this thesis (including any appendices and/or schedules to this thesis) owns certain copyright or related rights in it (the "Copyright") and he has given The University of Manchester certain rights to use such Copyright, including for administrative purposes.

**ii.** Copies of this thesis, either in full or in extracts and whether in hard or electronic copy, may be made **only** in accordance with the Copyright, Designs and Patents Act 1988 (as amended) and regulations issued under it or, where appropriate, in accordance with licensing agreements which the University has from time to time. This page must form part of any such copies made.

**iii.** The ownership of certain Copyright, patents, designs, trademarks and other intellectual property (the "Intellectual Property") and any reproductions of copyright works in the thesis, for example graphs and tables ("Reproductions"), which may be described in this thesis, may not be owned by the author and may be owned by third parties. Such Intellectual Property and Reproductions cannot and must not be made available for use without the prior written permission of the owner(s) of the relevant Intellectual Property and/or Reproductions.

**iv.** Further information on the conditions under which disclosure, publication and commercialisation of this thesis, the Copyright and any Intellectual Property and/or Reproductions described in it may take place is available in the University IP Policy (see <http://documents.manchester.ac.uk/DocuInfo.aspx?DocID=487>), in any relevant Thesis restriction declarations deposited in the University Library, The University Library's regulations (see <http://www.manchester.ac.uk/library/aboutus/regulations>) and in The University's policy on Presentation of Theses

## Glossary

AADH	Amino-acid dehydrogenase
ATA	Amine transaminase
NH <sub>3</sub> BH <sub>3</sub>	Ammonia-borane complex
CAR	Carboxylic acid reductase
CHAO	Cyclohexylamine oxidase
DEA	Diethylamine
DHQ	3,4-dihydroquinoline
DMAP	4-dimethylaminopyridine
DMF	<i>N,N</i> -dimethylformamide
DMSO	Dimethylsulfoxide
dH <sub>2</sub> O	Deionised water
<i>E. coli</i>	<i>Escherichia coli</i>
ERED	Enoate reductase
EtOAc	Ethyl acetate
EtOH	Ethanol
FAD	Flavin adenine dinucleotide
FID	Flame ionisation detector
GC	Gas chromatography
GDH	Glucose dehydrogenase
6-HDNO	6-hydroxy-D-nicotine oxidase
HPLC	High performance liquid chromatography
HRP	Horseradish peroxidase
IPTG	Isopropyl-β-D-1-thiogalactopyranoside
IR	Infrared

IRED	Imine reductase
KRED	Ketoreductase
LB	Luria broth
LDH	Lactate dehydrogenase
MAO-N	Monoamine oxidase (from <i>Aspergillus niger</i> )
MeOH	Methanol
MS	Mass Spectrometry
MTQ	1-methyl-1,2,3,4-tetrahydroisoquinoline
NMR	Nuclear magnetic resonance
NAD(P)H	Nicotinamide adenine dinucleotide (phosphate)
Pr	Propyl
PCR	Polymerase chain reaction
OTf	Trifluoromethanesulfonate (triflate)
TA	Transaminase
TB	Terrific broth
THQ	1,2,3,4-tetrahydroquinoline
<i>t</i> -Bu	<i>tert</i> -butyl
<i>t</i> -BuOK	Potassium- <i>tert</i> -butoxide
$\omega$ -TA	$\omega$ -transaminase
THF	Tetrahydrofuran

## **Acknowledgements**

First and foremost, I would like to thank my supervisor, Professor Nicholas Turner, for giving me the opportunity to complete my PhD project (as well as my Master's project) in your research group, as well as for the help, support and guidance (and faith!) that you have offered to me throughout the past four and a half years. Ultimately, you shuttled me down the career path that I now pursue and you continue to serve as an inspiration to me to this day.

I would like to offer my thanks to my industrial supervisor, Dr. Keith Mulholland, for being fully supportive throughout the whole PhD process, for allowing me the opportunity to work at AstraZeneca in Macclesfield during my third year and for making me feel welcome during my time there. Despite the (many) injuries I accumulated through my inability to stay upright on a bike, I thoroughly enjoyed the experience.

I would like to extend my gratitude to Dr. Gideon Grogan, Henry Man and Lilly Wells at the University of York, whom we have collaborated with on several occasions and who have been extremely helpful during the course of my PhD project.

On the same token, I have to thank Dr. Elaine O'Reilly, who served as my guide during my Master's Project and for being a fantastic teacher. I was able to take on everything that I learned with you and apply it to my PhD research project and beyond. I am the scientist that I am today because of you.

I would like to thank Dr. Marta Pontini, Dr. Rachel Heath and Dr. Anthony Green for their guidance, help and input in various aspects throughout my project.

I must offer my gratitude to Dr. Mark Corbett, Dr. Rachel Heath, Matthew Thompson, Lorna Hepworth and Scott France for proof-reading my thesis during the month of intense writing up against the clock. It was probably the most stressful period of my life and I couldn't have put together a coherent piece of work without you. You are all stars.

Thank you also to Paula Tipton for being helpful and generally lovely through the entire process of my PhD.

A special mention goes to Fox's Party Rings, which also lent its support during the writing-up period. A combination of delicious incentive and a necessary late-night sugar rush helped me complete my work in record time. I could not have done it without it.

I want to thank the people in the Turner-Flitsch research group for making it such a welcoming and enjoyable place to work over the years. In particular: the dream team (Niki, Anthony, Sarah, Cesar, Michel), Team IRED (Friedemann, Scott, Godwin, Juan, Sarah), Andy, Peter, Rachel, Mark and the golden bay (Lorna, Scott, Steph, Matthew, Nick). Thanks to Anna Hauck, who also made the PhD experience much more enjoyable!

I should also thank Carly Phelan, who put up living with me for so many years during my PhD, through the highs and lows and was still supporting me until the end (and beyond).

Finally, I want to thank my family and friends for being supportive through all the ventures in my life.

You all make my world.

## Chapter 1: Introduction

### 1.1 Chirality and chiral amines

The natural world has evolved to conform to the phenomenon of chirality: non-superimposable mirror images of a molecule which have distinct left- and right-handed enantiomeric forms. The fundamental building blocks of life exist predominantly in single enantiomer form in nature, notably L-amino acids and D-sugars. As our understanding of biochemistry and pharmacology progressed, it became readily apparent in biological systems that opposing enantiomers of the same molecule can have profoundly different effects in the physiological environment, due to chirality at the receptor point which affects recognition and binding of these molecules. An example of this effect can be observed with tramadol, an analgesic consisting of two enantiomers which contribute to its activity via different mechanisms (Figure 1). (+)-tramadol (+)-**29** is a  $\mu$ -opioid receptor agonist and inhibits the reuptake of the neurotransmitter serotonin. (-)-**29** inhibits norepinephrine reuptake, enhancing inhibitory effects on pain transmission within the spinal cord.<sup>1</sup> The drug is sold as the racemate, as the two enantiomers contribute to a synergistic analgesic effect.

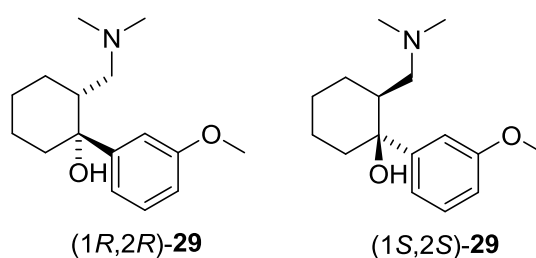


**Figure 1:** Enantiomers of (+)-tramadol and (-)-tramadol **29**, which exhibit different physiological effects. The drug is prescribed as the racemate as it was found to be more effective as an analgesic overall than when prescribed in single-enantiomer form.<sup>1</sup>

The most infamous example of the profound variation in effects that two enantiomers can possess can be found in the case of Thalidomide, a drug developed and distributed by the German pharmaceutical company Grünenthal and once prescribed to pregnant women to treat morning sickness. It was withdrawn soon after its launch to the public, after the teratogenic activity of the (*S*)-enantiomer of the compound became apparent.<sup>2</sup> The failure to detect such side-effects arising from enantiomeric forms led to a complete overhaul of the system used to assess the safety of drugs in both the U.S. and Europe and now each enantiomer of a potential drug molecule must be independently tested and verified for safety.<sup>3</sup>

Chiral amines are moieties that constitute a number of “privileged scaffolds” that are pervasive in natural products, pharmaceuticals, agrochemicals and fine chemicals.<sup>4</sup> Figure 2 illustrates some drugs currently on the market which feature chiral amines as an integral part within their framework. The preparation of chiral amines in single-enantiomer form continues to attract a significant amount of research attention.

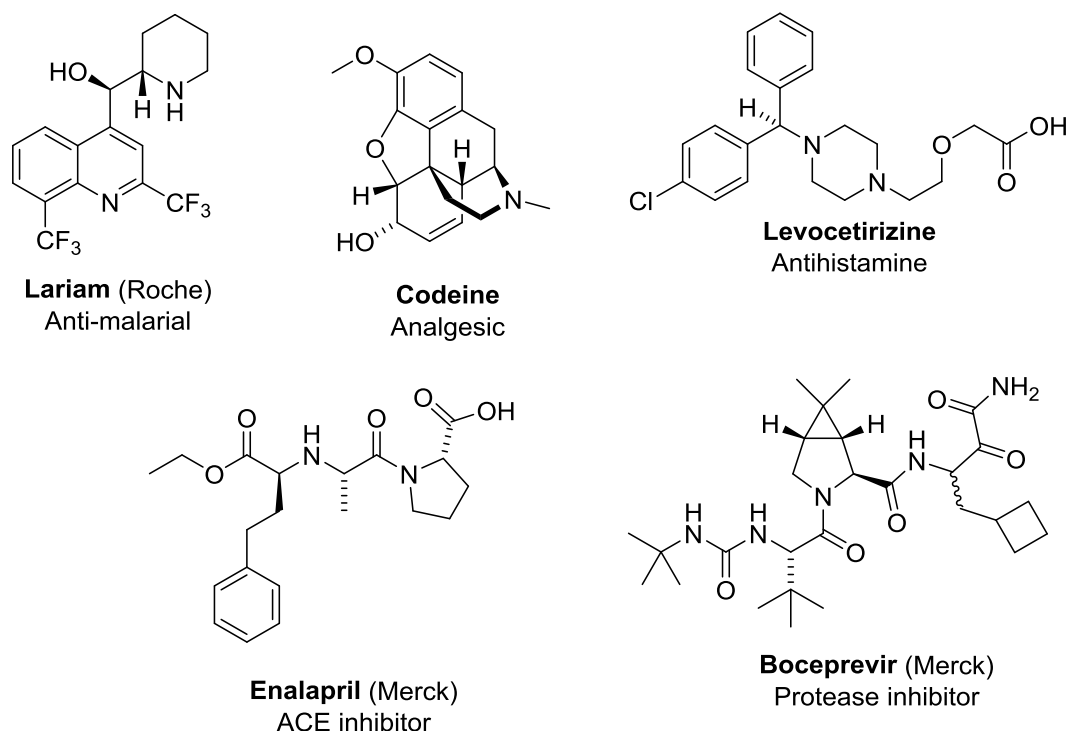


**Figure 2:** Structures of drugs currently on the market which feature a chiral amine as an integral part of their structure.

## 1.2 Strategies for the production of chiral amines

### 1.2.1 Resolution

There are two main strategies employed to obtain chiral amines in single-enantiomer form: resolution of the two enantiomers or direct asymmetric synthesis. The first resolution process to come about was spontaneous resolution through crystallization, which was demonstrated by L. Pasteur in 1882 when seed crystals of opposing enantiomers of tartaric acid were placed at opposite ends of a vessel containing super-saturated ammonium tartrate.<sup>5</sup> The crystals grew spontaneously to yield larger crystals of enantiomerically-pure tartrate.

Diastereomeric salt formation for classical resolution represents another technique used to separate enantiomers. Unlike enantiomers, diastereomers have different physical

properties and so can be separated using techniques such as chromatography. An example which utilizes this aspect to great success is in the synthesis of the serotonin-norepinephrine reuptake inhibitor duloxetine, which is used as an antidepressant (Figure 3). (*S*)-mandelic acid is used as a chiral resolving agent, forming diastereomeric salts with the amines; salts of the (*S*)-enantiomer of the intermediate precipitate and can be filtered off, whereas salts of the (*R*)-enantiomer remain in solution.<sup>6</sup>

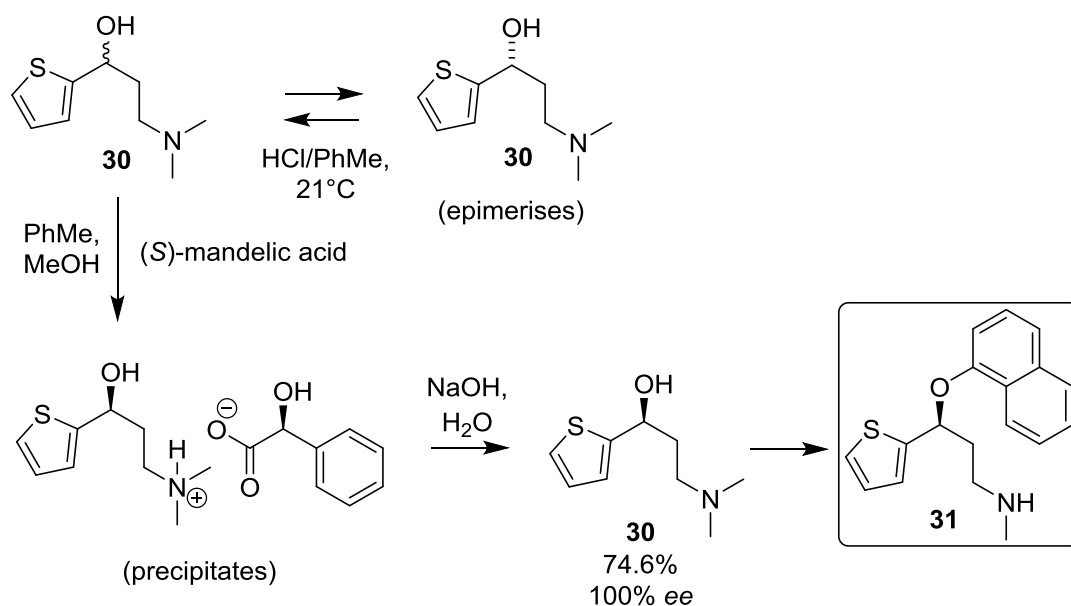


**Figure 3:** Synthesis of duloxetine **31**, which harnesses (*S*)-mandelic acid as a chiral resolving agent to form diastereomeric salts. The (*S*)-enantiomer of the amine (*S*)-**30** precipitates out of the solution as the salt forms, whereas the (*R*)-enantiomer (*R*)-**30** remains in solution where it epimerises to give the racemic alcohol **30**. The process is an example of a dynamic resolution.<sup>6</sup>

A disadvantage of classical resolution or diastereomeric salt formation is the theoretical yield is limited to 50%, as the undesired enantiomer is left behind as a waste product. For large-scale processes, this could lead to significant waste if there is no further use of the unwanted enantiomer, resulting in lower atom economy processes. In spite of this, classical resolution often remains the method of choice in industry for production of chiral molecules.<sup>7</sup> A contrasting approach for the resolution of enantiomers is kinetic resolution. In this case, the two enantiomers react with another reagent or catalyst at differing rates. The method relies on one of the enantiomers having a significantly faster reaction velocity than the other; thereby the *ee* of the less reactive enantiomer effectively increases as the more reactive enantiomer is consumed in the reaction (Figure 4). The drawback to this approach lies on a cap of the theoretical yield at a maximum of 50%, though again this method is a common practice in industry.

In order to reduce waste, a recycling/racemisation process can be employed on the unwanted enantiomer, in order to reinsert it into the reaction for resolution to occur. By this strategy, the product yield could theoretically reach 100% with 100% *ee* using a dynamic kinetic resolution. However, the racemisation would also be a competing reaction in this case and must have a faster rate of reaction than the rate of conversion of the single enantiomer (Figure 4). This was used to great success in Eli Lilly's synthesis of duloxetine **31**, where the diastereomer salt formed from the (*R*)-enantiomer alcohol (*R*)-**30** is epimerised in solution to give the racemic alcohol, which then begins the resolution process with (*S*)-mandelic acid again (Figure 3).

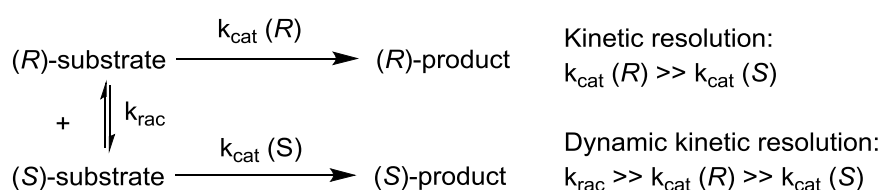


**Figure 4:** Scheme outlining the basic principles of a kinetic resolution reaction. In this example, the *ee* of the (*S*)-enantiomer increases with time as the (*R*)-enantiomer is consumed in reaction. When *in-situ* racemisation is employed, the theoretical yield of the reaction is no longer capped at 50% and the process becomes a dynamic kinetic resolution.

Kinetic resolution remains an important strategy for chiral amine synthesis, which was demonstrated in a recent example from the group of Bode. By employing an achiral *N*-heterocyclic carbene **34** in combination with a novel hydroxamic acid co-catalyst **33**, the kinetic resolution of cyclic secondary amines was accomplished via an amidation reaction (Figure 5).<sup>8</sup> The hydroxamic acid catalyst **33** was used to convert the acylating agent **32** into a more reactive species, which then facilitated the stereoselective acylation of the racemic amine, leading to an enantio-enrichment of the unreacted amine enantiomer. The catalyst was regenerated by the *N*-heterocyclic carbene and no non-volatile by-products were formed in the reaction. The system was successfully used with a diverse range of nitrogen heterocycles, including piperidines, azepanes, morpholines, piperazines and even tetrahydroisoquinolines. A simple cleavage of the acyl group following separation of the two products results in the recuperation of the reacted amine enantiomer. Subsequently, a polymer-supported version of the catalyst was developed which conferred stability to the catalyst so that it could be used multiple times without loss of efficiency or selectivity.<sup>9</sup>

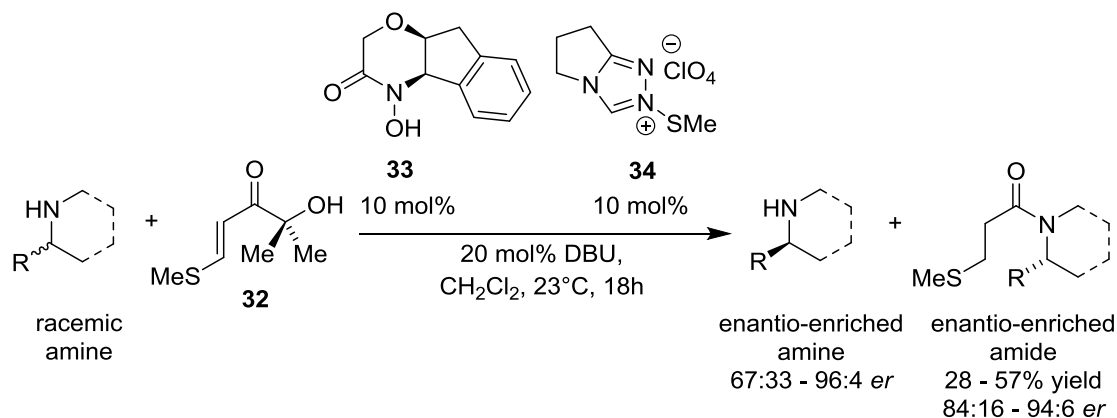


**Figure 5:** Catalytic kinetic resolution of cyclic amines using a combination of an achiral *N*-heterocyclic carbene working in concert with a novel chiral hydroxamic acid co-catalyst.<sup>8</sup>

### 1.2.2 Asymmetric synthesis

There are several methodologies for the synthesis of chiral amines through direct asymmetric synthesis. These includes careful selection of reagents from the large collection of naturally-occurring chemicals with existing chirality, such as enantiomerically-pure L-amino acids and D-sugars, dubbed the chiral pool, or by attachment of chiral auxiliaries to molecules prior to performing a chemical reaction, in order to direct the stereoselectivity of the modification. The disadvantage of this approach lies in the additional reaction steps necessary to attach and then cleave the auxiliary from the starting material and product. Transition-metal catalyzed asymmetric reactions remain a widely-employed and successful strategy, which can be used to perform such reaction steps as asymmetric reduction reactions.

### 1.2.3 Chemical imine reduction as a means to access chiral amines

Asymmetric hydrogenation technologies continue to attract a significant amount of research interest, for which transition metal catalysts can be used to effect asymmetric reduction reactions. One area of focus was the design of bulky, chiral ligands for the transition metal catalyst centres, which facilitate asymmetric reduction of double bonds under a molecular hydrogen atmosphere. This was described in work by Knowles, who detailed the substitution of the achiral phosphine ligands in Wilkinson's catalyst with a chiral phosphine group, increasing the stereoselectivity in the reduction of an olefin and the resulting *ee* of the product.<sup>10</sup>

Imine reduction is a particularly attractive strategy for the synthesis of chiral amines. While the chiral reduction of ketones has been well-documented, the reduction of

their nitrogenous analogues has been explored less extensively. This could be due in part to the relative difficulty of the synthesis of imines, which are often unstable. For acyclic imines, *E*- and *Z*-isomerism of the imines presents another variable to consider, which could affect the enantioselectivity of the reduction reactions. As both the imine and amine product can coordinate to the catalyst, catalyst poisoning can also be an issue.<sup>11</sup>

Arguably the most successful chiral catalyst for asymmetric hydrogenation is an iridium complex **37**, derived from chloro(cycloocta-1,5-diene)iridium(I) ( $[\text{Ir}(\text{cod})\text{Cl}]_2$ ) and a Xyliphos chiral ligand (Figure 6). Although a number of different ligands were tested, the Xyliphos ligand proved to effect a more stereoselective reduction and was applied to the asymmetric hydrogenation of a panel of *N*-aryl imines, including the cyclic imine 2,3,3-trimethylindolenine and the precursor **35** to the agrochemical (*S*)-metolachlor **36**. Subsequently, the process was optimised for the synthesis of (*S*)-**36** on production plant-scale from 1996 onwards in multi-tonne quantities. Although only a modest 79% *ee* was obtained from the reaction, the enantioenrichment requirement for the active chemical was fulfilled.<sup>12,13</sup>

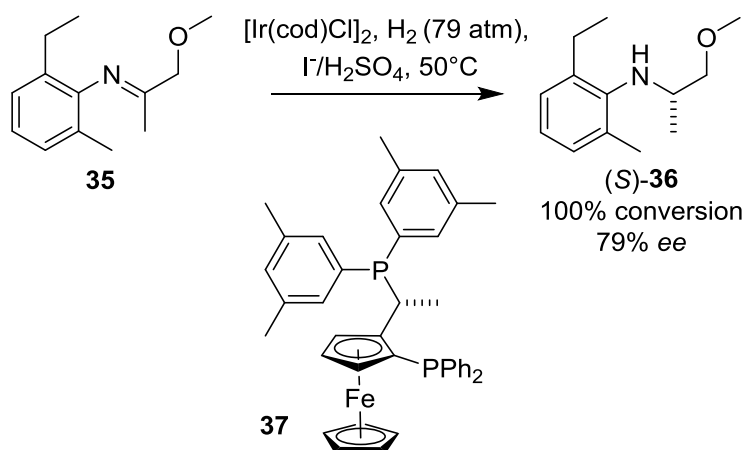


**Figure 6:** Asymmetric hydrogenation using an iridium-based catalyst complex **37** in combination with the chiral ligand Xyliphos (structure shown) for the production of the agrochemical (*S*)-metolachlor **36**.<sup>12</sup>

Han and co-workers were able to develop a spiro[4,4]-1,6-nonadiene-based phosphine-oxazoline ligand, which was used for the asymmetric hydrogenation of a range of *N*-aryl imines cyclic imines with an iridium-based catalyst **40**.<sup>14</sup> The utility of the SpinPHOX ligand (shown in complex with Ir(I) in Figure 7) was demonstrated in the synthesis of the chiral antidepressant drug sertraline. When fed the (*S*)-enantiomer imine **38**, the iridium catalyst (*S,S*)-**40** showed excellent *cis*-diastereoselectivity, furnishing sertraline **39** in the enantiopure form (> 99:1 *dr*) in quantitative yield.

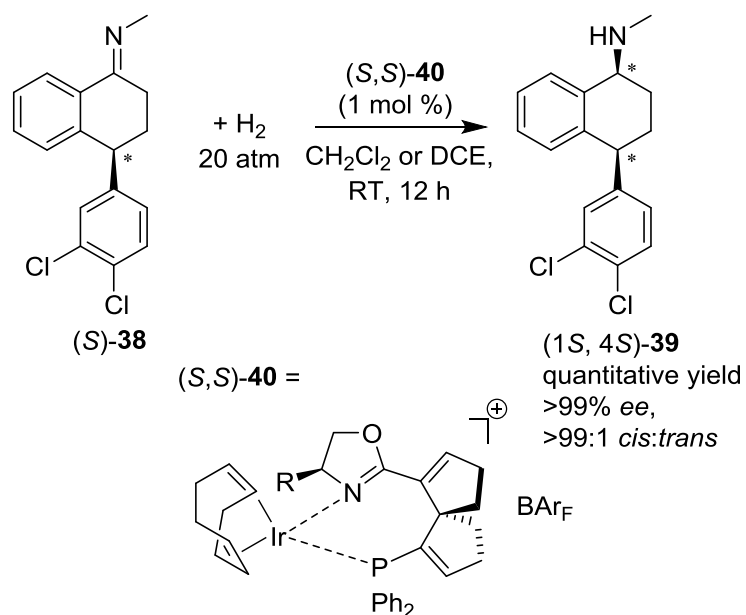


**Figure 7:** Synthesis of the antidepressant sertraline **39** by asymmetric hydrogenation of the corresponding (*S*)-enantiomer imine **38** using an iridium catalyst in combination with the SpinPHOX chiral ligand. Sertraline **39** was obtained in quantitative yield in >99:1 *dr*.<sup>14</sup>

In another example, Feaster demonstrated the use of a rhodium catalyst with a 1,2-*bis*-(phospholano)benzene ligand (Et-DuPHOS) in an asymmetric reductive amination procedure (**45**, Figure 8).<sup>15</sup> Beginning with a ketone **41**, a condensation reaction produced the *N*-aroylhydrazone **42**, which was then subjected to asymmetric hydrogenation by reacting with the catalyst  $[(\text{cod})\text{Rh}((R,R)\text{-Et-DuPHOS})]^+\text{OTf}^-$  **45** under hydrogen at 4 atm. At temperatures of 20 °C and below, stoichiometric conversion of the substrate was observed, giving predominantly the (*S*)-enantiomer of the corresponding hydrazines **43** in moderate to very good *ee* (72 – 97%). It was found that under the relatively mild hydrogenation conditions, <2 % reduction of unfunctionalised alkenes and alkynes and no reduction of ketones, aldehydes, esters, nitriles, imines, carbon-halogen and nitro groups was observed in competing reactions, demonstrating the excellent chemoselectivity of the catalyst. Cleavage of the N-N bond with  $\text{SmI}_2$  was then carried out to obtain the final secondary amine product **44**.

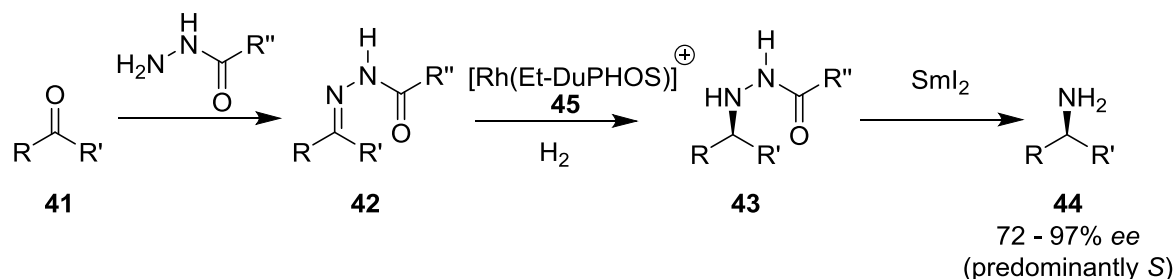


**Figure 8:** Procedure for the asymmetric reductive amination using a chiral rhodium catalyst **45**. Following formation of the *N*-arylhidrazine **42**, the C=N imino bond was reduced by the rhodium catalyst **45** to furnish the *N*-arylhidrazine **43**. Cleavage of the N-N bond was then effected to obtain the final amine product **44**, which in all but one case was in the (*S*)-enantiomer configuration.<sup>15</sup>

A chiral titanocene catalyst **48** was successfully employed by Willoughby and Buchwald to hydrogenate a series of *N*-aryl acyclic imines, 2-substituted cyclic imines **46** and 6,7-dimethoxy-1-methyl-3,4-dihydroisoquinoline **7b** (Figure 9).<sup>16</sup> The corresponding amines **47** were obtained in moderate yields of 86 – 93% and in 58 – 98% *ee* with reaction hydrogen pressures of 80 – 2000 psig (typically 80 psig). The cyclic amines in particular were produced with excellent enantioselectivity, with the tetrahydroquinoline amine alkaloid salsolidine (*S*)-**8b** produced in 82% yield, 98% *ee*.

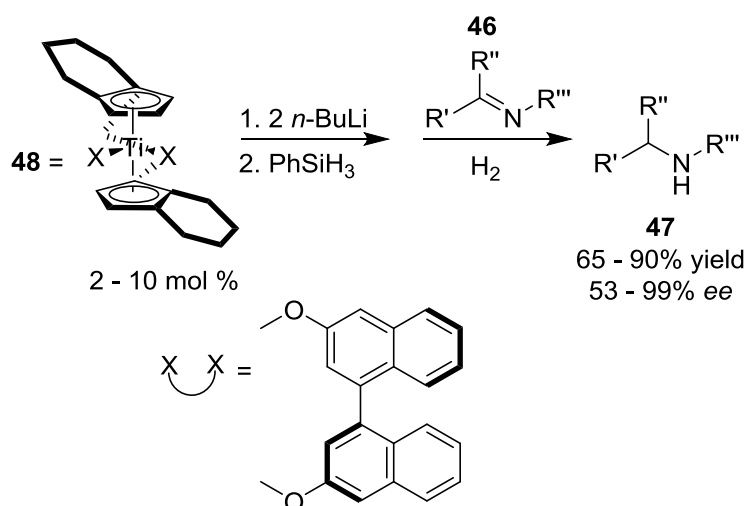


**Figure 9:** Asymmetric hydrogenation of imines catalysed by a titanocene-based system. Treatment of the 1,1'-binaphth-2,2'-diolate-titanocene complex **48** with two equivalents of *n*-BuLi and 2.5 equivalents of phenylsilane produced the active catalyst.<sup>16</sup>

Xiao demonstrated the feasibility of a cationic Rh(III) diamine catalyst for the asymmetric hydrogenation of cyclic imines (Figure 10).<sup>17</sup> It was suggested that the catalyst **51** would be converted to the active cationic Rh(III) form **50** in the reaction with SbF<sub>6</sub>, which contributed

to the success of the catalyst by acting as a bulky counter ion. The reaction was screened against a panel of dihydroisoquinolines **7** and dihydro- $\beta$ -carbolines **49**, affording the corresponding tetrahydroisoquinoline and tetrahydro- $\beta$ -carboline amines in typically excellent (>90%) *ee*.

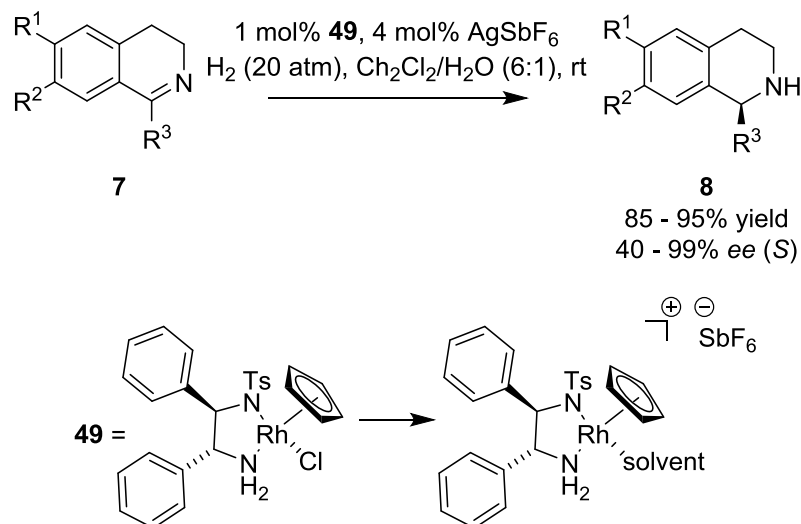


**Figure 10:** Asymmetric hydrogenation of cyclic imines catalysed by a cationic rhodium catalyst, which is converted to the active catalyst from **49** under the reaction conditions. The cationic nature and the bulky non-coordinating counterion were said to be key to the success of the catalyst.<sup>17</sup>

Rather than using molecular hydrogen as a source of hydride for reduction of imino bonds, the concept of asymmetric transfer hydrogenation uses less hazardous reducing agents, such as formic acid or propan-2-ol, as a source for the reductive hydride and is operationally more facile to carry out. Noyori's Nobel prize-winning work in this field used a chiral ruthenium catalyst to hydrogenate various imines, including substituted 6,7-dimethoxy-3,4-dihydroisoquinoline derivatives, dihydro- $\beta$ -carbolines and even acyclic imines, to provide access to the corresponding amines in up to 97% *ee* (Figure 11).<sup>18</sup> Crucially, a hydrogen atmosphere was not required in the reaction as formic acid acts as the hydrogen donor via transfer hydrogenation. The catalyst was found to be less effective with acyclic imines, however. It was also possible to control the configuration of the reduction product obtained by varying the chiral ligand in the ruthenium catalyst complex. A scheme was provided to rationalise the selectivity observed in the reduction reactions.

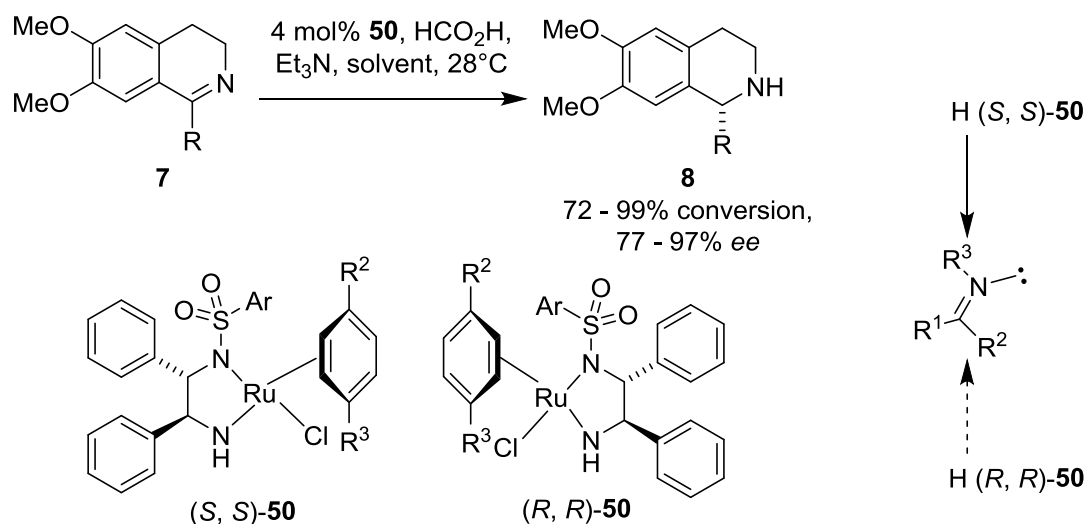


**Figure 11:** Asymmetric transfer hydrogenation of dihydroisoquinoline derivatives catalysed by chiral Ru(II) complexes. The chiral Ru species is able to formally discriminate the prochiral faces of the imine at the  $\text{sp}^2$  nitrogen atom, with hydride attack promoted at opposing faces of the imine depending on the chirality of the ruthenium catalyst complex.<sup>18</sup>

Asymmetric hydroboration has been reported for the production of 1,2-diphenylethylenediamine (Figure 12).<sup>19</sup> Harnessing a borane-tetrahydrofuran complex with an oxazaborolidine derived from L-threonine, the corresponding 1,2-diimine was reduced in an asymmetric fashion by the borane reductant. This yielded (*R,R*)-1,2-diphenylethylenediamine in excellent *ee* when the chiral ligand was used at greater than 0.5 mol %. When lower than stoichiometric amounts of the ligand were used in the reaction, a slightly larger amount of the *meso* by-product was formed from the reaction.

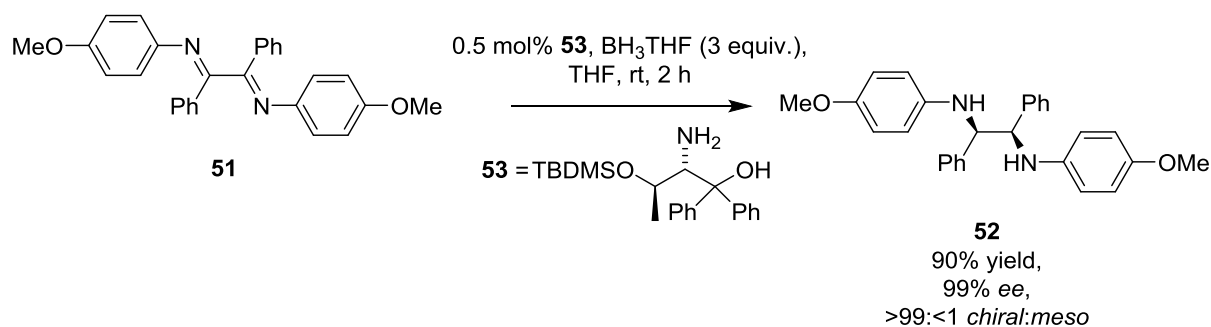


**Figure 12:** Asymmetric hydroboration of a 1,2-diimine using L-threonine-derived chiral ligand **53** and  $\text{BH}_3\cdot\text{THF}$  complex, furnishing (*R,R*)-1,2-diphenylethylenediamine **52** in typically 99% *ee* and with very low proportion of *meso* isomer (<1%) formed.<sup>19</sup>

### 1.3 Background on the evolution of biocatalysis

Enzymes are biological catalysts, which by definition lower the activation energy of a chemical reaction to increase the rate at which it occurs. Most enzymes are proteins – a chain of amino acids which produces a three-dimensional structure that defines the enzyme's function. Some enzymes have long been known to perform chemical transformations and have been harnessed by humans for this specific purpose, for example in the age-old reduction of the simple sugar glucose by yeast to yield ethanol. In nature, enzymes are particularly efficient in carrying out their processes, typically demonstrating high enantio- regio-, and chemoselectivity and high substrate turnover rates when doing so. However, as wild-type enzymes have evolved to perform a specific function, they typically possess narrow substrate scopes (particularly enzymes originating from prokaryotic organisms) and poor thermo- and solvent stability outside of their normal operating environment. These challenges have historically made it difficult to employ enzymes for the purpose of catalysing synthetic organic chemistry reactions.

However, the field of biocatalysis has greatly benefited from the advent of techniques such as DNA sequencing, gene cloning and synthesis, and recombinant DNA expression.<sup>20</sup> As a consequence, it is now possible to engineer enzymes to tailor them to our own specific requirements, for example through the use of techniques such as directed evolution to accelerate the development of the protein catalysts.<sup>21</sup> As enzymes can often catalyse reactions which are otherwise challenging to carry out by traditional chemical means, biocatalysis is taking an increasingly prominent role in the production of complex chiral molecules. It has been argued that enzymatic reactions should be regarded as a subset of transformations to be considered and applied by the synthetic organic chemist when designing novel syntheses. This offers an approach analogous to the established design strategies of organic chemistry and is therefore often dubbed "biocatalytic retrosynthesis."<sup>22</sup>

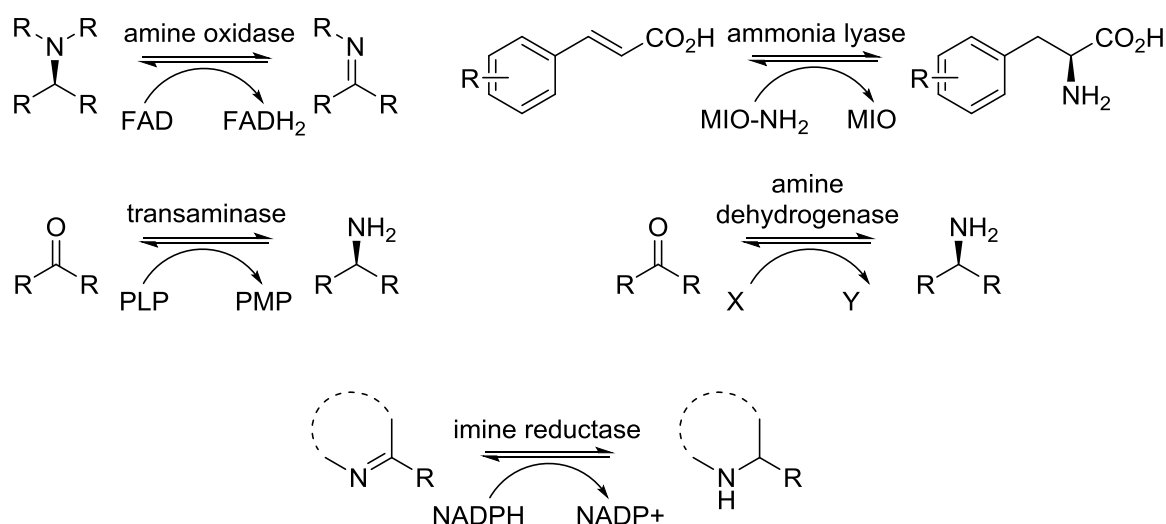


**Figure 13:** Examples of several biotransformations utilised for the synthesis of chiral amines. Amine oxidases, transaminases and phenylalanine ammonia lyases are well-established routes to chiral amines. Amine dehydrogenases represent a new class of biocatalyst specifically engineered to catalyse a non-native reaction.

Enzymes have played an increasingly prominent role in the synthesis of enantiomerically-pure amines. Lipases are well-established in this area and have typically catalysed kinetic resolutions for the production of chiral amines.<sup>23</sup> The array of tools available to the synthetic chemist for the synthesis of chiral amines continues to expand as more biocatalysts are described. Some of the main biocatalytic strategies used for the synthesis of amines will be discussed in the following sections.

#### 1.4 Reduction reactions – imine reduction

##### 1.4.1 Artificial metalloenzymes for the reduction of imines

Novel artificial metalloenzymes, comprised of inorganic scaffolds mounted within the organic environment of a protein, have received considerable attention for their ability to catalyse artificial transfer hydrogenation of imines. These catalysts represent the cutting-edge of research combining traditional transition-metal catalysis with protein biochemistry. The work by the group of Ward pioneers in this rather specialised research area. Previous reports have demonstrated the applicability of a biotinylated aminosulfonamide ligand mounted inside wild-type streptavidin for the production of salsolidine **8b** (Figure 14).<sup>24</sup> Further genetic optimisation of the streptavidin protein through screening of mutants produced variants of the artificial metalloenzymes capable of furnishing salsolidine **8b** in both the (*R*)- (96% *ee*) and (*S*)-configurations (78% *ee*).

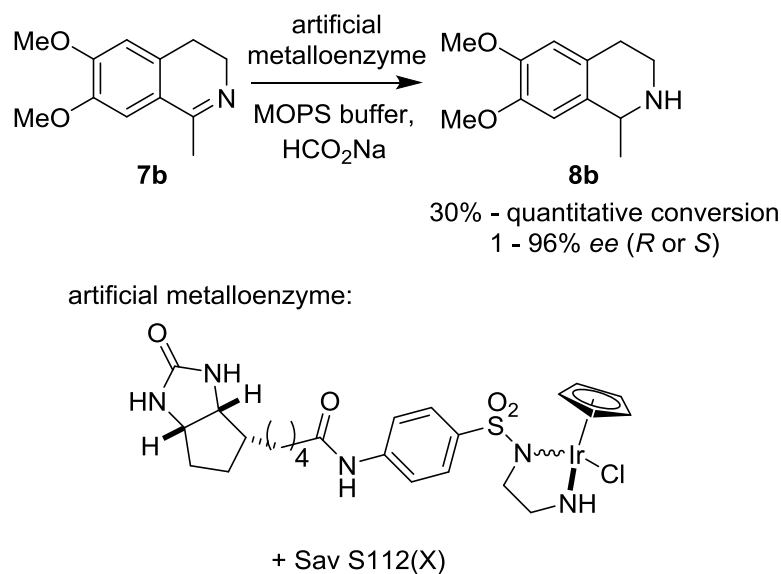


**Figure 14:** Artificial transfer hydrogenation of dihydroisoquinoline **7b** for the production of salsolidine **8b** catalysed by an artificial metalloenzyme. The most favourable results were obtained by combining an iridium metal catalyst with a biotinylated aminosulfonamide ligand, which was mounted in the protein environment of variants of streptavidin.<sup>24</sup>

A more recent report describes the anchoring of an iridium metal complex bearing an aryl-sulfonamide ligand within the enzyme human carbonic anhydrase II. Variation of the bidentate ligand, as well as of the protein, enhanced the activity and selectivity of the artificial metalloenzymes to give salsolidine **8b** in up to 68% *ee*.<sup>25</sup>

#### 1.4.2 Imine reductases

Recently, imine reductases have emerged as a class of enzymes holding great potential for biocatalytic production of chiral amines. As the majority of existing biocatalytic routes for direct formation of chiral amines provide access to primary amines only, the asymmetric biocatalytic reduction of imines presents an attractive route to optically active secondary and tertiary amines.

Imine reductases (IREDs) catalyse the reduction of pre-formed imines to the corresponding amines. Enzymatic imine reduction as a reaction type is not unknown in literature. One of the most studied imine reductases is dihydrofolate reductase (DHFR, EC 1.5.1.3), an enzyme that is ubiquitous in the cells of organisms. DHFR catalyses the reduction of 7,8-dihydrofolate **54** to give 5,6,7,8-tetrahydrofolate **55** (Figure 15), a cofactor used in single carbon transfer chemistry and which is involved in the biosynthesis of purines, pyrimidines as well as several amino acids. As a result of this essential function, the enzyme has been the target of important antineoplastic and antimicrobial drugs.<sup>26</sup> DHFR has been

studied extensively and crystal structures of the protein have been published.<sup>27</sup> Other enzymes capable of reducing imines that are ubiquitous in living organisms include ketimine reductases.<sup>28</sup> Most known imine reductases are dependent on the cofactor NAD(P)H as a source of hydride for the reduction step, although some imine reductases which are able to exploit the unusual F<sub>420</sub> deazeflavin cofactor have been implicated in biosynthetic pathways.<sup>29,30</sup>

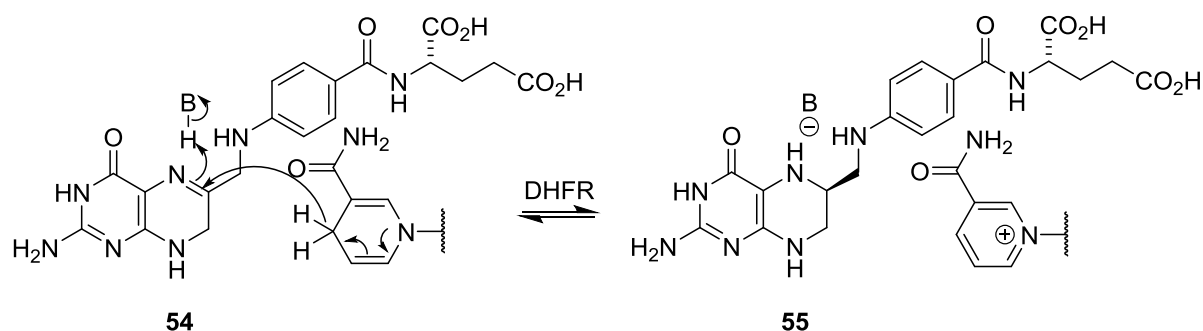


**Figure 15:** Mechanism of action of dihydrofolate reductase, which reduces substrate 7,8-dihydrofolate to the corresponding 5,6,7,8-tetrahydrofolate, a cofactor used in single carbon transfer chemistry.

Enzymes capable of imine reduction were described in 1957; an enzyme was purified from rat liver, which was found to be able to reduce  $\Delta^1$ -piperidine-2-carboxylic acid **5o** (Pip2C) to L-pipecolate **6o**. The structural homologue  $\Delta^1$ -pyrroline-2-carboxylic acid **1f** was also reduced to L-proline **2f**, a step involved in the catabolism of ornithine.<sup>31</sup> An enzyme capable of reduction of Pip2C, the  $\Delta^1$ -piperidine-2-carboxylate reductase (Pip2CR, EC 1.5.1.21), was later isolated from *Pseudomonas putida*, where its function is to reduce Pip2C to L-pipecolic acid in the catabolism of L-lysine in the pipecolate pathway (D-lysine is degraded primarily through the  $\delta$ -aminovalerate pathway – refer to Figure 16A).<sup>32</sup> The isolated enzyme was found to be very unstable following isolation, limiting its use as a potential biocatalyst. The related enzyme  $\Delta^1$ -pyrroline-2-carboxylate reductase (Pyr2CR, EC 1.5.1.1) catalyses the reduction of the structural homologue of Pip2C:  $\Delta^1$ -pyrroline-2-carboxylic acid (Pyr2C, Figure 16B). A gene was later isolated from *P. putida* which encodes for an imine-reducing enzyme capable of both Pip2CR and Pyr2CR related activity.<sup>32</sup>

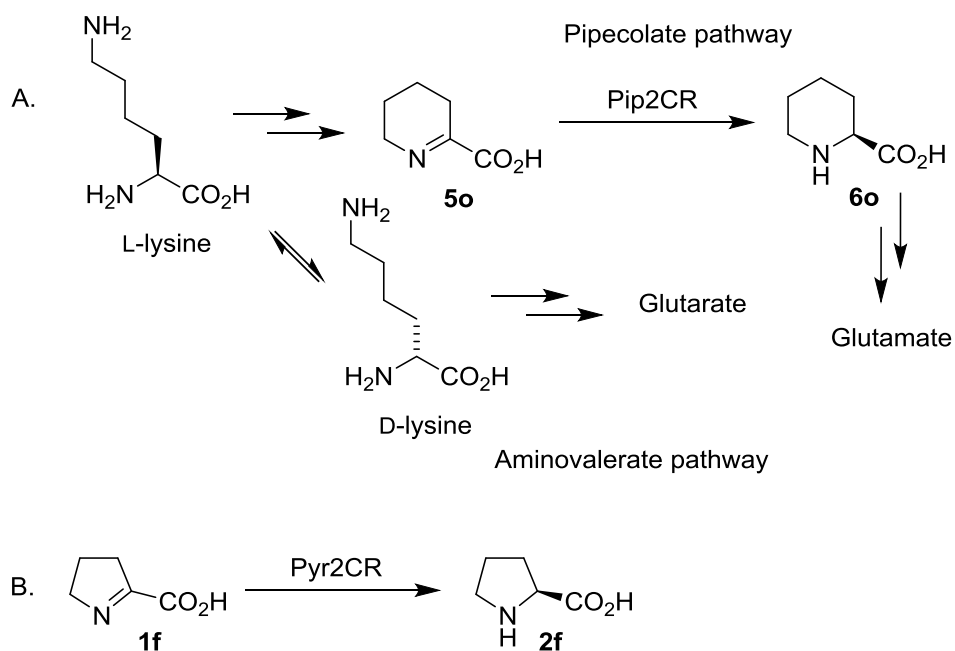


**Figure 16A:** Imine reduction reaction catalysed by Pip2CR, an imine-reducing enzyme involved in the catabolic pathway for lysine (pipecolate and  $\delta$ -aminovalerate pathways for L and D-lysine respectively) which reduces the Pip2C substrate **5o** to L-pipecolic acid **6o**. **16B:** Imine reducing reaction catalysed by Pyr2C, which catalyse the reduction of pyrroline-2-carboxylic acid **1f** to produce L-proline **2f**.<sup>31</sup>

A significant challenge for the use of imines is their instability in water, where they readily undergo hydrolysis to form the corresponding ketone. In the aqueous buffer environment of typical biotransformations, acyclic imines enjoy little success as substrates for imine reductases as the equilibrium position lies heavily towards the ketone. This imposes a limitation on the range of imines which can be screened with imine reductases. In spite of this, Vijayanthi *et al.* showed that it was possible to biocatalytically reduce benzylic acyclic imines **56**, which are hydrolytically stable despite bearing an acyclic imine.<sup>33</sup> Using whole-cells of *Candida parapsilosis* ATCC 7330 in mild aqueous conditions with no additional cofactors, yields of 55 – 80% of the (*R*)-enantiomer amine product were obtained in 95–99% *ee* (Figure 17). The screen was applied to a panel of imines with varying aromatic substituents. It was found that electron-withdrawing substituents led to a reduction in the isolated yield of product, although the *ee* remained high.

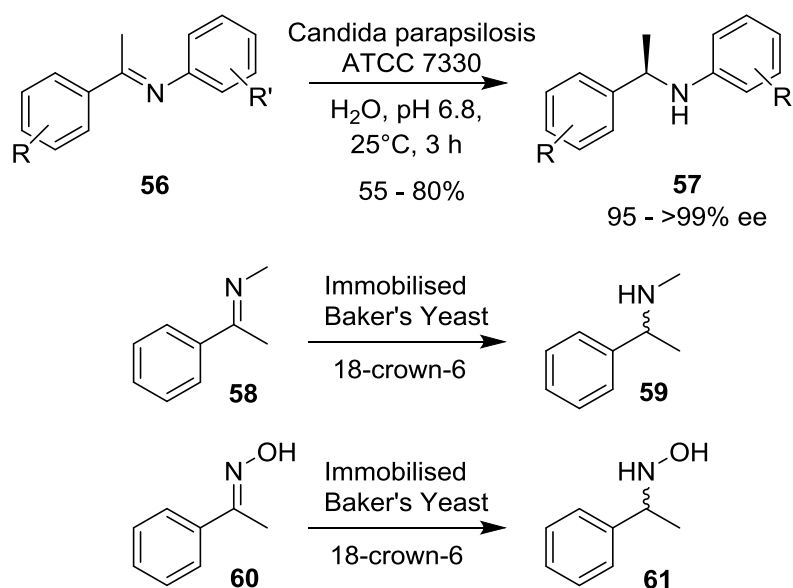


**Figure 17:** Imine reduction reactions catalysed by whole cells of *Candida parapsilosis* (top) and baker's yeast (middle and bottom). The whole cells of baker's yeast were harnessed as immobilised cells on calcium alginate beads in organic solvent.

In addition, organic solvent-tolerant baker's yeast has been shown to reduce imine C=N bonds to produce primary amines.<sup>34</sup> The report outlines a procedure employing whole-cells immobilised on calcium alginate beads, which were used in an aprotic solvent (THF or hexane) with 18-crown-6 as an additive. The substrate *N*-benzylidenemethylamine **58** was converted to the corresponding *N*-benzylmethylamine **59** using the system. The reduction of an oxime C=N bond was also attempted in a biphasic solvent system of hexane-water (1:9). With immobilised baker's yeast and additives 18-crown-6 and glucose, benzaldoxime **60** was reduced to *N*-benzylhydroxylamine **61**. However, neither yield nor *ee* was given for these transformations (Figure 17).

Cyclic imines, such as those based on substituted monocyclic systems as well as polycyclic systems, are also more hydrolytically stable and have therefore enjoyed success as potential substrates for IREDs. Espinoza-Moraga and co-workers have experimented with whole-cells from *Saccharomyces bayanus*, used to ferment grape sugars, for the biocatalytic reduction of dihydro- $\beta$ -carboline.<sup>35</sup> Under anoxic conditions, yields of 57 – 68% were reported for the asymmetric reduction of the imines. *Ee* values were in the range of 50 – 97%, with the configuration of the amine product dependant on the size of the substituent present. Interestingly, a model was proposed for the bioreduction of the dihydro- $\beta$ -carboline with whole cells of *S. bayanus* in order to rationalise these changes in stereochemical outcome, where the presence of a larger, bulkier substituent adjacent to the imine nitrogen facilitated hydride attack to the opposite face of the prochiral imine (Figure 18A).

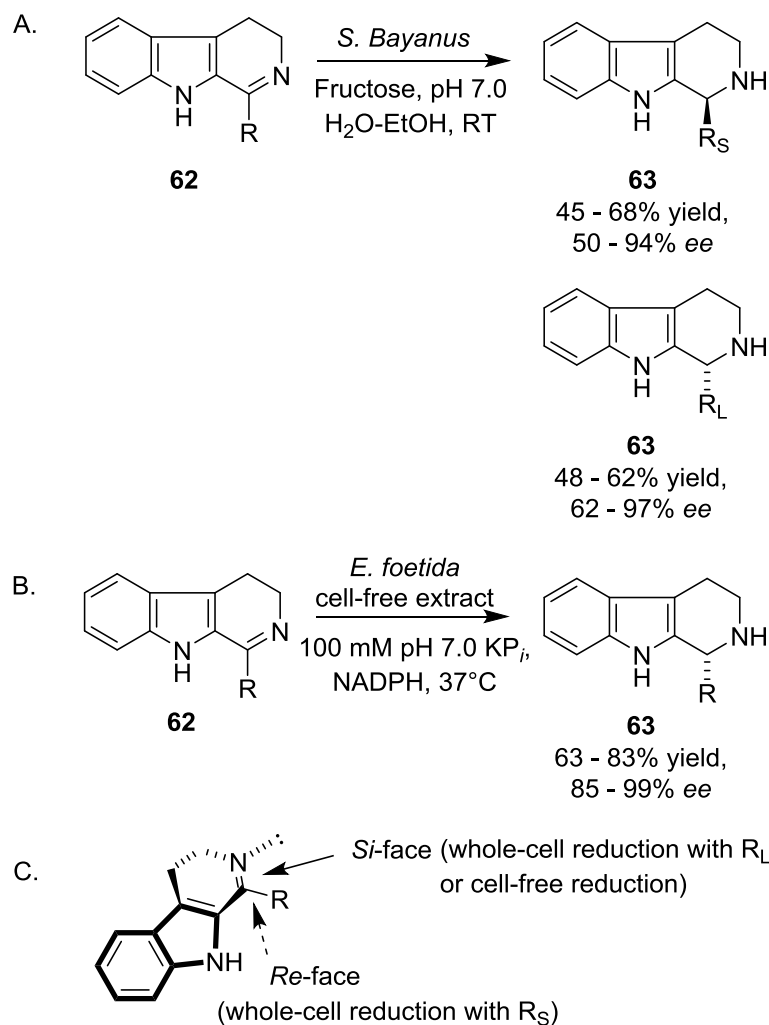


**Figure 18A:** Reduction of dihydro- $\beta$ -carboline **62** by whole cells of the yeast *Saccharomyces bayanus*, produced tetrahydro- $\beta$ -carboline with varying selectivity (both (*R*)- and (*S*)-enantiomers produced, depending on the substituent R group of the molecule). **18B:** Reduction of dihydro- $\beta$ -carboline **62** using cell-free lysate produced from homogenised earthworms *Eisenia foetida*, where delivery of the hydride proceeded exclusively on the top face of the molecule. **18C:** A proposed model for the explanation and determination of the stereochemical outcome of the reduction reactions with *S. bayanus* and *E. foetida*. Delivery of the hydride occurs on the top face of the molecule when the R group is large with *S. bayanus*, or in every case irrespective of the size of the R-group with *E. foetida*. Hydride delivery on the bottom *Re*-face of the molecule occurs with *S. bayanus* when the size of the R-group is small.<sup>35,36</sup>

Further to this work, Mirabal-Gallardo *et al.* subsequently reported the bioreduction of dihydro- $\beta$ -carboline using cell-free extracts from homogenised red Californian earthworms (*Eisenia foetida*).<sup>36</sup> Biotransformations of a panel of dihydro- $\beta$ -carboline compounds were conducted in aqueous medium with addition of NADPH cofactor in potassium phosphate buffer (Figure 18B). In comparison with the whole-cell approach using *S. bayanus*, higher yields (63 – 80%) and *ee* values (92 – 99%) were obtained. Interestingly, the substituent adjacent to the C=N bond had no influence the stereochemical outcome of the reaction, with the (*R*)-enantiomer of the amine produced in all cases. It was suggested that the lower

yields obtained using *S. bayanus* were a consequence of using the whole-cell system, as the cell wall could impede entry and exit of the substrate/product.

Having previously shown limited potential for application as biocatalysts, the turning point for imine reductases came when Mitsukura *et al.* reported the screening of the cyclic imine 2-methylpyrroline **1a** against organisms including bacteria, yeasts, actinomyces and fungi.<sup>37</sup> Imine reducing activity was found in strains of *Streptomyces* and in particular, two strains were said to display enantiocomplementary activity. *Streptomyces* sp. GF3587 reduced 2-methyl-1-pyrroline **1a** to the corresponding (*R*)-2-methylpyrrolidine (*R*)-**2a** whereas *Streptomyces* sp. GF3546 furnished the opposite (*S*)-**2a** in excellent yield and *ee* (Figure 19).

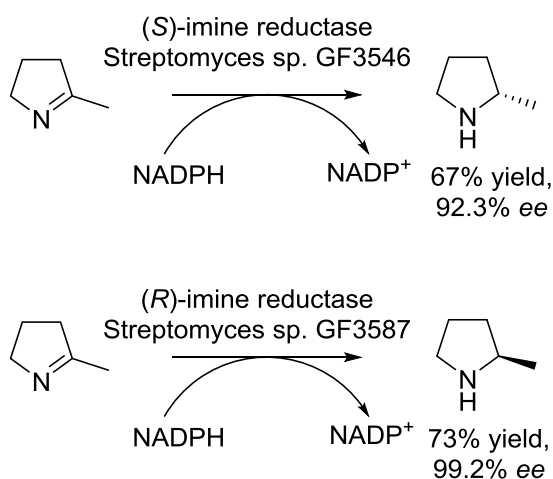


**Figure 19:** Reduction of cyclic imine 2-methyl-1-pyrroline **1a** to the corresponding (*R*)-2-methylpyrrolidine (*R*)-**2a** and opposing enantiomer (*S*)-**2a** using whole cells of *Streptomyces* sp. GF3587 and GF3546 respectively. It was from this biotransformation that the designation as (*R*)-IRED and (*S*)-IRED originated.<sup>37</sup>

The (*R*)-imine reductase from *Streptomyces* sp. GF3587 [(*R*)-IRED] was subsequently isolated, characterised and screened against a range of structurally-diverse compounds containing imine groups, although no further activity was detected beyond 2-methyl-1-pyrroline **1a**.<sup>38</sup> Interestingly, BLAST (Basic Local Alignment Search Tool) analysis of the (*R*)-imine reductase with sequences contained in the UniProt database,<sup>39</sup> revealed that the protein shared 100% sequence identity with that of the recently sequenced *Streptomyces fulvissimus* DSM 40593. It is unclear whether *Streptomyces* sp. GF3587 corresponds to the same *S. fulvissimus* strain, or if the protein sequence is conserved in multiple strains of *Streptomyces*.<sup>40</sup>

In contrast to the (*R*)-IRED, the (*S*)-imine reductase from *Streptomyces sp.* GF3546 [(*S*)-IRED] was found to possess a much broader substrate scope.<sup>41</sup> The protein was isolated and described as a homodimer composed of 30.5 kDa subunits. Recombinant expression of the (*S*)-IRED was achieved in *E. coli* for the first time in the report. The IRED was screened against a range of compounds, including dihydroisoquinolines, cyclic iminoacids and even the natural product dihydrofolic acid (Figure 20); 2-methyl-1-pyrroline was found to be the best substrate for the enzyme, with the highest reported level of activity.

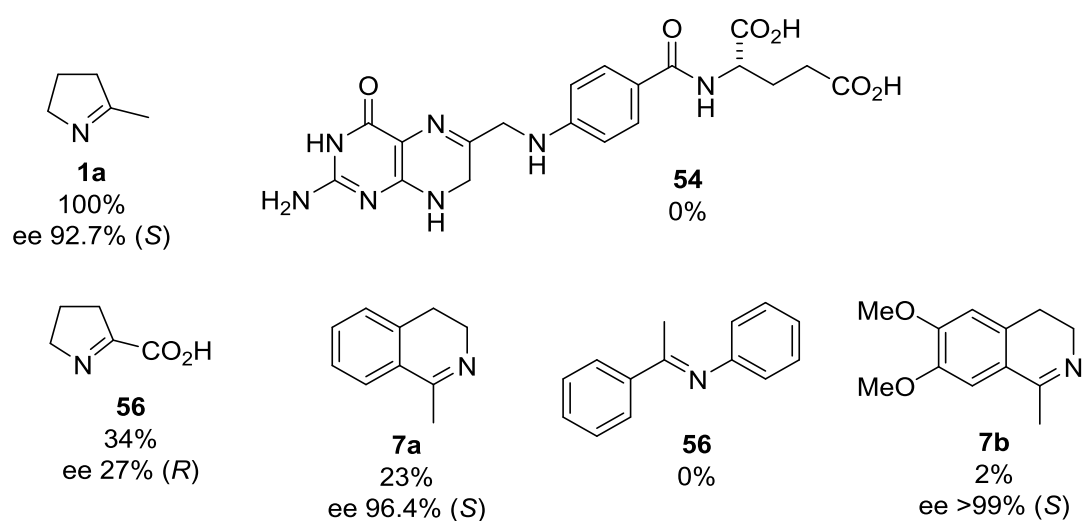


**Figure 20:** Compounds screened against the (*S*)-IRED, detailing the observed conversion as well as enantioselectivity of the reduction reaction.<sup>41</sup>

Both (*R*)-IRED and (*S*)-IRED were used as isolated enzymes to carry out biotransformations in aqueous medium. For the (*R*)-IRED, stoichiometric quantities of the cofactor NADPH were used in the biotransformation reactions. For the (*S*)-IRED, a system employing the commercially available glucose dehydrogenase in the presence of glucose was used to recycle the NADPH cofactor, negating the requirement for stoichiometric quantities of expensive NADPH to be added to the reaction.

Li *et al.* described an imine reductase from *Paenibacillus lactis* (*PSIR*) which was capable of reducing 3*H*-indoles and 3*H*-indole iodides to give the corresponding indolines and *N*-alkyl indolines in high conversion and ee (Figure 21).<sup>42</sup> The substrate panel was limited to 2,3,3-trimethyl-3*H*-indoles **64**, which possess the inability to undergo tautomerisation to the corresponding indoles, although bulkier substituents on the 2 and 3 positions appeared to inhibit enzyme activity. The *PSIR* also displayed the capability of reducing the more typical IRED substrates 2-methyl-1-pyrroline **1a** and 2-methyl-1-

piperideine **5a** in high *ee*, although no activity was observed towards 1-methyl-3,4-dihydroisoquinoline **7a**.

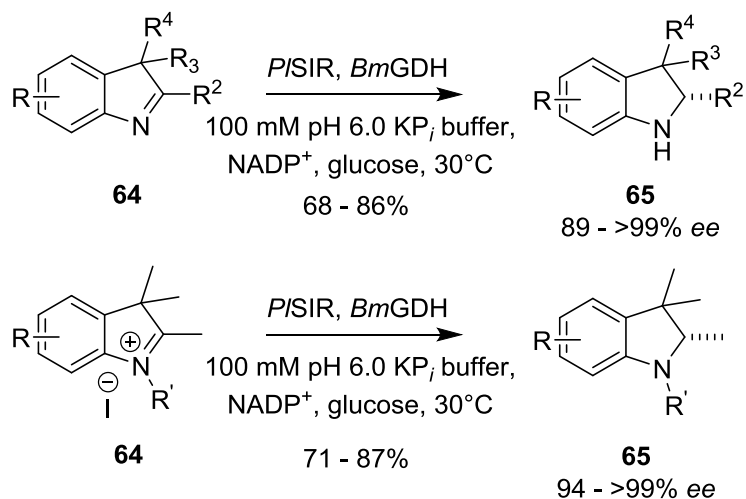


**Figure 21:** Reduction of 2,3,3-trimethyl-3*H*-indoles and the corresponding *N*-alkyl derivatives by the (*S*)-selective IRED from *Paenibacillus lactis* (*PISIR*).<sup>42</sup>

A more recent report from the same research group subsequently identified an (*R*)-selective IRED from *Paenibacillus lactis* (*PRIR*) using a genome data mining approach (Figure 22).<sup>43</sup> The *PRIR* shared 35% sequence identity with the (*R*)-IRED from *Streptomyces* sp. GF3587 as well as 40% sequence homology with the (*S*)-IRED from *Streptomyces* sp. GF3546 and the previously mentioned *PISIR*. The IRED was capable of converting 2,3,3-trimethyl-3*H*-indoles **64** to give the corresponding indolines in the opposite configuration to the *PISIR* products. In addition, 2-methyl-1-pyrroline **1a**, 2-methyl-1-piperideine **5a** and 1-methyl-3,4-dihydroisoquinoline **7a** were confirmed as substrates for the enzymes. High conversions were also reported for *N*-alkyl-3*H*-indoles, although interestingly the opposite (*S*)-enantiomer of the amine products was furnished in these cases as products.

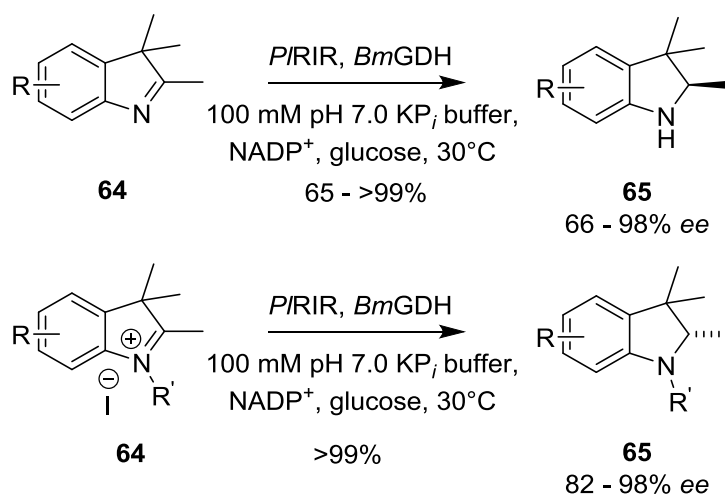


**Figure 22:** Reduction of 2,3,3-trimethyl-3H-indoles and the corresponding *N*-alkyl derivatives by the (*R*)-selective IRED from *Paenibacillus lactis* (*PIRIR*). Unlike the *PSIR*, a reversal of stereoselectivity was observed when reducing *N*-alkyl-3H indoles with *PIRIR*.<sup>43</sup>

As the number of new imine reductase reports has rapidly expanded, additional (*R*)- and (*S*)-selective IREDs have recently been described that share varying levels of sequence homology with the two from *Streptomyces* sp. These are typically characterised using the archetypal 2-methyl-1-pyrroline **1a** substrate. Grogan and co-workers described an oxidoreductase from *Streptomyces kanamyceticus*, which was found to catalyse the asymmetric reduction of **1a** to give (*R*)-2-methylpyrrolidine **2a** in >99% ee.<sup>44</sup> Following successful crystallisation of the protein, the structure for the protein was described and represented the first crystallisation of a recent IRED biocatalyst from the advent of the enzyme class.

Gand and co-workers described three novel imine reductases including an example from *Pseudomonas putida* KT2440 (*RIR-Ppu*), for which a crystal structure was previously known but imine reductase activity was never identified.<sup>45</sup> Interestingly, the report detailed screening of a variety of cyclic and acyclic amines in the oxidation direction of the enzymes, in order to identify novel activity towards acyclic imines which would otherwise be labile in aqueous environments. The structure of *RIR-Ppu* revealed the residue His180, which was proposed as a possible catalytic residue and was subsequently mutated to produce the variant H180V which displayed ten-fold reduced activity compared to the wild-type.

Huber *et al.* identified a novel (*S*)-IRED from *Streptomyces aurantiacus* JA4570, which shared a sequence identity of 57% with the (*S*)-IRED from *Streptomyces* sp. GF3546. Crystal structures of the novel IRED as well as those of the GF3546 (*S*)-IRED in apo form and with cofactor NADPH bound were reported. The paper also reported the first IRED-catalysed direct reductive amination of ketones, although the yields from the reactions were very poor ( $\leq 8.8\%$ ).<sup>46</sup>

Scheller *et al.* recently identified several novel IREDs: two (*R*)-selective IREDs, one from *Streptosporangium roseum* DSM 43021 [(*R*)-IRED-*Sr*] which shares 60.8 % sequence identity with the *Streptomyces kanamyceticus* (*R*)-IRED and another IRED from *Streptomyces turgidiscabies* [(*R*)-IRED-*Sf*] with 80.7 % sequence identity with the GF3587 (*R*)-IRED. In addition, an (*S*)-IRED from *Paenibacillus elgii* [(*S*)-IRED-*Pe*], which shares 60.5% sequence identity with the GF3546 (*S*)-IRED and displayed comparable activity was described.<sup>47</sup> The (*R*)-IRED-*Sr* was determined to be the most active IRED of the three and was able to catalyse intermolecular reductive amination reactions in a subsequent report (Figure 23). Interestingly, the work examined the formation of imines in aqueous medium and followed the equilibrium between imine and aldehyde using proton NMR at varying pH, with imine found to be favoured at higher pH ranges.<sup>48</sup>

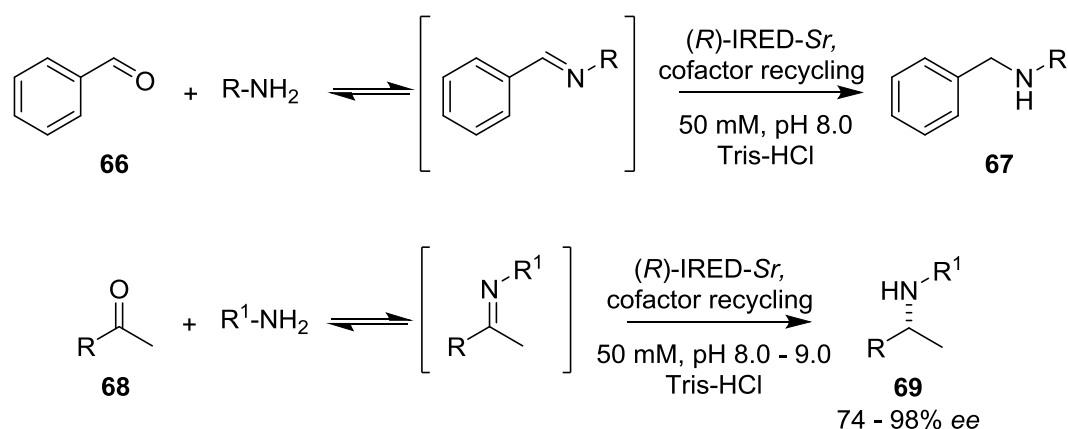


**Figure 23:** Intermolecular reductive amination reactions catalysed by the (*R*)-IRED *Sr* from *Streptomyces roseum* DSM 43021 with both aldehyde and ketone substrates. Higher conversions were observed with the benzaldehyde substrate.<sup>48</sup>

Hauer's group also produced an IRED sequence database<sup>49</sup> which aligns and compares the sequences of more than 530 putative imine reductases based on residues that are conserved within known imine reductase, to aid the discovery of novel IREDs *in silico*.<sup>50</sup> The work by Wetzl *et al.* built on this by using C-terminal domain clustering of the bacterial protein sequence space to mine protein sequences. Using this approach, 20 novel IREDs of differing activity and selectivity were identified, based on taking sequences from distinct sequence clusters, and screened against a panel of representative IRED substrates.<sup>51</sup>

As the number of IRED enzymes known and described for use as biocatalysts continues to expand, review articles have also been published which detail the rapid and ongoing developments with regards to this class of enzyme, including extensive articles by

Schrittwieser,<sup>52</sup> Grogan<sup>53</sup> and Gamenara.<sup>54</sup> Finally, a focussed examination of the synthetic applications of IRED enzymes can be found in a Science of Synthesis book chapter.<sup>55</sup>

### 1.5 Reduction reactions – carboxylic acid reduction

For the production of aldehydes from carboxylic acids, the reduction of the carboxylic acid to the alcohol and then subsequent selective re-oxidation to produce the aldehyde is routinely used. This selective re-oxidation can be accomplished via use of pyridinium chlorochromate, Swern oxidation or even using Dess-Martin periodinane. The alternative route, involving selective reduction of carboxylic acid groups to produce aldehydes, remains an area of synthetic chemistry that is difficult to accomplish cleanly. General strategies involve chemical activation of the carboxylic acid group, in order to generate a more reactive intermediate that can then be reduced to yield the corresponding aldehyde.

Carboxylic acid reductase (CAR) enzymes represent the biocatalytic alternative for the production of aldehydes and they have garnered significant attention recently due to the selectivity exhibited in the reduction of the carboxylic acid group. For a comprehensive review summarising carboxylic acid-reducing activity in a number of different organisms, dealt with briefly here, see that of Winkler and co-workers.<sup>56</sup> CARs are dependent on ATP and NADPH cofactors, required by the enzyme to activate and reduce the carboxylic acid respectively. The mechanism by which they operate involves activating the deprotonated carboxylic acid as adenosyl phosphate using ATP. This is accomplished in the adenylating domain of the holo-CAR enzyme. Following this activation, the adenosyl phosphate is then attacked by a phosphopantetheine arm with the release of AMP. The 4'-phosphopantetheine arm serves as a shuttle to transfer the resulting thioester to the reduction domain, where NADPH can finally reduce the thioester to the aldehyde product (Figure 24). Due to the dependence of NADPH and ATP, CAR enzymes are most conveniently used as whole-cell biocatalysts, as the cofactors can be regenerated within the host organism.

As the mechanism of the enzyme relies on the 4'-phosphopantetheine to shuttle the acyl acid intermediate between adenylating and reduction domains, a post-translational modification of the apo-CAR enzyme is required for maximum activity.<sup>57</sup> This is accomplished by transferring a 4'-phosphopantetheine prosthetic group from a CoA donor to the serine residue of the enzyme, catalysed by a 4'-phosphopantetheinyl transferase.

CARs, such as the enzyme from *Mycobacterium marinum*, have been shown to be able to reduce a number of medium- and long-chain fatty acids for the production of fuels and fragrance molecules.<sup>58</sup> Furthermore, it was found that the isolated CAR enzyme from

*Nocardia* was able to reduce vanillic acid to vanillin, with no further reduction observed and demonstrating the selectivity of CARs for carboxylic acid reduction only.<sup>59</sup>

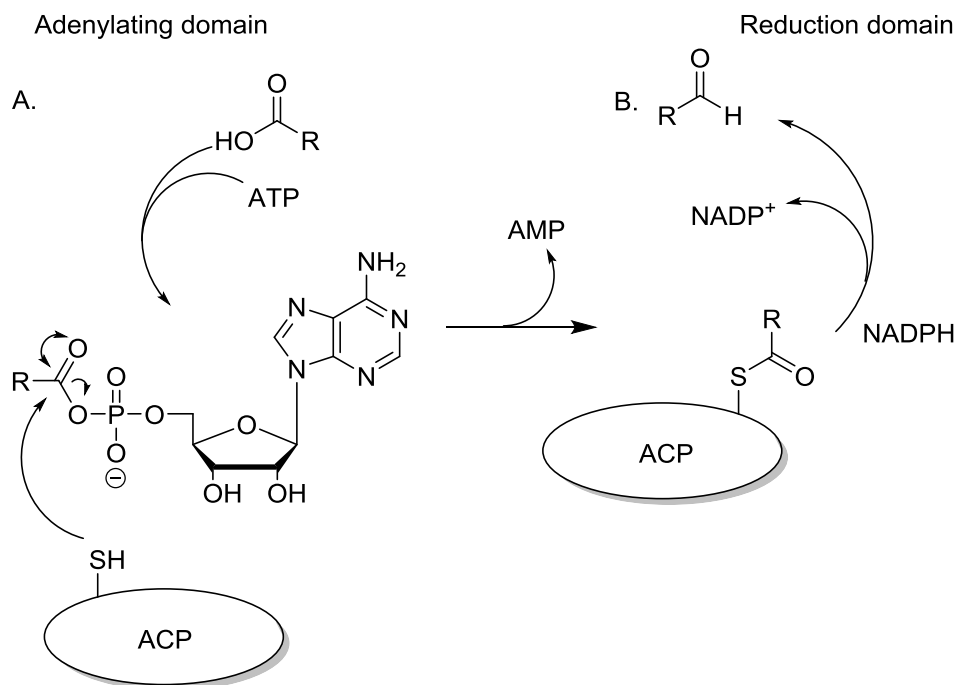


**Figure 24:** Enzyme mechanism for CAR-mediated reduction of carboxylic acids, which contains multiple domains to facilitate the transformation within the holo-CAR enzyme (which has undergone post-translational modification by *Sfp*). **A.** The deprotonated acid is first adenyated in the adenylation domain of the enzyme to activate the acid. The substrate adenosyl phosphate is subsequently attacked by the thiol of the 4'-phosphopantetheinyl arm of the ACP domain. This forms an acyl acid (thioester) intermediate, accompanied with the release of AMP. **B.** The ACP shuttles the thioester to the reduction domain of the enzyme using the 4'-phosphopantetheinyl arm, where NADPH can proceed to reduce the thioester to obtain the aldehyde product.<sup>56</sup>

### 1.6 Biocatalytic asymmetric synthesis - $\omega$ -transaminases

$\omega$ -transaminases (amine transaminases) are well-established enzymes for the direct asymmetric synthesis of chiral amines. These enzymes can act on aliphatic amines/ketones and can catalyse the reductive amination of carbonyl groups to generate primary amines enantioselectively, at the expense of a sacrificial amine donor such as alanine or isopropylamine. The mechanism of  $\omega$ -transaminases relies on the pyridoxal 5'-phosphate (PLP) cofactor, which transfers the amine from the donor to the carbonyl-containing substrate via a ping-pong mechanism.

As the reaction is fully-reversible,  $\omega$ -TAs can also catalyse the oxidation and subsequent hydrolysis of an amine to form a carbonyl. Indeed, it is more favourable for the transaminase to catalyse the formation of carbonyls from amines and this has been exploited to great success for the kinetic resolution of amines. One such example was

demonstrated by Kroutil's group in the deracemisation of a panel of  $\alpha$ -chiral primary amines, via a two-step enzymatic process exploiting enantiocomplementary transaminases (Figure 25).<sup>60</sup> The first stage involves a kinetic resolution of the racemic amine via a transaminase-catalysed hydrolysis of the (*R*)-enantiomer of the amine, leaving behind the opposing (*S*)-enantiomer of the amine. In order to effect a dynamic kinetic resolution, the ketone is then reacted with an (*S*)-selective  $\omega$ -transaminase, giving rise to the (*S*)-enantiomer amine, with the product produced overall in >99% *ee*.

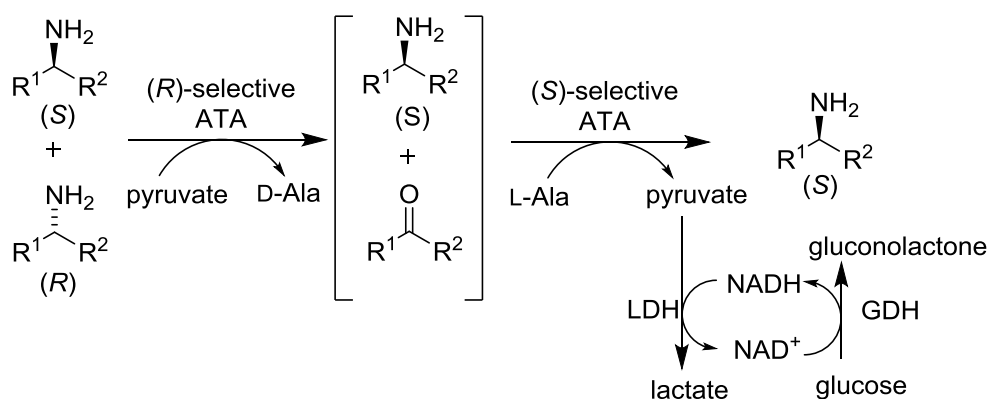


**Figure 25:** Deracemisation of primary amines by a one-pot, two-step reaction cascade employing two transaminases of opposing enantioselectivity. A kinetic resolution of the racemic amine is first carried out by an (*R*)-selective ATA, followed by transamination using an enantiocomplementary (*S*)-ATA, furnishing the desired (*S*)-amine product in >99% *ee*.<sup>60</sup>

The favoured reaction for amine transaminases (ATAs) is the formation of carbonyls from amines, difficulties are encountered regarding reaction equilibrium and stereoselectivity during asymmetric synthesis of amines. In order to help shift the reaction equilibrium to favour formation of the product, a number of enzyme cascades can be employed to effect *in-situ* product removal. This includes the use of lactate dehydrogenase (LDH), which has been shown to reduce the pyruvate generated when alanine is expended as an amine donor to lactate (Figure 26). Glucose dehydrogenase (GDH) was then used to regenerate the NADH cofactor required by LDH.<sup>61</sup>

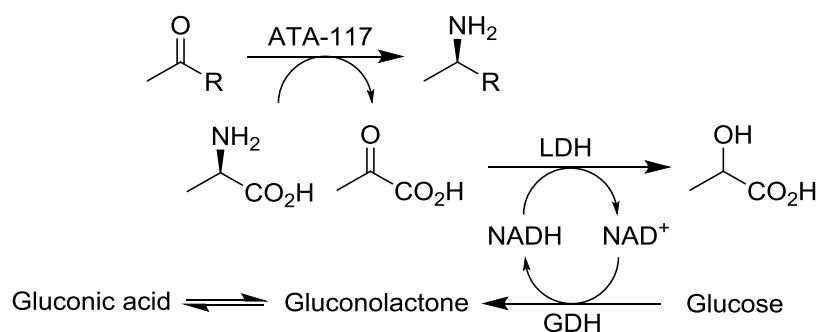


**Figure 26:** GDH/LDH enzyme cascade used to shift the transaminase reaction equilibrium towards product amine formation during asymmetric transamination of ketones and aldehydes. Here, D-Ala is used as the sacrificial amine donor during the enantioselective amination of a ketone by the commercially available (*R*)-selective transaminase ATA-117.

Kroutil's group has worked to construct the "ideal" reductive amination reaction of ketones, utilising ammonium as the amine donor together with a cheap reducing agent such as formate or glucose. To this end, they developed an elegant enzymatic cascade for producing enantiopure amines where L-alanine is used as the amine donor to the target ketone in a catalytic quantity.<sup>62</sup> However, the alanine is then regenerated from the resulting pyruvate by employing an L-amino acid dehydrogenase (L-AADH), where ammonium is used in the key regenerative step, thereby negating the necessity for stoichiometric amounts of the amine donor (Figure 27).

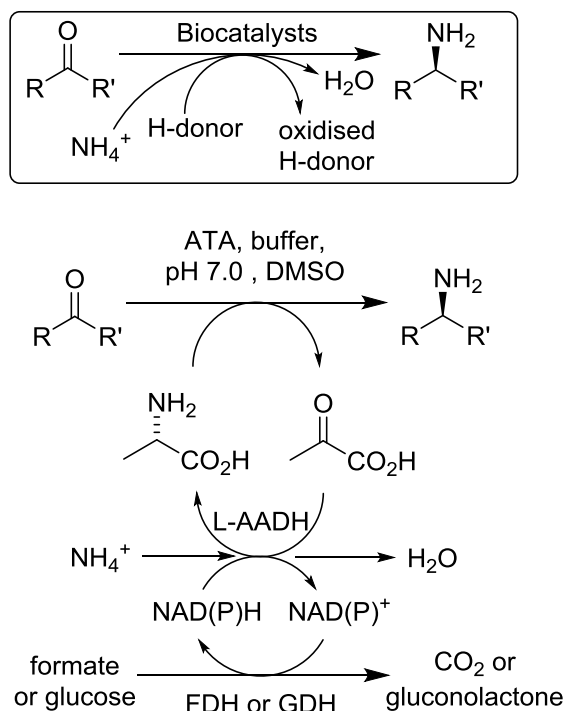


**Figure 27:** Enzyme cascade for the enantioselective amination of ketones, employing L-Ala as the sacrificial amine donor in the reaction. Here, L-Ala is used in less than stoichiometric quantities and is regenerated from pyruvate by an L-AADH using formate. The boxed reaction scheme represents the "ideal" reductive amination reaction, exploiting cheap amine donors.<sup>62</sup>

From this method, a number of different (*S*)-primary amines were prepared from their corresponding aliphatic, aromatic and aryl-alkyl ketones using  $\omega$ -transaminase ATA-113. Conversions and *ee* values observed varied but were typically above 90%, although acetophenone (6% conversion) and 4-phenyl-2-butanone (34% *ee*) produced less impressive results.

For the asymmetric synthesis of primary amines from ketones, enantiomerically-pure amine donors are also required. For the formation of (*R*)-amines, this can be quite costly as unnatural amino donors such as D-alanine must be used, rendering the use of (*R*)-selective amine transaminases far more expensive than their (*S*)-selective counterparts. Richter and co-workers devised an ingenious way to use the cheaper L-Ala as the amine donor in (*R*)-ATA-mediated reactions, by using an alanine racemase enzyme (AlaR) to provide the necessary D-Ala (Figure 28).<sup>63</sup>

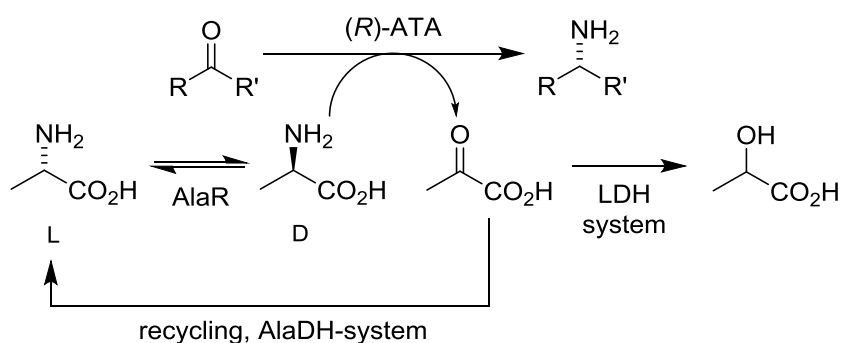


**Figure 28:** (*R*)-amination of ketones by an (*R*)-selective ATA using L-Ala as the amine donor. The L-Ala is racemised *in-situ* by the AlaR enzyme, providing the D-Ala amine donor. The pyruvate product can then be removed from the reaction using the LDH system or used to produce more L-Ala by employing the enzyme AlaDH.<sup>63</sup>

Transaminases have been used to great success for the manufacture of APIs in industry, including the antidiabetic drug sitagliptin (Figure 29).<sup>64</sup> An (*R*)-selective transaminase was subjected to 11 rounds of directed evolution in order to tailor the enzyme to the specific requirements for manufacturing the substance: increased activity towards the substrate **70**, thermostability, organic solvent tolerance and enhanced preference for IPA as an amine donor. The final variant, consisting of 27 mutations in total, was able to produce the API from 200 g/L pro-sitagliptin ketone in >99.95% *ee* by using 6g/L of the enzyme in 50% DMSO, with an assay yield of 92%. Compared to the previous state-of-the-art rhodium-catalysed process, this transaminase-catalysed biocatalytic process offered the API product in a 10 – 13% increase in overall yield, a 53% increase in productivity, 19% reduction in total waste, the elimination of all heavy metals from the process and an overall reduction in total manufacturing cost.

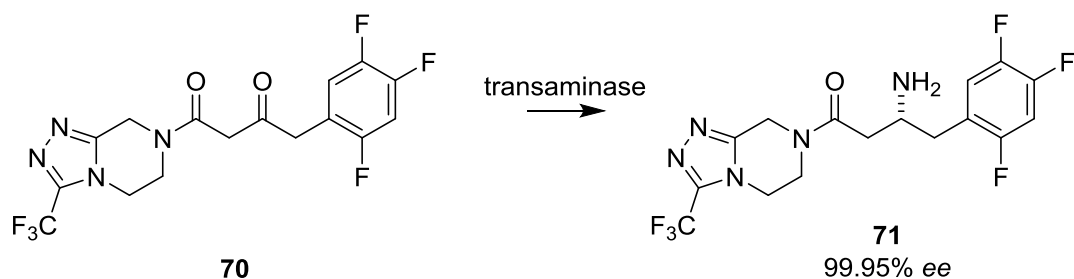


**Figure 29:** Manufacture of the antidiabetic drug sitagliptin **71**, using an evolved ATA to catalyse the final enantioselective amination step.<sup>64</sup>

Turner's group has recently reported several putrescine transaminases (pATAs), capable of catalysing the transfer of amino groups from terminal diamine donor molecules to ketoacid acceptors.<sup>65</sup> A spontaneous condensation of the resulting aminoaldehyde intermediates formed from the pATA-catalysed transformation allowed access to a range of *M*-heterocycle products. The system was employed successfully in the biomimetic synthesis of the bioactive alkaloid ficuseptine (Figure 30).

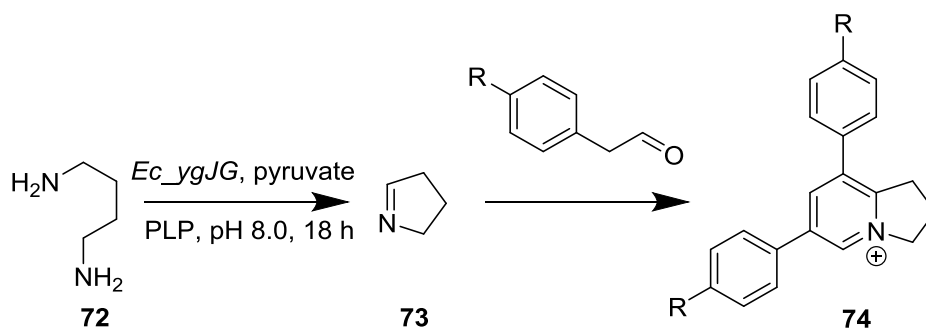


**Figure 30:** Biomimetic synthesis of 2,3-dihydro-1*H*-indolizinium motifs **74** employing the putrescine transaminase (pATA).<sup>65</sup>

### 1.7 Biocatalytic asymmetric synthesis – phenylalanine ammonia lyase

Phenylalanine ammonia lyase (PAL) enzymes catalyse the removal of ammonia from phenylalanine and its derivatives in order to afford cinnamic acid. This deamination reaction is generally implied to be catalysed by a 4-methylideneimidazole-5-one (MIO) cofactor. Although the mechanism of the PAL reaction is still under debate, recently an alternative mechanistic pathway was suggested which is independent of the MIO cofactor.<sup>66</sup>

In high ammonia concentrations, PAL enzymes are known to catalyse the reverse reaction for the formation of chiral  $\alpha$ -amino acids **76**. Turner's group has recently reported

an ammonia lyase from *Streptomyces maritimus*.<sup>67</sup> The EncP ammonia lyase was shown to be able to catalyse the formation of both  $\alpha$ -amino acids **76** and  $\beta$ -amino acids **77**, where the regioselectivity was said to be “tunable” in order to control the ratio of  $\alpha$ -amino acid to  $\beta$ -amino acid formed.

A related enzyme, phenylalanine aminomutase, catalyses the isomerisation of  $\alpha$ - and  $\beta$ -amino acids, by shuttling the amine group of the amino acid substrate across from the  $\alpha$ -position of the molecule to the  $\beta$ -position (Figure 31).<sup>68</sup>

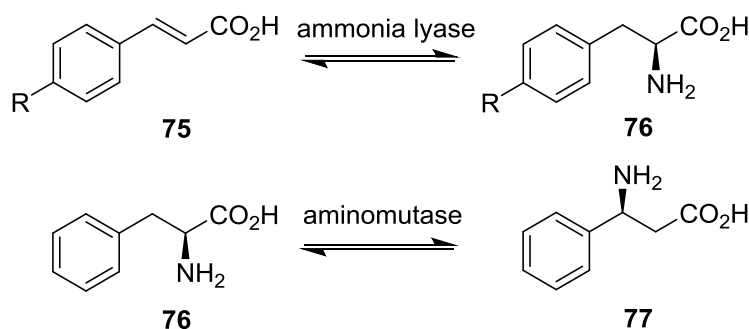


**Figure 31:** Biotransformation of cinnamic acid and its derivatives catalysed by phenylalanine ammonia lyases (PAL), which adds ammonia across a double bond (top) and phenylalanine aminomutases (PAM), which shuttles the amino group across the  $\alpha$ - and  $\beta$ -positions and produces a stereoinversion of the amino group on the molecule.<sup>68</sup>

The success of PALs as biocatalysts for the synthesis of chiral amine intermediates has been demonstrated by the development of a process by DSM for the synthesis of (*S*)-2-indolinecarboxylic acid **26f**, used as a key intermediate for angiotensin 1-converting enzyme inhibitors (ACE inhibitors).<sup>69</sup> The process marries the enzyme-catalysed asymmetric amination reaction of the PAL enzyme with a copper-catalysed cyclisation to afford the desired (*S*)-enantiomer building block (Figure 32).

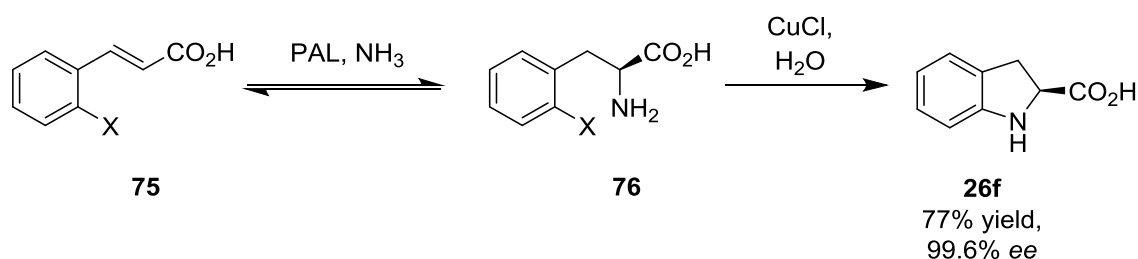


**Figure 32:** Formation of (*S*)-indoline-2-carboxylic acid **26f** from the enantioselective amination of cinnamic acid derivatives **75** with a PAL enzyme, followed by a copper-catalysed cyclisation.<sup>69</sup>

## 1.8 Biocatalytic asymmetric synthesis - amine dehydrogenase

Recently, a new class of enzyme has emerged for the synthesis of chiral amines. An amine dehydrogenase, which catalyses the asymmetric reductive amination of ketones to afford the corresponding primary amines, was engineered to accept non-natural ketones as substrates for the reaction (Figure 33).<sup>70</sup> The wild-type Leucine dehydrogenase from *Bacillus stercorophilus* catalyses the amination of  $\alpha$ -ketoacids **78**. This served as the protein scaffold which was subjected to several rounds of evolution, in order to produce the NADPH-dependent amine dehydrogenase that subsequently accepted the analogous methyl isobutyrate ketone **80** as the substrate for amination. The success in engineering the protein to accept non-natural substrate motifs is a testament to the advances gained from modern molecular biology techniques and protein engineering strategies.

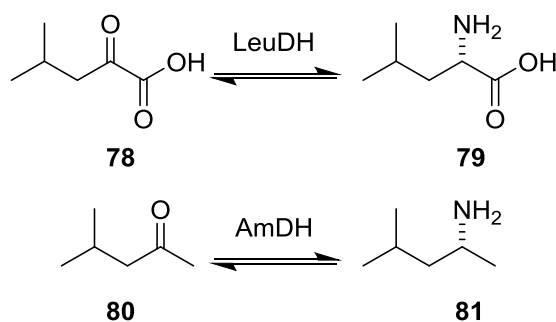


**Figure 33:** Biotransformation of wild-type Leucine dehydrogenase enzyme (LeuDH, top) and the transformation of the corresponding ketone catalysed by the engineered amine dehydrogenase (AmDH, bottom).<sup>70</sup>

## 1.9 Deracemisation of racemic amines

### 1.9.1 Chemical deracemisation methods

The deracemisation of racemic amines presents a particularly attractive route to enantiomerically-pure chiral amines. Unlike kinetic resolution reactions, the theoretical yield from the enantioenrichment reaction is >99%. Also, since the starting material and product are simply enantiomers of the same molecule, the treatment and containment of the chemical remains the same. The main challenge in constructing a successful deracemisation cascade is rooted in the two mechanistically-different reactions being able to work simultaneously without quenching one another. For oxidation/reduction orientated deracemisation cascades, this presents a significant problem for chemocatalytic routes as the oxidant and reductant are usually mutually nullified in the presence of the other.

The Toste group overcame this problem by keeping the oxidant and reductant separated in an aqueous/organic/solid-phase separation strategy, allowing the oxidation-reduction cycles to proceed in the same pot (Figure 34).<sup>71</sup> Employing a water-soluble oxidant, a Hantzsch ester as the solid-phase reductant and a phosphoric acid catalyst, they were able to achieve the enantio-enrichment of 3*H*-indolines in up to 96% *ee*.

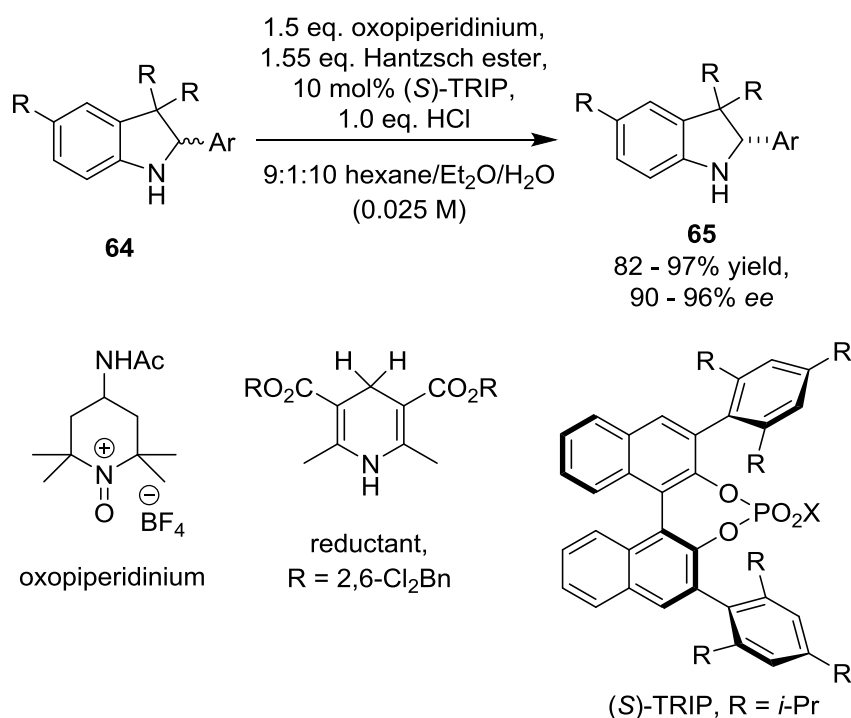


**Figure 34:** Chemocatalytic deracemisation of 2-substituted 3*H*-indoles **64** using the combined approach of an oxidant, reductant and phosphoric acid catalyst in an aqueous/organic/solid tri-phasic approach. The multi-phase reaction allowed effective separation of the oxidant and reductant, which would otherwise quench one another in the same pot.<sup>71</sup>

An excellent example of a chemocatalytic deracemisation of amines was reported by Ji *et al.*, who managed to combine *N*-bromosuccinimide oxidation with an iridium-catalysed asymmetric hydrogenation to affect the deracemisation of substituted racemic tetrahydroisoquinolines.<sup>72</sup> The strategy allowed the facile deracemisation of a broad range of 1-substituted-1,2,3,4-tetrahydroquinolines as well as *N*-methyl and *N*-benzyl 1-aryl-1,2,3,4-tetrahydroquinolines, for the production of optically-pure tertiary amines. The process was successfully applied to 1-phenyl-1,2,3,4-tetrahydroisoquinoline **7b** on a preparative-scale, affording (*S*)-**7b**, a precursor to drug molecules such as (+)-solifenacin and (+)-FR115427, in 90% yield and 97% *ee* (Figure 35).

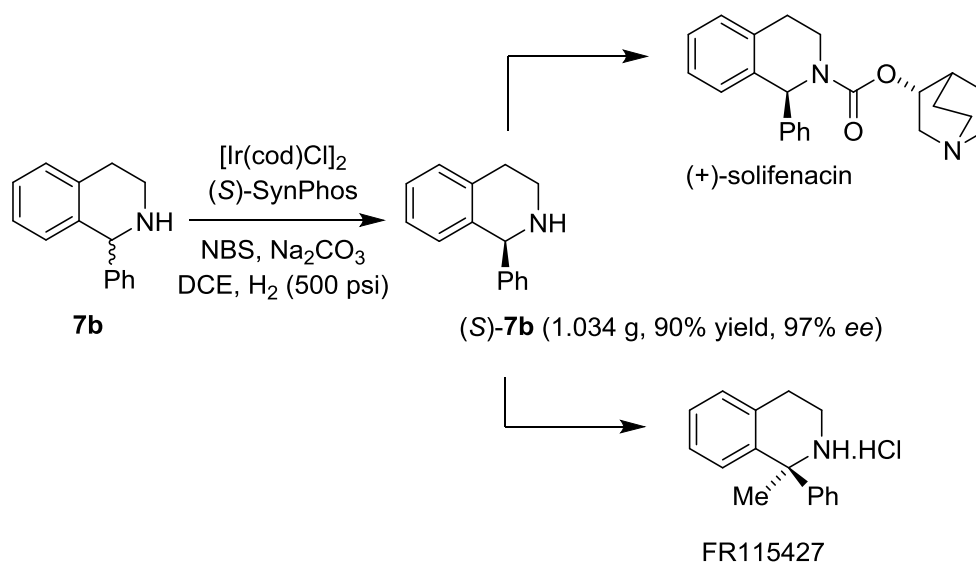


**Figure 35:** Chemocatalytic deracemisation strategy for the enantio-enrichment of racemic amines, employing an iridium catalyst with *N*-bromosuccinimide as the oxidant. This was used successfully in the preparative-scale deracemisation of 1-phenyl-1,2,3,4-tetrahydroisoquinoline **7b**, which is an intermediate to drug molecules.<sup>72</sup>

### 1.9.2 Amine oxidases for the biocatalytic deracemisation of amines

The majority of the work completed to date on deracemisation systems employs enzymes. Monoamine oxidase (MAO-N) from *Aspergillus niger* is an FAD-dependent flavoprotein capable of the enantioselective oxidation of amines to furnish the corresponding imines. The enzyme itself has been through many rounds of directed evolution in order to increase its activity and substrate scope. As a result, several variants of the oxidase have been described which have been tailored for activity towards a broad range of structurally-diverse amines (Figure 36).<sup>73</sup>

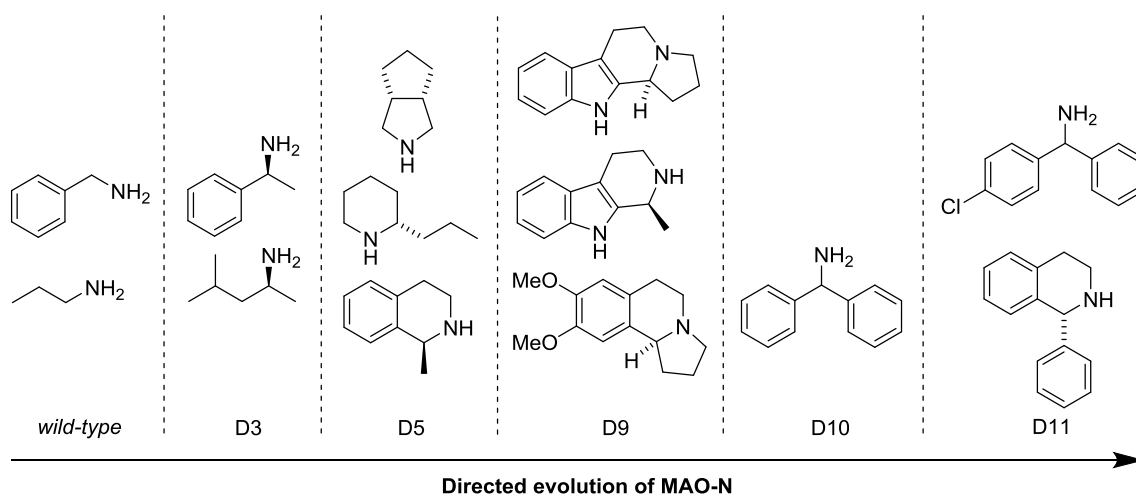


**Figure 36:** The toolbox of MAO-N variants available for activity towards a broad range of structurally-diverse amines. The enzyme has been through multiple rounds of engineering in order to tailor its function to the specific requirements of substrates and is broadly accepted as a prime demonstration of the power of directed evolution.<sup>73</sup>

MAO-N is very well-established for the chemo-enzymatic deracemisation of racemic amines, by combining the (*S*)-selective amine oxidase with ammonia-borane complex, a non-selective chemical reducing agent which is water-stable. The compatibility of the chemo-enzymatic redox deracemisation approach lies in the ability for the AO enzyme and reductant to remain inert to one another in solution. The underlying principle exploits the amine oxidase as a chiral catalyst to affect a kinetic resolution of the racemic amine, oxidising it to the corresponding imine at a faster rate than with the opposing enantiomer. The non-selective chemical reducing agent then proceeds to reduce the imine to reproduce a racemic mixture of the amine. Following subsequent cycles of the redox reaction, the unreacted enantiomer gradually accumulates in high yield and *ee*. Several syntheses to intermediates of alkaloid natural products and pharmaceuticals have been demonstrated by employing this technique, which include tetrahydro- $\beta$ -carbolines<sup>74</sup> and the intermediates to the drug solifenacin and the alkaloid product eleagnine (Figure 37).<sup>73</sup>

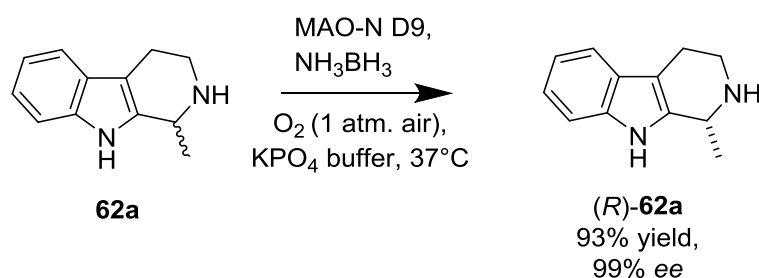


**Figure 37:** Chemo-enzymatic redox deracemisation of eleagnine **62a** employing MAO-N D9 in combination with a non-selective chemical reductant.<sup>73</sup>

The chemo-enzymatic deracemisation approach using MAO-N could also be extended to encompass desymmetrisation, for the production of optically-pure amines from their meso isomers. This process was applied to the synthesis of 3,4-disubstituted proline analogues, which are found in several protease inhibitors including Boceprevir, used in the treatment of hepatitis C (Figure 38).<sup>75</sup> Taking the symmetrical disubstituted pyrrolidine precursor, the  $\text{sp}^3$  carbon at the  $\alpha$ -position was oxidised to the imine by monoamine oxidase with high *ee*. This was followed by nucleophilic attack at the prochiral carbon, forming the diastereomeric product in 90% yield and 99% *ee*. Similarly, desymmetrisation was also applied successfully in the synthesis of a related chiral disubstituted pyrrolidine moiety found in the protease inhibitor Telaprevir.<sup>76</sup>

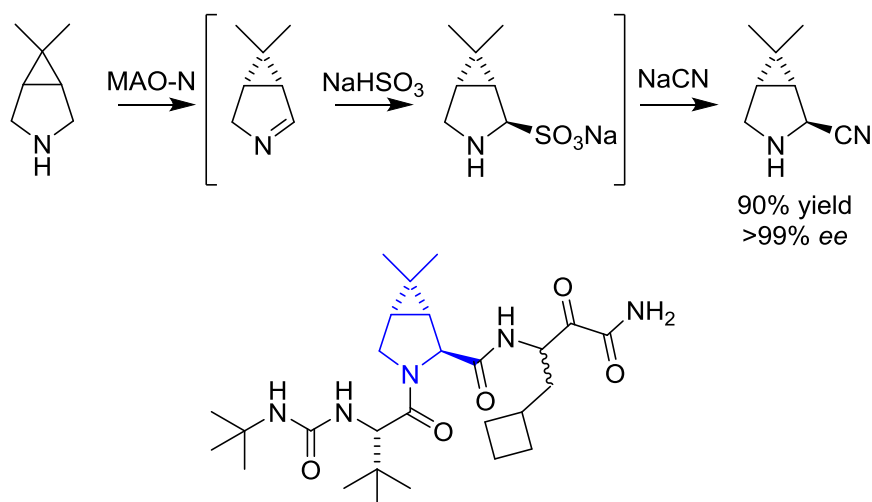


**Figure 38:** Desymmetrisation of the bicyclic disubstituted pyrrolidine employing MAO-N for enantioselective oxidation, followed by nucleophilic attack to furnish the pyrrolidine intermediate in high *ee*. The moiety, a key component of the protease inhibitor produced by Merck, is highlighted in blue within the structure of Boceprevir.<sup>75</sup>

### 1.10 Research project aims

The principle aim of this research project was to investigate novel biocatalytic routes for the production of chiral amines in single-enantiomer form. As highlighted through the introductory section, chiral amines are moieties that are prolific within natural products and pharmaceutical drugs. Biocatalytic routes have been recognised by savvy synthetic chemists as offering an alternative means to access these valuable chemicals and the uptake of enzymatic processes for the production of chemicals in industry is increasing. A number of different enzymes exist for chiral amine synthesis, providing a toolbox of biocatalysts which could be harnessed depending on the synthetic target.

Biocatalytic imine reduction, at the beginning of this research project, was underdeveloped and undervalued as a means to access chiral amines. The first aim was to characterise imine reductase enzymes in the context of biocatalysis. Although a breadth of reports on imine reductases was available, the potential of these enzymes for use as biocatalysts for the preparation of chemical products was not evaluated. Important considerations which were investigated include the substrate scope of the enzyme, the relative activity of the enzyme towards these substrates, the enantioselectivity of the reduction reactions and the general applicability of the enzyme systems to be used as catalysts in synthetic chemical processes.

In a much broader context of the research aim of this project, novel routes for the biocatalytic production of chiral amines were assessed. This was accomplished in several ways. Previously established processes for the production of amines in single-enantiomer form, such as deracemisation, were investigated and optimised to extend the scope of these techniques for accessing new motifs. Furthermore, the suitability of these processes for the production of chiral amines was investigated for the production of natural products and pharmaceutically-relevant targets. This could be accomplished through optimisation and application of existing enzyme-catalysed processes to the synthetic target or even engineering of the protein used within a specific process, in order to tailor the catalyst to be able to carry out the transformation required more efficiently.

Finally, methods for the preparation of larger quantities of chemicals via biocatalytic means were investigated. When novel enzymes are described, often they are screened against substrates in very small-scale reactions in order to characterise latent activity and substrate scope. For industrial purposes, the scalability of biocatalytic reaction processes was investigated.

## Chapter 2: Characterisation of the (*R*)-imine reductase from *Streptomyces* sp. GF3587 and comparison of the enzyme with the (*S*)-imine reductase from *Streptomyces* sp. GF3546

### 2.1. Overview

#### 2.1.1 Brief background on imine reductases as biocatalysts

Since the initial report by Mitsukura *et al.* of two *Streptomyces* strains, GF3587 and GF3546, capable of enantiocomplementary imine reduction, the proteins responsible for the observed activity have been isolated from their respective organisms and characterised. It was suggested that these enzymes could be used as biocatalysts for the production of 2-methylpyrrolidine **2a**, a chiral building block for the H<sub>3</sub> histamine receptor antagonist, ABT-239.<sup>77</sup> The (*S*)-IRED from *Streptomyces* sp. GF3546 was successfully expressed in *E. coli* and shown to be active towards further imine-containing compounds, further enhancing its potential applicability as a biocatalyst.<sup>41</sup> Work from our group expanded the substrate scope for this enzyme further, in addition to the protein showing increased activity towards known substrates versus previous reports.<sup>78</sup>

#### 2.1.2 Aims

The aim of this section of the research project was to develop a biocatalytic route to enantiomerically-pure chiral amines through the reduction of the corresponding imines. K. Mitsukura *et al.* described two enzymes from *Streptomyces*, which were shown to be enantiocomplementary in their reduction of the cyclic imine 2-methyl-1-pyrroline **1a**. As the means of accessing both enantiomers of end products remains a significant challenge in biocatalysis, the (*R*) and (*S*)-IREDs from *Streptomyces* sp. GF3587 and GF3546 offer a potential means of addressing this, so the enzymes presented ideal candidates to be characterised further through probing of their substrate scope. In particular, owing to the extremely narrow reported substrate scope of the (*R*)-IRED, this enzyme was characterised more extensively. This was to be accomplished by screening the enzymes against a panel of imines with varying structural features in order to detect novel activity. Due to the susceptibility to hydrolysis of imines in aqueous environments, the screening effort was limited to cyclic imines, which would be less labile in the buffer environment. The compounds would then be screened against the enzyme in biotransformation reactions monitored via chiral HPLC/GC.

In order to provide a feasible example of a challenging enzymatically catalysed synthetic process, a whole-cell biocatalytic system capable of reducing imines was

developed. The (*R*)-IRED protein was produced through heterologous expression of the gene in *E. coli* as previously described.<sup>78</sup> The utility of the protein as a whole-cell biocatalyst was assessed through the biotransformation reactions and the synthetic utility as a potential industrial biocatalyst was examined through the demonstration of reactions at a preparative-scale. Finally, the catalytic activity and mechanism of the (*R*)-IRED was characterised through the establishment of substrate kinetic parameters and mutagenesis of the wild-type protein.

## 2.2 Characterisation of the (*R*)-imine reductase from *Streptomyces* sp. GF3587

### 2.2.1 Previously reported substrate scope and synthesis of screening compounds

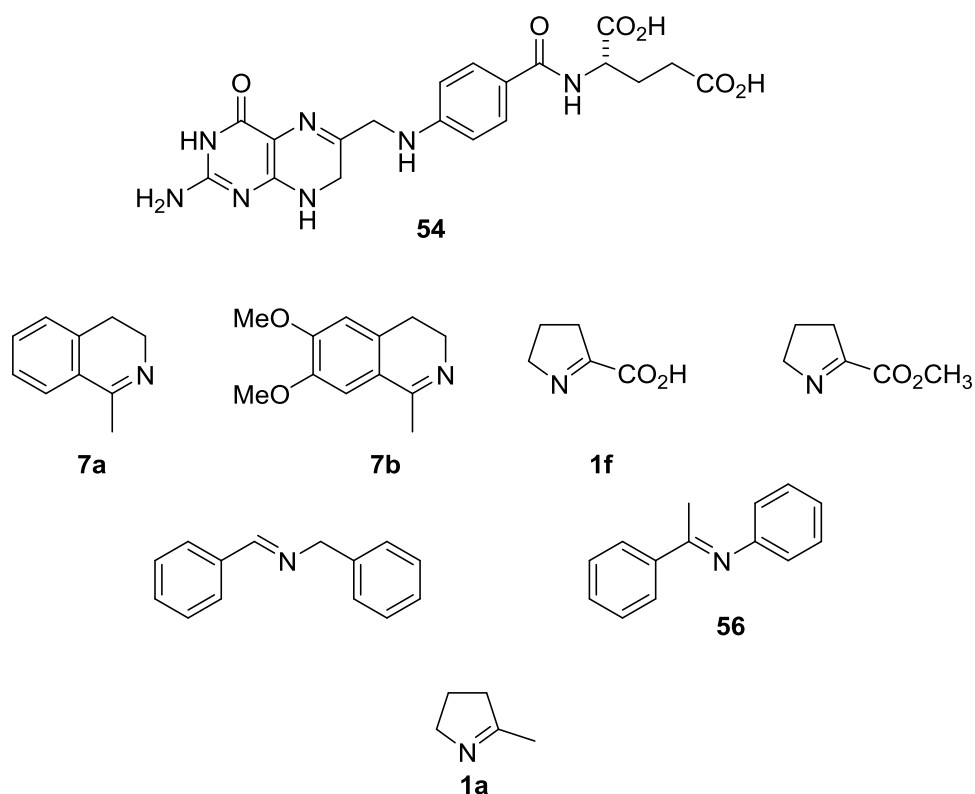


**Figure 39:** Structure of imine-containing compounds screened against the (*R*)-IRED from *Streptomyces* sp. GF3587 by Mitsukura *et al.*; only activity towards 2-methyl-1-pyrroline **1a** was detected.<sup>79</sup>

A previous report by Mitsukura and co-workers on the isolation of the (*R*)-imine reductase from *Streptomyces* sp. GF3587 described a homodimer composed of 32 kDa subunits in solution.<sup>79</sup> When the enzyme was screened against a panel of imines (Figure 39), only activity towards 2-methyl-1-pyrroline **1a** was detected and the enzyme was described to

have a very narrow substrate scope. In order to probe the substrate scope of the imine reductase further, a panel of cyclic imines was screened against the enzyme. As **1a** was a proven substrate, this motif was chosen to be explored further, as 2-substituted cyclic imines are also important scaffolds in a variety of pharmaceuticals and natural products.<sup>80,81</sup> Cyclic imines **1a** and **7a** were readily available from commercial sources (Figure 40). Dihydroisoquinolines **7b** and **7c**, as well as the corresponding tetrahydroisoquinolines **8b** and **8c** were synthesised by Dr. Diego Ghislieri in-house (Manchester, UK).

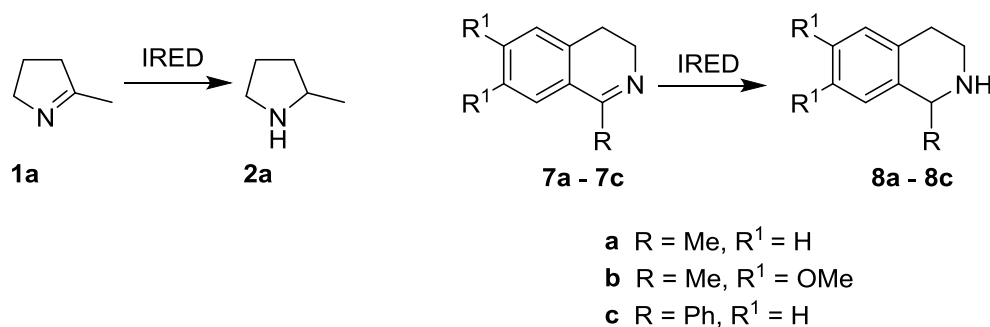


**Figure 40:** Structure of the commercially-available cyclic imines screened against the (R)-IRED. These included the mono 2-substituted cyclic pyrroline IRED substrate 2-methyl-1-pyrroline **1a** as well as substituted dihydroisoquinolines **7a – 7c**.

As the majority of the cyclic imines tested were not commercially available, they were synthesised according to an adapted version of a reported procedure.<sup>82</sup> The strategy involved Boc-protecting a lactam and then subsequently performing a Grignard reaction, leading to the formation of a Boc-protected aminoketone (Figure 41A). Following removal of the Boc-group, the aminoketone product spontaneously cyclised through a condensation reaction to yield the freebase cyclic imine product. All Grignard reagents used were commercially available and the flexible strategy allowed a panel of cyclic imines of varying ring size (by altering the starting lactam) as well as substituent (by changing the Grignard reagent used) to be quickly accessed.

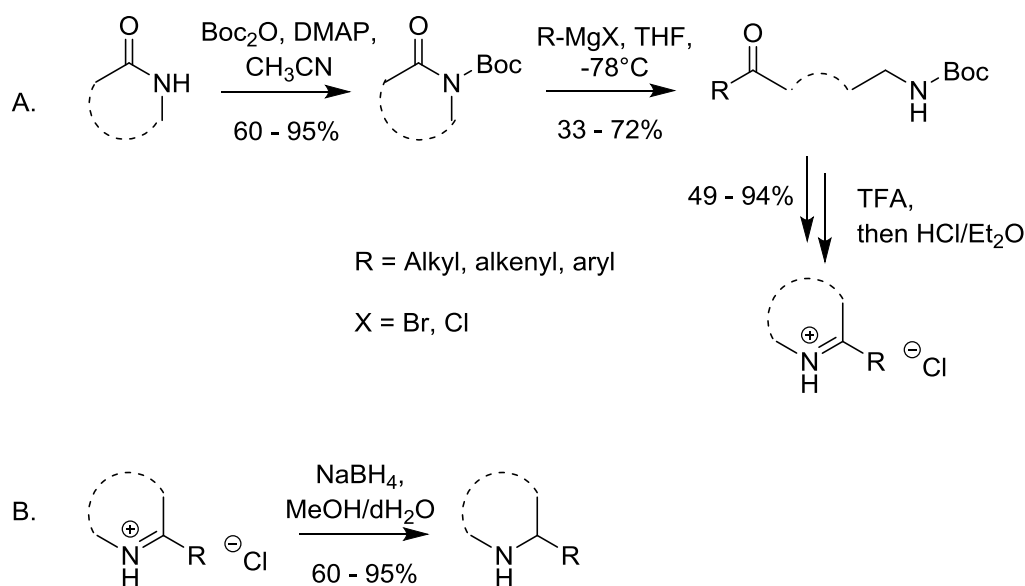


**Figure 41A:** Synthetic route followed for the synthesis of 2-substituted cyclic imines, which were isolated as their hydrochloride salts. The flexible strategy allowed a variety of imines to be accessed by altering the Grignard reagent used or the starting lactam. **41B:** Synthesis of racemic amines to be used as analytical standards by non-selective reduction of the corresponding imine hydrochloride salts.

In order to control selectivity of the Grignard reaction and also prevent double-addition to the carbonyl of the lactam leading to the corresponding Boc-protected aminoalcohol product, the temperature of the reaction was maintained at  $-78^{\circ}\text{C}$  by slow addition of the Grignard reagent. The number of equivalents of Grignard reagent to Boc-protected lactam used also played an important role, where typically 1.2 equivalents was used depending on the compound being prepared. For the synthesis of Boc-protected aminoketone **13j**, formation of the double-addition product proceeded more readily. In order to inhibit this unwanted side-reaction, only 1.1 equivalents of the Grignard reagent were used.

Despite being less thermodynamically favoured than formation of five- or six-membered rings, the seven-membered rings readily cyclised from their respective aminoketones. The substituents on the ring varied from simple alkyl groups to bulky aromatic groups (Figure 42) in order to fully explore the tolerance of the enzymes towards these different functionalities. The imines were isolated as hydrochloride salts rather than in the freebase form as the instability of the latter in long-term storage became readily apparent. The tendency to decompose was most likely due to the active lone pair on the nitrogen atom of the Schiff base. The corresponding hydrochloride salts conferred the advantage of stabilising the imines in storage and also making them easier to handle in their salt form rather than as an oily freebase imine.

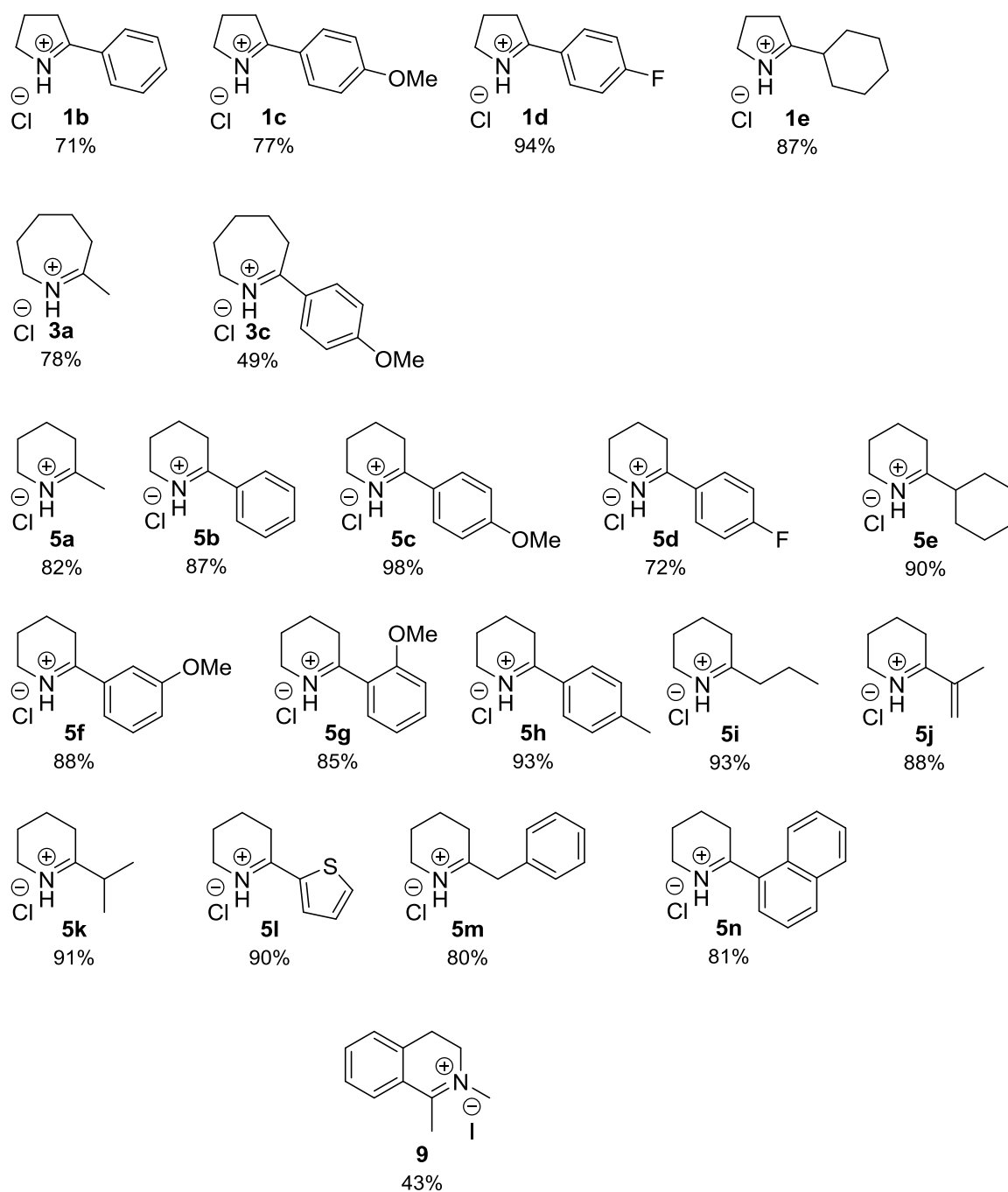


**Figure 42:** Structure of the synthesised cyclic imines screened against the (*R*)-IRED. These included mono 2-substituted cyclic imines **1**, **3**, **5** and iminium ion **9**. Yields obtained for each chemically synthesised imine are given below the structure. All imines were isolated as their hydrochloride salts for improved stability and usability of the compound. Iminium ion **9** was isolated as its iodide salt.

Analytical standards of the amine products expected following reduction of the corresponding imines were either purchased from commercial suppliers, or synthesised by effecting a simple  $\text{NaBH}_4$  reduction of the imine hydrochloride in  $\text{MeOH}/\text{dH}_2\text{O}$  (Figure 41B; for details of the chemical synthesis please refer to Experimental Section 7.3.2). The

racemic amine **4a** was isolated as its hydrochloride salt owing to the free amine's volatility (Figure 43).

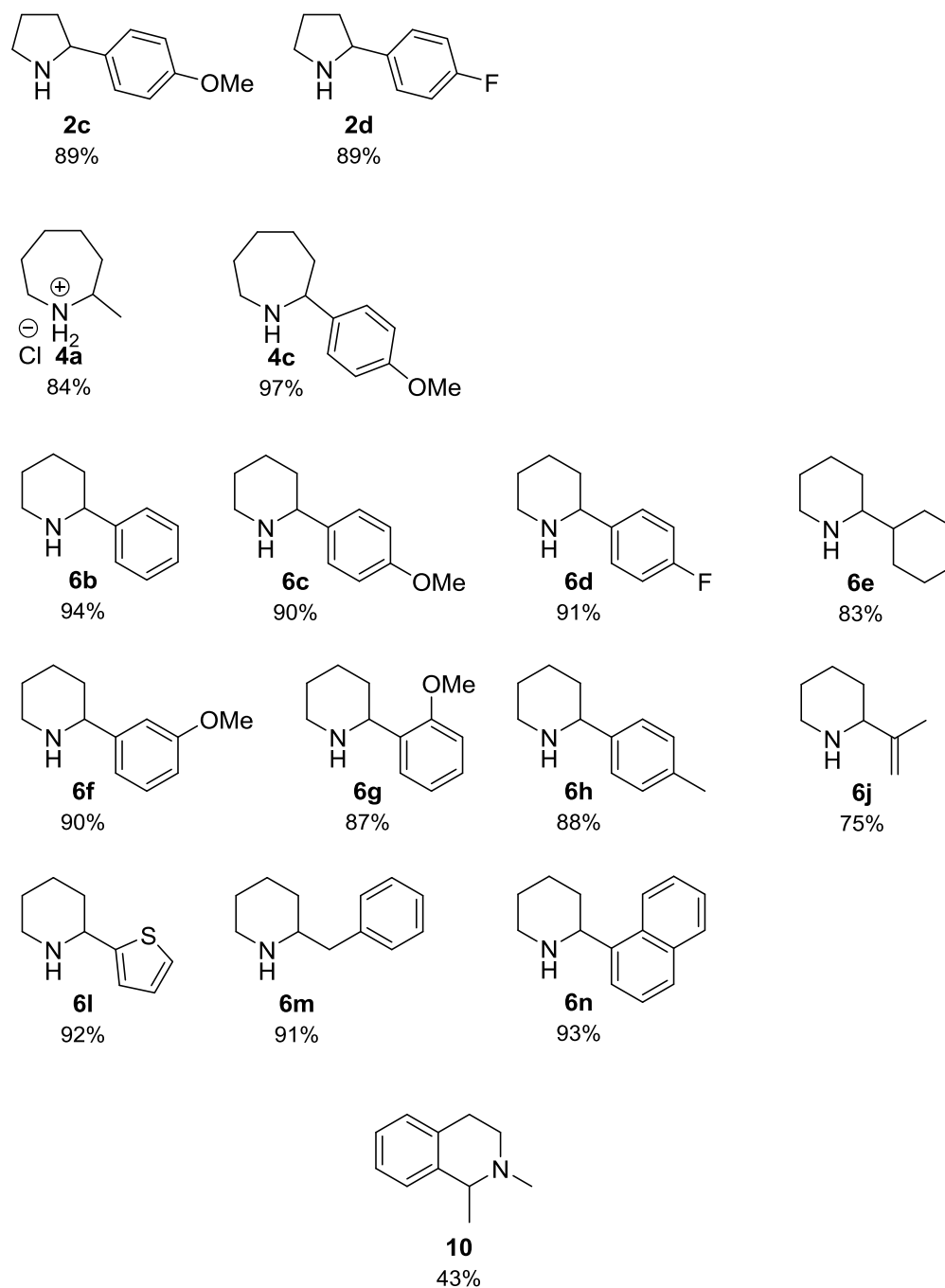


**Figure 43:** Structures of the cyclic amines which were chemically synthesised to be used as analytical standards. The yields obtained for each compound is displayed under the structure. Amine **4a** was isolated as its hydrochloride salt.

The use of IRED enzymes in whole-cell biocatalysts conferred the advantage of NADPH cofactor recycling by the endogenous proteins within the resting *E. coli* cells. Given the

potential expense and complexity of employing *in vitro* recycling systems and purified IREDs, if viable this system would also be preferred for industrial application. Previous reports analysing cofactor recycling in whole-cells have suggested that glucose-fed systems in resting *E. coli* cells can replenish NADPH-dependent proteins such as Baeyer-Villiger monooxygenases, with around 83% of the NADPH resulting from the action of isocitrate dehydrogenase in the citric acid cycle.<sup>83</sup> 50 mM glucose was therefore added to the reaction mixture to aid cofactor recycling. The biotransformations were carried out in 100 mM pH 7.0 sodium phosphate buffer at a substrate concentration of 5 mM. Cells were either resuspended to a final OD<sub>600</sub> of 30 or resuspended from pellets to a concentration of 50 mg/mL, which roughly equates to an OD<sub>600</sub> of 30. For compounds which were insoluble in aqueous medium (ie. compounds which were not hydrochloride salts), substrates were added to the reaction mixture from 250 mM stock solutions in DMSO. Biotransformations were quenched after 24 h and then extracted for analysis, as no further activity was detected after this time during preliminary investigations (see Experimental Section 7.5.1.1).

For selected substrates, biotransformations were also carried out using purified (*R*)-IRED protein (see Experimental Section 7.6 for purification procedures), in addition to either stoichiometric or lower amounts of NADPH in conjunction with a cofactor recycling system employing glucose dehydrogenase (GDH) from *Bacillus megaterium*.<sup>84</sup> In this setup, 50 mM glucose was also added to the reaction mixture in 100 mM pH 7.0 sodium phosphate buffer (Figure 44).

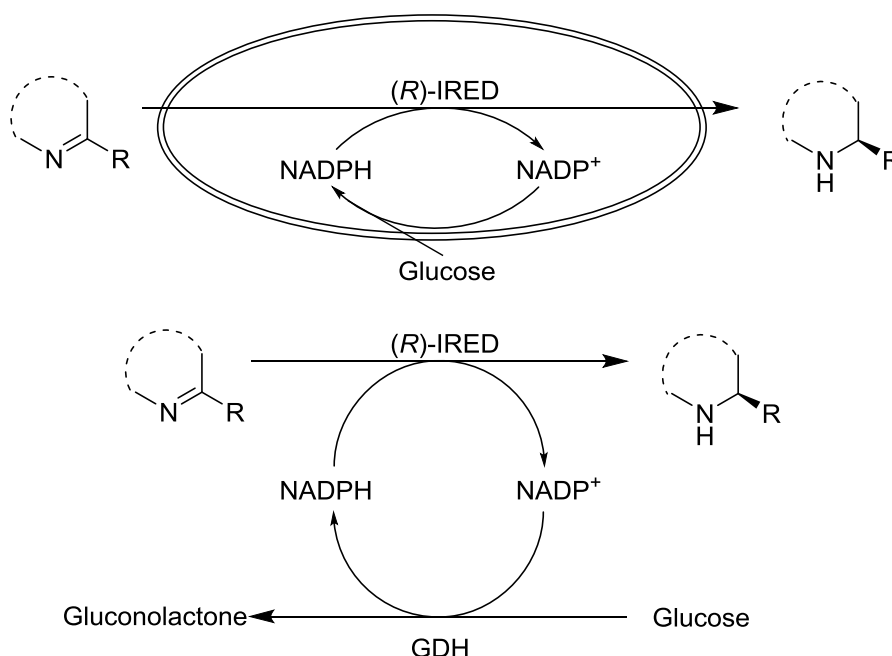
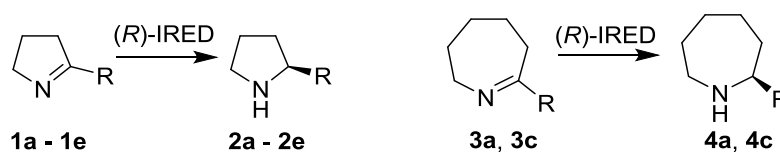


**Figure 44:** Diagrams depicting the biotransformation conditions with the (*R*)-IRED employing either a whole-cell biocatalyst (top) or using the isolated (*R*)-IRED protein in addition to a glucose dehydrogenase (GDH) cofactor recycling system (bottom).

Biotransformation reactions of the imine compounds were also run in parallel with *E. coli* cells harbouring the empty plasmid vector pET28a, in order to rule out any background activity from the endogenous proteins within the whole-cells. No conversion of the imine compounds was detected in these biotransformations.

### 2.2.2 Biotransformation results with (*R*)-IRED and characterisation of the enzyme substrate scope

**Table 1:** Biotransformation of cyclic imines **1a – 1e**, **3a** and **3c** with the (*R*)-IRED

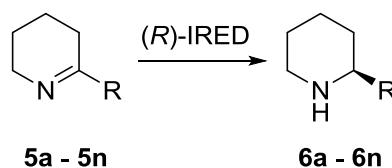


Substrate	R	Product	Conversion [%] <sup>[a]</sup>	<i>ee</i> [%] <sup>[b]</sup>	Absolute configuration
<b>1a</b>	Me	<b>2a</b>	>98	>98	( <i>R</i> ) <sup>[c, 78]</sup>
<b>1b</b>	Ph	<b>2b</b>	>98	8	( <i>S</i> ) <sup>[c, 85]</sup>
<b>1c</b>	<i>p</i> -MeOPh	<b>2c</b>	20	>98	( <i>S</i> ) <sup>[c, 85]</sup>
<b>1d</b>	<i>p</i> -FPh	<b>2d</b>	86	26	( <i>S</i> ) <sup>[c, 78]</sup>
<b>1e</b>	cyclohexyl	<b>2e</b>	>98	66	( <i>S</i> ) <sup>[c, 86]</sup>
<b>3a</b>	Me	<b>4a</b>	>98	>98	( <i>R</i> ) <sup>[c, 78]</sup>
<b>3c</b>	<i>p</i> -MeOPh	<b>4c</b>	50	>98	( <i>S</i> ) <sup>[d]</sup>

**Reaction conditions:** 5 mM substrate, 50 mg/mL (*R*)-IRED whole-cells, 50 mM glucose, 100 mM pH 7.0 sodium phosphate buffer, 30°C, 250 rpm, 24 h. [a] Conversion determined by comparison of peak areas of the starting material and product from HPLC/GC-FID analysis on a chiral stationary phase; [b] *ee* determined by comparison of peak areas of resolved enantiomers from HPLC/GC-FID analysis on a chiral stationary phase; [c] absolute configuration determined by comparison of retention times of the compound to published literature data; [d] absolute configuration determined by analogy of compound to structural homologues **3c** and **5c**

Contrary to the initial characterisation of the (*R*)-IRED by Mitsukura,<sup>79</sup> the enzyme showed a remarkable substrate scope and was tolerant of varying ring sizes and substituent groups (Table 1). A number of new substrates were confirmed beyond 2-methyl-1-pyrroline **1a**. The (*R*)-IRED was first screened against several 2-substituted pyrrolines, for which it showed a remarkable tolerance for the varying substituent groups. Methyl, phenyl and cyclohexyl-substituted pyrrolines **1a**, **1b** and **1e** were fully converted after 24 h, although enantioselectivity was lower towards the bulkier substituents. It should be noted that the apparent change in configuration of the amine products is due to changes in assignment according to Cahn-Ingold-Prelog priority rules, whereas the orientation of the bond in space remains the same. When comparing the conversions of *p*-MeOPh-substituted homologues **1c**, **3c** and **5c** (20%, 50% and >98% respectively, see Table 1 and Table 2) by the (*R*)-IRED, higher levels of activity were apparent towards the six-membered ring imine. It was for this reason that six-membered rings were explored more extensively than the five- and seven-membered counterparts, in order to fully gauge the effects of varying substituents on enzyme activity and selectivity.

**Table 2:** Biotransformation of cyclic imines **5a** – **5n** with the (*R*)-IRED

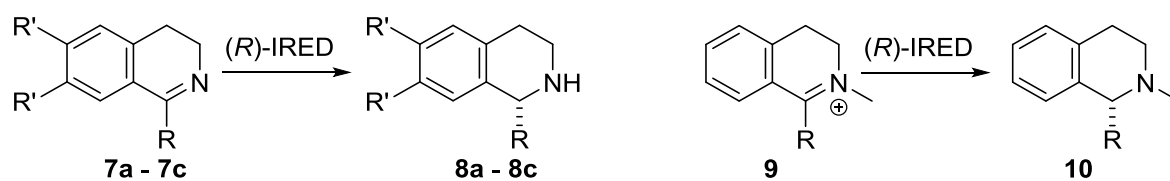


Substrate	R	Product	Conversion [%] <sup>[a]</sup>	<i>ee</i> [%] <sup>[b]</sup>	Absolute configuration <sup>[c]</sup>
<b>5a</b>	Me	<b>6a</b>	>98	>98	( <i>R</i> )
<b>5b</b>	Ph	<b>6b</b>	>98	37	( <i>S</i> )
<b>5c</b>	<i>p</i> -MeOPh	<b>6c</b>	>98	>98	( <i>S</i> )
<b>5d</b>	<i>p</i> -FPh	<b>6d</b>	>98	91	( <i>S</i> )
<b>5e</b>	cyclohexyl	<b>6e</b>	>98	66	( <i>S</i> )
<b>5f</b>	<i>m</i> -MeOPh	<b>6f</b>	>98	89	( <i>S</i> )

<b>5g</b>	<i>o</i> -MeOPh	<b>6g</b>	>98	77	(S)
<b>5h</b>	<i>p</i> -tolyl	<b>6h</b>	>98	>98	(S)
<b>5i</b>	<i>n</i> -Pr	<b>6i</b>	>98	>98	(R)
<b>5j</b>	<i>i</i> -propenyl	<b>6j</b>	>98	96	(S) <sup>[d]</sup>
<b>5k</b>	<i>i</i> -propyl	<b>6k</b>	>98	>98	(S)
<b>5l</b>	2-thienyl	<b>6l</b>	>98	78	(-) <sup>[e]</sup>
<b>5m</b>	benzyl	<b>6m</b>	54	78	(S)
<b>5n</b>	1-naphthyl	<b>6n</b>	4	27	(-) <sup>[e]</sup>

**Reaction conditions:** 5 mM substrate, 50 mg/mL (*R*)-IRED whole-cells, 50 mM glucose, 100 mM pH 7.0 sodium phosphate buffer, 30°C, 250 rpm, 24 h. [a] Conversion determined by comparison of peak areas of the starting material and product from HPLC/GC-FID analysis on a chiral stationary phase; [b] *ee* determined by comparison of peak areas of resolved enantiomers from HPLC/GC-FID analysis on a chiral stationary phase; [c] absolute configuration determined by comparison specific rotation of compound to published literature values; [d] absolute configuration determined by analogy of compound to **5k**; [e] absolute configuration undetermined

The (*R*)-IRED exhibited higher levels of catalytic activity towards six-membered rings in general, with piperidine substrates **5a** – **5l** fully converted after 24 hours. The (*R*)-IRED readily accepted a variety of substituents, with activity towards simple alkyl chains and bulkier saturated groups recorded, as along with more rigid aromatic moieties and even other heterocycles such a thiophene ring in **5l**. Surprisingly, rings bearing bulkier benzyl and 1-naphthyl groups (**5m** and **5n**) were also substrates, albeit with lower conversions. In both 5- and 6-membered rings, reduction of phenyl-substituted rings **1b** and **5b** proceeded with poor enantioselectivity (8% *ee* for **2b** and 37% *ee* for **6b**). The selectivity was greater once a substituent on the ring was introduced, giving up to ≥98 *ee*. Both electron-donating and electron-withdrawing groups on the ring were readily accepted, with no significant change in activity or selectivity for **5c**, **5d** and **5h**. Interestingly, as the position of the methoxy substituent was moved around the ring going from *p*-MeOPh **3c** through to *m*-MeOPh **3f** and *o*-MeOPh **3g**, the *ee* of the final amine product dropped significantly, signifying the increased contribution from a competing substrate binding mode.

**Table 3:** Biotransformation of bicyclic imines **7a – 7c** and bicyclic iminium ion **9** with the (*R*)-IRED

Substrate	R	R'	Product	Conversion [%] <sup>[a]</sup>	<i>ee</i> [%] <sup>[b]</sup>	Absolute configuration
<b>7a</b>	Me	H	<b>8a</b>	>98	71	( <i>R</i> ) <sup>[c]</sup>
<b>7b</b>	Me	OMe	<b>8b</b>	0	-	-
<b>7c</b>	Ph	H	<b>8c</b>	0	-	-
<b>9a</b>	Me	H	<b>10a</b>	24	74	( <i>R</i> ) <sup>[d]</sup>

**Reaction conditions:** 5 mM substrate, 50 mg/mL (*R*)-IRED whole-cells, 50 mM glucose, 100 mM pH 7.0 sodium phosphate buffer, 30°C, 250 rpm, 24 h. [a] Conversion determined by comparison of peak areas of the starting material and product from HPLC analysis on a chiral stationary phase; [b] *ee* determined by comparison of peak areas of resolved enantiomers from HPLC analysis on a chiral stationary phase; [c] absolute configuration determined by comparison of retention times of compound to published literature values; [d] absolute configuration determined by comparison specific rotation of compound to published literature values

With simple alkyl and alkenyl substituents, the (*R*)-IRED showed excellent enantioselectivity. In addition, reduction of  $\alpha,\beta$ -unsaturated imine **5j** proceeded exclusively at the carbon-nitrogen double-bond, with no reduction of the alkene bond observed, demonstrating the chemoselectivity exhibited by the (*R*)-IRED enzyme. Reduction of *n*-propyl-substituted piperidine **5i** resulted in the formation of the more active (*R*)-enantiomer (>98% *ee*) of the natural product coniine, which is found as a mixture of enantiomers in the plant genus *Conium* (poison hemlock). In addition to simple 2-substituted piperidines, 1-methyl-3,4-dihydroisoquinoline **7a** was also confirmed as a substrate for the enzyme, in contrast to previously reported findings.<sup>79</sup> No conversion was recorded with substituted isoquinolines **7b – 7c**. Significantly, the corresponding *N*-methyl iminium derivative **9** was reduced to tertiary chiral amine **10** with comparable selectivity (74% *ee*), albeit with reduced conversion, demonstrating the potential application of this biocatalyst for the synthesis of tertiary chiral amines. A selection of ketones and oximes was also screened for activity against the (*R*)-IRED, with no conversion detected (Figure 45). The absence of activity here further lends

support to the chemoselectivity of IREDs towards reduction of imines without promiscuous activity. This selectivity is useful for future applications in organic synthesis where other sensitive functionalities on a molecule must remain intact e.g. reductive amination reactions.

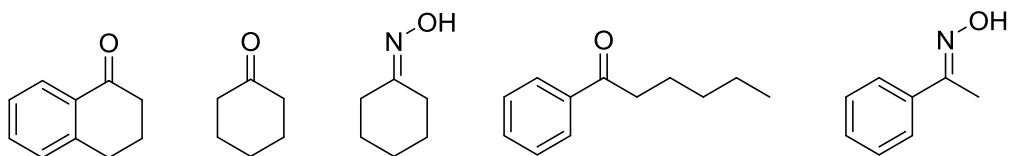


**Figure 45:** Structure of carbonyl- and oxime-containing compounds screened for activity against the (*R*)-IRED. No conversion was detected with these compounds.

To assess the suitability of the (*R*)-IRED as an industrial biocatalyst for preparative-scale synthesis of chiral amines, the reduction of **5j** was carried out on a 1.0 g scale. A series of analytical-scale biotransformations were performed in order to determine the substrate loading tolerance of the enzyme. It was found that after 24 h, reactions went to completion with a substrate concentration of up to 25 mM. Subsequently, a preparative-scale whole-cell biotransformation was conducted under the same conditions as previously described for the screening protocol, with a substrate loading of 25 mM, yielding (*R*)-coniine **6i** (90% yield, >98% *ee*) after 24 h (Figure 46). Owing to the volatility of the compound, the biotransformation product was extracted into diethyl ether and then isolated as its hydrochloride salt, which formed as needle-like crystals.

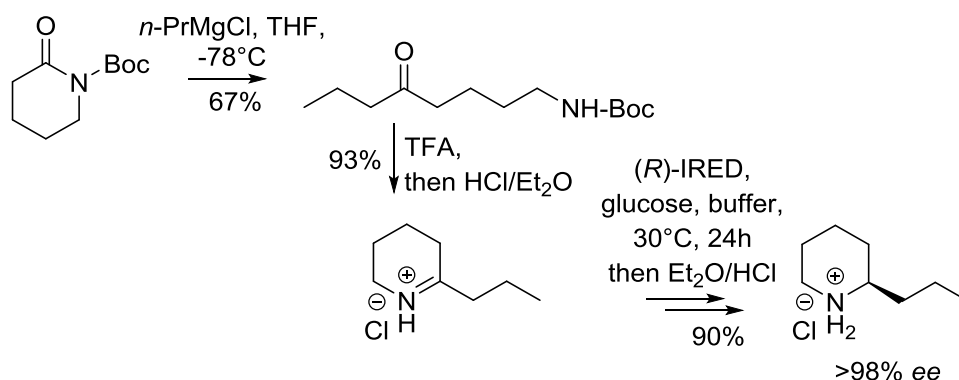
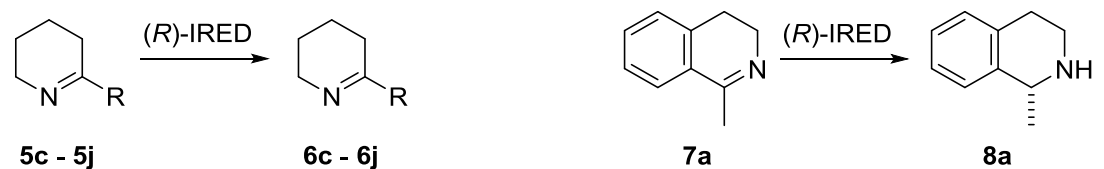


**Figure 46:** Procedure for the preparative-scale biotransformation of imine **5i**, yielding (*R*)-coniine **6i** (90% yield, >98% *ee*) after 24 h.

Biotransformations with the (*R*)-IRED were carried out using the isolated protein in addition to a GDH-based cofactor recycling system for a selection of piperidine substrates, in order

to determine if the selectivity remained consistent with whole-cell biotransformations (Table 4).

**Table 4:** Biotransformations of cyclic imines **5c – 5j** and dihydroisoquinoline **7a** with purified (*R*)-IRED enzyme



Substrate	R	Product	Conversion [%] <sup>[a]</sup>	<i>ee</i> [%] <sup>[b]</sup>	Absolute configuration
<b>5c</b>	<i>p</i> -MeOPh	<b>6c</b>	>98	>98	( <i>S</i> )
<b>5e</b>	cyclohexyl	<b>6e</b>	>98	71	( <i>S</i> )
<b>5i</b>	<i>n</i> -Pr	<b>6i</b>	>98	98	( <i>R</i> )
<b>5j</b>	<i>i</i> -propenyl	<b>6j</b>	>98	91	( <i>S</i> )
<b>7a</b>	Me	<b>8a</b>	>98	47	( <i>R</i> )

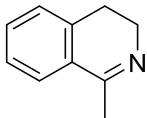
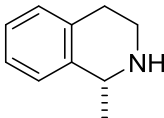
**Reaction conditions:** 5 mM substrate, 1000  $\mu\text{g/mL}$  (*R*)-IRED isolated protein, 1000  $\mu\text{g/mL}$  (GDH-II) isolated protein, NADPH (1.7  $\mu\text{L}$  from a 150 mM stock solution in  $\text{dH}_2\text{O}$ ), 50 mM glucose, 100 mM pH 7.0 sodium phosphate buffer, 30°C, 250 rpm, 24 h 5 mM substrate, 50 mg/mL (*R*)-IRED whole-cells, 50 mM glucose, 100 mM pH 7.0 sodium phosphate buffer, 30°C, 250 rpm, 24 h. [a] Conversion determined by comparison of peak areas of the starting material and product from HPLC/GC-FID analysis on a chiral stationary phase; [b] *ee* determined by comparison of peak areas of resolved enantiomers from HPLC/GC-FID analysis on a chiral stationary phase

In general, the selectivity observed in the isolated protein biotransformations showed only nominal variation compared to the selectivity of whole-cell biotransformations, with the exception of dihydroisoquinoline **7a** which showed a significantly lower *ee* of the amine product **8a** (47% *ee*, versus 74% in whole-cells). In contrast, the biotransformation of cyclohexyl-substituted **5e** showed a slight increase in *ee* of the amine product.

In order to determine if the *ee* of the amine product varied as a function of time, and hence establish whether the reduction reaction is under kinetic or thermodynamic control, a time-point assay for the reduction of 1-methyl-3,4-dihydroisoquinoline **7a** was

conducted with (*R*)-IRED whole-cells (see Experimental Section 7.5.1 for details). The results of the experiment showed that the *ee* value of the product amine **8a** remained constant throughout the reaction (Table 5), therefore indicative of a reaction under kinetic control.

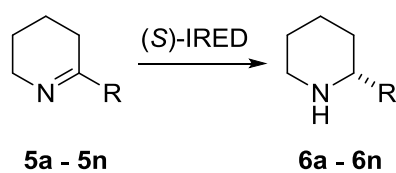
**Table 5:** Time-point assay biotransformations of 1-methyl-3,4-dihydroisoquinoline **7a** with whole-cell (*R*)-IRED

Substrate	Product	Time [h]	Conversion [%] <sup>[a]</sup>	<i>ee</i> [%] <sup>[b]</sup>
		1	17	69
		2	36	69
		3	53	70
		4	69	69
		5	81	70
		6	92	69
		24	>98	69

**Reaction conditions:** 5 mM substrate, 5 mg/mL (*R*)-IRED whole-cells, 50 mM glucose, 100 mM pH 7.0 sodium phosphate buffer, 30°C, 250. [a] Conversion determined by comparison of peak areas of the starting material and product from HPLC analysis on a chiral stationary phase; [b] *ee* determined by comparison of peak areas of resolved enantiomers from HPLC/GC-FID analysis on a chiral stationary phase

### 2.2.3 Comparison of (*R*)-IRED substrate scope with (*S*)-IRED

The (*S*)-IRED was also screened against the panel of 2-substituted piperideines in order to examine the enzyme's tolerance towards various functionalities on the imine substrate. The biotransformations substituting the (*S*)-IRED were conducted in parallel with the (*R*)-IRED reactions to offer a more direct comparison of the results (Table 6 and Table 7).

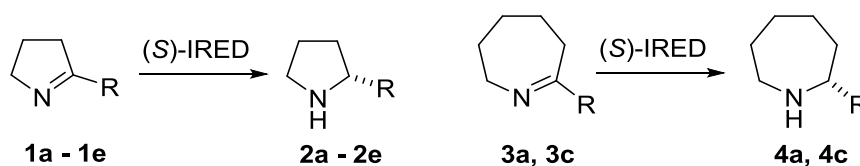
**Table 6:** Biotransformation of cyclic imines **5a** – **5n** with the (*S*)-IRED

Substrate	R	Product	Conversion [%]	<i>ee</i> [%]	Absolute configuration
<b>5a</b>	Me	<b>6a</b>	>98	>98	( <i>S</i> )
<b>5b</b>	Ph	<b>6b</b>	45	93	( <i>R</i> )
<b>5c</b>	<i>p</i> -MeOPh	<b>6c</b>	33	>98	( <i>R</i> )
<b>5d</b>	<i>p</i> -FPh	<b>6d</b>	>98	97	( <i>R</i> )
<b>5e</b>	cyclohexyl	<b>6e</b>	23	60	( <i>S</i> )
<b>5f</b>	<i>m</i> -MeOPh	<b>6f</b>	>98	97	( <i>R</i> )
<b>5g</b>	<i>o</i> -MeOPh	<b>6g</b>	14	94	( <i>R</i> )
<b>5h</b>	<i>p</i> -tolyl	<b>6h</b>	60	>98	( <i>R</i> )
<b>5i</b>	<i>n</i> -Pr	<b>6i</b>	58	51	( <i>S</i> )
<b>5j</b>	<i>i</i> -propenyl	<b>6j</b>	79	>98	( <i>R</i> )
<b>5k</b>	<i>i</i> -propyl	<b>6k</b>	-	0	(-)
<b>5l</b>	2-thienyl	<b>6l</b>	82	78	(-)
<b>5m</b>	benzyl	<b>6m</b>	27	37	( <i>S</i> )
<b>5n</b>	1-naphthyl	<b>6n</b>	1	77	(-)

**Reaction conditions:** 5 mM substrate, 50 mg/mL (*S*)-IRED whole-cells, 50 mM glucose, 100 mM pH 7.0 sodium phosphate buffer, 30°C, 250 rpm, 24. [a] Conversion determined by comparison of peak areas of the starting material and product from HPLC/GC-FID analysis on a chiral stationary phase; [b] *ee* determined by comparison of peak areas of resolved enantiomers from HPLC/GC-FID analysis on a chiral stationary phase; [c] absolute configuration determined by comparison of results to biotransformation results with (*R*)-IRED

In comparison with the (*R*)-IRED, the (*S*)-IRED showed a lower level of activity towards the piperidine imines as lower levels of conversion were recorded overall. A preference for six-membered rings versus five- and seven-membered rings was observed, which emulates the preference seen with the (*R*)-IRED.<sup>78</sup> However, the enantioselectivity in the reduction of 2-substituted cyclic imines with the (*S*)-IRED was notably higher, with generally greater *ee* values for the corresponding amines. Mirroring the results obtained with the (*R*)-IRED, the configuration of the amine products furnished appeared to reverse from (*S*) to (*R*), once again due to changes in formal assignment according to Cahn-Ingold-Prelog priority rules. Unusually, biotransformations of **5e** and **5m** furnished amines of the same configuration as the (*R*)-IRED products, indicating a switch in enantioselectivity of the (*S*)-IRED with these substrates. It is clear that with the (*S*)-IRED more subtle binding interactions are involved during the reduction of the substrate in the active site, which can lead to opposing facial selectivity for hydride delivery. Interestingly, a significantly lower conversion was recorded for *para*-methoxyphenyl-1-piperidine **5c** compared to *meta*-methoxyphenyl-1-piperidine **5f** (33% versus >98% conversion) and a sharp reduction in conversion with *ortho*-methoxyphenylpiperidine **5g** (14% conversion). The positioning of the substituent on the ring in this instance leads to a more profound change in activity than was observed with the (*R*)-IRED.

Consistent with the results obtained with the 2-substituted piperidines, the (*S*)-IRED displayed lower conversions albeit with greater enantioselectivity than the (*R*)-IRED with pyrroline substrates **1a** – **1e** and azepine substrates **3a** and **3c** (of which **1a** had been previously described<sup>41</sup>). As for its six-membered ring analogue, cyclohexyl-substituted pyrroline **1e** was converted to the (*S*)-enantiomer product, thereby illustrating the unusual case of hydride delivery to the opposing face of the prochiral imine substrate.

**Table 7:** Biotransformation of cyclic imines **1a – 1e**, **3a** and **3c** with the (*S*)-IRED

Substrate	R	Product	Conversion [%]	<i>ee</i> [%]	Absolute configuration
<b>1a</b>	Me	<b>2a</b>	57	>94	( <i>S</i> )
<b>1b</b>	Ph	<b>2b</b>	36	87	( <i>R</i> )
<b>1c</b>	<i>p</i> -MeOPh	<b>2c</b>	17	>98	( <i>R</i> )
<b>1d</b>	<i>p</i> -FPh	<b>2d</b>	42	>98	( <i>R</i> )
<b>1e</b>	cyclohexyl	<b>2e</b>	12	64	( <i>S</i> )
<b>3a</b>	Me	<b>4a</b>	>98	>98	( <i>S</i> )
<b>3c</b>	<i>p</i> -MeOPh	<b>4c</b>	20	>98	( <i>R</i> )

**Reaction conditions:** 5 mM substrate, 50 mg/mL (*S*)-IRED whole-cells, 50 mM glucose, 100 mM pH 7.0 sodium phosphate buffer, 30°C, 250 rpm, 24. [a] Conversion determined by comparison of peak areas of the starting material and product from HPLC/GC-FID analysis on a chiral stationary phase; [b] *ee* determined by comparison of peak areas of resolved enantiomers from HPLC/GC-FID analysis on a chiral stationary phase; [c] absolute configuration determined by comparison of results to biotransformation results with (*R*)-IRED

#### 2.2.4 Establishing substrate-enzyme kinetic parameters

Kinetic parameters were determined for a panel of representative substrates using the isolated (*R*)-IRED protein Table 8, see Experimental Section 7.8 for details concerning the determination of these kinetic constants). The previously reported substrate 2-methyl-1-pyrroline **1a** had a notably lower  $k_{cat}/K_M$  value than several piperidine substrates tested. In particular, a >fifty-fold increase in  $k_{cat}/K_M$  for 2-methyl-1-piperidine **5a** over **1a** was observed. In common with the (*S*)-IRED was a preference for six- and seven-membered ring systems over five-membered rings. The enzyme also displayed greater affinity towards simple alkyl- and alkenyl-substituted imines rather than those bearing aromatic moieties.

**Table 8:** Kinetic constants obtained for a selection of imine substrates with the isolated (*R*)-IRED enzyme

Entry	R	V <sub>max</sub>	k <sub>cat</sub> [s <sup>-1</sup> ]	K <sub>M</sub> [mM]	k <sub>cat</sub> /K <sub>M</sub> [s <sup>-1</sup> mM <sup>-1</sup> ]
<b>1a</b>	Me	0.633	0.351	1.88	0.187
<b>3a</b>	Me	6.56	3.64	5.11	0.712
<b>5a</b>	Me	8.14	4.52	0.437	10.3
<b>5c</b>	<i>p</i> -MeOPh	0.474	0.263	1.05	0.250
<b>5e</b>	cyclohexyl	0.0343	0.0242	0.810	0.0235
<b>5i</b>	<i>n</i> -propyl	3.59	1.99	0.154	13.0
<b>5j</b>	<i>i</i> -propenyl	2.54	1.41	0.686	2.06
<b>5l</b>	2-thienyl	1.03	0.570	0.189	3.01
<b>7a</b>		0.340	0.189	0.155	1.22

Kinetic constants with the previously reported (*S*)-IRED from *Streptomyces* sp. GF3546 have been described with substrates **1a**, **3a**, **5a** and **7** (*i.e.* k<sub>cat</sub> = 0.024 s<sup>-1</sup>, 0.039 s<sup>-1</sup>, 0.137 s<sup>-1</sup> and 0.040 s<sup>-1</sup> respectively).<sup>78</sup> Significantly higher k<sub>cat</sub> values and lower K<sub>M</sub> were observed with the (*R*)-IRED, with 2-methyl-1-piperidine **5a** showing a 30-fold increase in reaction turnover rate when compared to the reduction of **5a** by the (*S*)-IRED. These results demonstrate the (*R*)-IRED as the more active enzyme of the two. However, when the activity of the (*R*)-IRED towards substrate **1a** was compared with previously reported IREDs by Scheller *et al.*, both the (*R*)-IRED from *Streptosporangium roseum* DSM 43021 and the (*R*)-IRED from *Streptomyces turgidiscabies* displayed higher turnover rates of 0.961 s<sup>-1</sup> and 0.446 s<sup>-1</sup> respectively, though the two (*R*)-selective enzymes exhibited significantly lower k<sub>cat</sub>/K<sub>M</sub>.<sup>47</sup>

## 2.2.5 Enzyme mechanistic study – mutagenesis of the (*R*)-imine reductase

The enzyme mechanism for IRED-mediated reduction remains unknown. Grogan and co-workers recently described an oxidoreductase from *Streptomyces kanamyceticus*, which was found to catalyse the asymmetric reduction of 2-methyl-1-pyrroline **1a** to give (*R*)-2-methylpyrrolidine **2a** in >99% *ee*.<sup>44</sup> The enzyme was characterised and crystal structures were acquired for the protein in both apo form and with the cofactor NADPH bound. The structure was said to be related to those known of  $\beta$ -hydroxyacid dehydrogenases, in particular HIBDH/2CVZ, which catalyses the reduction of isobutyrate. Superimposition of their structures revealed that a key catalytic lysine residue in 2CVZ (Lys165) is replaced by an aspartate residue (Asp187) in Q1EQE0. The residue in 2CVZ acts as a proton donor to the forming hydroxyl group in the ketone reduction step. It was thought that Asp187 functioned similarly in Q1EQE0, donating a proton to the imine nitrogen. Based on this, mechanism for the imine reduction step was proposed (Figure 47).

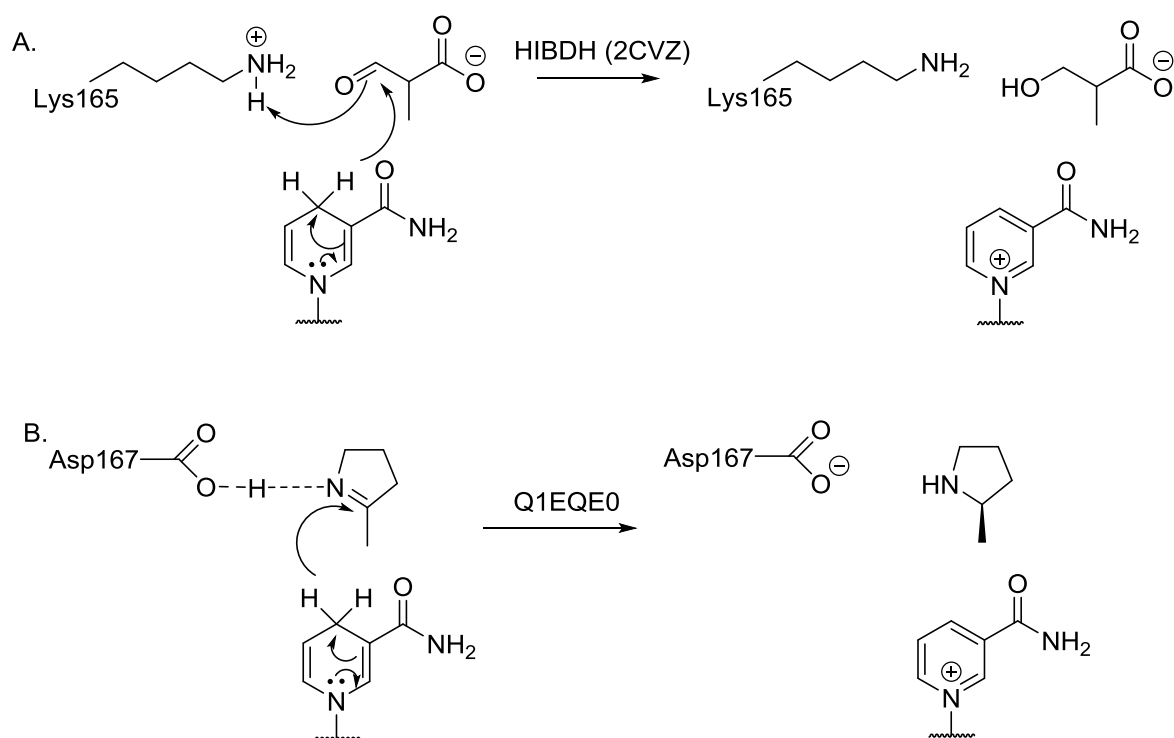


**Figure 47:** Mechanism for NADPH-mediated reduction in  $\beta$ -hydroxyacid dehydrogenase HIBDH/2CVZ, in which a lysine residue protonates the nascent alcohol during the hydride reduction step (A) and then the proposed mechanism for IRED-mediated imine reduction in Q1EQE0 (B), where an aspartate residue protonates the nascent amine in a similar fashion.

Two other protic residues within a 9Å sphere from the nicotinamide ring were identified as potentially having a role in the catalytic mechanism, Ser111 and Thr254 from subunit B. The imine reductase Q1EQE0 was found to share 50% sequence identity with the (*R*)-IRED from

*Streptomyces sp.* GF3587 with a further 19% strongly similar residues. In particular, the catalytic Asp167 residue is conserved in the *Streptomyces (R)*-IRED as Asp172 and most residues around the active site were conserved between the two proteins. Using the structural data obtained for Q1EQE0, a homology model of the (*R*)-IRED was constructed (Figure 48A).

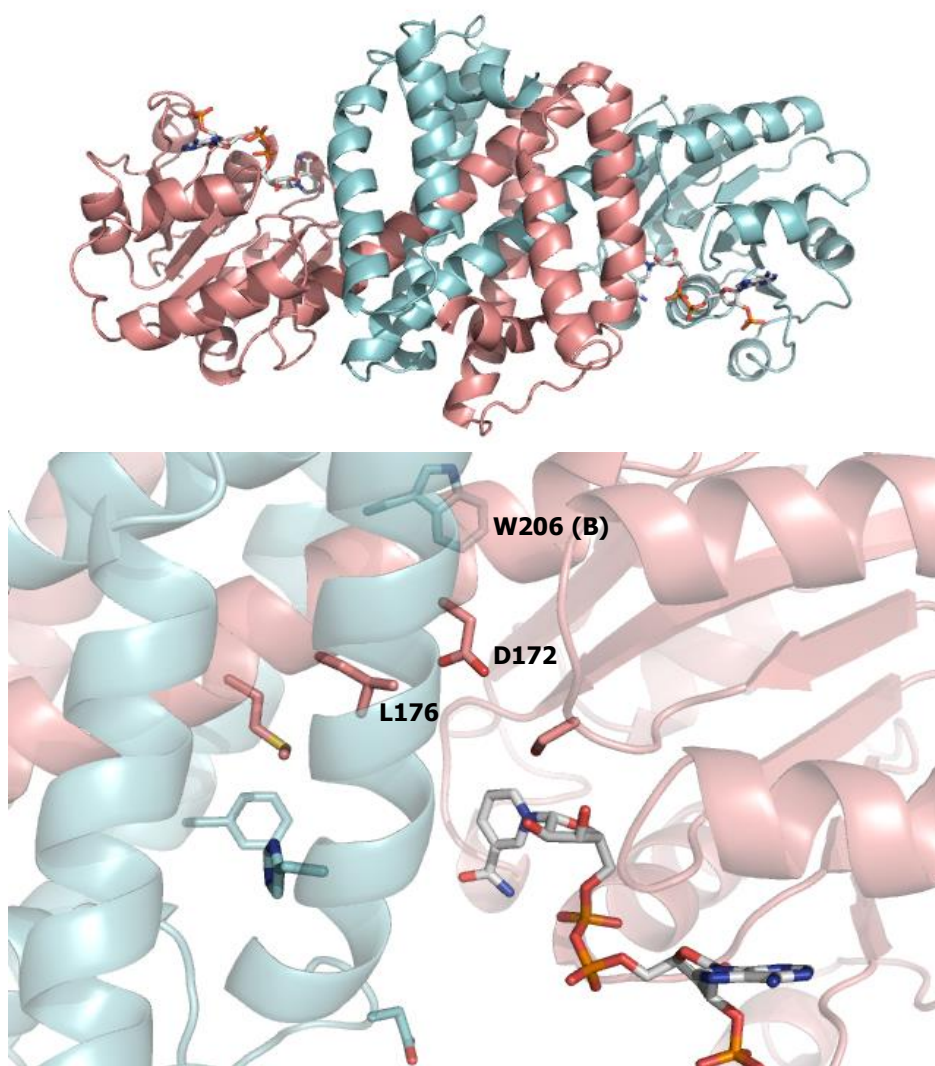


**Figure 48A:** Homology model of the (*R*)-IRED, based on the known structure of *SKRIR* Q1EQE0 from *Streptomyces kanamyceticus*, shown in cartoon format with cofactor NADPH bound (carbon atoms are in grey). Subunit A is displayed in salmon, subunit B in cyan. **48B:** Detail of the active site of the (*R*)-IRED, shown with NADPH bound and the C4 atom labelled from which hydride attack occurs and with conserved residues from Q1EQE0 labelled, except Trp206 (Phe in Q1EQE0) and Phe217 (Trp 232 in Q1EQE0). As the two subunits in the (*R*)-IRED participate in domain sharing, residues which originate from subunit B are labelled as such. Asp172 (Asp 187 in Q1EQE0) was selected for mutation studies as it was suggested to be a catalytic residue in the *SKRIR*.

Similar to the active site of Q1EQE0, the active site cavity is large in the (*R*)-IRED homology model. Protic residues Ser111 and Thr254 from Q1EQE0, which could be important in the catalytic mechanism of the enzyme, are also conserved in the (*R*)-IRED as Ser96 and Thr224 respectively. The active site cavity contains a large hydrophobic tunnel, lined by Met122, Leu176 and Met179, which would clearly be able to accommodate the substituent side chains of the 2-substituted cyclic imines (Figure 48B). The large active site of the protein may explain the impressive substrate scope demonstrated by the wild-type enzyme.

When Asp187 was mutated to Ala187 in Q1EQE0, imine reductase activity was nullified, which lent support to the role of Asp187 as a catalytic residue. In order to investigate this further and determine if the conserved residue Asp172 functioned similarly in the (*R*)-IRED, two variants of the wild-type (*R*)-IRED protein were generated, where the proton-donating aspartic acid was mutated to either Ala [(*R*)-IRED D172A] or Leu [(*R*)-IRED D172L]. It was hoped that if indeed Asp172 was a catalytic residue, the protein would be rendered inactive towards imine reduction. Mutagenesis of the protein was achieved through the use of the QuikChange® site-directed mutagenesis protocol (see Experimental Section 7.9.1 for details of the synthetic primers used to carry out the mutagenesis). The genes for the variants were then expressed in *E. coli* BL21 following the same procedures as for the wild-type protein and the mutant proteins were subsequently isolated from the whole-cells. Biotransformations were run using the two variants in parallel with the wild-type (*R*)-IRED against a selection of representative substrates, using the GDH-II cofactor recycling system (Table 9).

Interestingly, rather than rendering the protein inactive, the variants not only retained imine reducing activity but the observed selectivity of the reactions changed. In particular, variant D172A showed a significant drop in *ee* with substrate **5c** whereas both variants displayed an improvement in product *ee* upon reduction of 1-methyl-3,4-dihydroisoquinoline **7a** versus the wild-type protein. These results indicate that although the residue may not be fundamental for catalysis, it may represent a hotspot for mutagenesis in order to further engineer the enzyme for improved selectivity and/or activity in the future. Similar results were reported by P. Scheller *et al.*, where mutation of the conserved Asp residue in (*R*)-IRED-*Sr* and (*R*)-IRED-*St* resulted in significant decreases in conversion rates rather than complete inactivation of the enzymes for imine reduction, thereby implying the presence of other proton-donating residues in the active site involved in catalysis or even water acting as a proton donor.<sup>47</sup>

**Table 9:** Results for the biotransformation of a representative selection of cyclic imines by wild-type (*R*)-IRED and variants (*R*)-IRED D172A and (*R*)-IRED D172L

Substrate	<i>(R)</i> -IRED <i>wt</i>		<i>(R)</i> -IRED D172A		<i>(R)</i> -IRED D172L	
	Conversion [%]	<i>ee</i> [%]	Conversion [%]	<i>ee</i> [%]	Conversion [%]	<i>ee</i> [%]
<b>1a</b>	>98	98	96	97	98	93
<b>5a</b>	>98	>98	>98	98	>98	>98
<b>5c</b>	92	>98	40	2	72	80
<b>5i</b>	>98	98	98	93	92	93
<b>7a</b>	97	47	41	81	41	68
<b>9</b>	96	76	97	35	97	54

**Reaction conditions:** 5 mM substrate, 1000  $\mu\text{g/mL}$  (*R*)-IRED *wt*/D172A/D172L isolated protein, 1000  $\mu\text{g/mL}$  (GDH-II) isolated protein, NADPH (1.7  $\mu\text{L}$  from a 150 mM stock solution in  $\text{dH}_2\text{O}$ ), 50 mM glucose, 100 mM pH 7.0 sodium phosphate buffer, 30°C, 250 rpm, 24 h

The results signify that the catalytic mechanism of the enzymes may not be as simple as that observed in  $\beta$ -hydroxyacid dehydrogenases, as even in the absence of a proton-donating residue such as Asp172, the proton is available from elsewhere within the active site. The mechanism of IRED reduction was recently explored further by H. Man *et al.*, where the role of Asp187 in Q1EQE0 was compared with the role of Asp in dihydrofolate reductase (DHFR).<sup>87</sup> Asp 187 is located 7.9 Å from the C-4 atom of NADPH in Q1EQE0, which is similar to the equivalent distance in DHFR. The role of the Asp residue in DHFR is as part of a network of hydrogen bonds through to the substrate that assists proton donation from a water molecule to the imine during the reduction step, rather than direct proton transfer from the Asp itself. This differs for (*S*)-selective IREDs, where the distance between the proposed catalytic residue Tyr188 in the *Bacillus cereus* BAG3X2-2 IRED (*Bc*IRED) and the C-4 atom of NADPH is 5.0 Å. In this case, the Tyr residue is proposed to directly protonate the imine during the reduction step. However, there have been hints at domain movements between the apo-protein structure and upon binding of NADPH in the *Bc*IRED, which may also be responsible for observed IRED stereoselectivity in addition to the environment created by the amino acid residues around the active site.

### 2.3 Conclusions and outlook

The purpose of this section was to establish a robust approach for biocatalytic imine reduction using whole-cell imine reductase biocatalysts, in order to access secondary and potentially tertiary chiral amines. The (*R*)-IRED and (*S*)-IRED from *Streptomyces* sp. GF3587 and sp. GF3546 respectively were selected to be developed as enantiocomplementary biocatalysts based on previous reports. In particular, the substrate scope for the (*R*)-IRED was poorly understood despite the enzyme showing fairly high levels of catalytic activity towards 2-methyl-1-pyrroline **1a** in comparison with the (*S*)-IRED. Heterologous expression of the gene for the (*R*)-IRED was achieved for the first time in *E. coli* BL21 (DE3) cells, producing whole-cell biocatalysts which were then applied to a panel of mono-2-substituted cyclic imines in a series of biotransformation reactions. Parallel biotransformations of the panel of cyclic imines were carried out with the (*R*)-IRED and (*S*)-IRED. The results indicated that the wild-type proteins possessed a surprisingly broad substrate scope and were tolerant of cyclic imines of varying ring size as well as substituents at the C-2 position (Figure 49).

The (*R*)-IRED showed higher levels of catalytic activity in general, giving higher conversions (often >98% after 24 hours) and higher substrate turnover rates when kinetic parameters were established. Conversely, the (*S*)-IRED showed greater selectivity in its reductions by providing access to amines in higher *ee*. In the majority of cases, the enzymes were enantiocomplementary, except in the case of amines **2e**, **6e** and **6m** for the (*S*)-IRED. Although both enzymes were able to tolerate ring-size variation, the IREDs showed a preference for six-membered rings over five- and seven-membered rings. Contrary to previous reports, the (*R*)-IRED was capable of reducing dihydroisoquinoline **7a** with  $\geq 98\%$  conversion as well as the corresponding *N*-methyl iminium ion **9**, an example which demonstrates the potential use of the enzyme for the synthesis of tertiary amines (Figure 49).

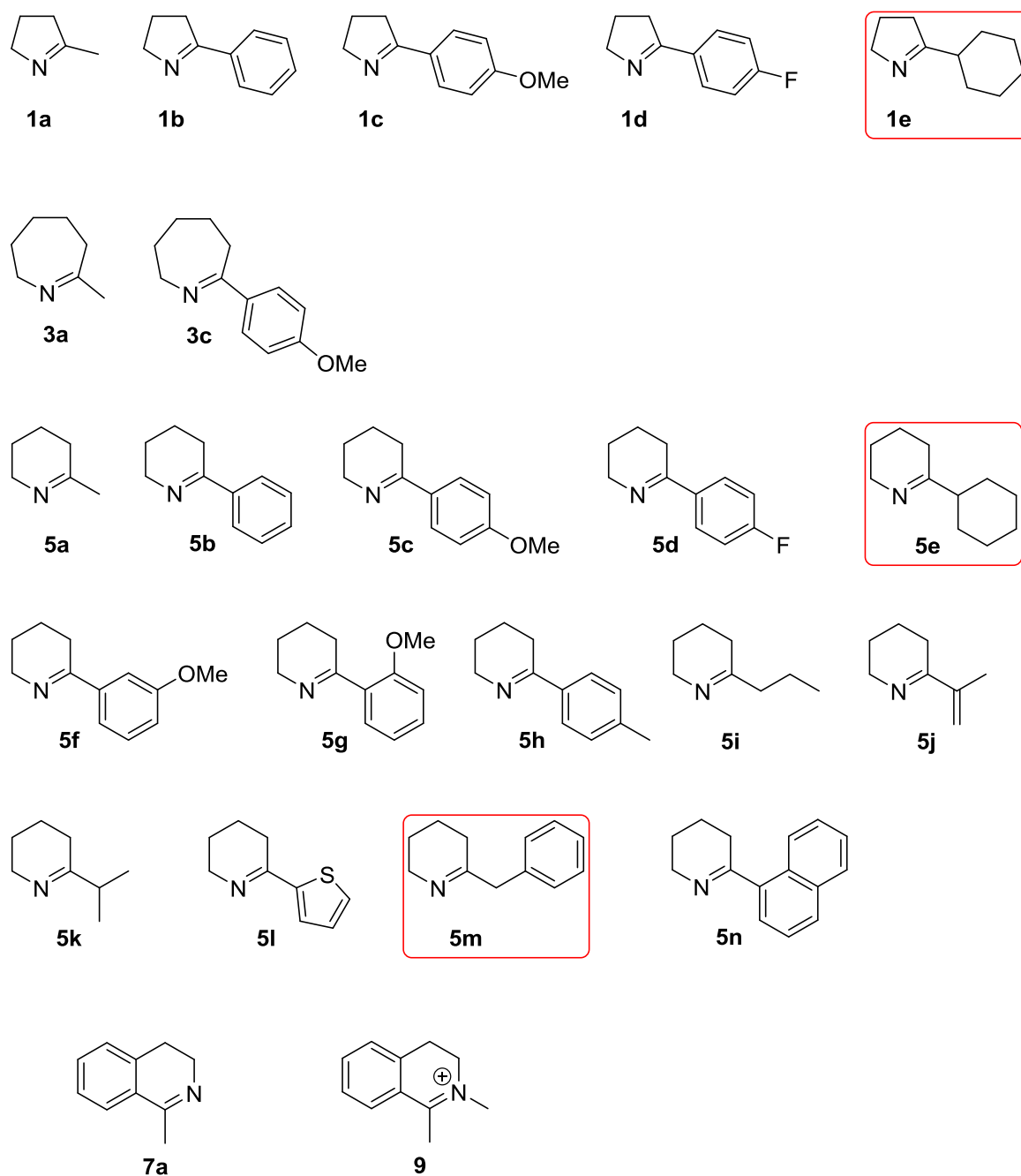


**Figure 49:** Structures of the 2-substituted cyclic imines and bicyclic imine **7a**, which were screened against the (*R*)-IRED and (*S*)-IRED and found to be substrates for both enzymes. The IREDs provided access to opposing enantiomer amine products upon bioreduction of these compounds. Structures in the red boxes indicate imines which were reduced to predominantly the same enantiomer by both enzymes. Iminium ion **9** was screened against the (*R*)-IRED only.

For the purpose of assessing the (*R*)-IRED whole-cell biocatalyst for industrial synthetic applications, the biotransformation of imine **5i** was conducted with the (*R*)-IRED whole-cells on a gram scale, yielding the enantiopure alkaloid (*R*)-coniine **6i** (90%, *ee* >98%) and complementing the reported prep-scale biotransformation of dihydroisoquinoline **7a** by the (*S*)-IRED (87%, *ee* 98%, Figure 50).<sup>78</sup>

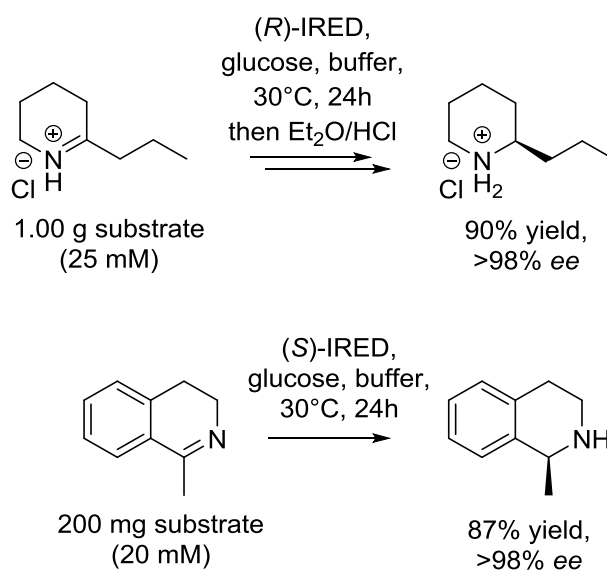


**Figure 50:** Comparison of preparative scale biotransformations accomplished with the IREDs. The (*R*)-IRED was used to produce the alkaloid (*R*)-coniine **6i** in 90% yield, >98% ee on a gram-scale, whereas the (*S*)-IRED has previously been shown to produce (*S*)-1-methyl-3,4-tetrahydroisoquinoline **8a** in 87% yield, >98% ee on a 200 mg-scale.<sup>78</sup>

A homology model of the (*R*)-IRED was constructed based on the known structure of a related (*R*)-selective imine reductase (Q1EQE0), where the residue Asp172 was postulated to be a catalytic residue. Experimental mutation of this residue produced variants which retained imine reductase activity yet possessed different enantioselectivity versus the wild-type protein.

The wild-type IRED proteins possess a surprisingly broad substrate scope whilst remaining selective for the reduction of imine functionalities. Further work could involve screening the enzymes against a more structurally diverse range of imines, for example tetrahydroquinolines, benzylic imines or even acyclic imines if the compounds were stable in buffer/the organic solvent intolerance of the imine reductases could be overcome. In particular, considering the chemoselectivity demonstrated by the IREDs, it would be interesting to explore the reduction of compounds with other functionalities present, which could then be exploited as building blocks by applying further chemistry following reduction and setting of the stereogenic centre by IREDs. Examples include a ketone in a conjugated system such as in 2-acetyl-1-piperidine, the principle component of the flavour of bread.

As only one example of the reduction of iminium ions was explored, it would be interesting to investigate this further in order to demonstrate the applicability of IRED biocatalysts in the synthesis of tertiary chiral amines. Undoubtedly, further IREDs will be described in quick succession, owing to the sheer attention garnered by this class of enzyme already in addition to the work which is being carried out in order to streamline approaches in the discovery of new IRED sequences. This has indeed been the case since the body of

work described in this chapter was completed and a number of IRED enzymes have appeared in the literature. One new IRED from *Amycolatopsis orientalis* ( *AoIRED*) from the Turner group is described as a (formally) (*S*)-selective IRED, based on the reduction of 2-methylpyrroline **1a**. The enzyme displays more activity towards **1a** than the (*S*)-IRED, with a  $k_{\text{cat}}/K_{\text{M}}$  value of  $0.17 \text{ s}^{-1} \text{ mM}^{-1}$ , thereby surpassing the (*S*)-IRED as a more catalytically active IRED in the same selectivity class. Interestingly, while the (*R*)- and (*S*)-IREDs have both been shown to (broadly) follow the same selectivity pattern when effecting their reductions of prochiral cyclic imines, this does not appear to be the case for the  *AoIRED*. Very subtle changes to the structure of a substrate (such as replacement of the OMe group in **5c** with an F atom in **5d**) lead to a complete reversal of stereoselectivity exhibited by the enzyme. In this case, the selectivity pattern is difficult to visualise for the IRED and each new substrate needed to be investigated on a case-by-case basis. Nevertheless, some of the cyclic imine substrates screened against the enzyme were loosely arranged into two groups to categorise the stereoselectivity of the enzyme towards the compounds [i.e. compounds with the imine bond on the right of the molecule (group A) and compounds with the imine bond on the left of the molecule (group B), as shown in Figure 51].

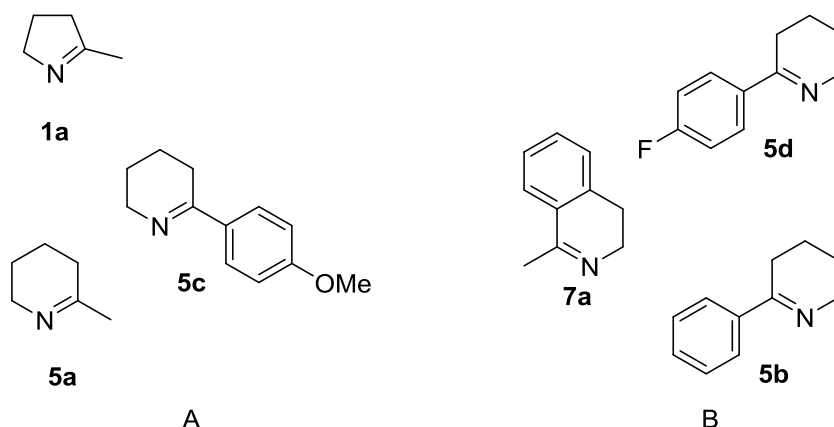


**Figure 51:** Two groups of prochiral imines reduced by the  *AoIRED* which are representative of the stereochemical outcomes from the bioreduction reaction. For both group, the incoming hydride from NADPH is delivered to the top face of the imines (from the front of the page).

Fascinatingly, the  *AoIRED* also exhibited a switch in stereoselectivity towards the same substrate (MDQ **7a**) based on the length of time the purified protein has been in storage. Whole-cell  *AoIRED* enzyme as well as freshly purified stocks of the protein yielded (*S*)-**8a**, whereas older purified enzyme stocks produced (*R*)-**8a** following biotransformation. The mechanism for this phenomenon remains poorly understood, but suggestions include conformational changes in the enzyme resulting in altered stereospecificity or even the presence of multiple binding sites. What this case highlights is the complex nature of IRED

enzymes, whose mechanism is not very well understood. However, it seems that we have only begun to scratch the surface with regards to the potential for this class of enzyme. As the number of reported and characterised IREDs increases, more enzymes may be found which possess different substrate scopes, activity and stability profiles. Very recently, an IRED from *Paenibacillus elgii* has been described as the most thermo stable IRED to date, with half-life of >400 h at T = 50°C.<sup>88</sup> Furthermore, two IREDs were reported to be much more efficient in catalysing reductive amination reactions than any previously reported IRED enzyme, which were used to produce the two enantiomers of the amine API rasagiline, which is used to treat Parkinson's (Figure 52).<sup>89</sup> This reactivity profile differs to that of the (*R*)- and (*S*)-IREDs, which are unable to carry out reductive amination reactions to such success. Although large equivalents of the amine and IRED were used to carry out these transformations, it is clear that the class of enzymes holds the potential to carry out reductive amination reactions effectively.

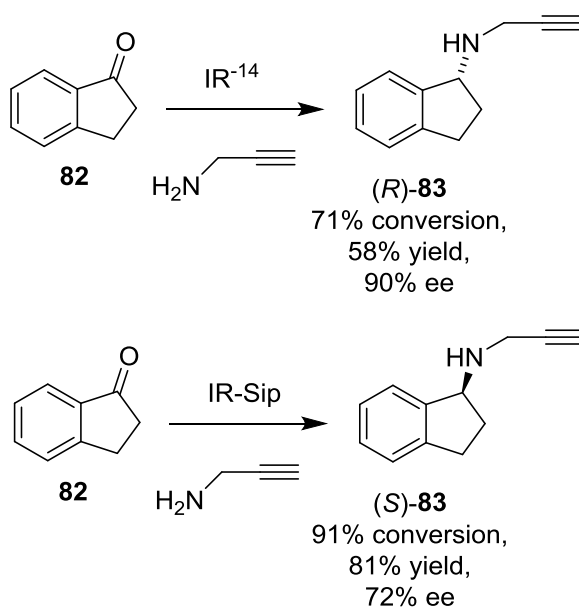


**Figure 52:** Conversion of indanone **82** to (*R*)-rasagiline (*R*-**83**) and (*S*)-rasagiline (*S*-**83**) using two new IREDs via reductive amination reactions.<sup>89</sup>

The chemoselectivity of the known imine reductases for the reduction of imine double-bonds lends itself well to combining the enzymes with other biocatalysts, to enable new multi-step enzymatic cascades, which will be explored in the next chapter.

### Chapter 3: One-pot enzymatic cascade reactions combining imine reductase (IRED) with amine transaminase (ATA) and carboxylic acid reductase (CAR) enzymes

#### 3.1 Overview of enzymatic cascade reactions

##### 3.1.1 Existing strategies for enzymatic cascade reactions

Taking inspiration from nature, where complex catabolic and metabolic pathways in living organisms operate as multi-step cascade reactions within the one-pot environment of cells, interest in multi-enzyme biocatalytic reactions is increasing. Owing to the orthogonality of enzyme reactions, multi-step reaction sequences can be built up by combining different enzymes to carry out single functional group modifications in sequence, in order to construct compounds of increasing complexity from simple starting materials. A recent review discusses the advantages of using such systems, as well as current developments in this field, which typically includes reduced reaction times, costs and waste as well as avoiding isolation of toxic or reactive intermediates.<sup>90</sup>

Recent examples of multi-enzyme cascade reactions include work by Bornscheuer *et al.*, who developed an enzymatic "redox toolbox" featuring an *in-vivo* multi-enzyme cascade in a single cell system for the synthesis of lactones (Figure 53).<sup>91</sup> A simple allylic alcohol was oxidised to the corresponding  $\alpha,\beta$ -unsaturated ketone by an alcohol dehydrogenase (ADH), which was then (stereo)selectively reduced by an enoate reductase (ERED), followed by a final oxidation step using a Baeyer-Villiger monoxygenase (BVMO) to produce a chiral lactone. The enzymes were selected such that the first two reactions were "redox self-sufficient," as the ADH and ERED utilised the oxidised and reduced forms of the cofactor NADPH respectively in a single cycle, whereas the final oxidation by the BVMO consumed another equivalent of NADPH which was not regenerated in the reaction sequence.

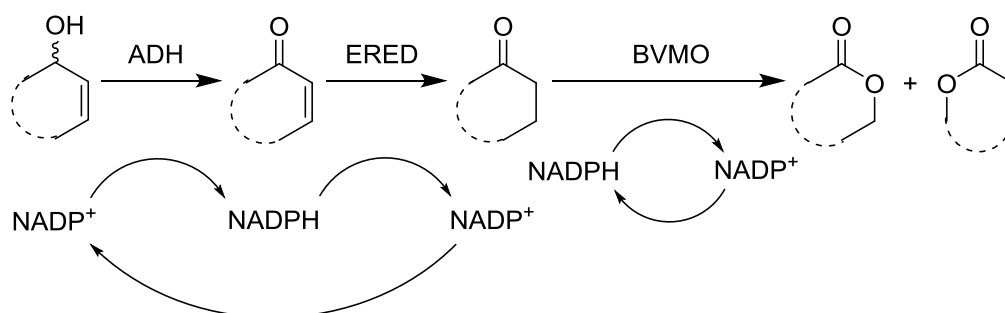


**Figure 53:** *In-vivo* multi-enzyme reaction cascade for the synthesis of chiral lactones from simple allylic alcohol starting materials, which includes a redox self-sufficient step with the cofactor NADPH regenerated in its oxidised form after the second reaction step. The enzymes employed in the report

were *Lactobacillus kefir* ADH (Lk-ADH), an ERED from *Pseudomonas* sp. (XenB) and finally the cyclohexanone monooxygenases from *Acinetobacter* sp. (CHMO<sub>Acineto</sub>).<sup>91</sup>

Subsequently, Bornscheuer and co-workers showed that it was possible to combine ERED enzymes with ATAs to enable a biocatalytic reaction cascade for the synthesis of 1-amino-3-methyl-cyclohexanes, starting from the corresponding 3-methylcyclohex-2-enone (Figure 54).<sup>92</sup> Two out of the four possible diastereomers of the product were accessed through this cascade, which employed an (*S*)-selective ERED for stereoselective reduction of the double bond in combination with an (*R*)- and an (*S*)-selective ATA. In order to access the two remaining diastereomers of the product, an ERED of opposing (*R*)-selectivity was required, though this reaction was not described in the report.

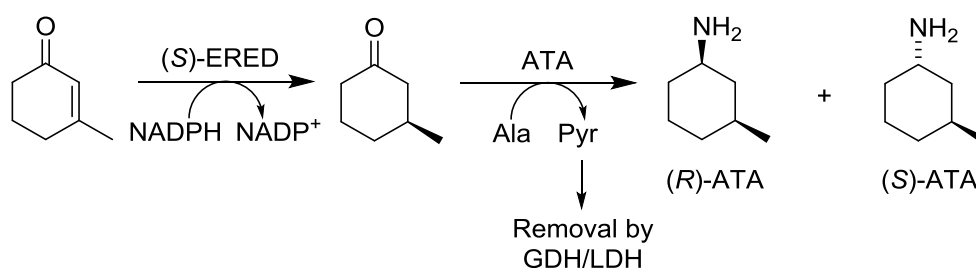


**Figure 54:** Two-step biocatalytic cascade employing an (*S*)-ERED with (*R*)- and (*S*)-selective ATA enzymes for the synthesis of 1-amino-3-methylcyclohexane. A GDH/LDH enzyme cascade was used to shift the transaminase biotransformation equilibrium towards product formation by removal of pyruvate from the reaction. The GDH also regenerated the NADPH cofactor used in the ERED reduction step.<sup>92</sup>

Turner *et al.* have successfully combined  $\omega$ -TA enzymes with an engineered variant of monoamine oxidase (MAO-N) from *Aspergillus niger* to create a one-pot cascade for the synthesis of enantio-enriched 2,5-disubstituted pyrrolidines (Figure 55).<sup>93</sup> A commercially-available (*S*)-selective ATA was used to regio- and enantioselectively transaminate the less-hindered carbonyl of a diketone substrate, producing a chiral disubstituted imine following a subsequent condensation/cyclisation reaction. This imine was then reduced using the non-selective chemical reducing agent ammonia-borane ( $\text{NH}_3\text{BH}_3$ ) which, in combination with the (*S*)-selective MAON D9 in the same pot, carried out a deracemisation cycle that enabled gradual accumulation of a single diastereomer of the amine product. This strategy was successfully employed to access disubstituted pyrrolidines in excellent enantioselectivity (>94% *ee*) and diastereoselectivity (>98% *de*).

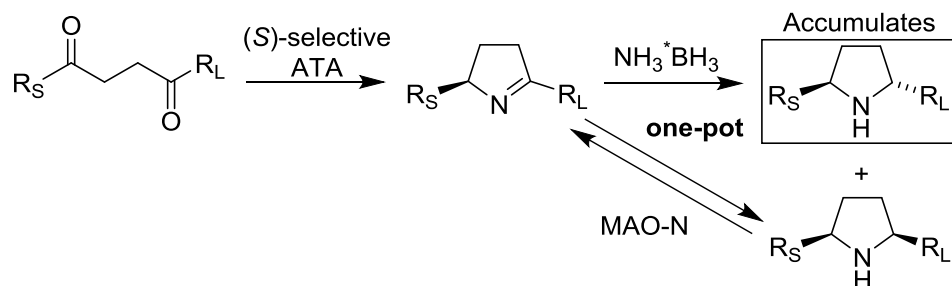


**Figure 55:** Chemoenzymatic cascade for the synthesis of chiral 2,5-disubstituted pyrrolidines, employing an (*S*)-selective  $\omega$ -transaminase and an (*S*)-selective amine oxidase in combination with a non-selective chemical reducing agent in a one-pot two-step reaction. The ATA regioselectively aminates the less sterically-hindered ketone adjacent to  $R_S$  in the first step and then subsequent redox cycles of the product chiral imine leads to a gradual accumulation of a single diastereomer of the pyrrolidine.<sup>93</sup>

Flitsch and co-workers recently reported the stereoselective benzylic amination of ethylbenzene derivatives using a three-step multi-enzyme cascade in a single whole-cell system (Figure 56). The cascade features four enzymes: a P450 monooxygenase (Y96F) which inserts molecular oxygen into the ethylbenzene substrate, followed by oxidation of the alcohol to the corresponding ketone by two enantiocomplementary ADHs and finally enantioselective amination of the ketone to afford (*R*)- $\alpha$ -methylbenzylamine derivative product by an (*R*)-selective ATA.

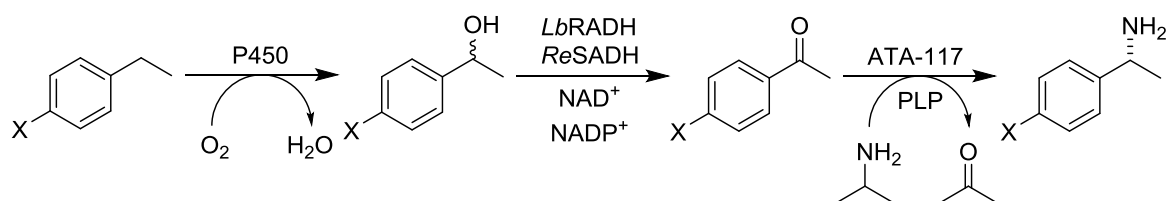


**Figure 56:** Enzyme cascade for the direct C-H amination of ethylbenzene and derivatives in a single-cell system. The sequence employed a chimeric self-sufficient P450 monooxygenase (Y96F), two enantiocomplementary ADHs (*Lb*RADH and *Re*SADH) and an (*R*)-selective  $\omega$ -TA (ATA-117).

The utility of these multi-enzyme reaction cascades is that more complex structural motifs (with one or more stereogenic centres) are accessed by transformation of simple starting materials, harnessing the enzymes' inherent enantioselectivity to set the stereogenic centres. These reactions are often difficult to accomplish chemically in a single pot due to the strict chemoselectivity required of the catalysts used for each transformation, as well as variations in reaction conditions used by each catalyst. Biocatalysts tend to operate under similar physiological conditions, enabling design of modular enzymatic reaction systems to provide access to a breadth of new chemical scaffolds.

### 3.1.2 Aims

The aim of this section of the project was to combine multiple enzymes to create reaction cascades for the synthesis of chiral amines. IREDs have already been shown to effectively reduce cyclic imine substrates asymmetrically, furnishing the amine products often in high *ee* and setting the stereogenic centre adjacent to the nitrogen atom of the molecule.

Previous work by Kroutil *et al.* exploited ATAs in the synthesis of disubstituted cyclic imines.<sup>94</sup> The ATAs catalysed the regioselective and enantioselective amination of the less-hindered ketone position of structurally-related 1,5-diketone substrates, leading to a spontaneous cyclisation of the aminoketone product and producing the disubstituted chiral imine following a spontaneous condensation reaction. This study builds on the biocatalytic approach to generate chiral imines by combining and treating the imine product with IREDs, which could reduce the chiral disubstituted imine in order to affect diastereoselective reduction, setting the second stereogenic centre of the molecule, to afford chiral disubstituted piperidine products. In a similar fashion, chiral disubstituted pyrrolidines could be accessed from the corresponding 1,4-diketones.

The ATAs employed in this cascade were commercially available from Codexis as cell lysates: the (*S*)-selective ATA-113 and the enantiocomplementary (*R*)-selective ATA-117. ATA-113 has been previously shown to regioselectively and enantioselectively aminate 1,4-diketones to produce chiral disubstituted pyrrolines in excellent *ee*.<sup>93</sup> Utilising ATAs of complementary selectivity allowed for the preparation of opposing enantiomers of the chiral cyclic imines in single enantiomer form. As the 2,6-disubstituted piperideines and 2,5-disubstituted pyrrolines would possess a pre-existing chiral centre, the effect of this chirality on the stereoselectivity of the IRED-mediated reduction reactions was examined. Chiral 2,6- and 2,5-disubstituted piperideines and pyrrolines treated with a non-selective chemical reducing agent (*e.g.* NaBH<sub>4</sub>) were reduced diastereoselectively to produce the amine products predominantly in the *syn* conformation. Based on the previously obtained results of the reduction of mono-substituted cyclic imines with the enantiocomplementary (*R*)- and (*S*)-IREDs, it was envisioned that the IRED's inherent stereoselectivity would override the stereochemical bias in the reduction reactions. This would grant access to the *anti*-disubstituted piperidines and pyrrolidines and hence all four possible diastereomers of the product amines (Figure 57).

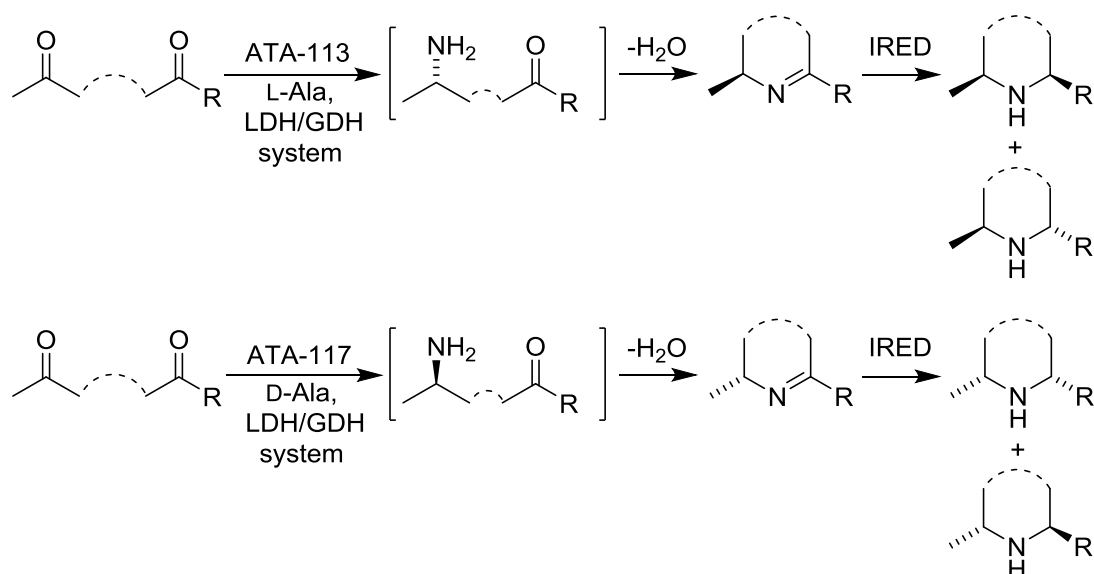


**Figure 57:** Envisaged reaction scheme for the enzyme cascade for the synthesis of 2,6-disubstituted piperidines and 2,5-disubstituted pyrrolidines. The enzyme cascade employs commercially-available ATAs ATA-113 and ATA-117, for the synthesis of chiral disubstituted imines from achiral diketones following a spontaneous cyclisation of the resulting aminoketone. IREDs could be employed to reduce the chiral imines to their corresponding amines, in order to gain access to all four diastereomer products. A pyruvate removal system of GDH and LDH is used to shift the transaminase equilibrium towards product amine formation (refer to Figure 26).

The ATA/IRED cascade was also extended to include carboxylic acid reductase (CAR) in the transformation sequence, which is able to catalyse the chemoselective reduction of the carboxylic acid functional group to the corresponding aldehyde. It was envisaged that starting from simple ketoacid compounds, CAR could be used to reduce the acid functionality to the aldehyde in the first stage of the reaction. The intermediate ketoaldehyde could then be intercepted by the ATA enzyme, which would preferentially aminate the less-hindered aldehyde carbonyl group, leading to a spontaneous cyclisation/intramolecular condensation of the aminoketone to produce a cyclic imine product. An IRED could then take this imine as a substrate and reduce the double-bond (setting the stereogenic centre) to furnish a chiral amine final product (Figure 58).

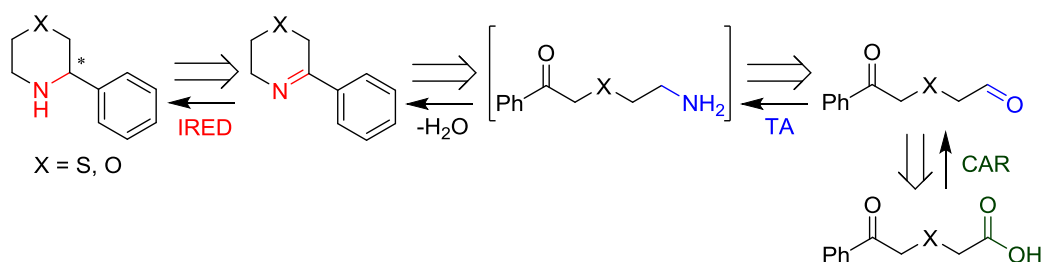


**Figure 58:** Synthetic scheme illustrating the multi-enzyme cascade for the synthesis of chiral 2-substituted morpholines and thiomorpholines via a three-enzyme reaction sequence harnessing CAR, TA and IRED enzymes. The biocatalytic retrosynthesis for the pathway is also displayed.

Building on the success of the cascade in the synthesis of several 2-substituted cyclic amines,<sup>95</sup> the multi-enzyme sequence was applied to the preparation of chiral cyclic imines possessing additional heteroatoms within their architecture, namely morpholines and thiomorpholines.

### 3.2 $\omega$ -transaminase/imine reductase cascade (ATA/IRED cascade)

#### 3.2.1 Principle and synthesis of screening compounds

1,5-diketones **11a** – **11d**, required for the preparation of chiral disubstituted piperideines **12a** – **12d**, were synthesised chemically using a literature method.<sup>94</sup> The flexible strategy allowed efficient access to diketones with varying substituents. The substituents chosen were based on diversifying the functionalities present as well as accommodating the requirement of the ATA to be able to differentiate between the two ketone groups present in the substrate. Bulkier substituents, such as rigid aromatic groups, were suitable in this respect. The four diketones **11a** – **11d** were synthesised through the addition of a Grignard reagent to a commercially-available lactone (Figure 59).

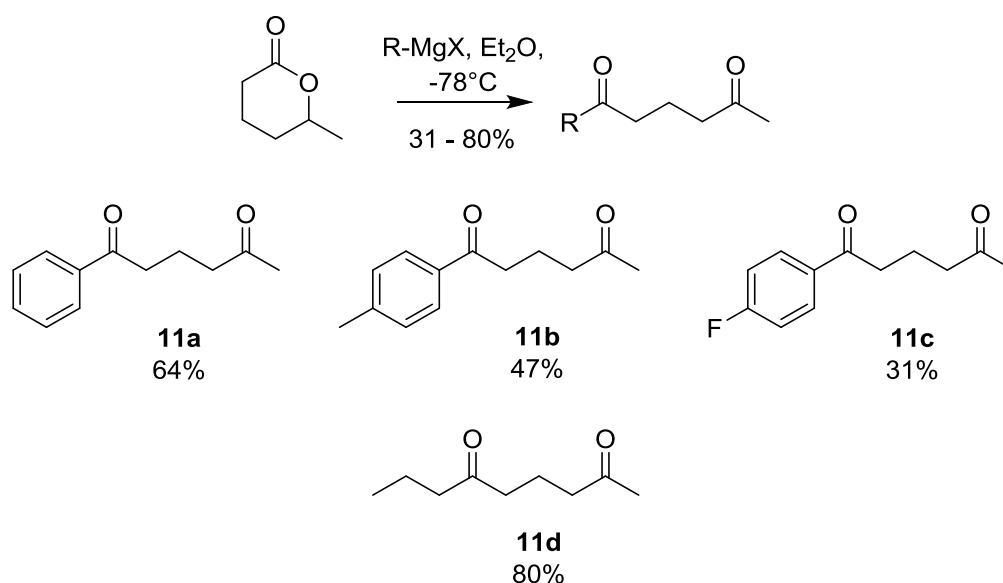


**Figure 59:** Reaction scheme for the synthesis of 1,5-diketones **11a** – **11d** from a commercially-available lactone. The yield obtained for each diketone is displayed under its structure.

Isopropyl-bearing diketone **11e** was synthesised through an alternative route, which has also been reported in the literature (Figure 60).<sup>94</sup> This route was devised as the Grignard addition of <sup>i</sup>PrMgCl or an alternative Grignard reagent to the starting lactone was reported to be extremely inefficient. The route employs a Krapcho decarboxylation reaction in the final step, where an  $S_N2$  reaction occurs at the carbon atom with chloride acting as a nucleophile.

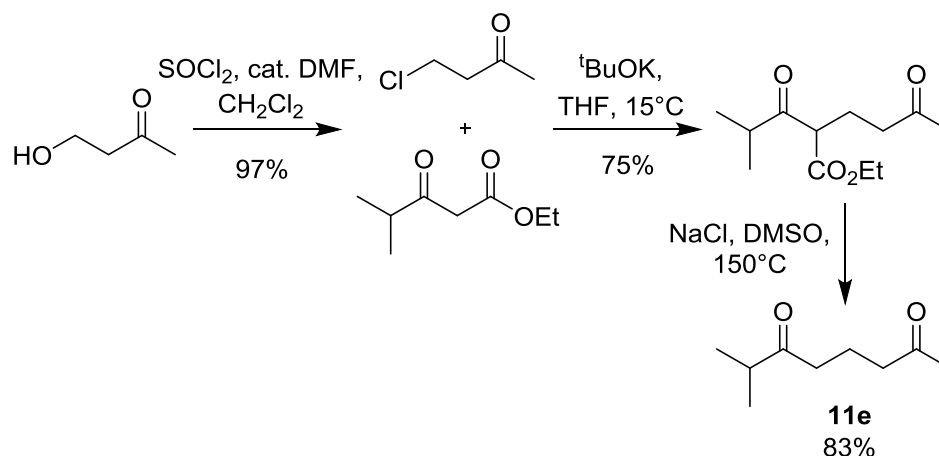


**Figure 60:** Synthesis of diketone **11e**, which involves the addition of a  $\beta$ -ketoester to 4-chlorobutan-2-one, followed by a Krapcho decarboxylation reaction to remove the ester group.

The conditions used for the transaminase reactions were adapted from a previously reported protocol.<sup>93</sup> In order to shift the equilibrium position of the ATA reaction towards formation of the aminoketone product, an additional enzyme cascade consisting of a commercially-available glucose dehydrogenase (CDX-901, GDH) and a lactate dehydrogenase (LDH-103, LDH) was harnessed. L-Ala and D-Ala were used as the sacrificial amine donors for the ATA-113 and ATA-117 biotransformations respectively and the GDH/LDH system allowed for *in-situ* removal of the pyruvate by-product via conversion of the pyruvate to lactate.

In the transaminase-catalysed reactions of the diketones, both ATA-113 and ATA-117 were able to differentiate between the two carbonyl groups in order to exclusively aminate the less hindered ketone with diketones **11a** – **11d**, producing chiral imines **12a** – **12d** in >98% *ee*. ATA-117 was observed to work more slowly than ATA-113, although both sets of reactions proceeded to completion after 24 h. With diketone **11e**, evidence of formation of the regioisomeric chiral piperidine **12e'** was observed, possibly due to the inability of the ATAs to distinguish between the similarly-sized methyl and isopropyl groups adjacent to the ketone groups. Therefore, no further experiments were conducted with this substrate. For the synthesis of chiral disubstituted pyrroline **15**, the commercially-available diketone **14** was used (Figure 61).

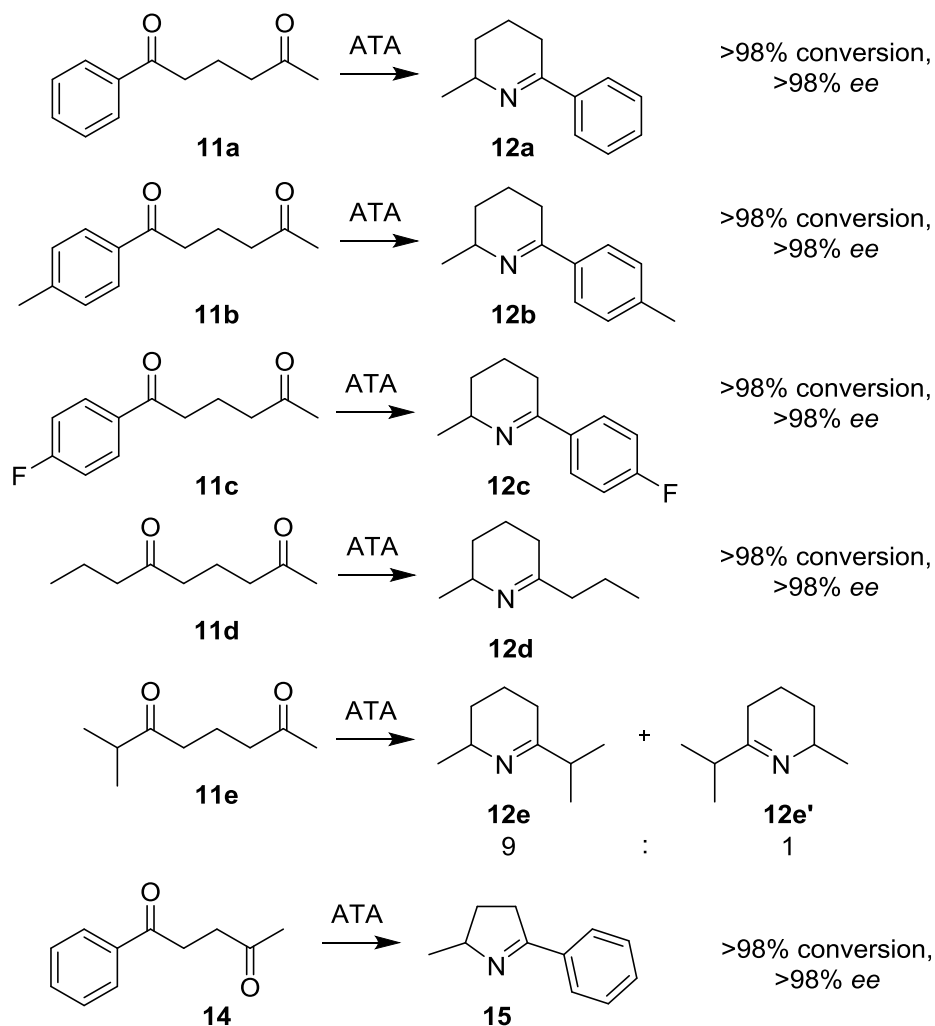


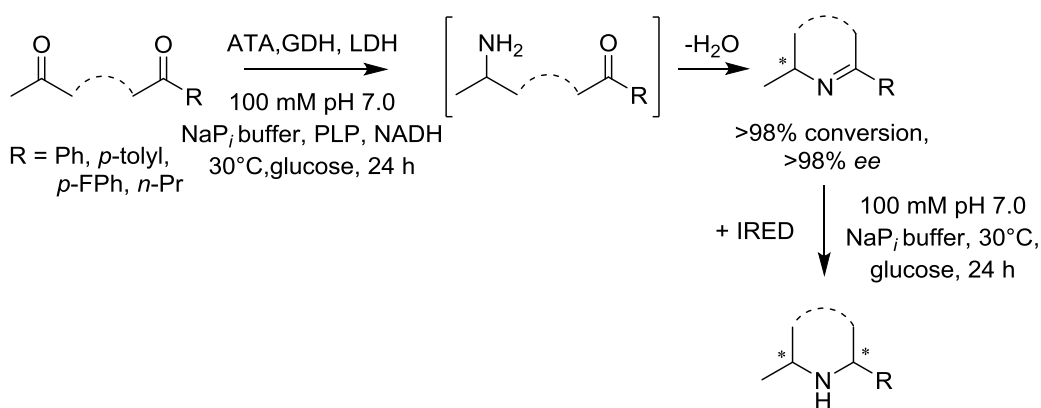
**Figure 61:** Reaction scheme displaying the ATA-catalysed amination of diketones **11a** – **11e** and **14** and the resulting products following cyclisation of the aminoketones. Although full conversion of the starting material was not observed, the amination of diketone **11e** was not completely selective, resulting in the formation of two regioisomeric disubstituted piperidines **11e** and **11e'** (in about 9:1 ratio).

### 3.2.2 One-pot two-step enzymatic cascade for the production of 2,6-disubstituted piperidines

The ATA-catalysed reaction was then coupled with IRED reduction in order to probe the stereoselectivity of IRED-mediated asymmetric reduction of imines with a pre-existing chiral centre. The reactions featured analogous conditions to those previously used in the screening of mono-substituted cyclic imines with the IREDs and were monitored by GC-MS and chiral GC-FID (see Experimental Section 7.5.2.1 for the reaction protocol).

The (*R*)-IRED and (*S*)-IRED were combined in the reaction mixture to affect the full ATA/IRED cascade. The IREDs were used as whole-cell biocatalysts in this procedure as it negated the cofactor recycling required when using the IREDs as isolated proteins. Although the ATA enzymes were able to fully convert the diketone starting material in 24 h, the

conversion of the diketone to the cyclic imine did not proceed to completion in the presence of IRED and the GDH/LDH system. The IRED whole-cells appeared to inhibit conversion of the starting material by ATAs. In order to overcome this problem, the reaction was optimised to allow complete consumption of the diketone by the ATAs by running the reactions without the IRED whole-cells for 24 h. Subsequently, the IRED whole-cell biocatalysts were added to the reaction mixture. This created a one-pot, two-step process overall (Figure 62). Preparation of analytical standards of the 2,6-disubstituted amines **13a** – **13d** was accomplished by transformation of diketones **11a** – **11d** to the corresponding imines **12a** – **12d** by ATA-113 and ATA-117 in the absence of the IRED enzymes, These imines were then reduced chemically in MeOH by treatment with NaBH<sub>4</sub>.

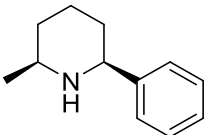
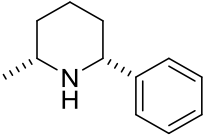
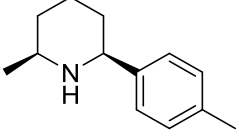
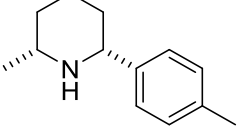
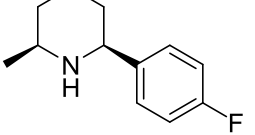
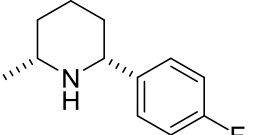


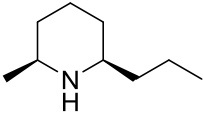
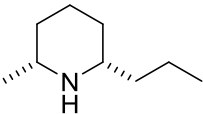
**Figure 62:** Reaction scheme displaying the conditions used in the proposed one-pot-two-step ATA/IRED cascade reaction with diketones **11a** – **11d** and **14**. The ATAs were allowed to work for 24 h in order to facilitate full conversion of the diketone before the IRED whole-cell biocatalysts were added to the reaction mixture. The stereogenic centres set by each biocatalyst is marked with an asterisk.

The 2,6-disubstituted piperideines proved to be challenging substrates for imine reduction, as observed from the moderate conversions of chiral imines **12a** – **12d** by the IRED enzymes. The IRED cell loading was subsequently increased to 200 mg/mL in order to achieve higher conversion rates. Interestingly, in contrast to the reduction of mono-substituted ring systems, formation of the *syn*-diastereomer product was consistent regardless of the IRED used. Though it was hoped that the inherent stereoselectivity of the IRED could override the preference for formation of the *syn*-product in order to provide a means to access the *anti*-diastereomer, it appeared that the pre-existing chirality of the substrate was the dominating factor in the stereochemical outcome of the biotransformation. This effect was particularly pronounced with bulky aromatic-substituted piperideines, which were converted to their corresponding amines in very high *de*.

Remarkably, there was evidence of a matched-mismatched pair effect: in cases where the inherent IRED stereoselectivity (based on the selectivity observed in the reduction of mono-substituted piperidines **5** and pyrrolines **1**) and the imine enantiomer produced by the ATA matched to afford a syn-diastereomer product, higher conversions and *de* of the resulting amine were achieved. In this respect, the (*R*)-IRED was best combined with ATA-113, which was reflected in higher conversions of the starting imine, whereas the (*S*)-IRED paired with ATA-117 with greater success (Table 10).

**Table 10:** Biotransformation of diketones **11a** – **11d** in the ATA/IRED cascade in the case of a matched pair between substrate/IRED

Substrate	ATA	Conversion to <b>12</b> [%] <sup>[a]</sup>	IRED	Amine product	Conversion [%] <sup>[a]</sup>	<i>de</i> [%] <sup>[b]</sup>	<i>ee</i> [%] <sup>[b]</sup>
<b>11a</b>	113	>98	( <i>R</i> )-IRED		81	>98	>98
<b>11a</b>	117	>98	( <i>S</i> )-IRED		32	>98	>98
<b>11b</b>	113	>98	( <i>R</i> )-IRED		71	>98	>98
<b>11b</b>	117	>98	( <i>S</i> )-IRED		61	>98	>98
<b>11c</b>	113	>98	( <i>R</i> )-IRED		42	>98	>98
<b>11c</b>	117	>98	( <i>S</i> )-IRED		63	>98	>98

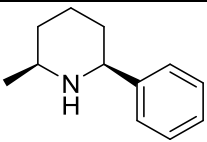
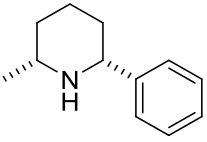
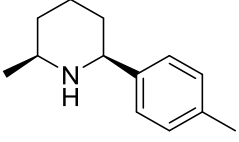
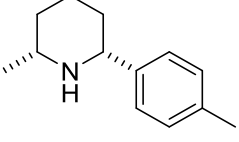
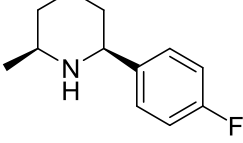
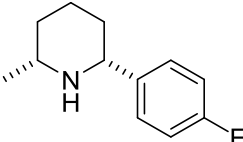
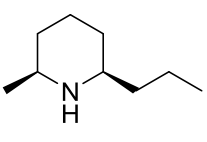
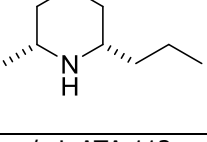
<b>11d</b>	113	>98	( <i>R</i> )- IRED		>98	95	>98
<b>11d</b>	117	>98	( <i>R</i> )- IRED		21	13	>98

**Reaction conditions:** 5 mM substrate, 2.5 mg/mL ATA-113 or ATA-117, 1 mg/mL GDH, 0.5 mg/mL LDH, 250 mM L- or D-alanine, 100 mM glucose, 1.5 mM NAD<sup>+</sup>, 1 mM PLP, 100 mM pH 7.0 NaP<sub>i</sub> buffer, 30°C, 250 rpm, 24 h followed by addition of 200 mg/mL IRED wet whole-cells and incubation at 30°C, 250 rpm for 24 h. [a] Conversion determined by comparison of peak areas of the starting material and product from GC-FID analysis on a chiral stationary phase; [b] *ee/de* determined by comparison of peak areas of resolved enantiomers from GC-FID analysis on a chiral stationary phase. Configuration assigned based on comparison of retention times on GC-FID to those of authentic standards produced chemically

In contrast, when the stereoselectivity of the IRED and the ATA no longer matched in combination, which would hypothetically grant access to the *anti*-diastereomer amine product, significantly lower conversions were recorded and the *de* of the amine products was also marginally lower (Table 11). The typically mismatched pairs were (*R*)-IRED with ATA-117 and (*S*)-IRED with ATA-113.

Diketone **11d** was transformed by ATA-113 in combination with the (*R*)-IRED to afford the natural product (-)-dihydropinidine, (*2S,6R*)-**13d** (>98% conversion, 95% *ee*), which is used as an anti-feedant against the pine weevil (*Hylobius abietis*) as well as being a component in the ladybird (*Coccinellidae*) defence mechanism.<sup>96,97</sup> Unusually, the (*R*)-IRED also displayed higher conversions of **11d** than the (*S*)-IRED when combined with ATA-117, producing amine (*2R,6S*)-**13d** in only 13% *de* and giving rise to a larger proportion of the *anti*-diastereomer product than was observed with diketones bearing bulkier aromatic substituents.

**Table 11:** Results for the biotransformation of diketones **11a** – **11d** in the ATA/IRED cascade in the case of a mismatched pair between substrate/IRED

Substrate	ATA	Conversion to <b>12</b> [%] <sup>[a]</sup>	IRED	Amine product	Conversion [%] <sup>[a]</sup>	<i>de</i> [%] <sup>[b]</sup>	<i>ee</i> [%] <sup>[b]</sup>
<b>11a</b>	113	>98	( <i>S</i> )-IRED		15	90	>98
<b>11a</b>	117	>98	( <i>R</i> )-IRED		23	96	>98
<b>11b</b>	113	>98	( <i>S</i> )-IRED		33	96	>98
<b>11b</b>	117	>98	( <i>R</i> )-IRED		7	93	>98
<b>11c</b>	113	>98	( <i>S</i> )-IRED		19	97	>98
<b>11c</b>	117	>98	( <i>R</i> )-IRED		25	98	>98
<b>11d</b>	113	>98	( <i>S</i> )-IRED		5	95	>98
<b>11d</b>	117	>98	( <i>S</i> )-IRED		3	87	>98

**Reaction conditions:** 5 mM substrate, 2.5 mg/mL ATA-113 or ATA-117, 1 mg/mL GDH, 0.5 mg/mL LDH, 250 mM L- or D-alanine, 100 mM glucose, 1.5 mM NAD<sup>+</sup>, 1 mM PLP, 100 mM pH 7.0 NaP<sub>i</sub> buffer, 30°C, 250 rpm, 24 h followed by addition of 200 mg/mL IRED wet whole-cells and incubation at 30°C, 250 rpm for 24 h. [a] Conversion determined by comparison of peak areas of the starting material and product from GC-FID analysis on a chiral stationary phase; [b] *ee/de* determined by comparison of peak areas of resolved enantiomers from GC-FID analysis on a chiral stationary phase. Configuration assigned based on comparison of retention times on GC-FID to those of authentic standards produced chemically

In order to test the scalability of the cascade reaction, a larger preparation of (-)-dihydropinidine was carried out with ATA-113 and the (*R*)-IRED. The reaction was run by emulating the analytical-scale procedure on a 50 mg scale of diketone **11d**. After 48 h, (*2S,6R*)-**13d** (51 mg, 90%, *de* >98%) was isolated as its hydrochloride salt following the full one-pot-two-step ATA/IRED cascade reaction. Formation of the *syn*-diastereomer of **13d** was confirmed by NOESY analysis, which showed correlation through space between the two axial protons H<sup>a</sup> and H<sup>h</sup> on C2 and C6 respectively (Figure 63; full details of the compound characterisation can be found in Experimental Section 7.5.4.2).

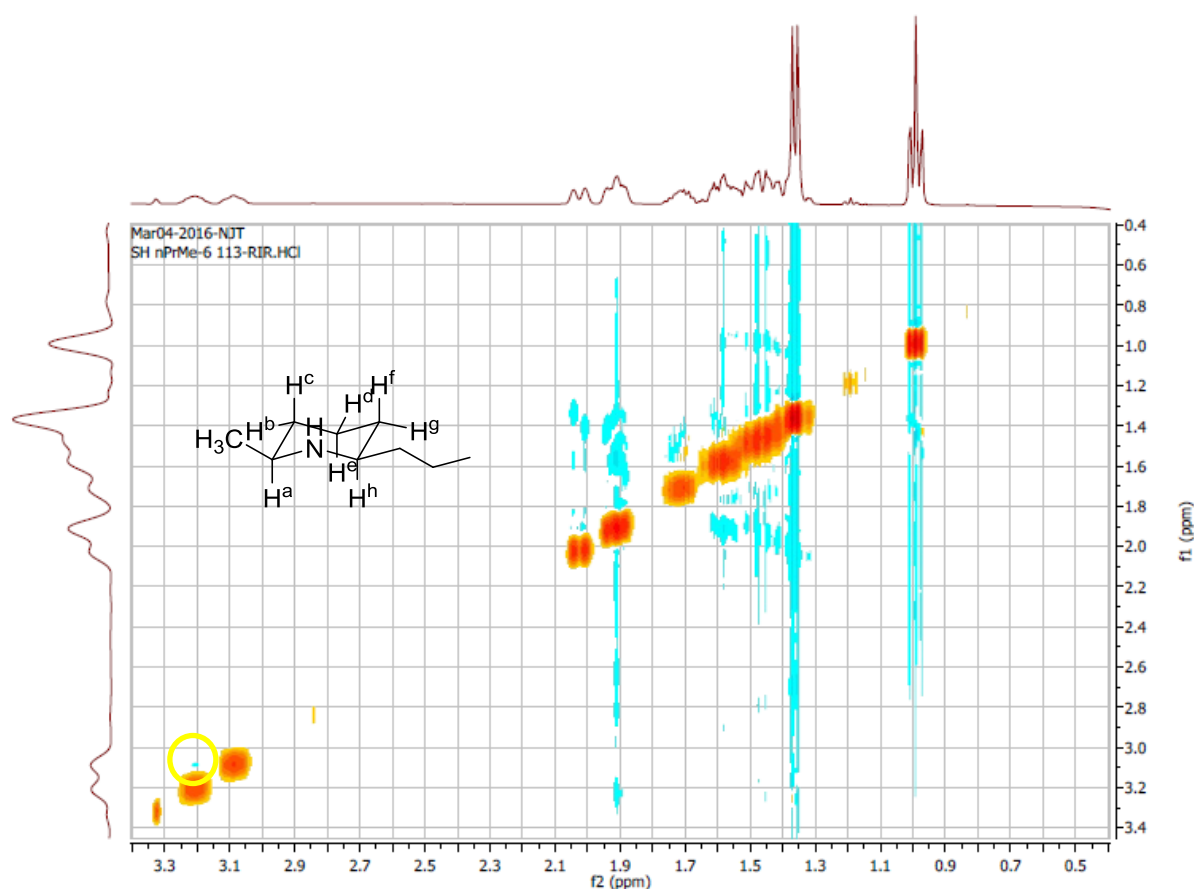


**Figure 63:** NOESY NMR analysis of (*2S,6R*)-**13d** produced from the preparative-scale biotransformation of **11d** with ATA-113 and (*R*)-IRED, showing correlation between the two axial protons H<sup>a</sup> and H<sup>h</sup> through space (circled in yellow).

A preparative-scale biotransformation of **13a** was also carried out starting from diketone **11a**. After 24 h, imine (*S*)-**12a** was isolated following treatment with ATA-113 as its hydrochloride salt (60 mg, 93%, *ee* >98%), which was subsequently reduced by the (*R*)-IRED in a separate reaction to yield (*2S,6S*)-**13a** (46 mg, 92% yield, *de* >98%) after 24 h. Formation of *syn*-(*2S,6S*)-**13a** was also confirmed by NOESY analysis, which showed correlation between the diaxial protons H<sup>a</sup> and H<sup>h</sup> on C2 and C6 (Figure 64). Additionally, <sup>1</sup>H NMR analysis confirmed a large coupling constant  $J^{ah} = 11.0$  Hz, which is consistent with

diaxial proton-proton coupling according to the Karplus equation, therefore indicative of the equatorial orientation of the both the methyl substituent on C2 and phenyl group on C6.

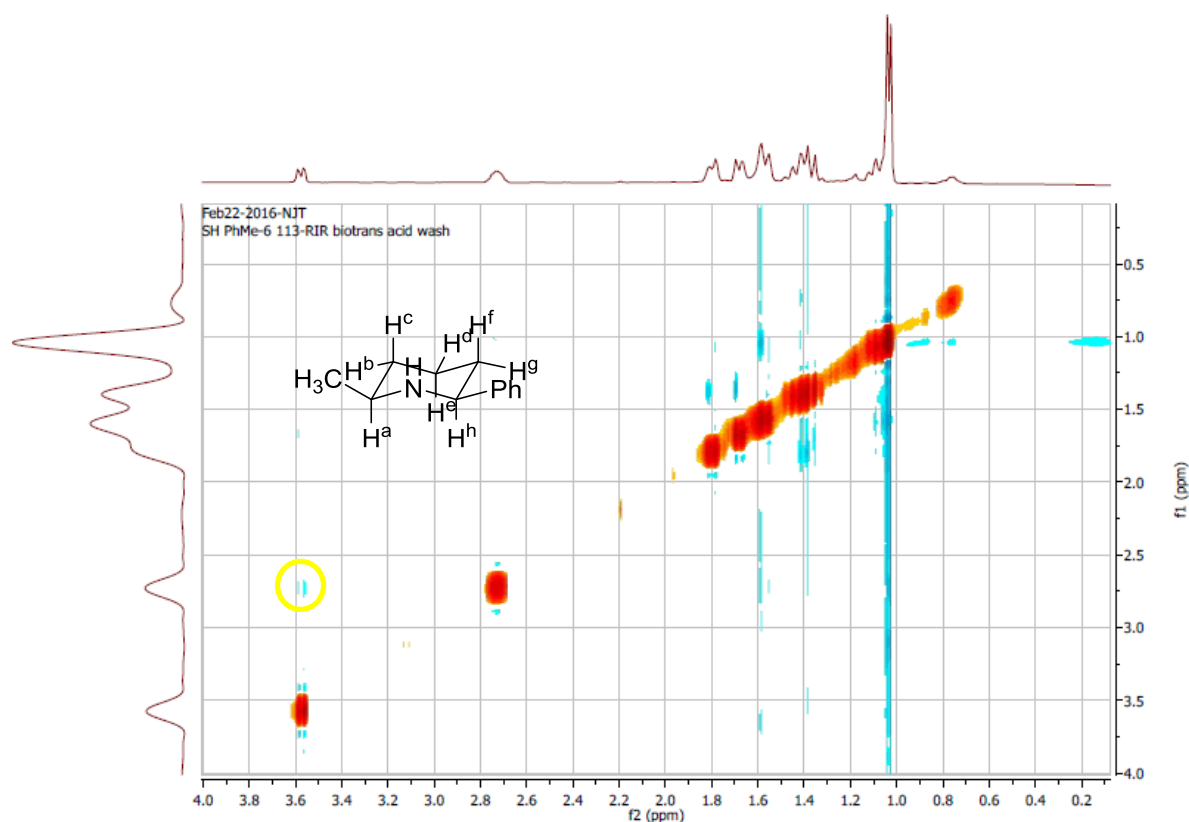


**Figure 64:** NOESY NMR analysis of (2*S*,6*S*)-**13a**, produced from the biotransformation of (*S*)-**12a** with the (*R*)-IRED, showing correlation between the two axial protons H<sup>a</sup> and H<sup>h</sup> through space (circled in yellow).

The observed stereoselectivity of the IRED reduction reactions, which gave rise to the *syn*-diastereomer products following reduction of the chiral disubstituted imines, can be rationalised based on the model described by Yamamoto *et al.*<sup>98,99</sup> This builds on theoretical work by Houk *et al.*, which states that “the tendency for staggering of vicinal bonds with respect to partially formed bonds is greater than for fully formed bonds,” thereby predicting a strong preference for antiperiplanar attack of the hydride ion with respect to the  $\sigma$ -C-H bond vicinal to the imino functional group.<sup>100</sup> The preference for axial attack of the hydride is also supported by Cieplak, who proposed that charge-transfer from the vicinal  $\sigma$ -C-H bond stabilises the transition state in nucleophilic addition to carbonyl groups, therefore favouring axial approach of the nucleophile.<sup>101</sup>

For the reduction of mono-substituted cyclic imines with each IRED, there is a preferred binding orientation of the substrate in the active site, allowing preferential delivery of the hydride from NADPH to the face of the imine and giving rise to the observed configuration of the amine product. The following rationale takes into account the work by

Yamamoto for the IRED-mediated reduction of the 2,6-disubstituted cyclic imines and assumes that the chiral cyclic imine is in its preferred binding orientation in the active site of the enzyme. When the hydride from NADPH approaches from above the imine, the most favoured axial attack occurs when the methyl substituent on C6 is in a pseudoequatorial position, thereby giving rise to the *syn*-diastereomer product (Figure 65A). However, when the opposite imine enantiomer is taken, whereby the methyl substituent is in a pseudoaxial position, approach by the hydride is hindered by a disfavoured 1,3-steric interaction (Figure 65B). It was proposed that in this case, it would be preferable for the imine to enter the active site of the enzyme in a 180° rotated orientation with an associated ring-flip of the imine. The hydride would therefore be delivered to the opposite face of the imine, thereby giving rise to the more configurationally-stable *syn*-diastereomer product and overriding the enzyme's inherent selectivity in this case. The proposal may explain the significantly lower conversions achieved with the mismatched imine enantiomer/IRED cases.<sup>95</sup>

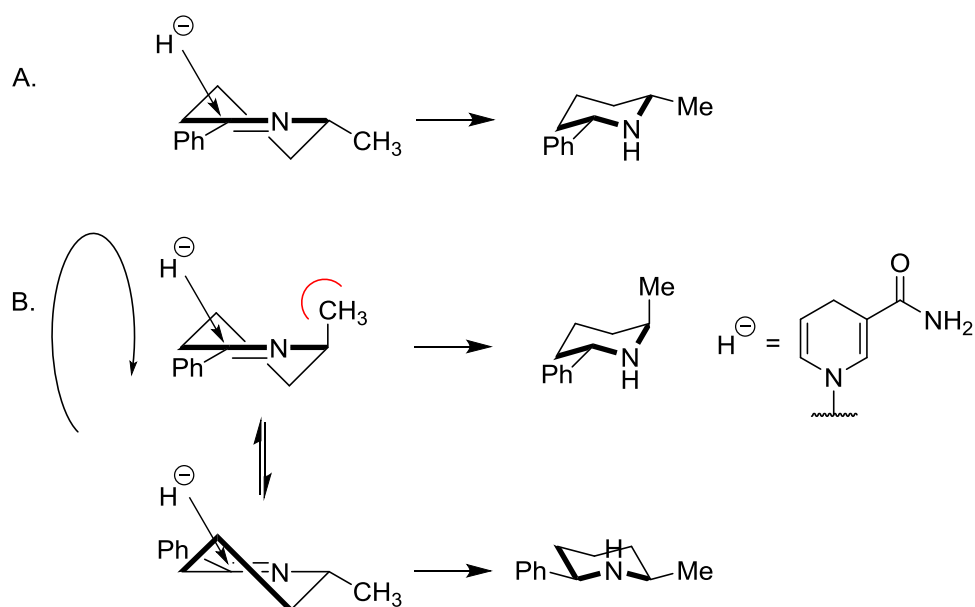


**Figure 65:** Proposed mechanism for hydride delivery from NADPH during the IRED-mediated reduction of chiral imines **12a** – **12d**. **A.** Hydride delivery during the matched pair scenario, showing formation of the *syn*-diastereomer amine product via the lowest energy route. **B.** Hydride delivery during the mismatched pair scenario, whereby a 1,3-steric clash between the incoming hydride and the pseudoaxial methyl substituent disfavours hydride delivery in this conformation. **C.** Hydride delivery during the mismatched pair scenario, whereby the opposite face of the prochiral imine is presented to the NADPH in the enzyme active site following a 180° flip of the imine. In this orientation, the 1,3-steric clash of the methyl substituent with the incoming hydride during its preferred axial nucleophilic attack pathway is minimised.

In order to access the *anti*-diastereomer product from the reduction of **11d**, Kroutil and co-workers (by extension of the work by Yamamoto *et al.*)<sup>98,99</sup> used a trialkylaluminium-mediated hydride reduction to force a conformation change in imine **12d**, whereby the methyl-substituent is in a pseudoaxial position due to steric repulsion between the methyl group and the Lewis acid coordinated to the nitrogen lone-pair. Subsequently, the preferred

antiperiplanar attack trajectory of the hydride is facilitated to afford the *anti*-diastereomer product in high selectivity (Figure 66).<sup>102</sup>

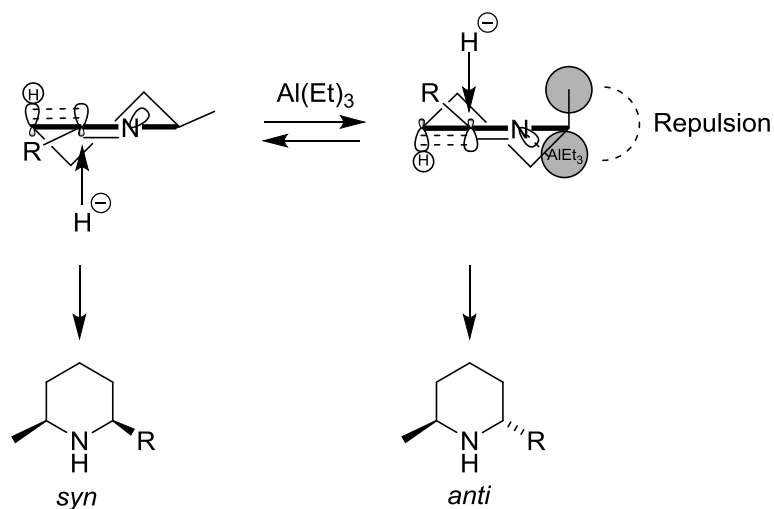


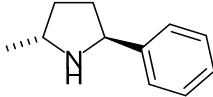
**Figure 66:** Reaction schemes for the formation of the *syn*-diastereomer of amine **11d** (from normal hydride reduction methods) and *anti*-diastereomer amine **11d** (from the trialkylaluminium-mediated hydride reduction method).<sup>102</sup>

### 3.2.3 One-pot two-step enzymatic cascade for the production of 2,5-disubstituted pyrrolidines

For the production of disubstituted pyrrolidines, 1,4-diketone **14** was treated with  $\omega$ -TA ATA-113 or ATA-117 for 24 h, before being subjected to reduction by either the (*R*)-IRED or (*S*)-IRED. Interestingly, investigation into the selectivity of IRED-mediated reductions of the chiral pyrrolines revealed a less predictable pattern (Table 12).

**Table 12:** Results for the biotransformation of diketones **14** in the ATA/IRED cascade

Entry	ATA	Conversion to <b>15</b> [%] <sup>[a]</sup>	IRED	Amine product	Conversion [%] <sup>[a]</sup>	<i>de</i> [%] <sup>[b]</sup>	<i>ee</i> [%] <sup>[b]</sup>
1	113	>98%	( <i>R</i> )-IRED		11	63	>98
2	113	>98%	( <i>S</i> )-IRED		17	65	>98
3	117	>98%	( <i>R</i> )-IRED		95	97	>98

4	117	>98%	( <i>S</i> )- IRED		68	>98	>98
---	-----	------	-----------------------	--	----	-----	-----

**Reaction conditions:** 5 mM substrate, 2.5 mg/mL ATA-113 or ATA-117, 1 mg/mL GDH, 0.5 mg/mL LDH, 250 mM L- or D-alanine, 100 mM glucose, 1.5 mM NAD<sup>+</sup>, 1 mM PLP, 100 mM pH 7.0 NaP<sub>i</sub> buffer, 30°C, 250 rpm, 24 h followed by addition of 200 mg/mL IRED wet whole-cells and incubation at 30°C, 250 rpm for 24. [a] Conversion determined by comparison of peak areas of the starting material and product from GC-FID analysis on a chiral stationary phase; [b] *ee/de* determined by comparison of peak areas of resolved enantiomers from GC-FID analysis on a chiral stationary phase. Configuration assigned based on comparison of retention times on GC-FID to those of authentic standards produced chemically

When ATA-113 product (*S*)-**15** was taken as a substrate by the IREDs, poor conversion of the imine was recorded and the corresponding amines were produced in only moderate *de* (63 – 65%). Unusually, the configuration of the diastereomer of the pyrrolidine produced appeared to contradict the selectivity pattern established with the analogous mono-substituted 2-phenyl-1-pyrroline **1b**. In this case, it appeared that the existing chirality on the substrate had overridden inherent stereoselectivity of both enzymes. When the IREDs were paired with ATA-117 in order to reduce the opposite (*R*)-enantiomer imine, significantly higher levels of conversion were observed and unusually, both IREDs furnished 2,5-disubstituted pyrrolidine **16** in the same configuration. These results indicate that both enzymes prefer the (*R*)-enantiomer imine as a substrate, although different binding modes operate for the two opposing enantiomers of the imine.

### 3.3 Carboxylic acid reductase/ $\omega$ -transaminase/imine reductase cascade

#### 3.3.1 Principle and synthesis of screening compounds

Extending the multi-enzyme cascade beyond ATA/IRED for the synthesis of cyclic amines, the conditions for the three-component multi-enzyme cascade incorporating CAR was optimised to take into account the nature of the proposed ketoacid starting material.<sup>95</sup> A stronger buffering capacity in the reaction solvent was imperative to allow the cascade to function efficiently, due to the large pH change experienced over the course of the reaction starting from the ketoacid on to the final chiral amine product. Therefore, 500 mM sodium phosphate buffer was used. The three enzymes were able to function well simultaneously in the same pot in contrast to the TA/IRED cascade, where the action of the ATA was inhibited by the presence of the IRED whole-cells. As the ATA enzymes transform a more sterically-accessible aldehyde carbonyl in this instance rather than a ketone, the ketoaldehyde may be a preferred substrate for the ATA. Mono-substituted imines were found to be less challenging substrates for the IREDs, so the IRED cell-loading was reduced to 50 mg/mL in this cascade.

By incorporation of a heteroatom into the alkyl chain of the ketoacid starting material, cyclic chiral amines possessing other heteroatoms, including morpholines and thiomorpholines, could be accessed through the cascade. To test this principle, two ketoacid compounds were synthesised (Figure 67). For the formation of 3-phenylmorpholine **19**, ketoacid **17** was synthesised following a patent procedure, where a commercially available anhydride was used to perform a Friedel-Crafts acylation reaction in neat benzene. Ketoacid **20**, which would provide access to 3-phenylthiomorpholine **22** upon treatment with the full CAR/ATA/IRED cascade, was approached through saponification of a ketoester intermediate, which was synthesised via a modified Williamson ether synthesis.<sup>103</sup>

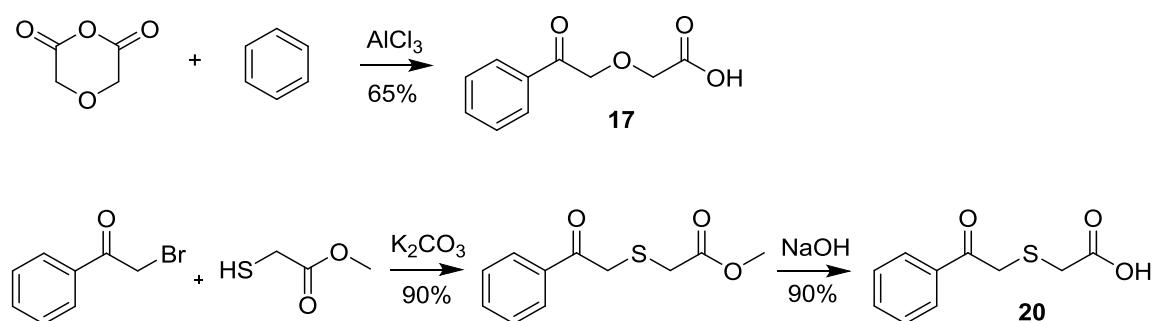


**Figure 67:** Synthesis routes for the production of ketoacids **17** and **20**.

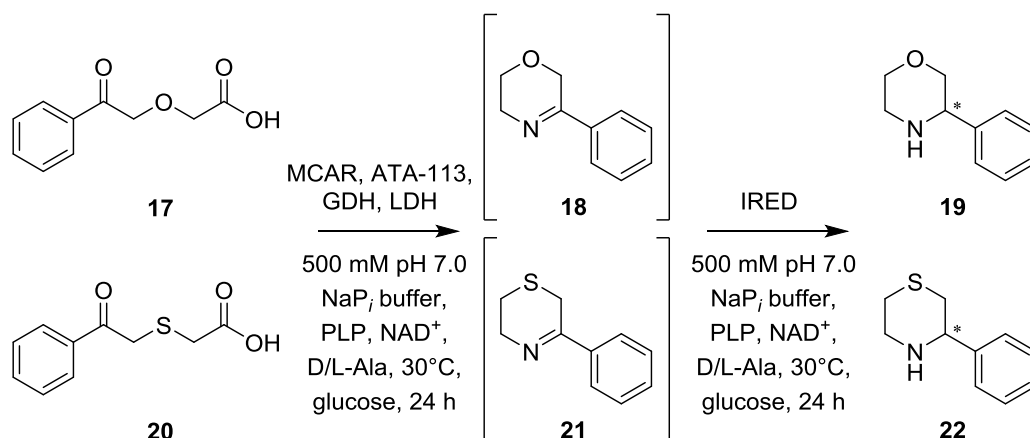
### 3.3.2 One-pot multi-enzyme cascade for the production of 3-phenylmorpholine **19** and 3-phenylthiomorpholine **22**

ATA-113 was employed as the  $\omega$ -transaminase of choice in this cascade, as the enantioselectivity of the ATA is irrelevant in the amination of the ketoaldehyde intermediate and ATA-113 was previously observed to work faster in the ATA/IRED cascade. The carboxylic acid reductase from *Mycobacterium marinum* (MCAR), which has been reported to reduce medium- and long-chain fatty acids, was also employed in the cascade. As CARs are ATP- and NADPH-dependent enzymes, the protein was produced in *E. coli* and used as a whole-cell biocatalyst. In order to obtain maximum levels of activity from the CAR whole-cells, a gene for a 4'-phosphopantetheinyl transferase (Sfp) from *Bacillus subtilis* was co-expressed in the same cell as the MCAR.<sup>58</sup>

The use of the pyruvate-removing GDH/LDH enzyme system was necessary in this cascade in order to shift the transaminase reaction equilibrium towards formation of the aminoketone. In the absence of the pyruvate removal system, overreduction of the aldehyde to the corresponding ketoalcohol has been observed.<sup>95</sup> This second reduction step is likely to be carried out by the endogenous enzymes present within the *E. coli* whole-cells

rather than the CAR itself. Previous studies into the transformation of vanillic acid by whole-cells of *Nocardia iowensis* (which contains the NCAR enzyme) produced the carboxylic acid reduction product vanillin, which was subsequently reduced to vanillyl alcohol. However, when the transformation of vanillic acid was carried out using the purified NCAR, the NADPH and ATP-dependent reduction to vanillin is quantitative, with no further reduction products observed.<sup>104</sup>

Both ketoacids **17** and **20** were treated with the one-pot CAR/ATA/IRED cascade with either the (*R*)-IRED or (*S*)-IRED (Figure 68). After 24 h, the pH of the biotransformation samples was adjusted to pH 12 with base and the aqueous mixture was extracted with organic solvent, in order to isolate the imine and amine products from the reaction. The remaining aqueous mixture was subsequently acidified and re-extracted with organic solvent to isolate any remaining ketoacid starting material (for full details for the experimental protocol, please see Experimental Section 7.5.2.2).

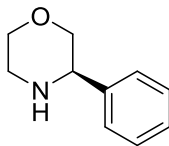
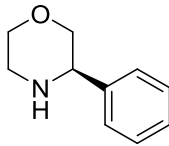
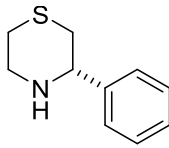


**Figure 68:** Conditions used for the one-pot multi-enzyme cascade employing MCAR, ATA-113 and IRED enzymes, in combination with a GDH/LDH cascade to drive the transaminase reaction towards amine formation. The flexibility of this modular approach would allow the cascade to be harnessed in part if required, *ie.* using CAR and ATA enzymes only in the first-stage to access the cyclic imine intermediate. Imines **18** and **21** were not isolated as they were found to be unstable intermediates.

When the CAR/ATA/IRED cascade was run in full, conversion of the ketoacids to the final 2-substituted amines was detected with both IREDs. The MCAR was able to consume the starting ketoacid completely and as no ketoalcohol by-product was detected by GC-MS, it is assumed that there was complete conversion of the ketoaldehyde by the ATA. Unusually, no imine could be detected by GC-MS or GC-FID analysis, even when the cascade was run in part in the presence of CAR and ATA-113 enzymes only. This may be attributed to potential instability of the imine intermediates **18** and **21**. When a preparative-scale reaction of **20** was carried out with the CAR/ATA cascade exclusive of the IRED, imine **21** could not be

isolated. The assays used for analysis of the biotransformations, based on chiral GC-FID and GC-MS, could not be used to determine the conversion of the imine intermediate to amine by the IREDs. Therefore, preparative-scale biotransformations with the full cascade were carried out using the (*R*)-IRED and the yields of the amine products **19** and **22** were calculated from the isolated product (Table 13).

**Table 13:** Results for the biotransformation of ketoacids **17** and **20** in the CAR/ATA/IRED cascade

Substrate	Conversion of ketoacid [%] <sup>[a]</sup>	IRED	Amine product	Yield [%] <sup>[b]</sup>	<i>ee</i> [%] <sup>[c]</sup>
<b>17</b>	>98	( <i>R</i> )-IRED		60	40
<b>17</b>	>98	( <i>S</i> )-IRED		-	>98
<b>20</b>	>98	( <i>R</i> )-IRED		72	90
<b>20</b>	>98	( <i>S</i> )-IRED		-	>98

**Reaction conditions:** 5 mM substrate, 75 mg/mL MCAR wet whole cells, 50 mg/mL IRED wet whole cells, 2.5 mg/mL ATA-113, 1 mg/mL GDH, 0.5 mg/mL LDH, 250 mM D/L-alanine, 100 mM glucose, 1.5 mM NAD<sup>+</sup>, 1 mM PLP, 500 mM pH 7.0 NaP<sub>i</sub> buffer, 30°C, 250 rpm, 24 h. [a] Conversion determined by comparison of peak areas of the starting material and product from GC-FID analysis on a chiral stationary phase; [b] isolated yield; [c] *ee/de* determined by comparison of peak areas of resolved enantiomers from GC-FID analysis on a chiral stationary phase. Configuration assigned by comparison of GC-FID retention times with published data.<sup>85</sup>

Treatment of ketoacids **17** and **20** with the full cascade employing either the (*R*)- or (*S*)-IREDs produced the corresponding 3-phenylmorpholine **19** and 3-phenylthiomorpholine **22** amines, demonstrating that the imine intermediates **18** and **21** are substrates for both

IREDs. The (*S*)-IRED was able to furnish both amines in excellent *ee*, whereas the (*R*)-IRED displayed varying levels of enantioselectivity (40% *ee* for **19** and 90% *ee* for **22**). The cascade with the (*R*)-IRED produced both amines in >60% yield, further demonstrating the synthetic utility of the cascade. As the biotransformations employing the (*S*)-IRED were run on an analytical-scale, no conversion of the imine to amine could be calculated.

### 3.4 Conclusions and outlook

Two biocatalytic reaction cascades were successfully employed for the synthesis of substituted cyclic amine scaffolds. The ATA/IRED cascade was used to produce chiral 2,6-disubstituted piperidine scaffolds starting from achiral 1,5-diketones, where each enzyme employed was able to set an individual stereogenic centre in discrete steps. Whole-cell IRED biocatalysts were utilised in the process, which appeared to inhibit the function of the ATA enzymes; therefore the biotransformation was conducted in two stages to produce a one-pot, two-step cascade. Access to the *syn*-diastereomer products was granted exclusively in all cases tested (Figure 69). An interesting selectivity pattern emerged where matching enzyme pairs of the (*R*)-IRED with ATA-113 and the (*S*)-IRED with ATA-117 achieved much higher conversions of the imine intermediate. Whereas with mono-substituted piperidines the (*R*)- and (*S*)-IREDs demonstrated enantiocomplementary behaviour by providing access to opposing enantiomers of the amine product, it appeared that the existing chirality of the 2,6-disubstituted imines exhibited control over the stereochemical outcome of the IRED-mediated reduction, thereby overriding the enzyme's inherent selectivity.

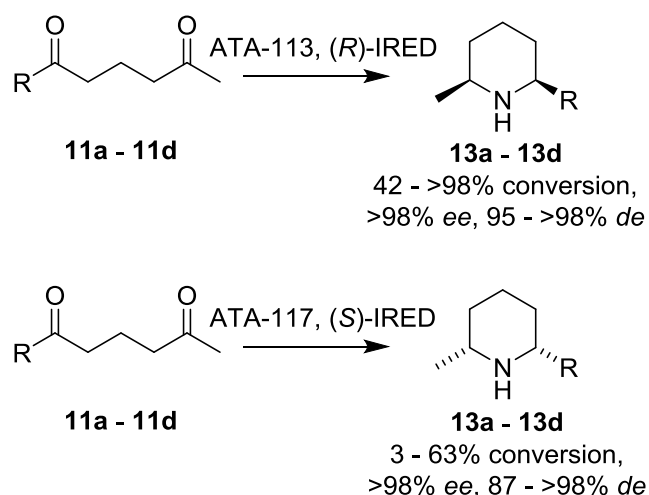


**Figure 69: A.** Reaction scheme of the TA/IRED catalysed one-pot, two-step cascade reaction of diketones **11a** – **11d**, which provided access to the *syn*-diastereomer amine products in all cases. The scheme illustrates the matched pair cases of ATA and IRED with the correct inherent selectivity to produce *syn* amine products, which were produced in higher conversion and *de* than when the selectivity of the two enzymes did not match up. The combination of ATA-117 with (*S*)-IRED with diketone **11d** produced the corresponding amine in only 3% conversion.

Interestingly, as the methyl group on chiral imine **12a** is systematically moved around the piperidine ring, the selectivity pattern changes depending on the position of the substituent.<sup>95</sup> It was shown that when the methyl group is on a position on the ring whereby a 1,3-steric clash could occur with the oncoming hydride (*i.e.* positions C-4 and C-6) or even a 1,2-steric interaction (position C-3), in these cases the chiral imine substrate will override the enzyme's inherent selectivity in order to minimise these unfavourable steric interactions. When the methyl is on position C-5, these effects are irrelevant, allowing the established stereoselectivity of IRED to then define the stereochemical outcome of the reaction (Figure 70).

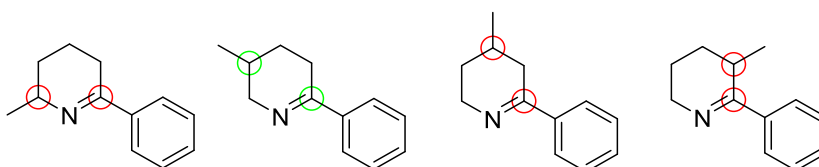


**Figure 70:** Structures of the isomers of the disubstituted piperidine imine **12a**, where the methyl substituent is systematically moved around the ring. The positions indicated by red circles indicate unfavourable interactions between the two substituents – resulting in the chiral substrate overriding the enzyme's selectivity in the reduction reaction. When the substituents are in a 1,5-arrangement, the unfavourable interactions are minimised (green circles), allowing the bioreduction reaction to proceed with the expected selectivity from the enzyme.<sup>95</sup>

In contrast to 2,6-disubstituted piperidines, a less predictable pattern of selectivity in the IRED reduction of 1,5-disubstituted pyrroline **15** emerged when applying the ATA/IRED cascade to 1,4-diketone **14**. Both the (*R*)- and (*S*)-IREDs showed a preference for (*R*)-**15** as a substrate, although both enzymes also furnished the disubstituted pyrrolidine product in the same (*2R,5S*) configuration.

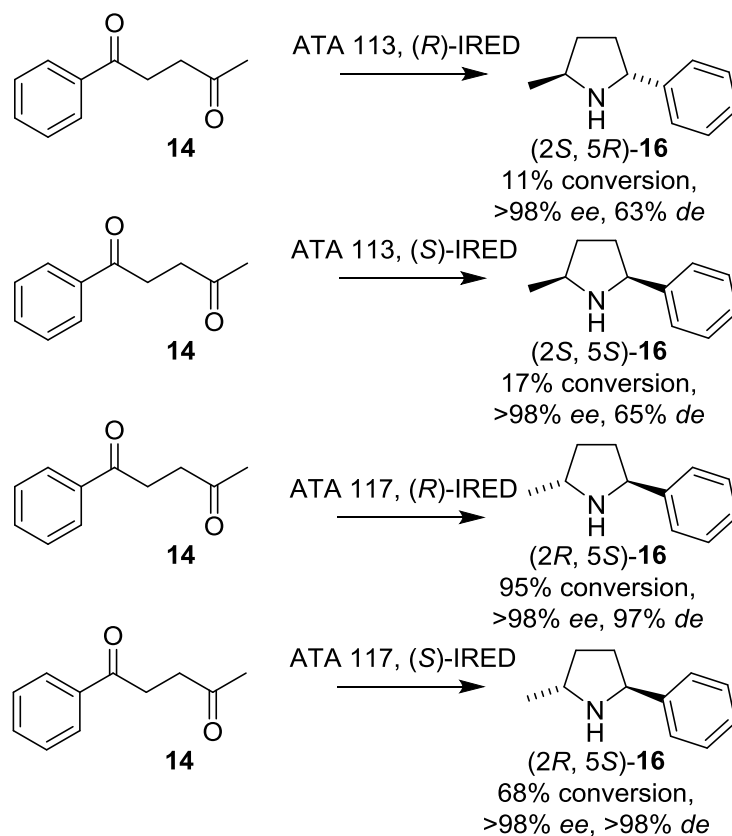


**Figure 71:** Synthesis of 2,5-disubstituted pyrrolidine **16** from the corresponding diketone **14** using the TA/IREd one-pot, two-step cascade.

The synthetic utility of the ATA/IREd cascade was demonstrated in the preparative-scale synthesis of the natural product (-)-dihydropinidine (2*S*,6*R*)-**11d**, which was accessed in 90% yield, >98% *de* (Figure 72).

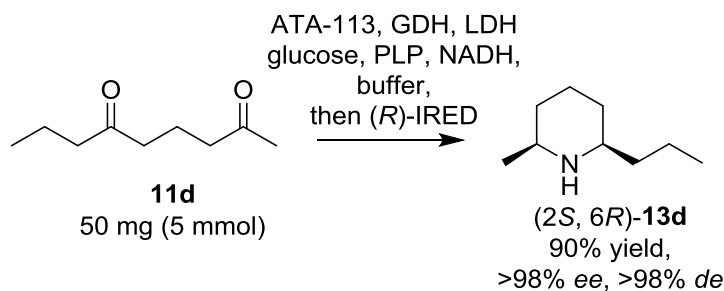


**Figure 72:** Preparative-scale synthesis of the natural product (-)-dihydropinidine **13d** using ATA-113 in combination with the (*R*)-IREd, producing the amine in 90% yield and >98% *de*.

The second cascade extended the ATA/IREd cascade by incorporation of CAR, to enable the synthesis of chiral cyclic amines starting from the corresponding ketoacids. This was successfully applied in the synthesis of 3-phenylmorpholine **19** and 3-phenylthiomorpholine

**22**, with the IREDs defining the stereogenic centre around the C-2 atom. The full cascade enables the construction of complex chiral *N*-heterocycles starting from relatively simple achiral ketoacids. This was applied successfully in the preparative-scale synthesis of (*R*)-**18** and (*R*)-**21** using MCAR and ATA-113 in combination with the (*R*)-IRED (Figure 73). The cascade allowed circumnavigation of the isolation of unstable chemical intermediates, such as imines **18** and **21**, in order to furnish the more stable amine products. The ability to add the enzymes into the reaction pot individually confers the advantage of control over the quantity of each active catalyst. This would be useful if a specific enzymatic step were identified as a bottleneck in the cascade, where increasing the quantity of the catalyst available could provide a solution. The use of separate enzymes also affords modularity to the approach, allowing the cascade to be employed in part if required *eg.* using CAR and ATA without the addition of the IRED in order to access the imine intermediate.

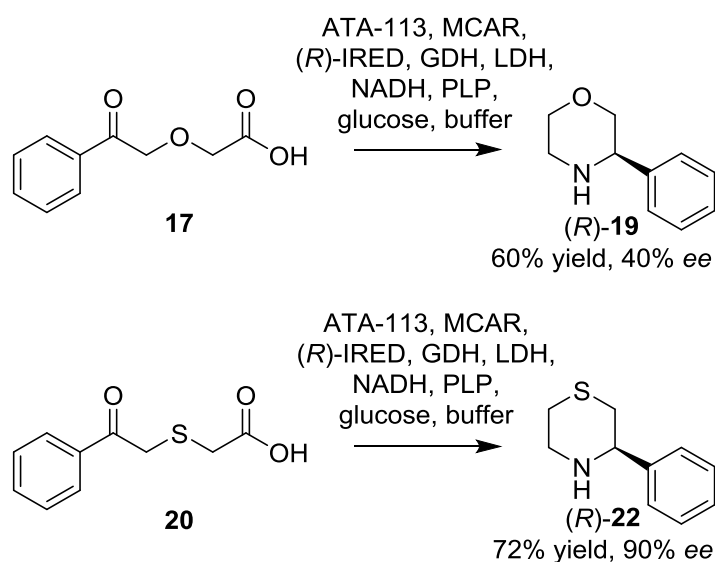


**Figure 73:** Preparative-scale synthesis of morpholine **19** and thiomorpholine **22** using the MCAR/ATA-113/(*R*)-IRED one-pot cascade. The yields of each amine product are displayed below the structures.

As most cascade reactions in nature have evolved to work within the same cell and are highly efficient in doing so, future work on the multi-enzyme cascade should be directed towards this goal. In particular, co-expression of all three enzymes involved, in a single cell, would allow a more facile preparation of an otherwise fairly complex reaction setup.

## Chapter 4: Amine oxidase-catalysed redox deracemisation reactions of 2-substituted cyclic amines, tetrahydroquinolines and indolines

### 4.1 Overview of deracemisation strategies

#### 4.1.1 Existing strategies for enzymatic deracemisation of amines

Although monoamine oxidase (MAO-N) remains the archetype enzyme employed in the redox deracemisation reactions of amines, typically only the (*R*)-enantiomer amine product is accessed through this route due to the selectivity of the oxidase biocatalyst, as most reported enzymes in this class are (*S*)-selective. This limitation was addressed recently by Turner's group, who reported the engineering of an (*R*)-selective amine oxidase with broad substrate scope.<sup>105</sup> The 6-hydroxy-D-nicotine oxidase (6-HDNO) from *Arthrobacter nicotinovorans* is a key enzyme in the nicotine metabolism pathway. The enzyme catalyses the oxidation of 6-hydroxy-D-nicotine to the corresponding imine, which then undergoes hydrolysis to yield 6-hydroxy-*N*-pseudooxynicotine which is then further metabolised to maleamic and fumaric acid (Figure 74).

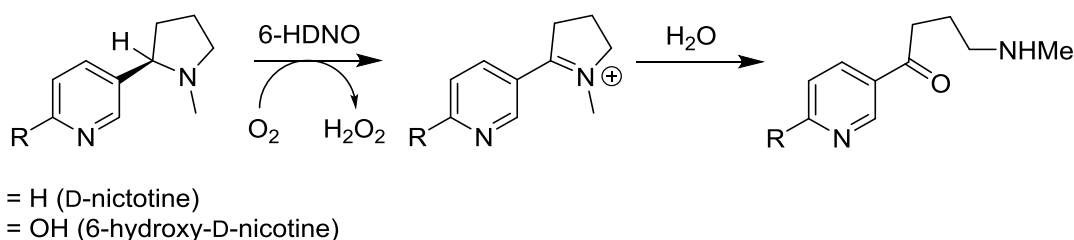


**Figure 74:** Metabolism of D-nicotine and 6-hydroxy-D-nicotine by 6-HDNO, a key enzyme in the nicotine degradation pathway.

The wild-type 6-HDNO enzyme was subjected to a CASTing approach for mutagenesis, resulting in the variant E350L/E352D which possessed a much broader substrate tolerance than the original enzyme applicable for biocatalysis. This variant was used to deracemise a broad panel of 2-substituted cyclic amines, including pyrrolidines, piperidines, tetrahydroisoquinolines and tetrahydro- $\beta$ -carbolines; granting access to predominantly (*S*)-enantiomer amines in up to >99% *ee* following the chemo-enzymatic deracemisation approach (Figure 75).

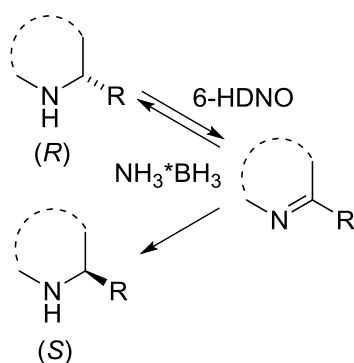


**Figure 75:** Chemo-enzymatic deracemisation of cyclic amines, utilising ammonia-borane as a non-selective reductant in combination with the (*R*)-selective amine oxidase 6-HDNO.<sup>105</sup>

Asano also reported the tailoring of a D-amino acid oxidase (D-AAO) originating from pig kidney to develop an (*R*)-selective AO, though the demonstration of deracemisation using this enzyme was limited to  $\alpha$ -methylbenzylamine.<sup>106</sup> An additional (*S*)-selective FAD-dependent amine oxidase originating from the bacterium *Brevibacterium oxydans* IH-35A has been described,<sup>107</sup> the cyclohexylamine oxidase (CHAO) is discussed in more detail in Section 4.3.1.

#### 4.1.2 Aims

The aim of this section of the project was to further develop the chemo-enzymatic deracemisation approach to access enantiomerically-pure chiral amines by substituting the ammonia-borane reductant in the reaction with a biocatalyst. In addition to the well-established monoamine oxidase-NH<sub>3</sub>BH<sub>3</sub> cascade, 6-HDNO has been used with great success in the deracemisation of cyclic amines to afford the opposite (*S*)-enantiomer amines. Work with the (*R*)- and (*S*)-IREDs has detailed their ability to reduce a broad panel of cyclic imines to their corresponding amines in an asymmetric fashion, providing complementary routes to each enantiomer amine product in high *ee* (see Section 2). It was envisaged that pairing the (*R*)-selective 6-HDNO with the (*R*)-IRED (which produces predominantly amines in the (*S*)-configuration when the substituent is bulky) would allow the redox deracemisation of cyclic amines to proceed as the selectivity of each enzyme would match, such that the IRED would selectively reduce the imine in the reaction to the amine enantiomer that remains untouched by the 6-HDNO (Figure 76).

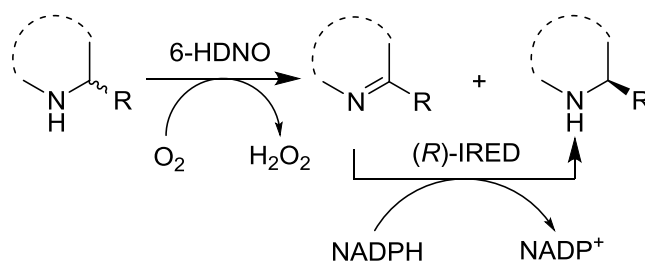


**Figure 76:** Scheme showing the proposed biocatalytic redox deracemisation of racemic cyclic amines, using the (*R*)-selective 6-HDNO and the (*R*)-IRED. The enzymes are able to work in tandem as the (*R*)-IRED produces amines in predominantly the enantiomer which is not oxidised by the 6-HDNO.

Additionally, the redox deracemisation approach was to be explored further by applying the technique to new classes of substrates. Using 6-HDNO and variants of MAO-N, the scope of AO/ $\text{NH}_3\text{BH}_3$  chemo-enzymatic deracemisation has included monosubstituted cyclic amines, tetrahydroisoquinolines, tetrahydro- $\beta$ -carbolines, *N*-methyl cyclic tertiary amines and also acyclic amines.<sup>73,74,108</sup> Despite the rather broad substrate scope of the technique, previous reports have paid little attention to the tetrahydroisoquinoline isomer, tetrahydroquinoline, as well as indoline scaffolds as targets for redox deracemisation (Figure 77).

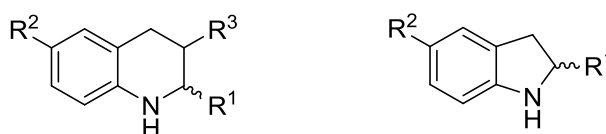


**Figure 77:** Structures of the proposed racemic amine scaffolds as targets for redox deracemisation in combination with amine oxidases and either the chemical reductant  $\text{NH}_3\text{BH}_3$  or IREDs.

A panel of substituted tetrahydroquinolines and indolines will be synthesised and subjected to redox deracemisation, either by the chemo-enzymatic route harnessing AO enzymes in combination with the non-selective chemical reducing agent  $\text{NH}_3\text{BH}_3$  or solely by biocatalytic means, harnessing IREDs in combination with AOs. It was hoped that the combination of enantiocomplementary AO enzymes (MAO-N and CHAO with HDNO) as well as (*R*)- and (*S*)-selective IREDs would provide routes to each enantiomer of the amine.

## 4.2 Amine oxidase/imine reductase catalysed deracemisation of 2-substituted cyclic amines

### 4.2.1 Optimisation of the biocatalytic deracemisation of amines with 6-HDNO and (*R*)-IRED

To effect the full amine oxidase/imine reductase (AO/IRED) biocatalytic redox deracemisation of amines without compromising the activity of the enzymes involved, the

conditions were optimised using 2-(*p*-methoxyphenyl)piperidine **6c** as a model substrate for the 6-HDNO/(*R*)-IRED reactions (Figure 78).<sup>85</sup>

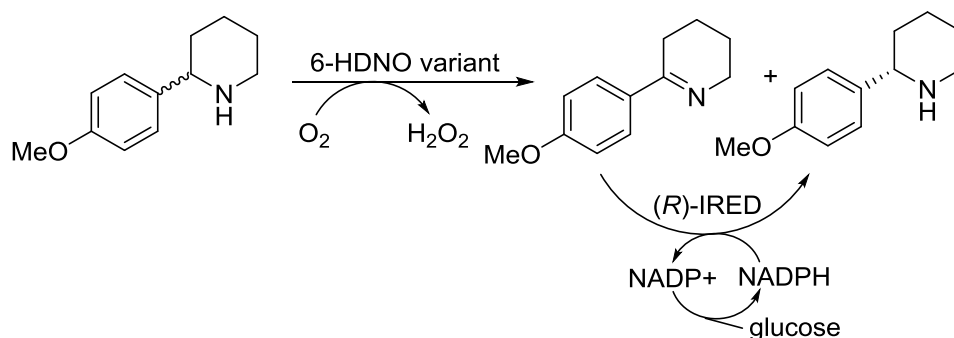


**Figure 78:** Reaction scheme showing the biocatalytic deracemisation of 2-(*p*-methoxyphenyl)piperidine **6c** employing the (*R*)-IRED in combination with 6-HDNO. **6c** was used as the model substrate for the optimisation of the biotransformation conditions.

The biotransformation optimisation work was carried out with Dr. Rachel Heath (Manchester, UK). Both enzymes were used as whole-cell biocatalysts, which for the IRED conferred the advantage of NADPH cofactor recycling by endogenous proteins within the *E. coli* cells. As the two enzymes typically operate in slightly different reaction environments, the biotransformation conditions required optimisation (Table 14). Specifically, buffer strength was found to be imperative in order to maintain the activity of the 6-HDNO. Therefore, 1 M potassium buffer was used, which was tolerated by the (*R*)-IRED when tested independently from the oxidase (Table 14, Entry 8). The presence of excess glucose, which was necessary to aid NADPH cofactor recycling for the (*R*)-IRED, was found to inhibit the activity of the 6-HDNO, so a compromise of 10 mM (2 x stoichiometric amount with respect to the final substrate concentration) was used. The pH of the buffer used was pH 7.4, which also lies midway between the two enzymes' optimum pH for operation. The H<sub>2</sub>O<sub>2</sub> generated from the AO did not appear to impede the function of the IRED. When the reduction of **5c** was examined with the (*R*)-IRED in 1 M phosphate buffer with H<sub>2</sub>O<sub>2</sub> present, full conversion was attained but this reduced to 95% conversion when the buffer strength was reduced to a concentration of 100 mM.

**Table 14:** Optimisation of conditions for deracemisation of racemic amine **6c** by combining 6-HDNO with (*R*)-IRED<sup>85</sup>

Entry	Amine or Imine	6-HDNO	( <i>R</i> )-IRED	pH	[Buffer] [M]	Glucose [mM]	Conversion [%]	<i>ee</i> [%]
1	amine	Y	Y	7.4	0.1	50	34	30
2	imine	N	Y	7.4	0.1	50	>99	>99
3	amine	Y	N	8	1	0	N/A	>99
4	amine	Y	N	7.4	1	0	N/A	>99
5	amine	Y	N	7.4	0.1	0	N/A	>99
6	amine	Y	N	7.4	0.1	50	N/A	30
7	amine	Y	N	7.4	1	50	N/A	>99
8	imine	N	Y	7.4	1	50	>99	>99
9	imine	N	Y	7.4	1	10	>99	>99
10	amine	Y	Y	7.4	1	10	>99	>99

Y = yes, N = no; Conditions: potassium phosphate buffer, 5 mM substrate, *E. coli* whole-cell biocatalyst

#### 4.2.2 Deracemisation of racemic cyclic amine 2-phenylpiperidine **6c** with 6-HDNO/(*R*)-IRED cascade

With the biotransformation conditions optimised for the deracemisation cascade, the procedure was screened and found to be applicable towards a broad panel of cyclic amines (Table 15).<sup>85</sup>

**Table 15:** One-pot deracemisation of racemic amines with 6-HDNO E350L/E352D and (*R*)-IRED<sup>85</sup>

Entry	rac-amine	Conversion [%] <sup>[b]</sup>	<i>ee</i> [%] <sup>[a]</sup>	<i>ee</i> with ( <i>R</i> )-IRED from imine [%]	Imine
1	<b>6b</b>	99	99 ( <i>S</i> )	37 ( <i>S</i> )	<b>5b</b>
2	<b>6f</b>	95	95 ( <i>S</i> )	89 ( <i>S</i> )	<b>5f</b>
3	<b>6c</b>	99	99 ( <i>S</i> )	>98 ( <i>S</i> )	<b>5c</b>
4	<b>6g</b>	99	17 ( <i>S</i> )	77 ( <i>S</i> )	<b>5g</b>
5	<b>6d</b>	99	93 ( <i>S</i> )	>98 ( <i>S</i> )	<b>5d</b>
6	-	99	99 ( <i>S</i> )	n.t.	-
7	<b>6e</b>	99	99 ( <i>S</i> )	66 ( <i>S</i> )	<b>5e</b>
8	<b>6l</b>	>99	76 (n.a.)	78 (n.a.)	<b>5l</b>
9	<b>2b</b>	71	72 ( <i>S</i> )	8 ( <i>S</i> )	<b>1b</b>
10	<b>2e</b>	99	99 ( <i>S</i> )	66 ( <i>S</i> )	<b>1e</b>

**Reaction conditions:** 5 mM substrate, 50 mg/mL amine oxidase wet whole-cells, 100 mg/mL (*R*)-IRED wet whole-cells, 1 M pH 7.4  $KP_i$  buffer, 30°C, 250 rpm, 24 h. [a] *ee* determined by chiral HPLC analysis, absolute configuration determined by comparison with previous results with (*R*)-IRED (see Section 2.2.2). [b] based on remaining imine. n.t. – not tested, n.a. = not assigned.

To demonstrate the practical applicability of this methodology, the deracemisation of 2-phenylpiperidine **6b** was carried out on a 250 mg scale, starting from the amine and the corresponding imine **5b** in parallel biotransformations. Time points were taken during the biotransformation, in order to determine if any variations existed in the two routes to the fully enantio-enriched amine product (Figure 79).

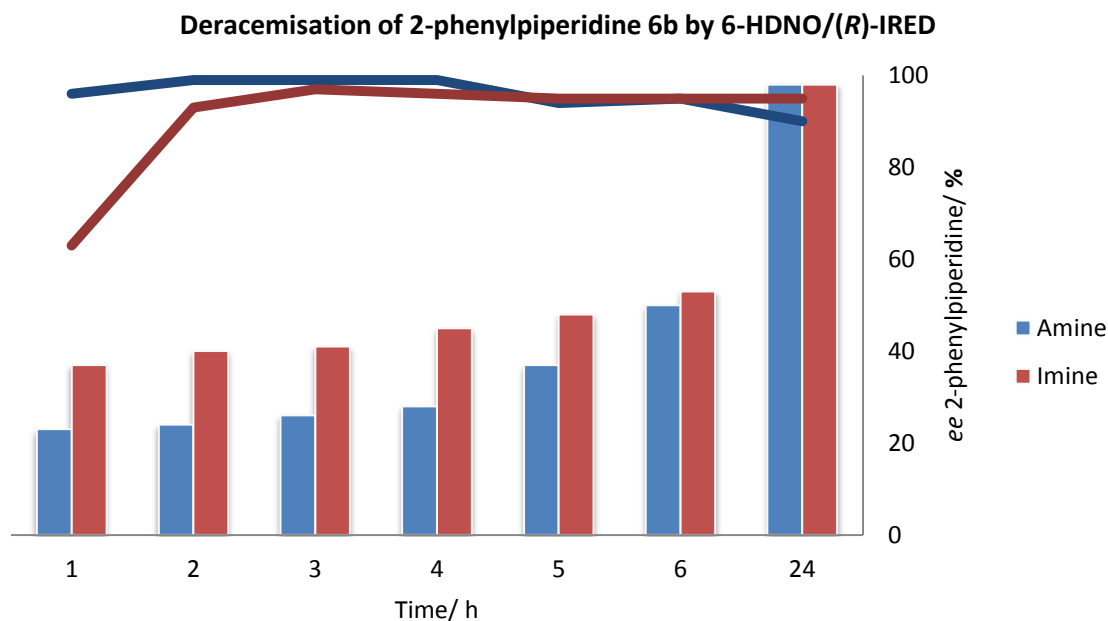


**Figure 79:** Time-point analysis of the preparative-scale deracemisation of 2-phenylpiperidine **6b** using the HDNO/(*R*)-IRED redox cascade, starting from the racemic amine (blue) and the corresponding imine hydrochloride (red). The bars on the chart represent the gradual increase in *ee* and the lines for each route represent the quantity of amine present in the reaction mixture relative to the quantity of imine.

As expected, the deracemisation reaction starting with the reduction of imine **5b** proceeds with greater *ee* of the amine product, although the amount of the amine in proportion to the imine present is lower due to incomplete reduction of the imine starting material by the (*R*)-IRED during the initial cycles. By contrast, when starting from the racemic amine the *ee* in the first few hours fails to reach the same level as seen for the reaction starting from the imine but gradually this increases through repeated cycles of oxidation/reduction, with no evidence of build-up of the imine seen. However, both deracemisation routes proceed to completion, with no imine detected in the final product after 24 h. 2-phenylpiperidine **6b** was isolated starting from the racemic amine (205 mg, 82%, *ee* >98%) and the corresponding imine hydrochloride **5b** (200 mg, 80%, *ee* >98%), demonstrating the broad applicability of this procedure for the deracemisation of racemic cyclic amines. Remarkably, it was observed that the *ee* of the amine **6b** obtained from the cascade beginning with the reduction of the imine was much higher than the *ee* of the amine obtained from the reduction of imine **5b** by the (*R*)-IRED in isolation (>98% *ee* vs. 37% *ee*, see Section 2.2.2). The technique could thus also be used as a means to 'fix' the imperfect *ee* of the amine products obtained from IRED-mediated biotransformations, in order to obtain single-enantiomer amines in excellent *ee*.

## 4.3 Amine oxidase-catalysed deracemisation of tetrahydroquinolines

### 4.3.1 Current strategies for the deracemisation of tetrahydroquinolines

Though deracemisation as a technique to access enantiomerically-pure chiral amines continues to attract significant research interest, the deracemisation of tetrahydroquinoline compounds remains relatively unexplored. The tri-phasic system developed by the Toste group (see Section 4.1.1) was also applied to 2-substituted tetrahydroquinoline compounds, though the conditions had to be adapted to the different compound class and 3 or more equivalents of the oxidant and reductant were needed in order to inhibit a second oxidation of the intermediate dihydroquinoline to the fully-aromatic quinoline, which occurred rapidly (Figure 80).

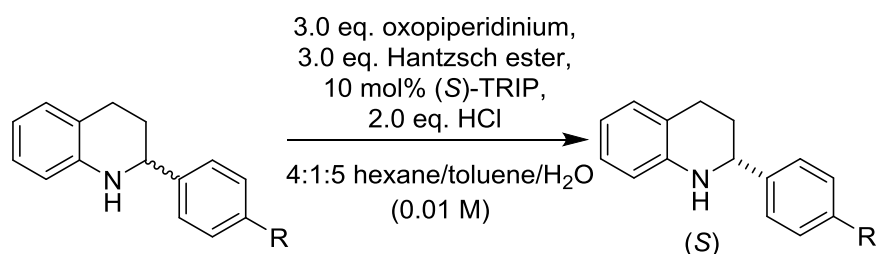


**Figure 80:** Enzymatic redox deracemisation of substituted tetrahydroquinolines, using the combined approach of an oxidant, reductant and phosphoric acid catalyst in an aqueous/organic/solid tri-phasic approach. The quantity of oxidant and reductant used for this class of compound had to be increased to 3 – 3.5 equivalents in order to inhibit a rapid second oxidation of the intermediate dihydroquinoline to the corresponding quinoline.

Reports of amine oxidase activity towards this class of compound are limited. The most prominent example originates from an FAD-dependent amine oxidase from the bacterium *Brevibacterium oxydans* IH-35A, which was isolated from the organism and found to be responsible for the initial step in the cyclohexylamine degradation pathway (Figure 68).<sup>107</sup> The heterologous expression of the gene for this (*S*)-selective cyclohexylamine oxidase (CHAO) was then achieved in *E. coli* by P. C. K. Lau's group, who also reported the success of initial chemoenzymatic deracemisation experiments on a panel of amines with the enzyme.<sup>109</sup> Although trace levels of activity were detected towards 2-methyl-1,2,3,4-tetrahydroquinoline in these experiments, it was not until G. Li *et al.* developed a triple mutation variant of the protein that the potential for deracemisation of tetrahydroquinolines by CHAO was realised.<sup>110</sup> The CHAO variant T198FL199SM226F, engineered using the iterative saturation mutagenesis technique, exhibited up to 406 times higher catalytic efficiency towards this compound class than the wild-type enzyme (Figure 81). The development of this amine oxidase biocatalyst represents the first example of a chemoenzymatic deracemisation of a tetrahydroquinoline substrate.

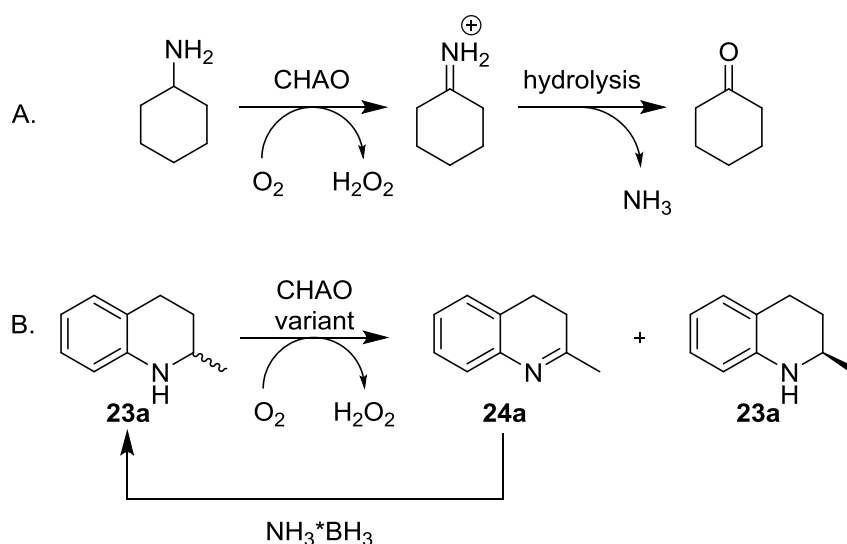


**Figure 81:** Reactions of the cyclohexylamine oxidase, showing **A.** natural function of the wild-type CHAO, which is involved in the degradation of cyclohexylamine to cyclohexanone (reaction shown takes place in buffer) and **B.** deracemisation of 2-methyl-1,2,3,4-tetrahydroquinoline **23a** by CHAO variant T198FL199SM226F.<sup>109,110</sup>

#### 4.3.2 Synthesis of tetrahydroquinoline compounds

Access to a panel of substituted tetrahydroquinolines to screen against the AOs was realised following the synthesis outlined in Figure 82. This involved the Heck-coupling of an allylic alcohol or ketone with an *o*-bromonitrobenzene, producing an *o*-butanone-substituted nitrobenzene intermediate. The conditions used in the Heck-coupling reaction were adapted from a previously reported protocol.<sup>111</sup> Where  $\alpha,\beta$ -unsaturated *o*-nitrophenylbutanone intermediates were produced from the coupling reaction, these were made exclusively as the *trans*-configuration. Reduction of the nitro group by catalytic hydrogenation with Pd/C to the corresponding aniline affected a spontaneous cyclisation/condensation reaction to afford the desired racemic tetrahydroquinoline **23** via *in-situ* reduction of the intermediate 3,4-dihydroquinoline **24**. Conveniently for  $\alpha,\beta$ -unsaturated *o*-nitrophenylbutanone intermediates, the hydrogenation step also reduced the alkene double bond in addition to the nitro group, producing the cyclic tetrahydroquinolines in a single reaction.

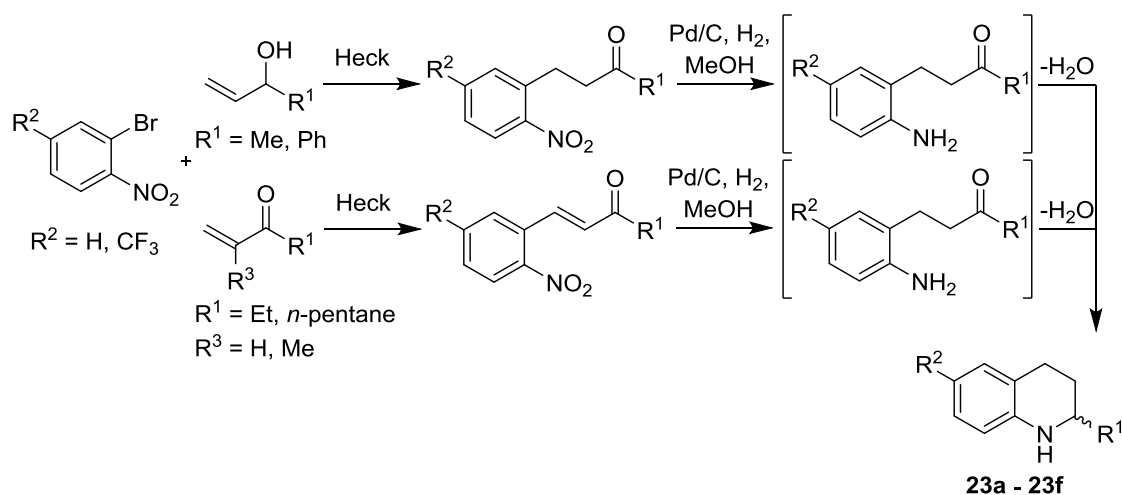


**Figure 82:** Reaction scheme displaying the synthetic route employed for the production of substituted 1,2,3,4-tetrahydroquinolines **23** – **23f**, involving a Heck-coupling reaction in the first stage, followed by catalytic hydrogenation of the intermediate using Pd/C.

The synthesis of analytical standards for the substituted 3,4-dihydroquinoline (DHQ) intermediates was also attempted. These imine-containing compounds could also be screened against the IREDs in isolation. As the 3,4-dihydroquinoline intermediate was easily reduced under the previously specified reduction conditions under molecular hydrogen, an alternative pathway using microwave-assisted transfer hydrogenation from 4-methylcyclohexene was employed (Figure 83).<sup>112</sup> The milder reduction conditions resulted in the formation of a mixture of products. Silica-gel chromatography of the crude separated the desired dihydroquinoline products **24a** and **24c**; in spite of this, the products were unstable and spontaneously underwent further reactions to afford a mixture of products, including the corresponding tetrahydroquinoline and quinoline compounds. A previous report has suggested that the dihydroquinolines undergo disproportionation reactions, resulting in equimolar amounts of the tetrahydroquinoline and fully-aromatic quinoline.<sup>113</sup> Contrary to this, following the transfer hydrogenation for the synthesis of DHQ **24**, predominantly the fully-aromatic product was isolated, suggesting further oxidation of the dihydroquinoline occurred. As the isolation of the DHQs proved to be difficult, their synthesis was not pursued further.

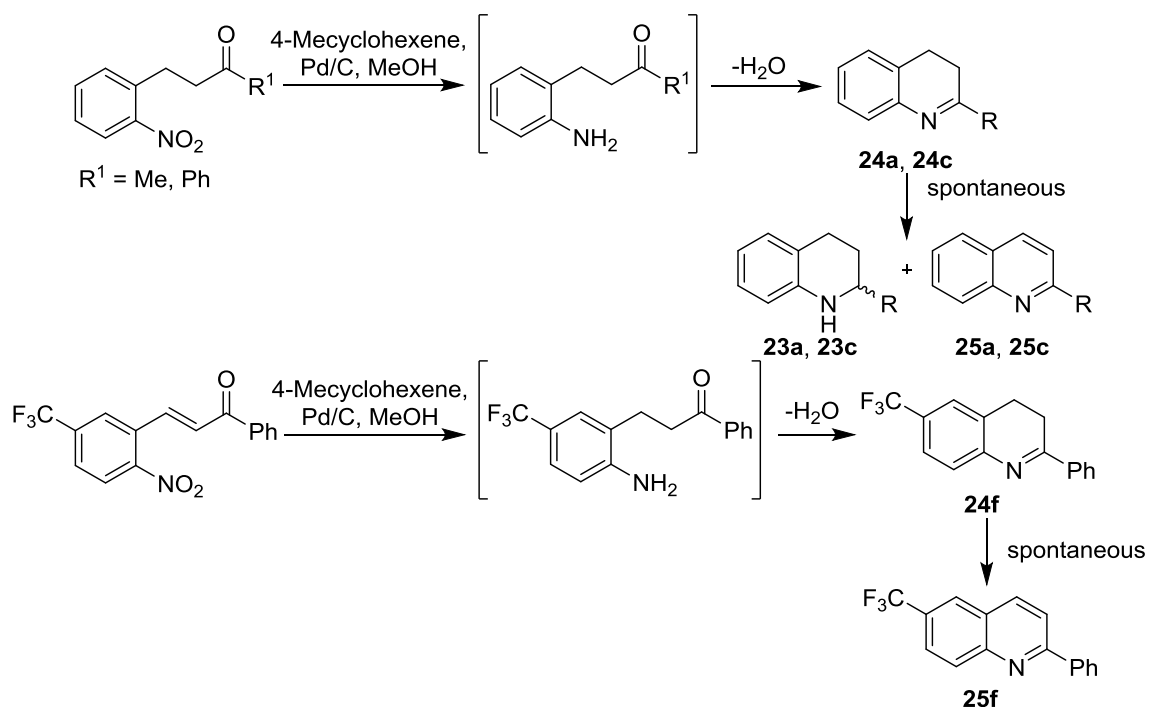


**Figure 83:** Reaction scheme displaying the synthetic route attempted for the production of substituted 3,4-dihydroquinolines **24** following on from *o*-nitrophenylbutanones. A milder microwave-assisted transfer hydrogenation, using 4-methylcyclohexene, was carried out to reduce the aromatic nitro group, which left the resulting dihydroquinoline intact. However, it was found that the dihydroquinoline product was prone to undergo disproportionation to the corresponding 1,2,3,4-tetrahydroquinoline and quinoline. In the case of **24e**, predominantly the fully-aromatic quinoline product was isolated, presumably from further oxidation of the dihydroquinoline.

Six substituted tetrahydroquinoline compounds **23a** – **23g** were screened in order to determine if deracemisation could be applied to this class of compound (Figure 84). Apart from **23a**, which was commercially available, all the other racemic THQs were chemically synthesised.

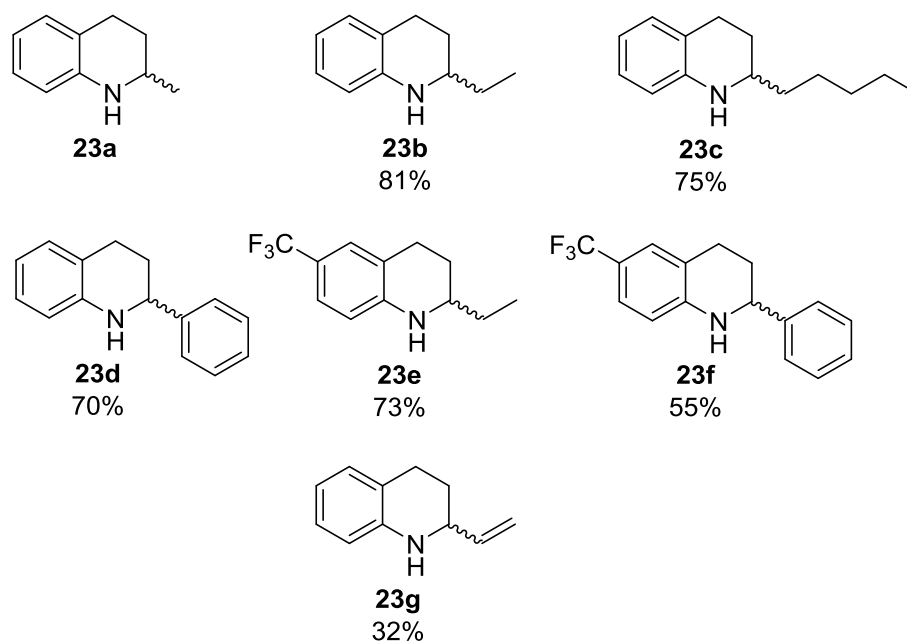


**Figure 84:** Structures of racemic tetrahydroquinolines **23a** – **23g**, which were screened for amine oxidase-catalysed deracemisation. The yields obtained for each tetrahydroquinoline are stated below the structures.

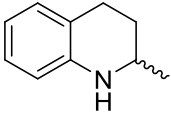
#### 4.3.3 Establishing an autoinduction protocol for the expression and growth of CHAO

The previously reported engineered variant of CHAO, CHAO T198FL199SM226F, was acquired as a synthetic gene. This gene was then sub-cloned into a pET-16b expression vector with an ampicillin antibiotic resistance, with which *E. coli* BL21 (DE3) cells were subsequently transformed with. Although the heterologous expression of CHAO had been achieved in *E. coli*, no protocol for the expression of the gene in auto-induction medium had been described. According to F. W. Studier's method, growth of bacterial cultures which use an inducible T7 expression system in auto-inducing medium achieves typically higher cell densities from the same quantity of medium as well as increasing the overall yields of the target protein by several fold.<sup>114</sup> This method for preparation of cell stocks of amine oxidases, such as 6-HDNO biocatalysts, has been used employed previously to obtain large quantities of the biocatalyst.<sup>105</sup> Therefore, for an efficient production of whole-cells for biocatalysis, the auto-induction methodology was extended to the expression of CHAO.

Expression trials for CHAO were conducted in order to determine the conditions which are best suited for the production of the protein. Three different temperatures were chosen (20°C, 25°C and 30°C) and expression of the protein was tracked by taking samples of the bacterial cell culture at 24 h intervals (24 h , 48 h and 72 h). Analysis of the cell lysate by SDS-PAGE revealed that the CHAO was overexpressed in all cell batches, producing similarly large amounts of soluble protein at all three temperatures. Finally, for

determination of the levels of activity of each cell batch, parallel biotransformations for the deracemisation of model substrate **23a** were conducted, using a wet-cell loading of 25 mg/mL, from which the relative rate of deracemisation was extracted in order to identify the batch of cells with the highest levels of activity (Table 16).

**Table 16:** Screen for the deracemisation of 2-methyl-1,2,3,4-tetrahydroquinoline **23a** with CHAO expressed at different temperatures

Substrate	R	Temperature [°C]	Time [h]	<i>ee</i> [%] <sup>[a]</sup>
	Me	20	24	91
		20	48	77
		20	72	73
		25	24	81
		25	48	92
		25	72	36
		30	24	2
		30	48	0
		30	72	0

**Reaction conditions:** 5 mM substrate, 50 mg/mL amine oxidase wet whole-cells, 50 mM NH<sub>3</sub>BH<sub>3</sub>, 1 M pH 7.4 KPi buffer, 30°C, 250 rpm, 24 h. [a] *ee* determined by comparison of peak areas of resolved enantiomers from HPLC analysis on a chiral stationary phase

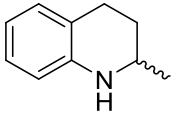
The biotransformations revealed that comparable levels of activity from the cells grown at 20°C and 25°C, though growth at 30°C appeared to produce inactive enzyme. The cell batch that achieved the highest level of deracemisation was grown at 25°C for 48 h, therefore these conditions were adopted for future preparations of the CHAO.

#### 4.3.3 Chemo-enzymatic deracemisation of THQs – AO/NH<sub>3</sub>BH<sub>3</sub>

As the tetrahydroquinoline scaffold as a target for enzymatic redox deracemisation has been relatively unexplored, model compound **23a** was screened against the available amine oxidases under chemo-enzymatic deracemisation conditions (Table 17). The CHAO variant, engineered for activity towards this particular class of compound, was able to fully deracemise **23a** in 24 h. 6-HDNO acted on the opposite enantiomer of the racemic amine,

granting access to (*S*)-**23a** in 77% *ee* after 48h. When screened against variants of MAO-N, mutant D9 was found to be active towards **23a** and lead to the accumulation of (*R*)-**23a** in 77% *ee*, whilst D11 showed only residual levels of enantio-enrichment. For this reason, D9 was used in further deracemisation experiments with the THQs.

**Table 17:** Initial screen of 2-methyl-1,2,3,4-tetrahydroquinoline **23a** with amine oxidases under deracemisation conditions

Substrate	R	Amine oxidase	<i>ee</i> [%] <sup>[a]</sup>	Absolute configuration <sup>[b]</sup>
	Me	6-HDNO	77	( <i>S</i> )
		CHAO	>98	( <i>R</i> )
		MAO-N D5	0	( <i>R</i> )
		MAO-N D9	78	( <i>R</i> )
		MAO-N D11	2	( <i>R</i> )

**Reaction conditions:** 5 mM substrate, 100 mg/mL amine oxidase wet whole-cells, 25 mM NH<sub>3</sub>BH<sub>3</sub>, 1 M pH 7.4 KP<sub>i</sub> buffer, 30°C, 250 rpm, 48 h. [a] *ee* determined by comparison of peak areas of resolved enantiomers from HPLC analysis on a chiral stationary phase; [b] absolute configuration determined by comparison of compounds retention times on HPLC to published data

During the initial screen of **23a** against the AOs, there was evidence of the formation of the fully-aromatised quinoline **24a** (identified by comparison of biotransformation samples with an authentic standard of **24a** by HPLC) in the reactions catalysed by 6-HDNO and MAO-N variants (Figure 85). Since the fully-aromatised quinoline form of the compound is inert to reduction by borane, this represented a dead-end product. The formation of the quinoline would proceed via the 3,4-dihydroquinoline intermediate, therefore in order to inhibit formation of the aromatised product a number of different water-stable borane reducing agents were screened, to try to intercept the 3,4-dihydroquinoline intermediate before any unwanted side-reaction occurred to further oxidise the compound (Table 18).

**Table 18:** Screening of various borane reducing agents in the deracemisation of 2-methyl-1,2,3,4-tetrahydroquinoline **23a** with CHAO and MAO-N D9

Entry	Reducing agent	Amine oxidase	<i>ee</i> [%] <sup>[a]</sup>	Quinoline [%] <sup>[b]</sup>
1	NH <sub>3</sub> BH <sub>3</sub> (4 eq.)	CHAO	>98	>98
2	NH <sub>3</sub> BH <sub>3</sub> (4 eq.)	MAO-N D9	84	12

3	NH <sub>3</sub> BH <sub>3</sub> (5 eq.)	CHAO	>98	68
4	NH <sub>3</sub> BH <sub>3</sub> (5 eq.)	MAO-N D9	84	0
5	NH <sub>3</sub> BH <sub>3</sub> (10 eq.)	CHAO	>98	0
6	NH <sub>3</sub> BH <sub>3</sub> (10 eq.)	MAO-N D9	83	0
7	NH <sub>3</sub> BH <sub>3</sub> (20 eq.)	CHAO	>98	0
8	NH <sub>3</sub> BH <sub>3</sub> (20 eq.)	MAO-N D9	83	0
9	<i>t</i> -BuNHBH <sub>3</sub>	CHAO	>98	29
10	<i>t</i> -BuNHBH <sub>3</sub>	MAO-N D9	47	0
11	Me <sub>2</sub> NHBH <sub>3</sub>	CHAO	>98	42
12	Me <sub>2</sub> NHBH <sub>3</sub>	MAO-N D9	83	12
13	MorpholineBH <sub>3</sub>	CHAO	>98	42
14	MorpholineBH <sub>3</sub>	MAO-N D9	84	50
15	PyridineBH <sub>3</sub>	CHAO	>98	77
16	PyridineBH <sub>3</sub>	MAO-N D9	11	81

**Reaction conditions:** 5 mM substrate, 100 mg/mL amine oxidase wet whole-cells, 50 mM reducing agent (5 eq., unless stated otherwise), 1 M pH 7.4 KPi buffer, 30°C, 250 rpm, 48 h. [a] *ee* determined by comparison of peak areas of resolved enantiomers from HPLC analysis on a chiral stationary phase; [b] quantification of the quinoline formed was based on the percentage peak area for the quinoline compound compared with the peak area for the amine on the HPLC chromatograms

The reducing agent screen revealed the NH<sub>3</sub>BH<sub>3</sub> complex to be the most effective reductant, with minimal formation of the quinoline by-product detected by HPLC in redox reactions employing CHAO or MAO-N D9. With 10 molar equivalents of reductant to substrate or greater, no quinoline product was detected so this quantity of NH<sub>3</sub>BH<sub>3</sub> reducing agent was used in all further experiments. In the deracemisation reactions **23a** employing CHAO, the use of all borane reducing agents apart from NH<sub>3</sub>BH<sub>3</sub> led to the formation of the quinoline by-product to some degree. Interestingly, when MAO-N was employed as the oxidant in the reaction, the quinoline by-product appeared to form to a lesser degree than for reactions employing CHAO, and in the case of using *t*-BuNH<sub>2</sub>BH<sub>3</sub> as the reductant, no quinoline was formed. This may be reasoned by the fact that the MAO-N enzyme has a lower activity towards THQ **23a** than the CHAO, so less of the amine is oxidised to the DHQ per unit time. Therefore, the concentration of the DHQ intermediate present in the reaction employing MAO-N D9 would effectively be lower than the analogous reaction harnessing CHAO, which would increase the chance for the reductant to intercept the DHQ before it undergoes further oxidation. For the biotransformations employing CHAO, if the oxidation of amine **23**

to the corresponding DHQ **24** occurred faster than the reduction of intermediate **24**, the DHQ concentration in the reaction mixture would effectively remain much higher and would linger in the reaction for longer, therefore increasing the likelihood for the compound to undergo oxidation to the fully-aromatic quinoline **25**.

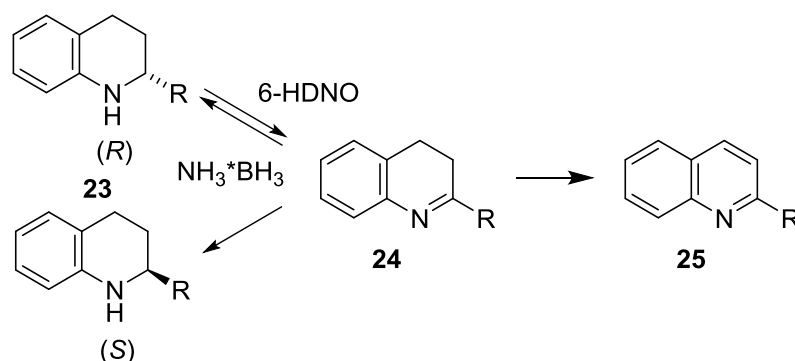
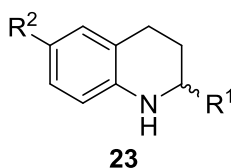


**Figure 85:** Reaction scheme for chemo-enzymatic deracemisation of substituted tetrahydroquinolines **23**, catalysed by 6-HDNO in this example, as well as the formation of the quinoline **25** via a side reaction proceeding from the dihydroquinoline **24**.

The amine oxidases were used as whole-cell biocatalysts resuspended in buffer from frozen wet cell pellets. For screening purposes, substrate concentration was kept to 5 mM. With the exception of CHAO with **23a**, the deracemisation of THQs proceeded more slowly when compared with the deracemisation of 2-substituted cyclic imines. Therefore, the reactions were allowed to continue for at least 48 h and beyond before being quenched, extracted and analysed (Table 19).

**Table 19:** Screen of 2-substituted-1,2,3,4-tetrahydroquinolines **23** with amine oxidases under chemo-enzymatic deracemisation conditions



Compound	$\text{R}^1$	$\text{R}^2$	Amine oxidase	<i>ee</i> [%] <sup>[a]</sup>	Absolute configuration <sup>[b]</sup>
<b>23a</b>	Me	H	6-HDNO	77	( <i>S</i> )
<b>23a</b>	Me	H	CHAO	>98	( <i>R</i> )
<b>23a</b>	Me	H	MAO-N D9	78	( <i>R</i> )

<b>23b</b>	Et	H	6-HDNO	69	( <i>S</i> )
<b>23b</b>	Et	H	CHAO	-[ <sup>d</sup> ]	N/A
<b>23b</b>	Et	H	MAO-N D9	45	( <i>R</i> )
<b>23c</b>	<i>n</i> -pentyl	H	6-HDNO	13	( <i>R</i> )
<b>23c</b>	<i>n</i> -pentyl	H	CHAO	70	( <i>R</i> )
<b>23c</b>	<i>n</i> -pentyl	H	MAO-N D9	13	( <i>R</i> )
<b>23d</b>	Ph	H	6-HDNO	7	(-) <sup>[c]</sup>
<b>23d</b>	Ph	H	CHAO	0	N/A
<b>23d</b>	Ph	H	MAO-N D9	0	N/A
<b>23e</b>	Et	CF <sub>3</sub>	6-HDNO	3	(-) <sup>[e]</sup>
<b>23e</b>	Et	CF <sub>3</sub>	CHAO	72	(-) <sup>[e]</sup>
<b>23e</b>	Et	CF <sub>3</sub>	MAO-N D9	0	N/A
<b>23f</b>	Ph	CF <sub>3</sub>	6-HDNO	0	N/a
<b>23f</b>	Ph	CF <sub>3</sub>	CHAO	0	N/A
<b>23f</b>	Ph	CF <sub>3</sub>	MAO-N D9	0	N/A
<b>23g</b>	CHCH <sub>2</sub>	H	6-HDNO	72	(-) <sup>[e]</sup>
<b>23g</b>	CHCH <sub>2</sub>	H	CHAO	38	(-) <sup>[e]</sup>
<b>23g</b>	CHCH <sub>2</sub>	H	MAO-N D9	29	(-) <sup>[e]</sup>

**Reaction conditions:** 5 mM substrate, 100 mg/mL amine oxidase wet whole-cells, 50 mM NH<sub>3</sub>BH<sub>3</sub>, 1 M pH 7.4 KPi buffer, 30°C, 250 rpm, 48 h. [a] *ee* determined by comparison of peak areas of resolved enantiomers from HPLC analysis on a chiral stationary phase; [b] absolute configuration determined by comparison of compounds retention times on HPLC to published data; [c] absolute configuration undetermined; [d] no amine observed following deracemisation reaction; [e] absolute configuration undetermined; however, 6-HDNO enriches the amine to the opposite configuration to CHAO and MAO-N

### Deracemisation of 2-substituted THQs

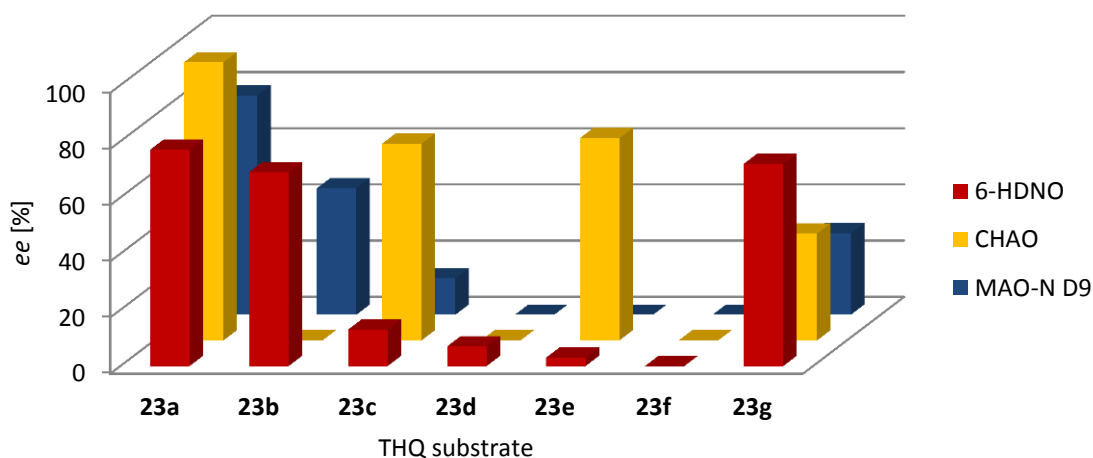


**Figure 86:** Graph showing levels of enantioenrichment achieved by 6-HDNO, CHAO and MAO-N D9 amine oxidases with each THQ. The CHAO enzyme was able to achieve higher levels of enantioenrichment overall, though the 6-HDNO showed deracemisation activity towards a broader range of THQ compounds.

The amine oxidases tolerated both alkyl and alkenyl substituents, with reasonable levels of enantio-enrichment achieved. With the 2-ethyl substituted THQ **23b**, both HDNO and MAO-N were able to enrich the amine to 69% *ee* in (*S*)-configuration and 45% *ee* in (*R*)-configuration respectively. Unusually, the amine could not be isolated from the reaction with CHAO; only the fully-aromatic quinoline could be detected in this reaction. The same result could be obtained from the stand-alone oxidation reaction in the absence of reducing agent, which suggests that the CHAO enzyme is completely non-selective with regards to oxidation of this substrate. In this instance, the DHQ presumably undergoes further oxidation to the quinoline as it remains in a high concentration in the reaction mixture. When the CF<sub>3</sub> group was introduced to the aromatic ring of the THQ in **23e**, the 6-HDNO appeared to be far less active with the THQ and a very low level on enantioenrichment was achieved. Interestingly, the CHAO enzyme displayed greater stereoselectivity with **23e** than with **23b**, with the amine enriched to 72% *ee*.

With the *n*-pentyl-substituted **23c**, which is a precursor to the tetrahydroquinoline alkaloid angustureine,<sup>115</sup> CHAO and MAO-N enriched the expected (*S*)-enantiomer amine to 70% *ee* and 13% *ee* respectively. 6-HDNO also performed comparatively with MAO-N, though the enantioselectivity of the enzyme appeared to switch as the enriched (*R*)-enantiomer amine was also obtained following deracemisation. Bulky phenyl group substituted **23d** and **23f** did not appear to be substrates for the AOs, with the exception of

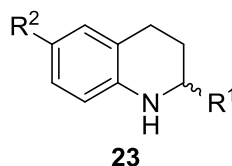
6-HDNO with **23d** where a residual amount of enantio-enrichment was detected. This also follows a previous report with the CHAO enzyme, which was unable to deracemise **23d**.<sup>110</sup> All three oxidases were able to enrich THQ **23e** bearing an allyl substituent, with HDNO (72% *ee*) outperforming CHAO and MAO-N (38% *ee* and 29% *ee*) and granting access to the opposing enantiomer.

All three enzymes showed the greatest level of enantio-enrichment with THQ **23a**. Overall, CHAO appeared to achieve the highest levels of enrichment, although the 6-HDNO showed activity and/or enantioselectivity towards a broader range of THQ compounds (Figure 86).

#### 4.3.4 Biocatalytic deracemisation/kinetic resolution of tetrahydroquinolines – with AO/IRED combination

Following the chemo-enzymatic redox reactions, the deracemisation of THQs using IREDs as the reducing agent was explored for THQs **23a** with HDNO and CHAO, **23b** with HDNO only and **23e** for CHAO only. The substrate-AO combinations were chosen as the amine oxidases had previously shown the greatest levels of enantio-enrichment with these particular THQs. The IREDs were harnessed as whole-cell biocatalysts in the reactions, which enabled cofactor recycling via endogenous proteins within the cell. As no formal selectivity has been established with the IREDs with this class of compound, each combination of IRED with the selected amine oxidase was tested. Of course, in this instance it would be entirely possible for the IRED to be paired with the AO which does not complement its selectivity *i.e.* the IRED could selectively reduce the DHQ intermediate predominantly to the amine enantiomer that is then re-oxidised by the AO. Using the same conditions as previously established for the deracemisation of 2-substituted cyclic amines (see Section 4.2.1), the deracemisation reactions were allowed to proceed for 24 h as the IRED reducing agents would no longer be active after this time (Table 20).

**Table 20:** Screen of 2-substituted-1,2,3,4-tetrahydroquinolines **23** with amine oxidases and IREDs under biocatalytic redox conditions



Compound	R <sup>1</sup>	R <sup>2</sup>	Amine oxidase	IRED	<i>ee</i> [%] <sup>[a]</sup>	Absolute configuration <sup>[b]</sup>
<b>23a</b>	Me	H	6-HDNO	( <i>R</i> )-IRED	39	( <i>S</i> )
<b>23a</b>	Me	H	6-HDNO	( <i>S</i> )-IRED	53	( <i>S</i> )
<b>23a</b>	Me	H	6-HDNO	<i>Ac</i> -IRED	83	( <i>R</i> )
<b>23a</b>	Me	H	CHAO	( <i>R</i> )-IRED	>98	( <i>R</i> )
<b>23a</b>	Me	H	CHAO	( <i>S</i> )-IRED	>98	( <i>R</i> )
<b>23a</b>	Me	H	CHAO	<i>Ac</i> -IRED	>98	( <i>R</i> )
<b>23b</b>	Et	H	6-HDNO	( <i>R</i> )-IRED	34	( <i>S</i> )
<b>23b</b>	Et	H	6-HDNO	( <i>S</i> )-IRED	46	( <i>S</i> )
<b>23b</b>	Et	H	6-HDNO	<i>Ac</i> -IRED	71	( <i>R</i> )
<b>23e</b>	Et	CF <sub>3</sub>	CHAO	( <i>R</i> )-IRED	89	(-) <sup>[c]</sup>
<b>23e</b>	Et	CF <sub>3</sub>	CHAO	( <i>S</i> )-IRED	60	(-) <sup>[c]</sup>
<b>23e</b>	Et	CF <sub>3</sub>	CHAO	<i>Ac</i> -IRED	60	(-) <sup>[c]</sup>

**Reaction conditions:** 5 mM substrate, 100 mg/mL amine oxidase wet whole-cells, 100 mg/mL IRED wet whole-cells, 10 mM glucose, 1 M pH 7.4 KP<sub>i</sub> buffer, 30°C, 250 rpm, 24 h. [a] *ee* determined by comparison of peak areas of resolved enantiomers from HPLC analysis on a chiral stationary phase; [b] absolute configuration determined by comparison of compounds retention times on HPLC to published data; [c] absolute configuration undetermined

For **23a**, a significant quantity of the aromatic 2-methylquinoline was present in all reactions with 6-HDNO and CHAO, suggesting that the DHQ was not intercepted fast enough before formation of the quinoline proceeded. 6-HDNO in combination with *Ac*-IRED produced the opposite enantiomer amine, signalling the selectivity of the IRED as (*R*)-selective for this particular substrate and overriding the 6-HDNO's own enantioselectivity to enrich the enantiomer that is oxidised. This was also the case with the 6-HDNO in combination with *Ac*-IRED with **23b**, where again the opposite (*R*)-configuration product was obtained. In both instances, a higher *ee* of the resulting amine was also achieved when compared with NH<sub>3</sub>BH<sub>3</sub> used as a reducing agent.

CHAO in combination with all three IREDs produced the expected (*R*)-enantiomer in all cases with **23a**, clearly demonstrating the higher level of activity of the oxidase than the IREDs towards this particular compound. With **23e** as a substrate, remarkably all three CHAO-IRED combinations produced enriched amines with very little quinoline present in the reaction mixture, implying that the THQ itself is a better substrate for the three IREDs. In particular, both the (*R*)- and (*S*)-IREDs in combination with the CHAO produced amines in excellent *ee*, outperforming  $\text{NH}_3\text{BH}_3$  as a reductant in both cases.

#### 4.4 Deracemisation of indolines

##### 4.4.1 Brief background on chiral indolines and synthesis of indolines

Chiral indolines, such as analogues of 2-methylindoline **26a**, can be found in molecules with diverse biological activities.<sup>116</sup> Therefore, their preparation in single-enantiomer form is very desirable. Current methods utilised for the preparation of 2-substituted indolines in single-enantiomer form include a lipase-catalysed kinetic resolution of the racemic indolines, where a range of structurally-diverse 2-substituted racemic indolines were resolved by selective acylation of one of the enantiomers. Of course, this strategy carried the expected drawback of a limited 50% final yield of the remaining enantiomer of the indoline (Figure 87).<sup>117</sup>

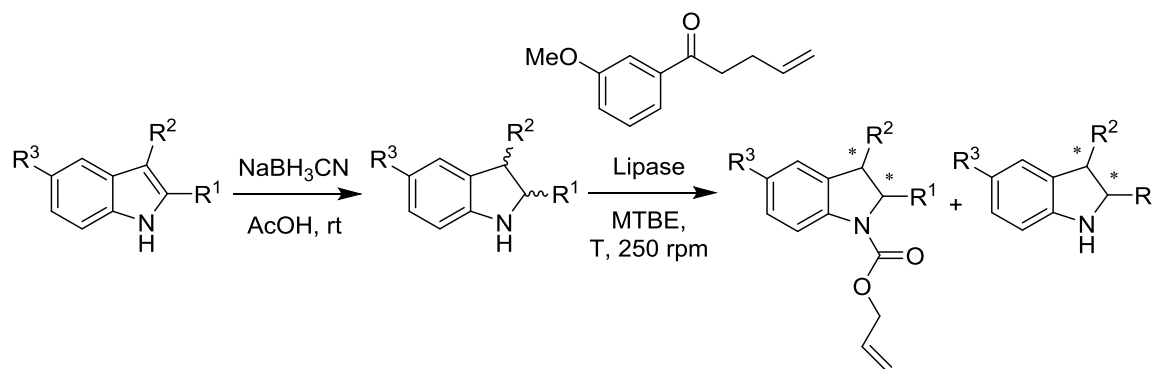


**Figure 87:** Scheme for the chemo-enzymatic preparation of chiral indolines, by effecting a reduction of the corresponding indole using  $\text{NaCNBH}_4$  in acetic acid in the first step and then carrying out a lipase-catalyzed acylation reaction on the racemic indoline.<sup>117</sup>

Due to the success of applying chemo-enzymatic and biocatalytic deracemisation to racemic tetrahydroquinolines, the five-membered bicyclic analogues, 2-substituted indolines, were investigated as possible targets for enantioenrichment. Racemic indolines **26b** – **26d** were synthesised via reduction of the corresponding indoles **28b** – **28d** by refluxing in  $\text{Sn}$  with

conc. HCl and EtOH (Figure 88).<sup>118</sup> The reductions proceeded efficiently and following purification of the crude product on silica, the racemic indolines were obtained in fairly high yield (for details relating to the synthesis of the racemic indolines **26b** – **26d**, refer to Experimental Section 7.3.7).

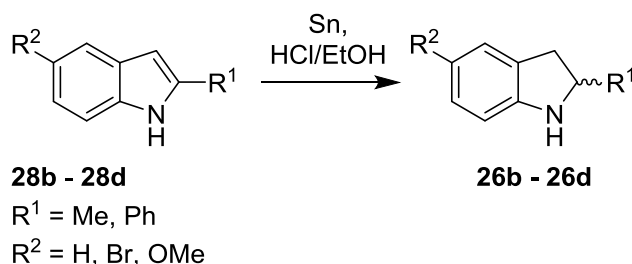


**Figure 88:** Synthesis of racemic indolines **26b** – **26d** via reduction of the corresponding indoles **28b** – **28d**, using Sn in conc. HCl/EtOH mixture under reflux conditions.<sup>118</sup>

The investigation of the 2-substituted indolines as targets for deracemisation was undertaken following a similar approach to that carried out with the 2-substituted THQs. Indolines **26a** – **26e** were screened against the amine oxidases in combination with  $\text{NH}_3\text{BH}_3$  as a reducing agent and then subsequently with IREDs as the reductant in the redox cascade reactions (Figure 89). The same reaction conditions established for the screening of the THQs was utilised for the deracemisation of the indoline compounds.

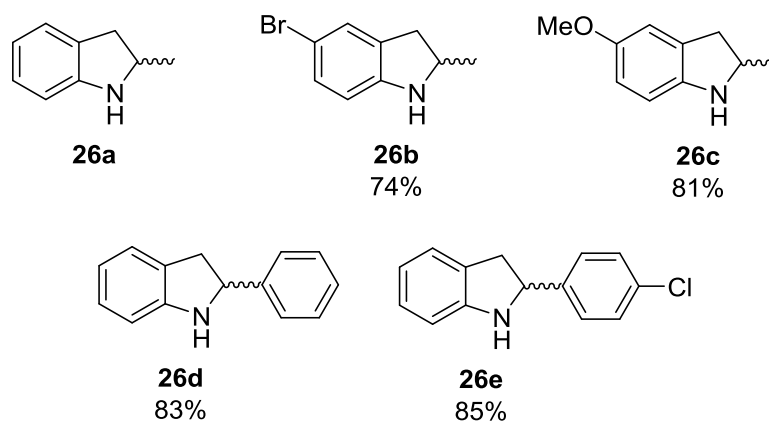


**Figure 89:** Structures of substituted indolines **26a** – **26e**. Indolines **26b** – **26e** were synthesised by reducing their corresponding indoles. The yields obtained are given below the structures.

#### 4.4.2 Kinetic resolution of indolines

Preliminary screening results of the chemo-enzymatic AO/NH<sub>3</sub>BH<sub>3</sub> cascade with racemic indoline **26a** suggested formation of a by-product from the reaction in a significant quantity. This was identified as the fully-aromatic 2-methylindole by comparison of the HPLC chromatogram of the authentic standard of 2-methylindole to the HPLC chromatogram of the biotransformation sample. In a similar fashion to the spontaneous oxidation of the DHQ intermediate in the deracemisation reactions of THQs, a competing side reaction following oxidation of the indoline had occurred: thermodynamically-driven tautomerisation of the oxidised 3*H*-indole intermediate to produce the corresponding indole. Once at the indole stage, reduction would no longer occur and the deracemisation cycle would be broken (Figure 90).

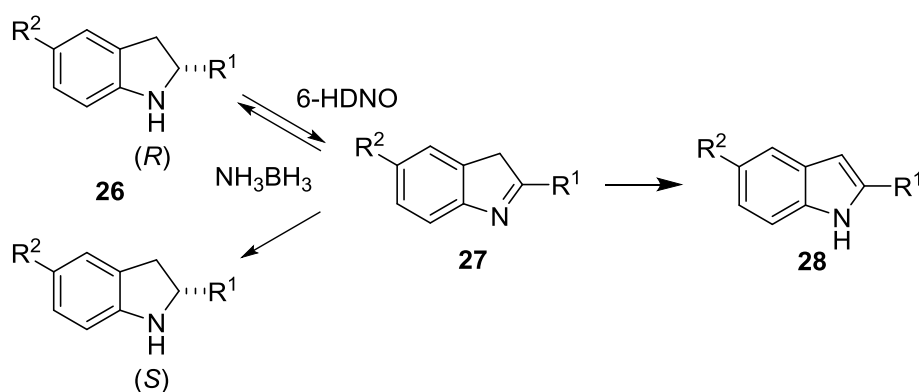


**Figure 90:** Reaction scheme for chemo-enzymatic deracemisation of 2-substituted indolines **26a** – **26e**, catalysed by 6-HDNO in the example shown. Following oxidation of the indoline, the 3*H*-indole **27** rapidly underwent tautomerisation to afford the fully-aromatic indole **28**.

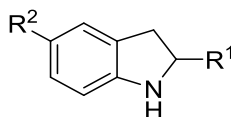
To inhibit tautomerisation of the oxidised indoline to the indole, the redox reaction employing 6-HDNO and NH<sub>3</sub>BH<sub>3</sub> as a reducing agent was screened under a range of different pHs (pH 6.8 to pH 8.2 in increments of 2) as well as varying the stoichiometric concentration of NH<sub>3</sub>BH<sub>3</sub> reducing agent (2 – 50 stoichiometric equivalents relative to the substrate). However, the screen did not yield conditions which were less favourable for 3*H*-indole-indole tautomerism, as the indole by-product **28** was present in all biotransformation reactions.

As the oxidation and subsequent tautomerisation of the indoline to the indole during the redox process would ultimately represent a net change in the composition of the amine, the process cannot be referred to as a deracemisation. Instead, it would be classed as a dynamic kinetic resolution reaction. By definition, the DKR process combines an enantioselective transformation (selective oxidation of the indoline by the amine oxidase)

with an *in-situ* racemisation process (non-selective reduction of the 3*H*-indole). In this process, both enantiomers of the amine can theoretically be converted to the product, which happens to be one enantiomer of the starting material in this case. The process would not be considered a kinetic resolution due to the presence of an *in-situ* racemisation process, which should ultimately drive the formation of the (single enantiomer) amine product beyond 50%. It is important to note that any incidence of the indole by-product from this process represents a loss of overall yield of the amine product.

The chemo-enzymatic DKR approach, using the conditions set out for the deracemisation of the 2-substituted THQs, was applied despite the aforementioned issue (Table 21 and Figure 91).

**Table 21:** Screen of 2-substituted-indolines **26** with amine oxidases under chemo-enzymatic DKR conditions



Compound	R <sup>1</sup>	R <sup>2</sup>	Amine oxidase	<i>ee</i> [%] <sup>[a]</sup>	Absolute configuration <sup>[b]</sup>
<b>26a</b>	Me	H	6-HDNO	9	( <i>R</i> )
<b>26a</b>	Me	H	CHAO	– <sup>[c]</sup>	N/A
<b>26a</b>	Me	H	MAO-N D9	90	( <i>S</i> )
<b>26b</b>	Me	Br	6-HDNO	8	( <i>S</i> )
<b>26b</b>	Me	Br	CHAO	>98	( <i>R</i> )
<b>26b</b>	Me	Br	MAO-N D9	8	( <i>R</i> )
<b>26c</b>	Me	OMe	6-HDNO	40	( <i>S</i> )
<b>26c</b>	Me	OMe	CHAO	>98	( <i>R</i> )
<b>26c</b>	Me	OMe	MAO-N D9	97	( <i>R</i> )
<b>26d</b>	Ph	H	6-HDNO	70	( <i>S</i> )
<b>26d</b>	Ph	H	CHAO	0	(–)
<b>26d</b>	Ph	H	MAO-N D9	5	( <i>R</i> )
<b>26e</b>	<i>p</i> -ClPh	H	6-HDNO	11	( <i>S</i> )
<b>26e</b>	<i>p</i> -ClPh	H	CHAO	0	(–)

<b>26e</b>	<i>p</i> -CIPh	H	MAO-N D9	5	( <i>R</i> )
------------	----------------	---	----------	---	--------------

**Reaction conditions:** 5 mM substrate, 100 mg/mL amine oxidase wet whole-cells, 50 mM NH<sub>3</sub>BH<sub>3</sub>, 1 M pH 7.4 KP; buffer, 30°C, 250 rpm, 48 h. [a] *ee* determined by comparison of peak areas of resolved enantiomers from HPLC analysis on a chiral stationary phase; [b] absolute configuration determined by comparison of compounds retention times on HPLC to published data; [c] amine could not be detected in the reaction following deracemisation of **26a**, only the corresponding indole was present.

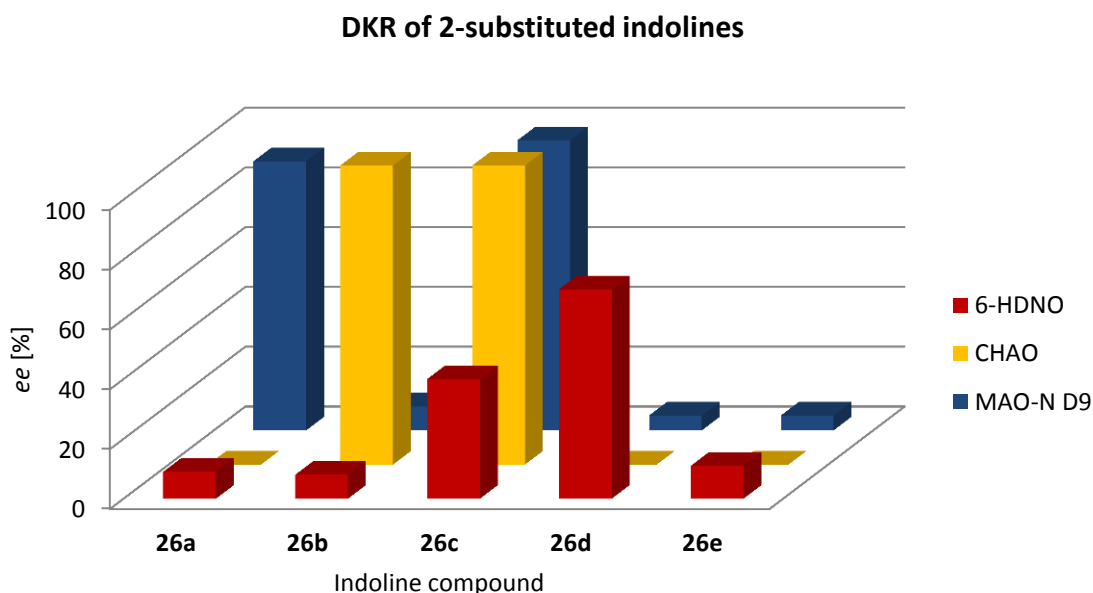


**Figure 91:** Graph showing levels of enantioenrichment achieved by 6-HDNO, CHAO and MAO-N D9 amine oxidases in the chemo-enzymatic DKR of 2-substituted indolines **26a** – **26e**. 6-HDNO was able to enantio-enrich all indoline compounds tested to some extent, although only CHAO and MAON D9 were able to almost completely enrich certain indoline compounds. For details of the configuration of the enriched amine products, refer to Table 21.

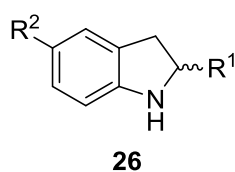
The three oxidases showed varying levels of DKR potential for indolines **26a** – **26e**. For 2-methylindoline **26a**, 6-HDNO and MAO-N enriched opposing enantiomers of the amine, although MAO-N achieved a greater DKR of the amine by enriching the (*S*)-enantiomer to 90% *ee*. Unusually, indoline **26a** could not be extracted from the biotransformation with CHAO, indicating that a complete transformation of the starting amine had taken place. In addition, only the corresponding indole was detected on the HPLC chromatogram of the biotransformation sample, implying that both enantiomers of the starting indoline had been oxidised. This suggests that CHAO is unable to selectively oxidise **26a**. With the introduction of a bromo- or methoxy- substituent on the aromatic ring portion of the indoline structure, CHAO was able to successfully enrich indolines **26b** and **26c** after 48h to produce the (*R*)-enantiomer amine in >98% *ee*. In addition, MAO-N also was able to carry out a DKR of methoxy-bearing indoline **26c** with the same selectivity as CHAO to produce (*R*)-**26c** in 97% *ee*. On the other hand, 6-HDNO appeared to act on the opposite enantiomers of **26b**

and **26c** to CHAO and MAO-N, although the *ee* upgrade of the (*S*)-enantiomer amine from these processes was modest by comparison.

Aromatic-substituted indolines **26d** and **26e** proved to be challenging substrates for the (*S*)-selective AOs, with CHAO unable to perform any resolution of the two enantiomers of these compounds. As neither an enantio-enrichment of the amine nor indole by-product was detected for the reaction of CHAO with **26d** and **26e**, this implies that CHAO is unable to display any oxidase activity towards these compounds. 6-HDNO displayed more promising results, with (*S*)-2-phenylindoline **26d** enriched to an impressive 70% *ee*.

The formation of the indole by-product was observed in all chemo-enzymatic DKR reactions conducted and was especially pronounced in the chromatograms from reactions with aromatic-substituted indoles **26d** and **26e**. A plausible explanation would be that the increased aromaticity of these systems would actively drive tautomerisation of the 3*H*-indoles to the fully-aromatic indole, as the phenyl/substituted phenyl group would be conjugated with the rest of the indole ring system. However, it is difficult to say whether the larger peak areas for the indole by-products from indolines **26d** and **26e** are representative of an increase in tautomerisation of the 3*H*-indole to the indole, or if the large peak areas are merely a consequence of the increased conjugation of the entire aromatic system from the inclusion of a phenyl/substituted phenyl substituent. As the UV response between the indoline and fully-aromatic indole would be very different on the HPLC UV-detector chromatograms, accurate quantitative analysis of the degree of tautomerisation of the 3*H*-indole to the indole occurring (and therefore the yield of amine product from the reaction) cannot be carried out.

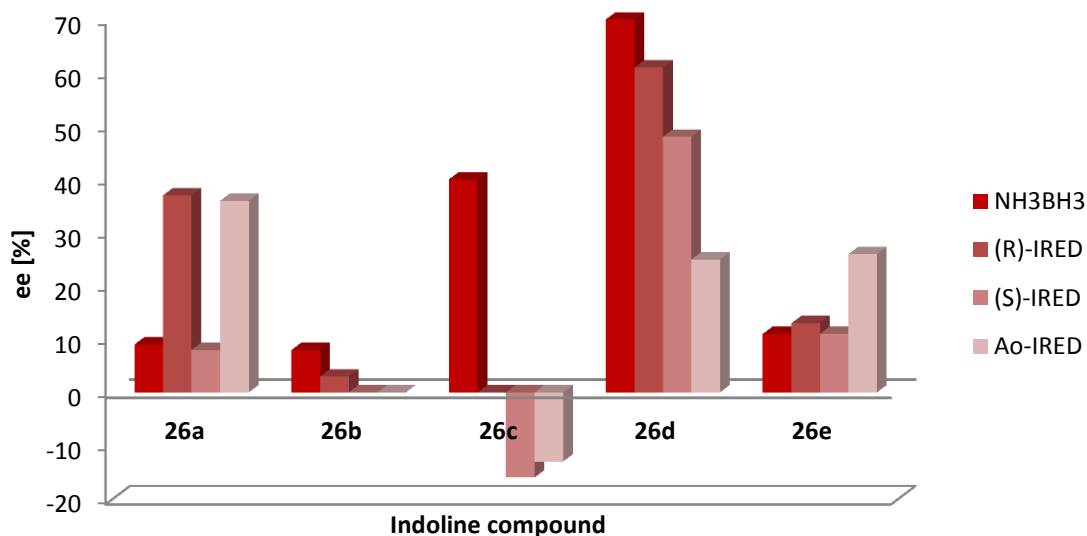
The DKR of racemic indolines **26a** – **26e** was subsequently tested with the previously established AO/IRED redox cascade, in order to determine if the fully-biocatalytic redox system could be applied to this class of compound. It was hoped that the IREDs could intercept and reduce the 3*H*-indole intermediate at a faster rate than the rate of tautomerisation of the 3*H*-indole to the indole. As 2-substituted-3*H*-indoles had not been investigated as IRED substrates previously, the enzymatic DKR was carried out in a wide screen by employing all combinations of amine oxidase and imine reductase (Table 22 – 24 and Figure 92 - 94).

**Table 22:** DKR of 2-substituted indolines **26** with 6-HDNO/IRED cascade

Compound	R <sup>1</sup>	R <sup>2</sup>	IRED	ee [%] <sup>[a]</sup>	Absolute configuration <sup>[b]</sup>
			( <i>R</i> )-IRED	37	( <i>R</i> )
<b>26a</b>	Me	H	( <i>S</i> )-IRED	8	( <i>R</i> )
			<i>Ao</i> -IRED	36	( <i>R</i> )
			( <i>R</i> )-IRED	3	( <i>S</i> )
<b>26b</b>	Me	Br	( <i>S</i> )-IRED	0	N/A
			<i>Ao</i> -IRED	0	N/A
			( <i>R</i> )-IRED	0	N/A
<b>26c</b>	Me	OMe	( <i>S</i> )-IRED	16	( <i>R</i> )
			<i>Ao</i> -IRED	13	( <i>R</i> )
			( <i>R</i> )-IRED	61	( <i>S</i> )
<b>26d</b>	Ph	H	( <i>S</i> )-IRED	48	( <i>S</i> )
			<i>Ao</i> -IRED	25	( <i>S</i> )
			( <i>R</i> )-IRED	13	( <i>S</i> )
<b>26e</b>	<i>p</i> -ClPh	H	( <i>S</i> )-IRED	11	( <i>S</i> )
			<i>Ao</i> -IRED	26	( <i>S</i> )

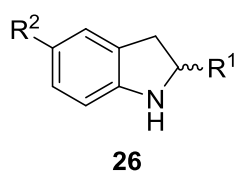
**Reaction conditions:** 5 mM substrate, 100 mg/mL 6-HDNO wet whole-cells, 100 mg/mL IRED wet whole-cells, 10 mM glucose, 1 M pH 7.4 KPi buffer, 30°C, 250 rpm, 24 h. [a] ee determined by comparison of peak areas of resolved enantiomers from HPLC analysis on a chiral stationary phase; [b] absolute configuration determined by comparison of compounds retention times on HPLC to published data

### DKR of 2-substituted indolines with 6-HDNO/IRED



**Figure 92:** Graph showing the levels of enantioenrichment achieved by the 6-HDNO/IRED biocatalytic redox cascade in 24 h in comparison with the value attained from the chemo-enzymatic redox cascade of 6-HDNO/NH<sub>3</sub>BH<sub>3</sub> in 48 h. Subjection of substrate **26c** to the biocatalytic redox cascade in combination with the (*S*)- and *Ao*-IREDs produced an inversion of stereochemistry for the enriched amine when compared with the analogous chemo-enzymatic redox process. For details of the configuration of the enriched amine products, refer to Table 22.

In general, the combination of 6-HDNO and the IREDs did not provide any significant advantage over using NH<sub>3</sub>BH<sub>3</sub> as the reducing agent of choice for the enantio-enrichment of 2-substituted indolines. All screening biotransformations employing 6-HDNO with IREDs produced some indole by-product, indicating either the indolines are poor substrates for the IREDs as they are unable to reduce the forming 3*H*-indole faster than the rate of tautomerisation of the oxidation product to its corresponding indole, or that the selectivity of the IRED in question does not match that of the 6-HDNO enzyme. In this instance, a constant cycle of oxidation-reduction of the substrate indoline occurs, increasing the concentration of 3*H*-indole in the reaction mixture which will ultimately tautomerise to the more stable indole form. In spite of this, 6-HDNO paired with the (*R*)-IRED or *Ao*-IRED enriched amine **26a** to 37% and 36% *ee* respectively, whereas (*S*)-**26e** was obtained from the combination of 6-HDNO and *Ao*-IRED in >two-fold increase of 26% over the chemo-enzymatic deracemisation equivalent process. Interestingly, **26c** was obtained in the opposite configuration to the chemoenzymatic deracemisation product with the use of (*S*)-IRED and *Ao*-IRED.

**Table 23:** DKR of 2-substituted indolines **26** with CHAO/IRED cascade

Compound	R <sup>1</sup>	R <sup>2</sup>	IRED	ee [%] <sup>[a]</sup>	Absolute configuration <sup>[b]</sup>
			( <i>R</i> )-IRED	- <sup>[c]</sup>	N/A
<b>26a</b>	Me	H	( <i>S</i> )-IRED	- <sup>[c]</sup>	N/A
			<i>Ac</i> -IRED	- <sup>[c]</sup>	N/A
			( <i>R</i> )-IRED	>98	( <i>R</i> )
<b>26b</b>	Me	Br	( <i>S</i> )-IRED	>98	( <i>R</i> )
			<i>Ac</i> -IRED	>98	( <i>R</i> )
			( <i>R</i> )-IRED	>98	( <i>R</i> )
<b>26c</b>	Me	OMe	( <i>S</i> )-IRED	>98	( <i>R</i> )
			<i>Ac</i> -IRED	>98	( <i>R</i> )
			( <i>R</i> )-IRED	12	( <i>R</i> )
<b>26d</b>	Ph	H	( <i>S</i> )-IRED	11	( <i>R</i> )
			<i>Ac</i> -IRED	4	( <i>R</i> )
			( <i>R</i> )-IRED	0	N/A
<b>26e</b>	<i>p</i> -ClPh	H	( <i>S</i> )-IRED	0	N/A
			<i>Ac</i> -IRED	0	N/A

**Reaction conditions:** 5 mM substrate, 100 mg/mL CHAO wet whole-cells, 100 mg/mL IRED wet whole-cells, 10 mM glucose, 1 M pH 7.4 KPi buffer, 30°C, 250 rpm, 24 h. [a] ee determined by comparison of peak areas of resolved enantiomers from HPLC analysis on a chiral stationary phase; [b] absolute configuration determined by comparison of compounds retention times on HPLC to published data; [c] amine could not be detected in the reaction following deracemisation of **26a**, only the corresponding indole **28a** was present.

### DKR of 2-substituted indolines with CHAO/IRED

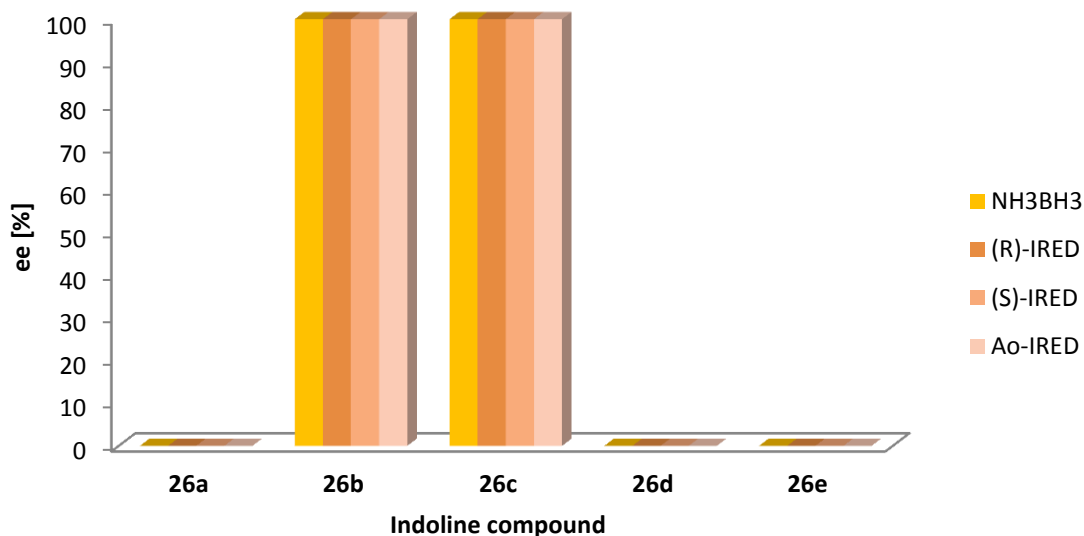


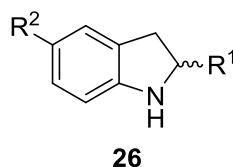
**Figure 93:** Graph showing the levels of enantioenrichment achieved by the CHAO/IRED biocatalytic redox cascade in 24 h in comparison with the value attained from the chemo-enzymatic redox cascade of CHAO/NH<sub>3</sub>BH<sub>3</sub> in 48 h. For details of the configuration of the enriched amine products, refer to Table 23.

Neither amine nor indole was detected from the biotransformation of indoline **26a** with CHAO/IRED, mirroring the result obtained with CHAO in combination with NH<sub>3</sub>BH<sub>3</sub>. Indolines **26d** and **26e** was also left intact following the biotransformation in a racemic mixture, indicating an inability of CHAO to oxidise the compounds at all. Previously, when CHAO was coupled with NH<sub>3</sub>BH<sub>3</sub>, an encouraging level of activity was displayed in the full chemo-enzymatic kinetic resolution of the two enantiomers of indolines **26b** and **26c**. Single enantiomers of the amines **26b** and **26c** were again detected following the biotransformation, regardless of the IRED enzyme used with the CHAO. Compared to the levels of enantio-enrichment seen with the HDNO/IRED combination, attaining a full kinetic resolution (i.e. single enantiomer of the amine) with **26b** and **26c** suggests a high level of activity of the CHAO enzyme towards the two particular amines. In addition, when CHAO was coupled with the (*R*)-IRED enzyme with **26b** and **26c**, the corresponding indolines were not detected from the biotransformation mixtures. These transformations represent true deracemisation reactions, as the net quantity of the amines would remain unchanged in the reaction mixtures since no conversion to another compound (the indole or otherwise) appears to have taken place.

For the remaining CHA/IRED biotransformations with **26b** and **26c**, a significantly larger proportion of the indole by-products appeared to form than was observed in the equivalent chemo-enzymatic redox process, from comparison of the percentage peak area

of the indole to the corresponding amine. This suggests that the (*R*)- and (*S*)-IREDs are not very active towards these compounds, or that the IREDs are simply reducing the oxidised 3*H*-indole intermediate to the enantiomer that is oxidised by CHAO in a greater proportion.

**Table 24:** DKR of 2-substituted indolines **26** with MAO-N D9/IRED cascade



Compound	R <sup>1</sup>	R <sup>2</sup>	IRED	<i>ee</i> [%] <sup>[a]</sup>	Absolute configuration <sup>[b]</sup>
<b>26a</b>	Me	H	( <i>R</i> )-IRED	75	( <i>R</i> )
			( <i>S</i> )-IRED	32	( <i>R</i> )
			<i>Ao</i> -IRED	68	( <i>R</i> )
<b>26b</b>	Me	Br	( <i>R</i> )-IRED	2	( <i>R</i> )
			( <i>S</i> )-IRED	3	( <i>R</i> )
			<i>Ao</i> -IRED	3	( <i>R</i> )
<b>26c</b>	Me	OMe	( <i>R</i> )-IRED	15	( <i>R</i> )
			( <i>S</i> )-IRED	0	N/A
			<i>Ao</i> -IRED	14	( <i>R</i> )
<b>26d</b>	Ph	H	( <i>R</i> )-IRED	19	( <i>S</i> )
			( <i>S</i> )-IRED	37	( <i>R</i> )
			<i>Ao</i> -IRED	14	( <i>R</i> )
<b>26e</b>	<i>p</i> -CIPh	H	( <i>R</i> )-IRED	0	N/A
			( <i>S</i> )-IRED	0	N/A
			<i>Ao</i> -IRED	0	N/A

**Reaction conditions:** 5 mM substrate, 100 mg/mL MAO-N D9 wet whole-cells, 100 mg/mL IRED wet whole-cells, 10 mM glucose, 1 M pH 7.4 KP<sub>i</sub> buffer, 30°C, 250 rpm, 24 h. [a] *ee* determined by comparison of peak areas of resolved enantiomers from HPLC analysis on a chiral stationary phase; [b] absolute configuration determined by comparison of compounds retention times on HPLC to published data

### DKR of 2-substituted indolines with MAO-N D9/IRED

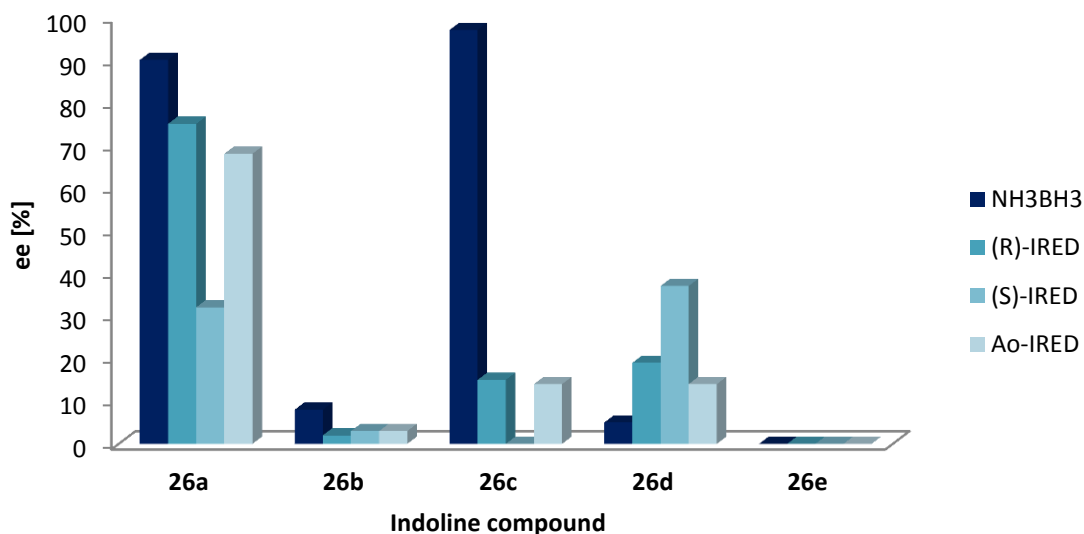


**Figure 94:** Graph showing levels of enantioenrichment achieved by the MAO-N D9/IRED biocatalytic redox cascade in 24 h in comparison with the value attained from the chemo-enzymatic redox cascade of MAO-N D9/NH<sub>3</sub>BH<sub>3</sub> in 48 h. For details of the configuration of the enriched amine products, refer to Table 24.

MAO-N in combination with the IREDs did not afford any significant advantage over using the non-selective chemical reducing agent in the process, producing amines which were not enriched to the same levels (except in the case of **26d**). Enantio-enrichment of 2-methylindoline **26a** to (*S*)-**26a** proceeded with comparable results when the oxidase was combined with the (*R*)-IRED and *Ao*-IRED. Surprisingly, the enrichment of (*R*)-**26d** proceeded with slight improvement with the IREDs.

#### 4.5 Conclusions and outlook

Owing to the theoretical yield of >99% for enantio-enrichment reactions, as well as the convenience of handling an enantiomerically-pure product that possesses the same structure as the starting material, deracemisation strategies are highly desirable for the production of chiral amines. Although challenging to implement chemically, chemo-enzymatic redox cascades have been previously used to great success and the investigation in this report has taken the work a step further by demonstrating a fully biocatalytic redox cascade for deracemisation of cyclic amines. This system, employing an amine oxidase with an IRED, was successfully demonstrated in the deracemisation of 2-phenylpiperidine **6b** by 6-HDNO and (*R*)-IRED enzymes. The reaction was completed on a preparative-scale, further

demonstrating the applicability of this system for the synthesis of practically-useful quantities of chiral amines.

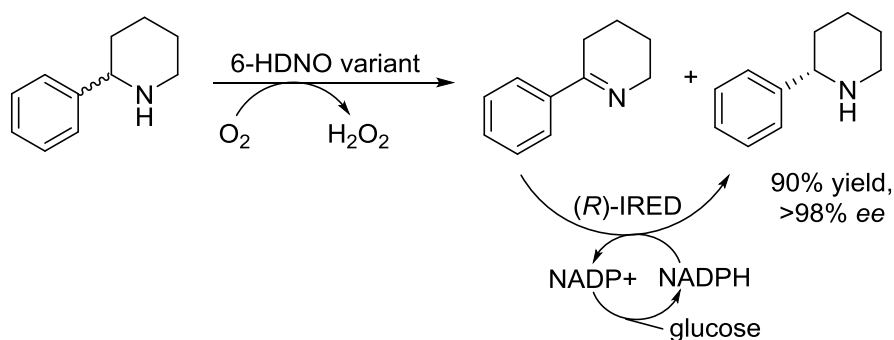


**Figure 95:** Prep-scale deracemisation of 2-phenylpiperidine **6b** with 6-HDNO and (*R*)-IRED

The deracemisation of tetrahydroquinolines remains an area of research where very few strategies, by chemical or biocatalytic means, are available to explore. The chemo-enzymatic deracemisation strategy employing an amine oxidase in combination with the non-selective chemical reducing agent  $\text{NH}_3\text{BH}_3$  was applied to this class of compounds, using a range of amine oxidases including (*S*)-selective MAO-N and CHAO enzymes as well as the enantiocomplementary (*R*)-amine oxidase 6-HDNO. For the CHAO variant, which was previously engineered for activity towards 2-methyl-1,2,3,4-tetrahydroquinoline **23a**, conditions for expression of the gene for the protein in auto-induction medium was established, for a more efficient means of producing of the biocatalyst.

Previously unseen activity with the MAO-N D9 variant was detected towards 2-substituted THQs. Although the THQs proved to be challenging substrates for the amine oxidases, with moderate levels of enantio-enrichment achieved after 48 h, the enzymes were broadly tolerant of this class of compound. A competing side reaction involving further oxidation of the dihydroquinoline intermediate formed from by the AO oxidation of THQs was observed in the deracemisation reaction, although tweaking the molar equivalent of the  $\text{NH}_3\text{BH}_3$  reducing agent with regards to the substrate concentration appeared to inhibit this side-reaction in most cases. When the fully biocatalytic redox deracemisation was applied to THQs by combining the AOs with IRED enzymes, limited success in deracemisation was observed as more quinoline by-product was formed in the biotransformations, suggesting that the dihydroquinoline compounds are challenging substrates for the IRED enzymes. In this case, the redox process cannot be labelled as a deracemisation reaction but rather a kinetic resolution instead, as the overall quantity of the amine in the reaction mixture is reduced as more is converted to the quinoline side-product.

The chemo-enzymatic deracemisation reaction was applied to 2-substituted indolines as a means of addressing the dearth of deracemisation strategies available to

access single enantiomers of this class of compound. Varying levels of enantioenrichment of the indoline amines were observed with the amine oxidases. Impressively, CHAO was able to produce (*R*)-**26b** and (*R*)-**26c** after 48 h in >98% *ee*. A competing side-reaction was evident in all the biotransformations conducted, whereby the imine-containing 3*H*-indole intermediate following oxidation of the indoline by the AOs isomerised readily to the corresponding indole. As this is inert to reduction in the reaction environment, a range of biotransformation conditions were screened to inhibit formation of the indole, though little success was attained.

IREDs were also tested as reducing agents in the deracemisation reactions and although in principle the reactions were functional, no immediate benefit was obtained from using the IRED biocatalyst over the chemical reducing agent. It is important to consider that the tautomerisation going from the 3*H*-indole following oxidation of the indoline to the corresponding indole occurred rapidly. For substrates tested in the AO/IREd cascade where there appeared to be an enantioenrichment, based on the formation of the amine product in higher *ee* at the end of the reaction, abstracting a positive conclusion from the data may not be possible as this may not directly translate to a deracemisation if the yield of the amine decreases. During the redox process, if the IRED acted significantly more slowly than the oxidase on a particular compound, the concentration of the 3*H*-indole intermediate **27** would effectively increase in the reaction mixture. This could drive the tautomerisation of **27** to the indole **28**, as the 3*H*-indole would be free to linger in the reaction for longer and therefore more likely to undergo isomerisation to the more stable indole.. A means to examine this further would be to carry out a preparative-scale reaction of an indoline deracemisation, in order to assess the mass balance of the reaction products and the extent of conversion of the amine/formation of the indole. This process of irreversible oxidation would also apply to the deracemisation of THQs and was also observed during the reducing agent screen to some degree, although the tautomerisation of the 3*H*-indole **27** to the indole **28** appeared to proceed more readily than oxidation of the DHQs **24** to the corresponding quinolones **25**, which appeared to be suppressed by using sufficient chemical reducing agent.

While the enantio-enrichment of indolines may not represent a true deracemisation reaction, the work is directly comparable to that of Saito *et al*, where a chiral phosphoric acid catalyst was deployed to facilitate a transfer hydrogenation reaction to indoline compounds, resulting in enantioselective oxidation of the indoline to the 3*H*-indole, which then isomerised to the more stable indole (Figure 96).<sup>119</sup> While in this resolution process an *in-situ* racemisation process was not deployed, capping the yield of enantiomerically-pure amine at 50%, in the enzymatic redox process employing amine oxidases discussed in this chapter the theoretical yield can go up to 100%, depending on the amount of isomerisation

to the indole that occurs in the biotransformation reactions. Although due to timing constraints the level of isomerisation and yield of amine product was not examined in more detail in this body of work, this can be investigated further in future work.

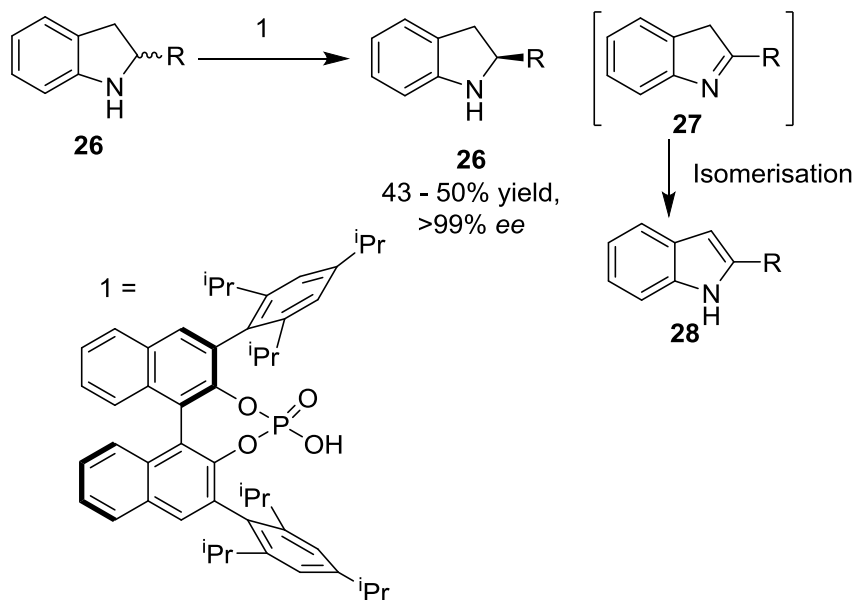


**Figure 96:** Kinetic resolution of indolines **26** catalysed by a phosphoric acid catalyst, which performs a transfer hydrogenation reaction to enantioselectively oxidise one enantiomer of the indoline. The resulting 3*H*-indole **27** rapidly isomerises to the more stable indole **28**.<sup>119</sup>

Where the level of deracemisation of the 2-substituted indoline (as well as for the 2-substituted THQs) using the AO/IREDC combination was comparable to the result obtained using  $\text{NH}_3\text{BH}_3$  as reducing agent, the advantage of using the fully-biocatalytic redox cascade lies in the fact that the enrichment of the amines was accomplished in half the time (24 h versus 48 h for the chemo-enzymatic redox cascade reactions). As the limiting factor of 24 h for reaction time was due to the inactivity of the IRED component beyond this point, further work could explore adding a second batch of IRED enzyme after this initial reaction period, in order to affect the redox process for longer and to increase the level of enantio-enrichment.

When using biological catalysts, it is often the case that the substrate must match the enzyme in order to attain high levels of substrate turnover. The corresponding imines to the indolines **26** and tetrahydroquinolines **23** represent largely untested compounds for the IREDs, so no previous activity of the IREDs towards these compounds is known. Unfortunately, the imines **27** and **24** do not remain as imines as they rapidly convert to their fully-aromatic counterparts, so it would pose a challenge to determine the reduction activity (and selectivity) of the IREDs for these class of substrates directly. The chemo-

enzymatic and indeed biocatalytic deracemisation processes can be broadly applied to provide access to enantiomerically-pure indolines and tetrahydroquinolines, although at this moment this does not represent the most efficient strategy for the preparation of enantiomerically-pure indolines and tetrahydroquinolines. It is clear that further reaction optimisation is needed before the system can be applied for the practical synthesis of these desirable amine-containing scaffolds.

## Chapter 5: (*R*)-IRED-catalysed bioreduction reaction in continuous flow

### 5.1 Brief introduction to reactions in flow and current strategies

While chemical synthesis performed in batch or semi-batch processes still dominate in small-scale laboratory set-ups and in industry, chemical reactions in flow have begun to attract significant research interest from both academic synthetic organic chemists and the pharmaceutical industry alike. Performing chemical reactions in flow is appealing for several reasons including: enhanced reaction rates, increased throughput, a reduction in cost and waste, improvement of worker safety and the ability to use hazardous reagents on all scales, as toxic and reactive intermediates do not have to be isolated.<sup>120</sup> Heider and co-workers, with the support of Novartis, developed an impressive multi-step synthesis and workup sequence for the continuous flow manufacture of the API aliskiren.<sup>121</sup> The fully-integrated flow sequence involved two discrete chemical reaction steps and included intermediate downstream processing, such as extraction, crystallisation, filtration and washing steps, even going as far to produce the final product in the tablet deliverable form. Running the process for 240 h at pilot plant-scale, they were able to achieve a nominal production rate of 41 g h<sup>-1</sup> of aliskiren. Continuous flow processes have also been applied to other APIs, several of which are featured in a review by Porta *et al.*<sup>122</sup>

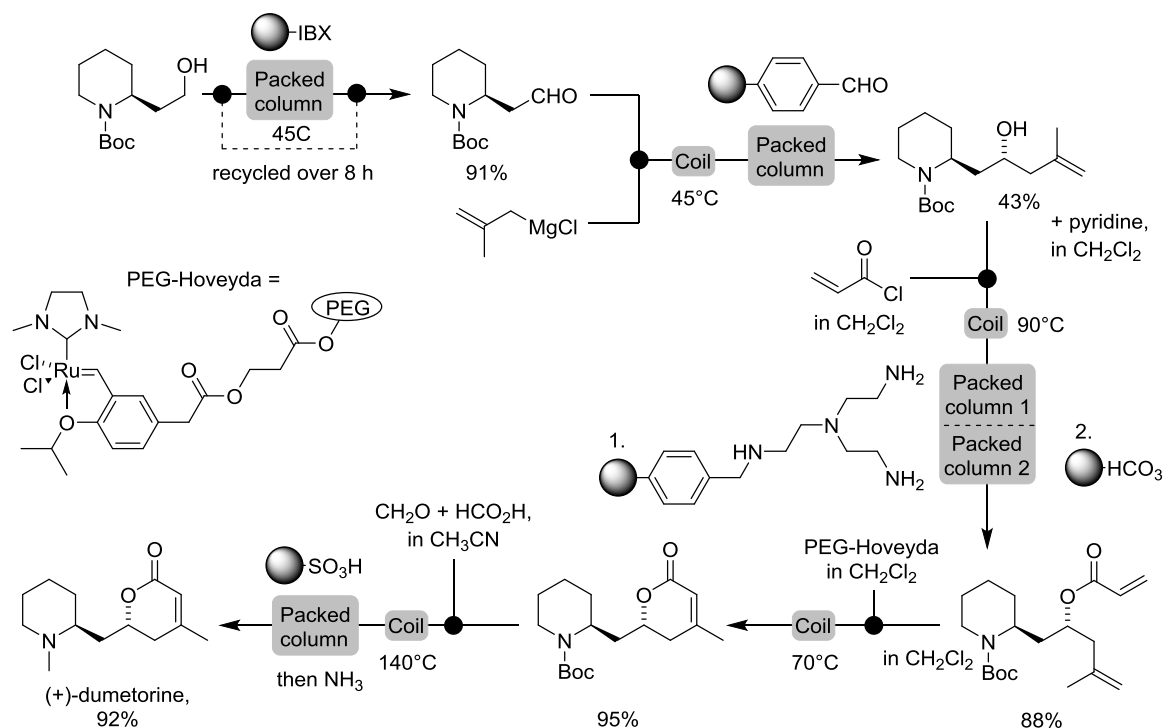


**Figure 97:** Continuous flow synthesis (+)-dumetorine via a 5-stage reaction sequence, which incorporated packed reactors containing scavengers and immobilised reagents, designed for continuous workup and intermediate/product isolation.<sup>123</sup>

A recent review article discussed the development of continuous flow processes applied to the synthesis of natural products, including the production of the 2-piperidinyl alkaloid (+)-dumetorine.<sup>123</sup> The five-step reaction was accomplished by employing packed columns containing immobilised reagents or scavengers to designed to facilitate in-line workup and isolation of any intermediates (Figure 97). The final product was isolated via a “catch and release” method utilising silica-supported sulfonic acid, from which the product was released by washing with methanolic ammonia solution. The productivity of the reaction in flow was vastly improved over the batch process, where the yield for the reaction sequence was 30%, a thirty-fold increase in comparison with the 1% yield obtained from the equivalent batch synthesis of the product. The reactions in flow were extended to include 2-substituted piperidine alkaloids (-)-sedamine and (+)-sedridine, highlighting the flexibility of this approach.

Enzymatic steps have also been incorporated in continuous flow syntheses. In one report, R. de Lopes *et al.* successfully employed a linked batch and continuous flow system for the chemo-enzymatic synthesis of the biaryl moiety of the selective cathepsin K inhibitor Odanacatib, used in the treatment of postmenopausal osteoporosis.<sup>124</sup> An ADH-catalysed reduction of the corresponding ketone was carried out to yield the (*R*)-enantiomer alcohol. The biocatalyst was then separated and, after the addition of the Pd catalyst to the supernatant, the aqueous mixture was pumped through a heated coil along with a separate feed of the boronic acid and potassium carbonate base to effect a Suzuki-Miyaura coupling reaction. The intermediate of Odanacatib was obtained in 73% crude yield (Figure 98).

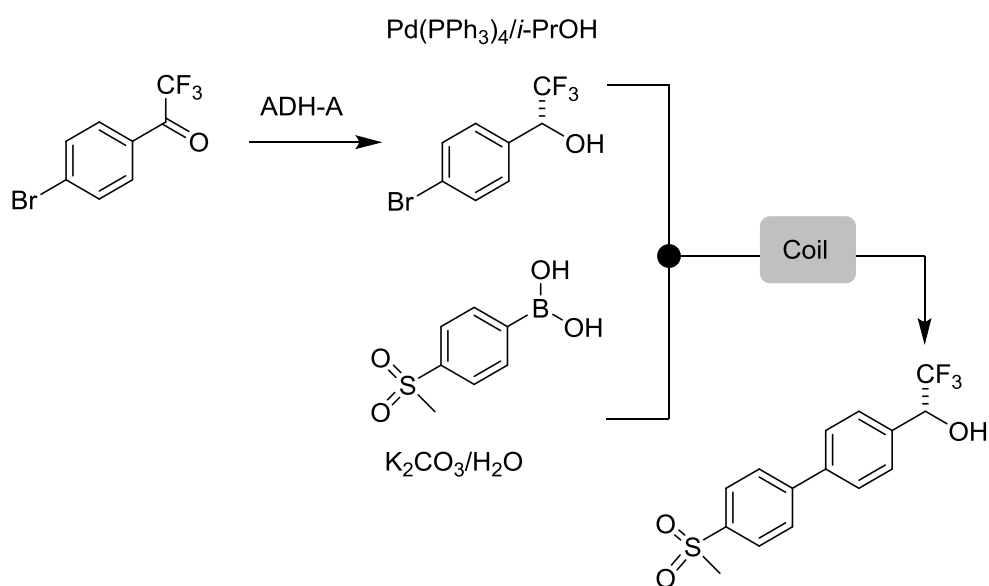


**Figure 98:** Flow diagram of a combined batch and continuous flow synthesis of an intermediate of the API Odanacatib, involving asymmetric reduction catalysed by an ADH from *Rhodococcus ruber* (ADH-A), followed by a Suzuki-Miyaura coupling in flow using the ADH-produced chiral aryl bromide.<sup>124</sup>

Andrade recently described the production of chiral amines by utilising an (*R*)-selective  $\omega$ -TA in continuous flow, where the enzymatic step was incorporated within the flow process.<sup>125</sup> *E. coli* cells containing an over-expressed (*R*)-selective ATA from *Arthrobacter* were immobilised on methacrylate beads. These were then set up in a packed-bed reactor, through which the substrate (methoxyacetone and its derivatives) and the sacrificial amine donor IPA dissolved in water-saturated MTBE were fed. The resulting amine products were isolated in up to 79% yield and >99% *ee*. As the reaction was carried out in MTBE, the cofactor PLP did not leak from the cells so this was not added to the reaction externally. The effective strategy allowed facile removal of the product amines from the reaction mixture via a silica cartridge inserted after the packed-bed reactor (Figure 99).

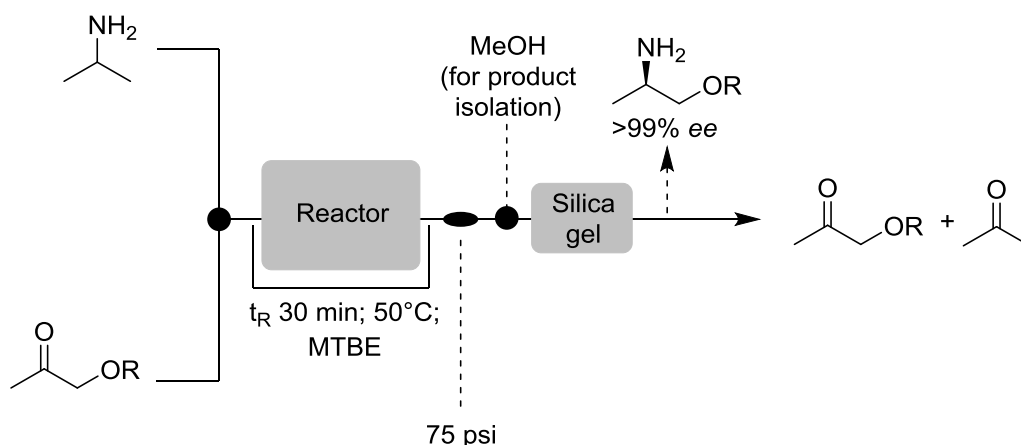


**Figure 99:** Continuous flow synthesis of chiral amines employing an (*R*)-selective ATA from *Arthrobacter* expressed in *E. coli* cells, which were immobilised on methacrylate beads. The reagents were fed into a packed-bed reactor system and the chiral amine product was isolated from the reaction via a “catch and release” mechanism using a silica gel cartridge and MeOH to elute the final product.<sup>125</sup>

Clearly flow chemistry offers significant advantages over batch process equivalents with regards to productivity and reduced reaction times. Provided the experimental needs of the reactions are met, this could provide great benefit to biocatalytic process. However, there have been very few examples of biocatalysis conducted in flow. There, the applicability of continuous flow chemistry in a biotransformation reaction was investigated.

## 5.2 Imine reductase reaction in flow using the Freactor modular flow reactor units – principle

In order to assess the suitability of a continuous flow approach for enzymatic reactions, the (*R*)-IRED-catalysed reduction of imine **5i** was carried out in a small-scale flow reactor

system developed by Blacker's group at the University of Leeds. The apparatus for the flow reaction system was composed of individual reactor units containing magnetic stirrer fleas, each possessing an internal volume of approximately 2 mL. These reactor units could be linked together, thereby increasing the internal volume of the entire reaction system. The individual units were mounted on bases which contained magnetic stirrers. Five of the modules were connected together in series to produce a system of approximately 10 mL internal volume (Figure 100). The first unit in the system was connected to two inlets linked to peristaltic pumps. These were used to feed two sets of reagents into the flow reactor system. The final unit in the system possessed the outlet for the mixture leaving the reaction system.

The conditions used for the reduction reaction in continuous flow were adapted from those used previously in the preparative-scale batch reaction of (*R*)-coniine (see Section 2.2.2). In the batch-scale process, whole-cell (*R*)-IRED biocatalysts were used to carry out the reduction reaction. However, to mitigate complexities associated with whole-cell systems (*e.g.* viscosity, oxygenation, shearing effects) the initial proof-of-concept experiment was conducted using isolated (*R*)-IRED protein in buffer solution in combination with a GDH cofactor recycling system.

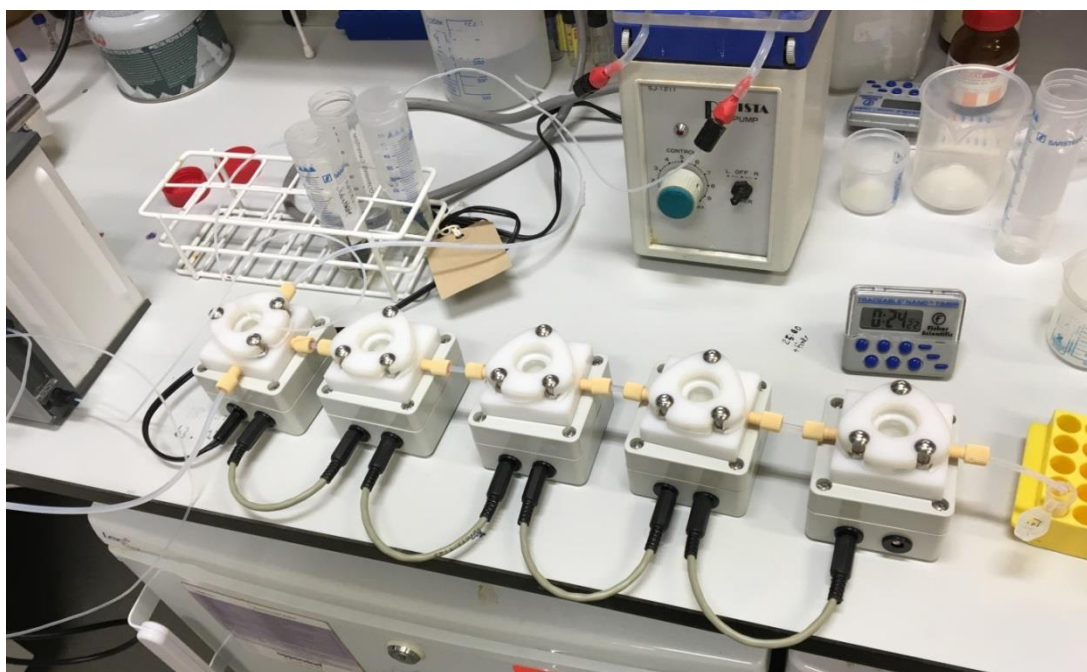


**Figure 100:** Set-up of the Freactor system for the reduction reaction of **5i** catalysed by the (*R*)-IRED enzyme in continuous flow. The system was composed of five reactor units linked in series. Two inlets, connected to peristaltic pumps, were used to feed the first module and the last module carried an outlet hose which collected the reaction mixture leaving the system into an Eppendorf tube (part-filled with a 10 M NaOH quench).

The whole reactor system was initially filled with water (being careful to purge the system of air bubbles) and then flushed with 100 mM pH 7.0 sodium phosphate buffer. The two peristaltic pumps were then set to feed the system at the same flow rate – in order to ensure that the two feeds were mixed in a 1:1 ratio within the system. The residence time for the reaction ( $t_R$ ), which corresponds to the total reaction time of the reagents within the system, is given by the following formula, where  $V_{system}$  is the total system volume:

$$t_R = \frac{V_{system}}{flow\ rate}$$

For reactions in flow, the residence time can be determined by injecting an inert chemical, known as a tracer, into the system and then waiting for the tracer to be detected once it has passed through the entire reaction system. It is assumed that the residence time equates to the time taken for a single system volume to be passed through in flow. The  $t_R$  value corresponds to the total reaction time that the reagent has in flow. In the case of the Freactor units, where the total system volume was 10 mL, the residence time (time taken to collect 10 mL flowing through the system) was determined to be approximately 19 min 20 seconds. IRED-mediated reductions performed in batch have been previously found to reach completion in several hours. It has been shown that reactions can occur more rapidly in flow systems when compared with an equivalent batch process.<sup>126</sup> It was hoped that despite the short residence time, efficient mixing within the Freactor would afford good overall conversion in the (*R*)-IRED reduction of **5i**.

The two inlets for the flow system consisted of isolated (*R*)-IRED protein and the GDH cofactor recycling system in buffer being fed through one inlet and the substrate with cofactor NADPH and glucose pumped through the other inlet. All enzymes and reagents in the prepared feed solutions were dissolved in 100 mM pH 7.0 sodium phosphate buffer at 2 x concentration, so that when mixed in a 1:1 molar ratio in the flow system they would be diluted to the expected concentration. Substrate loading was 50 mM final concentration in the flow system, with 1 mg/mL of IRED and GDH catalyst loading. The reaction was conducted under ambient conditions (20°C with no thermal regulation). To afford a direct comparison of the processes, a batch-scale reaction utilising the same reagent concentrations was carried out in parallel in a shaking incubator at 20°C, 250 rpm.

Samples from the reaction were collected every four minutes until approximately 6 system volumes were passed through (60 mL,  $t = 115$  min). The outlet collected the mixture leaving the reaction system in Eppendorf tubes containing 10 M NaOH as a reaction quench.

### 5.3 (*R*)-imine reductase reaction in flow – results

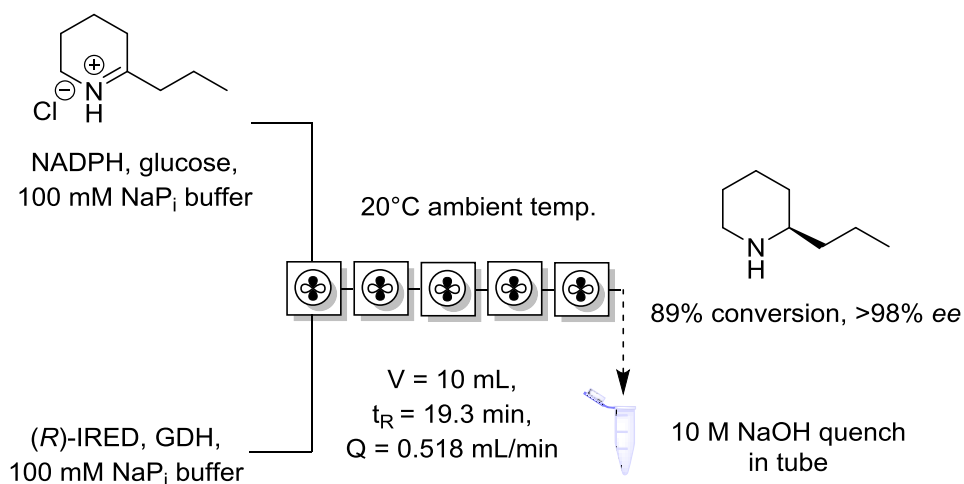
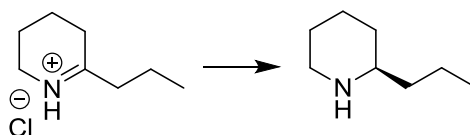


**Figure 101:** Continuous flow synthesis of (*R*)-coniine **6i**, catalysed by isolated (*R*)-IRED isolated protein in combination with a GDH cofactor recycling system. The residence time was approximately 19 min 20 s, the composition of the two inlets feeding the system are given and samples were collected at periodic intervals in Eppendorf tubes containing a 10 M NaOH reaction quench

For comparison purposes, the reduction of **5i** by the (*R*)-IRED was carried out in continuous flow (Figure 101) and in a 500  $\mu\text{L}$  scale batch process emulating the reaction conditions (Table 25). For the batch process, the reaction was conducted in an Eppendorf tube in a shaking incubator at 250 rpm. The conversion stated for the continuous flow process was obtained from the final reaction sample leaving the system prior to termination, in order to ensure that the reaction system had reached steady-state equilibrium since up until this stage the concentrations of the reagents within the reactor would be steadily increasing.

**Table 25:** Biotransformation of 2-(*n*-propyl)-1-piperideine **5i** by the (*R*)-IRED in batch and continuous flow processes



Substrate	Product	Reaction process	Reaction time [min]	Conversion [%]	<i>ee</i> [%]	Absolute config.	Space-time yield [g L <sup>-1</sup> h <sup>-1</sup> ]
<b>5i</b>	<b>6i</b>	Batch	60	>98	>98	( <i>R</i> )	6.36
		Flow	19.3	89	>98	( <i>R</i> )	17.6

**Reaction conditions:** 50 mM substrate, 1 mg/mL (*R*)-IRED isolated protein, 1 mg/mL GDH, 5 mM NADPH, 25 mM glucose, 100 mM pH 7.0 NaP<sub>i</sub> buffer, 20°C.

Comparing the batch and continuous flow process, both reactions produced the expected product (*R*)-coniine **6i** in >98% *ee*. However, the batch process achieved full conversion of the starting material within one hour, whereas the continuous flow process produced (*R*)-**6i** in 89% conversion. In spite of this, the 89% conversion in flow was achieved in effectively a third of the time experienced by the batch process ( $t_R = 19.3$  min, assuming the reaction was immediately quenched in the collection tube). Impressively, when comparing the space-time yields of the two reactions, more than double the amount of product (17.6 g L<sup>-1</sup> h<sup>-1</sup>) could potentially be obtained from the operation of the continuous flow process versus the equivalent batch process. This supports previous reports which have found continuous flow processes to be more productive than their batch counterparts.<sup>123</sup>

The continuous flow reaction reached steady-state equilibrium after approximately four system volumes had passed through, after which conversion remained effectively constant (Figure 102). The low levels of conversion recorded prior to reaching this state could be explained by the relatively low concentrations of the reagents/catalysts within the system, which would struggle to interact efficiently as conversion of the substrate relies on the reagents and catalysts meeting. The unsteady increases in conversion could also be a product of uneven mixing or even uneven flow rates at the two inlets, though this did not seem to lead to variations in conversion once steady-state equilibrium had been established. The pressure within the Freactor system was not monitored, quantitative analysis of the effect of pressure on the biocatalyst could not be undertaken.

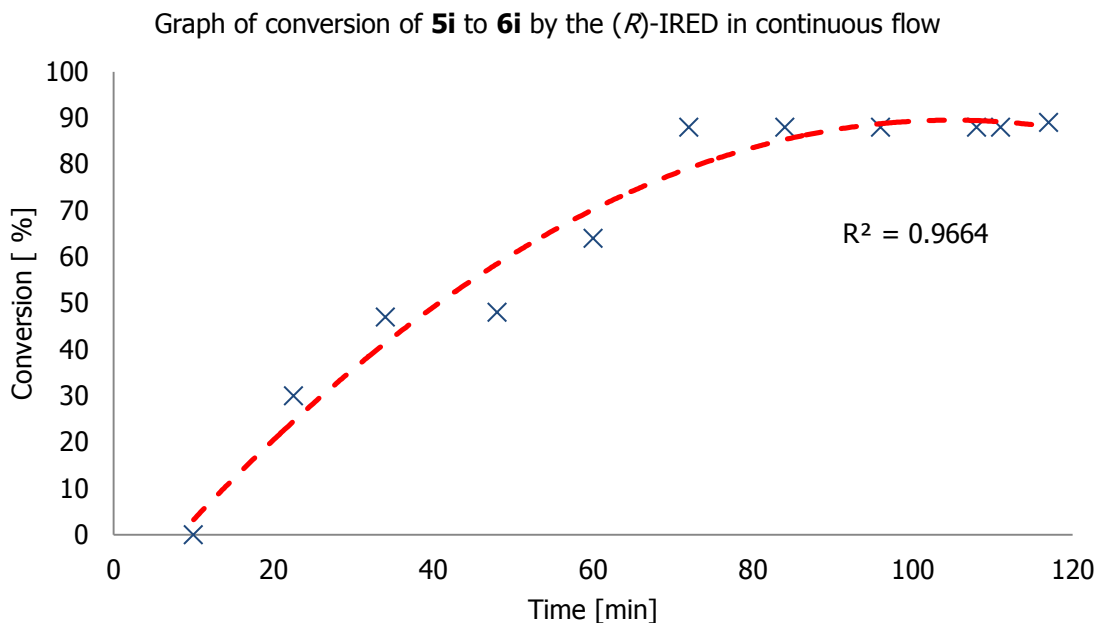


**Figure 102:** Graph showing conversion as a function of time for the continuous flow reduction of **5i** by the (*R*)-IRED, where the residence time of the reagents  $t_r = 19.3$  min. The level of conversion was minimal initially as the reagents filled the reaction vessel slowly and replaced the buffer solution. The conversion then increased in a non-linear fashion due to mixing effects within the flow system until the steady-state equilibrium point of the reaction was reached at approximately  $t = 70$  min, after which time the maximum conversion point from the reaction was reached (the level of conversion no longer increases) as the conditions within the flow reactor vessels had equilibrated.

#### 5.4 Conclusions and further work

Although batch process reactions continue to dominate the landscape of synthetic organic chemistry, reactions in continuous flow are garnering more interest. An enzymatic reaction in flow was demonstrated successfully, with the isolated (*R*)-IRED protein reducing imine **5i** to produce (*R*)-coniine **6i** in 89% conversion and >98% *ee*. Comparing the reaction in flow versus an equivalent batch process, 89% conversion of the starting material was obtained in a third of the time of the batch process, although the reaction in batch did proceed to completion. On examining the space-time yield of the reaction, the continuous flow process produced the product amine in  $17.6 \text{ g L}^{-1} \text{ h}^{-1}$ , a higher value than the batch process could produce and demonstrating the efficacy of this strategy. Of course, as no product was isolated from the reaction, this value is subject to change once downstream processes are taken into account (separation of the product from the aqueous reaction mixture of reagents and catalysts, any further purification steps required). This could be explored in further work.

The reaction conditions could also be optimised further. The (*R*)-IRED reduction reactions have previously been carried out  $30^\circ\text{C}$ , therefore future reactions in flow could be undertaken at this elevated temperature in order to increase the reaction rate and ultimately

the conversion. The conversion could also be increased by increasing the residence time, either by increasing the overall system volume or by decreasing the flow rate. Experiments into reducing the catalyst loading could also be carried out in order to make the process more atom-economic. As the pressure within the system was not monitored, it remains to be established whether the increased pressure had any effect on the function of the catalyst.

Previous reduction reactions with the (*R*)-IRED were conducted with predominantly whole-cell biocatalysts. Further experiments would be required to determine if this procedure could also be applied in flow. However, factors that would need to be considered include mixing of the more viscous reaction composition (as well as ensuring unimpeded flow through the system), the mechanical effect of the fast mixing experienced within the Freactor units on the whole-cell system (which relies on the correct functioning of the *E. coli* organism for *in-situ* cofactor regeneration) as well as amount of oxygen within the reaction system (again necessary for cofactor regeneration through cellular respiration). As the initial proof-of-principle reaction was conducted with isolated protein, it was expected that shearing would have negligible effect on the protein with regards to its structural integrity. The amount of dissolved oxygen/gas was also irrelevant to the reaction catalysed by the (*R*)-IRED, whereas this would have to be taken into account for a whole-cell biocatalyst relying on NADPH cofactor regeneration or if a different enzyme were to be used eg. amine oxidase.

Once conditions have been further optimised for a particular reaction in flow, further work could also attempt to use the biocatalysts immobilised on solid support. This would confer the advantage of facile insertion of the catalyst into the process as well as keeping the catalyst isolated from the product mixture following reaction. Reactions in organic solvents could then be tested under the conditions, which could further simplify the downstream processing steps. A major advantage of the continuous flow reaction is its scalability, as conversions and ultimately space-time yields should remain consistent if the process was scaled up. The same cannot be said of the batch process, where mixing and heat transfer become more of an issue as the reaction scale increases.

## Chapter 6: Conclusions and outlook

### 6.1 Conclusions

The aim of the research project was to assess and develop novel biocatalytic routes for the production of enantiomerically-pure chiral amines. Imine reductases and the concept of biocatalytic imine reduction were not previously unfounded in nature. The transformation itself, however, was relatively unexplored for the purpose of biocatalysis. Two reported imine reductases, which were found in strains of *Streptomyces*, were identified as promising candidates for performing biocatalytic applications based on their initial biotransformation of 2-methyl-1-pyrroline **1a**. The (*R*)-IRED from GF3587 and the (*S*)-IRED from GF3546 afforded the corresponding (*R*)- and (*S*)-enantiomer pyrrolidines respectively in high *ee*. During the course of this project, the (*R*)-IRED was screened against a panel of structurally-diverse imines, which included 2-substituted cyclic imines with varying substituents, dihydroisoquinolines and an iminium ion, and was found to possess a broad substrate scope, in contrast to reported findings. The IREDs were used as robust whole-cell biocatalysts, which enhanced their ease of use due to the convenience afforded by *in-situ* cofactor recycling within the cell. The (*R*)-IRED was also applied to the synthesis of the natural product coniine on a gram-scale, producing the (*R*)-enantiomer of the alkaloid product in excellent *ee* and demonstrating the suitability of the IRED biocatalyst for large-scale preparations of enantiomerically-pure amine products.

The application of multiple enzymes within a single reaction system was assessed. One system utilised commercially-available  $\omega$ -transaminase ( $\omega$ -TAs) lysates in combination with the (*R*)- and (*S*)-IREDs in two discrete reaction steps within the same pot, for the production of chiral disubstituted piperidines and pyrrolidines from achiral diketone starting materials. As the  $\omega$ -TAs were found to be inhibited by the presence of the whole-cell IRED biocatalysts, the reaction was carried out as a one-pot-two-step procedure, which afforded chiral disubstituted piperidines and pyrrolidines. The enzyme cascade was suitable for the preparation of *syn*-diastereomer 2,6-disubstituted piperidines, but as the *anti*-diastereomer products could not be accessed this imposed a limitation on this synthetic route. The cascade was then extended to include carboxylic acid reductase enzymes in the synthetic route, in order to access chiral 3-substituted morpholines and thiomorpholines starting from simple achiral ketoacid reagents.

Two enzymatic redox cascades were then assessed for their application in the deracemisation of racemic 2-substituted tetrahydroquinolines and 2-substituted indolines, which were scaffolds that were previously untested. The procedure employed amine oxidases in combination with the non-selective chemical reducing agent  $\text{NH}_3\text{BH}_3$ , or IRED

biocatalysts. For the AO/IREC cascade, the enzymatic redox deracemisation process showed applicability in the deracemisation of 2-phenylpiperidine **6b** to on a preparative-scale.

Both the THQs and the indolines proved to be challenging substrates for the AOs, as moderate amounts of enantioenrichment were attained from the attempted chemo-enzymatic deracemisation of a panel of the racemic amines. A side reaction for both compounds, whereby the intermediates following oxidation of the THQs underwent further oxidation to produce fully-aromatic quinolones and the oxidised indolines tautomerised to their corresponding indoles, prevented a full deracemisation of these compounds from being achieved as some of the amine would be lost to these undesired processes. This led to a net reduction of the amine starting material and so the enantio-enrichment process would have to be regarded as a kinetic resolution instead. This issue was addressed by optimising the quantity of the chemical reducing agent added into the process for deracemisation of the THQs. For the indolines, however, the indole side-product was present in most reactions carried out and the evidence suggests that further optimisation of the reaction conditions is needed.

Finally, an enzymatic reaction was carried out in continuous flow in order to determine if biocatalytic reactions could be conducted in these reaction systems. As the interest in continuous flow chemistry grows, due to the ease of applying the system to large-scale chemical production, the suitability of biocatalysis under these conditions will undoubtedly be questioned. The success of the proof-of-concept IRED-mediated reduction in flow demonstrated in this investigation can be added to the limited reports in order to stimulate further interest in the research area.

## 6.2 Outlook

While existing strategies offer a choice of enzyme catalysts to be harnessed as tools in the synthetic chemist's repertoire, there was still need to further expand the scope of the substrates that are accessible using these strategies, as well as to develop new methodologies to be able to make existing processes for the manufacture of chiral amines more efficient. IREDs undoubtedly hold great potential as biocatalysts, as they offer a direct route for the production of chiral secondary and tertiary amines. As the number of reports on novel IREDs grows, we have seemingly only just begun to scratch the surface with regards to the diverse range of chiral amine scaffolds that are accessible through IRED-mediated reduction. The enzymes appear to be able to catalyse enantioselective reductive amination reactions in limited capacity from previous reports; though as further IREDs are discovered and assessed this will undoubtedly change. The IREDs that were utilised

throughout this project possessed reasonable activity towards the breadth of compounds tested and yet it remains to be seen what their natural function is.

As the IRED enzymes formed the crux of many of the enzymatic cascades explored within the project, higher levels of activity as well as enantioselectivity would be beneficial to all these processes. This could be addressed through the discovery of more efficient enzymes for imine reduction, or even engineering the IREDs to tailor them to the specific requirements of the reactions wishing to be catalysed.

The ATA/IRED and CAR/ATA/IRED cascades have been successfully demonstrated in the asymmetric synthesis of cyclic piperidines, pyrrolidines, morpholines and thiomorpholines. The scope of the cascade could be expanded to include compounds possessing further functionalities, for the synthesis of more complex frameworks. This would be particularly insightful for access to more complex morpholines and thiomorpholines, possessing more than a single chiral centre, as this was not tested within the scope of this project. In addition, the possibility of combining more enzymes within the cascade exists. One such addition would be an amine oxidase, which could affect enzymatic or chemo-enzymatic deracemisation on the morpholine and thiomorpholine compound to enrich the *ee* of the products following IRED reduction. For the ATA/IRED cascade, the synthesis of (-)-dihydropinidine was demonstrated successfully and it would be interesting to see if the procedure could be readily applied for the synthesis of the 2,6-disubstituted piperidine alkaloid solenopsin, which is found in the venom of the Fire Ant, *Solenopsis saevissima*,<sup>127</sup> for which there is considerable research interest for its asymmetric synthesis.<sup>128</sup>

The deracemisation of 2-substituted tetrahydroquinoline and 2-substituted indolines proceeded with varying levels of enantioenrichment attained. The amine oxidases were not found to be particularly active (or possibly stereoselective) towards tetrahydroquinolines in general, as full deracemisation did not occur in many cases after 48 h or longer. This could be addressed by subjecting the oxidases to directed evolution methods, which have previously been used to engineer oxidases such as MAO-N and 6-HDNO to broaden their substrate specificity as well as activity. As the technique was applied to the variant of CHAO used within this report with success, and with the availability of a convenient high-throughput assay for detecting positive variants, the engineering of the enzymes appears to be the most obvious approach. The availability of IREDs which are more active towards indolines and THQs could also aid in the inhibition of the formation of the aromatic side-products encountered during the enantio-enrichment of these compounds, thereby producing a true deracemisation of these compounds rather than just a yield-limited kinetic resolution.

For the enzymatic reaction in flow, which was conducted in the modular vessel flow reaction system (Freactor), it would be interesting to see if the productivity of the reaction could be improved. Approaches to consider would be to increase the conversion from the reaction, possibly by running the reaction at an elevated temperature. The residence time could also be increased in order to increase the overall conversion to the product obtained at the end of the reaction, though this would not necessarily improve the space-time yield as the reaction rate would remain unchanged.

The next stage for enzymatic reactions in flow would be to attempt different reactions with other biocatalysts, in order to assess the applicability of the system to other enzymatic transformations. As a previous report on enzyme reactions in flow demonstrated the success of using immobilised whole-cell biocatalysts,<sup>125</sup> the same system could be applied to the IRED-reduction system. This would confer the advantage of keeping the catalyst isolated from the product mixture, reducing downstream processing. It would also be interesting to see if the reactions could be carried out in organic solvents or even biphasic systems, which could possibly increase the scope of the products that could be made in continuous flow as well as reduce downstream processing.

Finally, the modular nature of the Freactor flow reaction system, as well as continuous flow systems in general, would allow reaction sequences comprised of multiple stages to be set up and carried out in continuous flow in a convenient and facile fashion. It would be interesting to investigate whether the enzyme cascades, such as ATA/IRED or CAR/ATA/IRED, could be carried out in a continuous flow environment with the catalysts entering the system at different stages. This could improve processes such as the TA/IRED cascade, where the procedure was carried out in two stages, to improve the overall production of these cascade reactions.

## Chapter 7: Methods and experimental

### 7.1 Materials, equipment and general analysis procedures

#### 7.1.1 Chemicals

All commercially available reagents were used without further purification and purchased from Sigma-Aldrich (Poole, Dorset, UK), Melford Laboratories (Ipswich, Suffolk, UK), Alfa Aesar (Karlsruhe, Germany), Acros Organics (Geel, Belgium) and Fluorochem (Derbyshire, UK) unless stated otherwise. HPLC solvents were obtained from Sigma-Aldrich (Poole, Dorset, UK) or ROMIL (Waterbeach, Cambridge, UK) and GC gases from BOC gases (Guildford, UK). 2-methyl-1-pyrroline (**1a**), 2-methylpiperidine (**6a**), coniine (**6i**), 2-isopropylpiperidine (**6k**), 6,7-dimethoxy-1-methyl-1,2,3,4-tetrahydroisoquinoline (**7b**), 1-phenyl-1,2,3,4-tetrahydroisoquinoline (**7c**) and 2-methylindoline (**26a**) were purchased from Sigma-Aldrich (Poole, Dorset, UK). 2-methylpyrrolidine (**2a**) and 1-methyl-3,4-dihydroisoquinoline hydrochloride (**7a**) were sourced from Acros Organics (Geel, Belgium). 2-phenylpyrrolidine (**2b**) and 2-cyclohexylpyrrolidine (**2e**) were purchased from Apollo Scientific (Stockport, UK) and 1-methyl-1,2,3,4-tetrahydroisoquinoline (**8a**) was obtained from GlaxoSmithKline (Stevenage, UK). 2-methyl-1,2,3,4-tetrahydroquinoline (**23a**) was purchased from TCI (Oxford, UK).

#### 7.1.2 Equipment and general analysis procedures

Solvents were of HPLC grade and were purchased dried over molecular sieves where necessary. Column chromatography was performed on silica gel [Fluka (Buchs, Switzerland), 220-440 mesh].  $^1\text{H}$  and  $^{13}\text{C}$  NMR spectra were recorded on a Bruker Avance 400 instrument (400 MHz for  $^1\text{H}$  and 100 MHz for  $^{13}\text{C}$ ) in  $\text{CDCl}_3$  or  $\text{CD}_3\text{OD}$  without additional standard using residual protic solvent as an internal standard. Chemical shifts ( $\delta$ ) are reported in parts per million (ppm) relative to the residual protic solvent signal ( $\text{CHCl}_3$  in  $\text{CDCl}_3$ ,  $^1\text{H} = 7.26$ ;  $\text{CDCl}_3$ ,  $^{13}\text{C} = 77.16$ ;  $\text{CHD}_2\text{OD}$  in  $\text{CD}_3\text{OD}$ ,  $^1\text{H} = 3.31$ ;  $\text{CD}_3\text{OD}$ ,  $^{13}\text{C} = 49.0$ ).<sup>[1]</sup>

High-resolution mass spectrometry (HRMS) was recorded using a Waters LCT time-of-flight mass spectrometer, connected to a Waters Alliance LC (Waters, Milford, MA, USA). Waters Masslynx software was used for the data processing. Samples for IR spectroscopy were run on a Nicolet 5700 FT-IR (Thermo Electron, Madison, WI, USA) using a Smart Orbit Diamond accessory. Optical rotation measurements were taken on an AA-100 polarimeter at 25°C with the solvent and concentration stated.

Chiral normal phase HPLC was performed on an Agilent system (Santa Clara, CA, USA) equipped with a G1379A degasser, G1312A binary pump, a G1367A well plate

autosampler unit, a G1316A temperature controlled column compartment and a G1315C diode array detector. CHIRALPAK<sup>®</sup>IA, CHIRALPAK<sup>®</sup>IC, CHIRALPAK<sup>®</sup>IE and CHIRALCEL<sup>®</sup>OJ-H analytical columns (all Daicel (Osaka, Japan), 250 mm length, 4.6 mm diameter, 5 µm particle size) were used. The typical injection volume was 10 µl and chromatograms were monitored at 254 nm or 265 nm.

GC analysis was performed on a Agilent 6850 GC (Agilent, Santa Clara, CA, USA) with a flame ionization detector (FID) and autosampler equipped with a 25 m CP-Chirasil-DEX CB column with 0.25 mm inner diameter and 0.25 µm film thickness (Agilent, Santa Clara, CA, USA) or β-Dex 325 column with 0.25 mm inner diameter and 0.25 µm film thickness (Supelco, Bellefont, PA, USA). Samples which were run on the Chirasil-DEX CB column were derivatised using acetic anhydride with an excess of triethylamine at room temperature, whereas samples run on the β-DEX 325 column were derivatised with an excess of trifluoroacetic anhydride at room temperature.

## 7.2 Media, buffers and stock solutions

The following media were used in the growth and maintenance of bacterial cells harbouring the biocatalysts used in this report. These were prepared according to the manufacturer's instructions and were autoclaved before use.

### 7.2.1 Growth media

#### 7.2.1.1 IPTG induction media (all purchased from Formedium, Norfolk, United Kingdom)

LB-Broth Miller – Tryptone (10 g/L), yeast extract (5 g/L), NaCl (10 g/L)

2 x YT Medium – Tryptone (16 g/L), yeast extract (10 g/L), NaCl (5 g/L)

Terrific Broth Medium – Tryptone (12 g/L), yeast extract (24 g/L)

LB-Agar Miller - Tryptone (10 g/L), yeast extract (5 g/L), NaCl (10 g/L), Agar (15 g/L)

#### 7.2.1.2 Auto-induction media

CHAO/6-HDNO auto-induction medium (prepared according to Studier<sup>114</sup>)

The following solutions were prepared and sterilised by autoclave prior to use.

50 x M solution (1 L)

1M NH<sub>4</sub>Cl (53.49 g), 0.1M Na<sub>2</sub>SO<sub>4</sub> (14.2 g), 0.5M KH<sub>2</sub>PO<sub>4</sub> (68 g), 0.5M Na<sub>2</sub>HPO<sub>4</sub> (173 g) – made up to 1 L with dH<sub>2</sub>O

50 x 5052 solution (500 mL)

Glycerol (125 mL, 25% v/v), glucose (12.5 g, 2.5% w/v), α-lactose monohydrate (50 g, 10% w/v) – made up to 500 mL with dH<sub>2</sub>O

2 M MgSO<sub>4</sub> solution – made as is in dH<sub>2</sub>O and filter-sterilised by passing through a 0.2 μm syringe filter

1000 x trace elements solution (100 mL)

Solution A: 20 mM CaCl<sub>2</sub> (440 mg), 10 mM MnCl<sub>2</sub>·4H<sub>2</sub>O (400 mg), 10 mM ZnSO<sub>4</sub>·7H<sub>2</sub>O (1.15 g), 2 mM CoSO<sub>4</sub>·7H<sub>2</sub>O (112 mg), 2 mM CuCl<sub>2</sub>·2H<sub>2</sub>O (68 mg), 2 mM NiSO<sub>4</sub>·6H<sub>2</sub>O (105 mg), 2 mM Na<sub>2</sub>MoO<sub>4</sub>·2H<sub>2</sub>O (97 mg), 2 mM Na<sub>2</sub>SeO<sub>3</sub> (76mg), 2 mM H<sub>3</sub>BO<sub>3</sub> (25 mg) – made up to 100 mL with dH<sub>2</sub>O and autoclaved

Solution B: 50 mM FeCl<sub>3</sub>·H<sub>2</sub>O (2.7 g) was added to conc. HCl (1 mL) - made up to 100 mL with dH<sub>2</sub>O and then filter-sterilised by passing through a 0.2 μm syringe filter

Solution A and solution B were then mixed together to produce 1000 x trace elements solution (200 mL)

The auto-induction medium was prepared by charging a flask of tryptone (5 g) and yeast extract (2.5 g), made up in 480 mL and autoclaved, with (in the order listed) 2 M MgSO<sub>4</sub> (500 μL), 1000 x trace elements (100 μL), 50 x 5052 (10 mL), 50 x M (10 mL) and the appropriate antibiotic selection agent.

MAO-N D9 auto-induction medium

The auto-induction for the growth and expression of MAO-N was prepared from the same solutions listed for the auto-induction medium, with the addition of sodium succinate solution.

Succinate solution (1 L)

500 mM sodium succinate dibasic (81.03 g) – made up to 1 L with dH<sub>2</sub>O and autoclaved

The auto-induction medium was prepared by charging a flask of tryptone (19.7 g) and yeast extract (9.8 g), made up in 538 mL and autoclaved, with (in the order listed) 2 M MgSO<sub>4</sub> (600 μL), 1000 x trace elements (600 μL), 50 x 5052 (12 mL), 50 x M (30 mL), succinate (30 mL) and the appropriate antibiotic selection agent.

## 7.2.2 Buffers

### 7.2.2.1 Biotransformation buffers

The following buffers were used to maintain a constant pH environment during whole-cell as well as isolated protein biotransformations

Sodium phosphate buffer – prepared from dissolving a mixture of the salt  $\text{NaH}_2\text{PO}_4$  as the acidic component and salt  $\text{Na}_2\text{HPO}_4$  as the basic component in  $\text{dH}_2\text{O}$ . The pH was adjusted as required by addition of orthophosphoric acid or NaOH solution.

Potassium phosphate buffer – prepared from dissolving a mixture of the salt  $\text{KH}_2\text{PO}_4$  as the acidic component and salt  $\text{K}_2\text{HPO}_4$  as the basic component in  $\text{dH}_2\text{O}$ . The pH was adjusted as required by addition of orthophosphoric acid or KOH solution.

### 7.2.2.2 Protein purification buffers

The following buffers were used for the purification of the (*R*)-IRED

Loading buffer - 100 mM pH 7.0 sodium phosphate buffer + 300 mM NaCl

Elution buffer - 100 mM pH 7.0 sodium phosphate buffer + 300 mM NaCl + 300 mM imidazole

Size exclusion chromatography buffer - 100 mM pH 7.0 sodium phosphate buffer + 100 mM NaCl

## 7.2.3 Antibiotics and IPTG stock solutions

### 7.2.3.1 Antibiotic stock solutions

The following antibiotics were used as selection agents for cells containing the target plasmid vectors carrying the gene of interest. These were typically administered as a 1/1000 dilution. The antibiotic stock solutions were passed through a 0.2  $\mu\text{m}$  micron syringe filter (Sartorius, Surrey, UK) to ensure sterility prior to use.

Ampicillin – prepared as a 100 mg/mL stock solution, typical working concentration 100  $\mu\text{g}/\text{mL}$ .

Kanamycin – prepared as a 50 mg/mL stock solution, typical working concentration 30  $\mu\text{g}/\text{mL}$  although 50  $\mu\text{g}/\text{mL}$  was used in TB buffer, due to kanamycin resistance induced in the phosphate buffered medium

Spectinomycin – prepared as a 50 mg/mL stock solution, typical working concentration 50 µg/mL.

### 7.2.3.2 IPTG stock solution

IPTG, used as an analogue of lactose for the initiation of gene expression in plasmids bearing a T7 promoter, was prepared as a 1 M stock solution in dH<sub>2</sub>O and was used at a final concentration of 0.2 mmol – 1.0 mmol. The IPTG stock solution was passed through a 0.2 µm micron syringe filter (Sartorius, Surrey, UK) to ensure sterility prior to use.

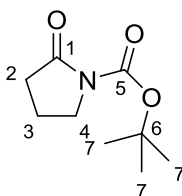
## 7.3 Synthesis of substrates and analytical standards

### 7.3.1 Synthesis of 2-substituted cyclic imines and amines

#### 7.3.1.1 General procedure for the preparation of *N*-Boc-protected lactams **11a** - **11c**

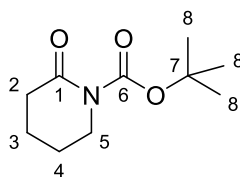
Under N<sub>2</sub>, to a solution of the starting lactam (53.0 mmol) and 4-dimethylaminopyridine (1.62 g, 13.3 mmol) in acetonitrile (90 mL) was slowly added a solution of Boc anhydride (14.5 g, 66.3 mmol) in acetonitrile (20 mL) and the mixture was stirred overnight at room temperature. The reaction mixture was then diluted with water (50 mL) and the layers separated before the aqueous phase was extracted with ethyl acetate (3 x 100 mL). The combined organic phases were washed with 1 M HCl (1 x 200 mL) and saturated brine (3 x 200 mL). The organic phase was then dried over MgSO<sub>4</sub> and concentrated *in vacuo* to yield the crude product. Purification on silica gel (15% v/v ethyl acetate-cyclohexane + 0.1% triethylamine) gave the *N*-Boc-protected lactam product.

#### ***N*-Boc-2-pyrrolidinone**



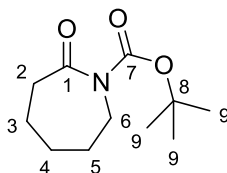
Reaction of 2-pyrrolidinone (4.51 g, 53.0 mmol) with Boc anhydride (14.5 g, 66.3 mmol) afforded *N*-Boc-2-pyrrolidinone **84a** (9.32 g, 95% yield) as pale yellow oil. **<sup>1</sup>H NMR** (400 MHz, CDCl<sub>3</sub>) δ: 3.78 – 3.69 (t, *J* = 7.2 Hz, 2H, C4-CH<sub>2</sub>), 2.54 – 2.46 (t, *J* = 8.3 Hz, 2H, C2-CH<sub>2</sub>), 2.05 – 1.93 (m, 2H C3-CH<sub>2</sub>), 1.51 (s, 9H, *t*-Bu); **<sup>13</sup>C NMR** (100 MHz, CDCl<sub>3</sub>) δ: 174.4 (C1), 150.2 (C5), 82.7 (C6), 46.5 (C4), 33.0 (C2), 28.0 (C7), 17.4 (C3). *Data consistent with literature values.*<sup>82</sup>

### ***N*-Boc- $\delta$ -valerolactam**



Reaction of  $\delta$ -valerolactam (5.25 g, 53.0 mmol) with Boc anhydride (14.5 g, 66.3 mmol) afforded *N*-Boc- $\delta$ -valerolactam **84b** (6.34 g, 60% yield) as pale yellow solid. **<sup>1</sup>H NMR** (400 MHz, CDCl<sub>3</sub>)  $\delta$ : 3.65 – 3.56 (m, 2H, C5-CH<sub>2</sub>), 2.50 – 2.41 (m, 2H, C2-CH<sub>2</sub>), 1.83 – 1.71 (m, 4H, C3-CH<sub>2</sub> and C4-CH<sub>2</sub>), 1.47 (s, 9H, *t*-Bu); **<sup>13</sup>C NMR** (100 MHz, CDCl<sub>3</sub>)  $\delta$ : 171.3 (C1), 152.7 (C6), 82.8 (C6), 46.3 (C5), 34.9 (C2), 28.0 (C8), 22.8 (C4), 20.5 (C3). *Data consistent with literature values.*<sup>82</sup>

### ***N*-Boc- $\epsilon$ -caprolactam**

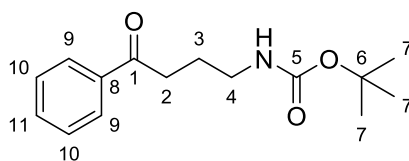


Reaction of  $\epsilon$ -caprolactam (6.00 g, 53.0 mmol) with Boc anhydride (14.5 g, 66.3 mmol) afforded *N*-Boc- $\epsilon$ -caprolactam **84c** (8.59 g, 76% yield) as a pale yellow solid. **<sup>1</sup>H NMR** (400 MHz, CDCl<sub>3</sub>)  $\delta$ : 3.77 – 3.70 (m, 2H, C6-CH<sub>2</sub>), 2.63 (dd, *J* = 6.6, 4.5 Hz, 2H, C2-CH<sub>2</sub>), 1.74 (ddd, *J* = 18.6, 16.7, 11.9 Hz, 6H, C3-CH<sub>2</sub>, C4-CH<sub>2</sub> and C5-CH<sub>2</sub>), 1.48 (s, 9H, *t*-Bu); **<sup>13</sup>C NMR** (100 MHz, CDCl<sub>3</sub>)  $\delta$ : 175.6 (C1), 152.7 (C7), 82.6 (C8), 46.0 (C6), 39.3 (C2), 29.0 (C4), 28.5 (C5), 27.9 (C9), 23.4 (C3). *Data consistent with literature values.*<sup>82</sup>

#### 7.3.1.2 Preparation of *N*-Boc-protected aminoketones

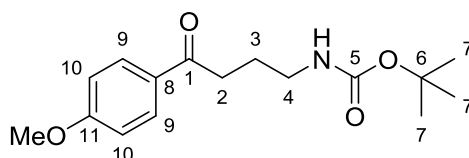
Under nitrogen atmosphere, a solution of *N*-Boc-protected lactam **84a** - **84c** (1 eq.) in THF (4mL/mmol of lactam) was cooled to -78°C. The Grignard reagent (1.1 – 1.4 eq.) was added dropwise and the mixture was stirred overnight at -78°C. The reaction was then warmed at room temperature and quenched by adding 1 M HCl solution until pH 1-2. The mixture was extracted with CH<sub>2</sub>Cl<sub>2</sub> (3 x 50 mL). The combined organic phases were dried over MgSO<sub>4</sub> and concentrated *in vacuo* to give the crude product. Purification on silica gel afforded the desired product.

### ***tert*-butyl(4-oxo-4-phenylbutyl)carbamate**



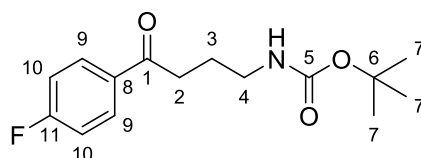
*N*-Boc-2-pyrrolidinone **84a** (1.53 g, 8.26 mmol) was reacted with phenylmagnesium bromide (1 M solution in THF, 11.6 mL, 11.56 mmol). Purification on silica (10-20% v/v ethyl acetate-cyclohexane + 0.1% triethylamine) gave **85a** (721 mg, 33% yield) as a white solid. **<sup>1</sup>H NMR** (400 MHz, CDCl<sub>3</sub>) δ: 7.97 - 7.90 (m, 2H, C9-H), 7.59 - 7.53 (m, 1H, C11-H), 7.49 - 7.43 (m, 2H, C10-H), 4.65 (bs, 1H, NH), 3.26 - 3.18 (m, 2H, C4-CH<sub>2</sub>), 3.03 (t, *J* = 7.1 Hz, 2H, C2-CH<sub>2</sub>), 1.94 (p, *J* = 7.0 Hz, 2H, C3-CH<sub>2</sub>), 1.42 (s, 9H, *t*-Bu); **<sup>13</sup>C NMR** (100 MHz, CDCl<sub>3</sub>) δ: 199.8 (C1), 156.1 (C5), 136.8 (C8), 133.1 (C11), 128.6 (C9), 128.1 (C10), 79.2 (C6), 40.1 (C4), 35.7 (C4), 28.4 (C2), 24.5 (C3). *Data consistent with literature values.*<sup>82</sup>

### ***tert*-butyl(4-oxo-4-(*p*-methoxyphenyl)butyl)carbamate**



*N*-Boc-2-pyrrolidinone **84a** (1.50 g, 8.10 mmol) was reacted with (*p*-methoxy)phenylmagnesium bromide (0.5 M solution in THF, 22.7 mL, 11.3 mmol). Purification on silica (10-20% v/v ethyl acetate-cyclohexane + 0.1% triethylamine) gave **85b** (782 mg, 33% yield) as an off-white solid. **<sup>1</sup>H NMR** (400 MHz, CDCl<sub>3</sub>) δ: 7.98 - 7.93 (m, 2H, 2 x C9-CH), 6.96 - 6.89 (m, 2H, 2 x C10-CH), 4.67 (bs, 1H, NH), 3.87 (s, 3H, OMe), 3.25 - 3.17 (m, 2H, C4-CH<sub>2</sub>), 2.97 (t, *J* = 7.2 Hz, 2H, C2-CH<sub>2</sub>), 1.92 (p, *J* = 7.2 Hz, 2H, C3-CH<sub>2</sub>), 1.42 (s, 9H, *t*-Bu); **<sup>13</sup>C NMR** (100 MHz, CDCl<sub>3</sub>) δ: 198.4 (C1), 163.6 (C5), 156.2 (C11), 130.5 (C9), 130.0 (C8), 113.9 (C10), 79.2 (C6), 55.6 (OMe), 40.1 (C4), 35.3 (C2), 28.5 (C7), 24.8 (C3); **HRMS** C<sub>16</sub>H<sub>23</sub>O<sub>4</sub>N, [M+Na]<sup>+</sup> found 316.1525.

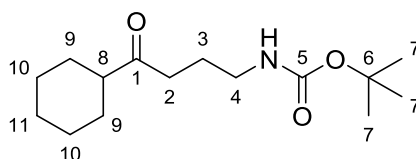
### ***tert*-butyl(4-oxo-4-(*p*-fluorophenyl)butyl)carbamate**



*N*-Boc-2-pyrrolidinone **84a** (1.20 g, 6.48 mmol) was reacted with (*p*-fluoro)phenylmagnesium bromide (1 M solution in THF, 9.07 mL, 9.07 mmol). Purification on silica (12.5% v/v ethyl acetate-cyclohexane + 0.1% triethylamine) gave **85c** (1.31 g, 72%

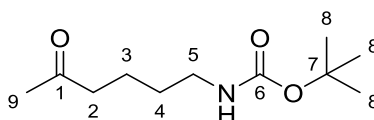
yield) as a white solid. **<sup>1</sup>H NMR** (400 MHz, CDCl<sub>3</sub>) δ: 7.92 - 7.85 (m, 2H, C10-CH), 7.05 - 6.97 (m, 2H, C9-CH), 4.97 (bs, 1H, NH), 3.17 - 3.09 (m, 2H, C4-CH<sub>2</sub>), 2.91 (t, *J* = 7.1 Hz, 2H, C2-CH<sub>2</sub>), 1.84 (p, *J* = 7.0 Hz, 2H, C3-CH<sub>2</sub>), 1.30 (s, 9H, *t*-Bu); **<sup>13</sup>C NMR** (100 MHz, CDCl<sub>3</sub>) δ: 198.1 (C1), 165.6 (d, *J* = 254.9 Hz, C11), 156.1 (C5), 133.2 (d, *J* = 3.1 Hz, C8), 130.6 (d, *J* = 9.7 Hz, C9), 115.6 (d, *J* = 22.3 Hz, C10), 78.9 (C6), 40.0 (C4), 35.5 (C2), 28.3 (C7), 24.4 (C3); **IR** *v*<sub>max</sub>(neat)/cm<sup>-1</sup>: 3383, 2986, 2872, 2360, 2050, 2016, 1702, 1671, 1594, 1502, 1365, 1277, 1244, 1205, 1153, 1005, 837, 751, 595; **HRMS** C<sub>15</sub>H<sub>20</sub>O<sub>3</sub>NF calculated [M<sup>+</sup>] 282.1505, found 304.1325 [M+Na]<sup>+</sup>.

#### ***tert*-butyl(4-cyclohexyl-4-oxobutyl)carbamate**



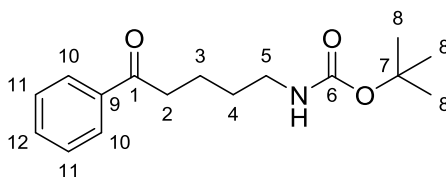
*N*-Boc-2-pyrrolidinone **84a** (1.01 g, 5.45 mmol) was reacted with cyclohexylmagnesium chloride (2 M solution in diethyl ether, 3.82 mL, 7.63 mmol). Purification on silica (12.5% v/v ethyl acetate-cyclohexane + 0.1% triethylamine) gave **85d** (726 mg, 49% yield) as a colourless oil. **<sup>1</sup>H NMR** (400 MHz, CDCl<sub>3</sub>) δ: 4.77 (bs, 1H, NH), 3.00 (m, 2H, C4-CH<sub>2</sub>), 2.38 (t, *J* = 7.1 Hz, 2H, C2-CH<sub>2</sub>), 2.24 (tt, *J* = 11.1, 3.4 Hz, 1H, C8-CH), 1.76 – 1.60 (m, 6H, C3-CH<sub>2</sub> and C9-CH<sub>2</sub>), 1.59 – 1.52 (m, 1H, C11-H), 1.33 (s, 9H, *t*-Bu), 1.27 – 1.04 (m, 5H, C10-CH<sub>2</sub> and C11-CH); **<sup>13</sup>C NMR** (100 MHz, CDCl<sub>3</sub>) δ: 213.6 (C1), 156.0 (C5), 78.9 (C6), 50.8 (C8), 40.0 (C2), 37.6 (C4), 28.4 (C7), 28.3 (C9), 25.8 (C11), 25.6 (C3), 23.9 (C10).

#### ***tert*-butyl(5-oxo-5-methylpentyl)carbamate**



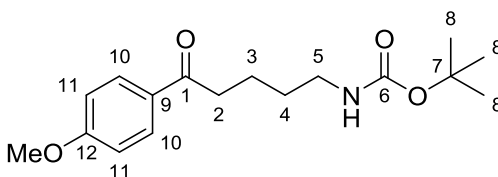
*N*-Boc-δ-valerolactam **84b** (1.35 g, 6.78 mmol) was reacted with methylmagnesium bromide (1.4 M solution in THF:toluene (1:3), 6.78 mL, 9.49 mmol). Purification on silica (15% v/v ethyl acetate-cyclohexane + 0.1% triethylamine) gave **86a** (1.08 g, 72% yield) as a white solid. **<sup>1</sup>H NMR** (400 MHz, CDCl<sub>3</sub>) δ: 4.67 (bs, 1H, NH), 3.03 (t, *J* = 6.8 Hz, 2H, C5-CH<sub>2</sub>), 2.40 (t, *J* = 7.2 Hz, 2H, C2-CH<sub>2</sub>), 2.07 (s, 3H, C9-CH<sub>3</sub>), 1.55-1.50 (m, 2H, C4-CH<sub>2</sub>), 1.41 (ddd, *J* = 4.1, 8.3, 9.2 Hz, 2H, C3-CH<sub>2</sub>), 1.36 (s, 9H, *t*-Bu); **<sup>13</sup>C NMR** (100 MHz, CDCl<sub>3</sub>) δ: 208.7 (C1), 156.0 (C6), 79.0 (C7), 43.0 (C9), 40.1 (C5), 29.8 (C2), 29.4 (C3), 28.4 (C8), 20.7 (C4); **IR**, *v*<sub>max</sub>(neat)/cm<sup>-1</sup>: 3361, 2972, 2937, 1682, 1672, 1518, 1364, 1247, 1161, 1020, 838, 781; **HRMS**: C<sub>11</sub>H<sub>21</sub>O<sub>3</sub>N, [M+Na]<sup>+</sup> found 238.1419. *Data consistent with literature values.*<sup>129</sup>

### ***tert*-butyl(5-oxo-5-phenylpentyl)carbamate**



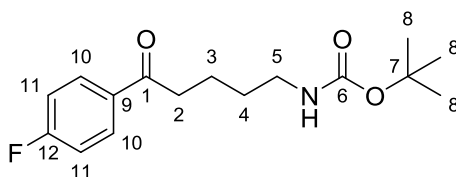
*N*-Boc- $\delta$ -valerolactam **84b** (1.21 g, 6.07 mmol) was reacted with phenylmagnesium bromide (1 M solution in THF, 8.5 mL, 8.5 mmol). Purification on silica (15% v/v ethyl acetate-cyclohexane + 0.1% triethylamine) gave **86b** (832mg, 49% yield) as a white solid. **<sup>1</sup>H NMR** (400 MHz, CDCl<sub>3</sub>)  $\delta$ : 7.96 - 7.93 (m, 2H, C10-CH), 7.56 - 7.52 (m, 1H, C12-CH), 7.46 - 7.42 (t,  $J$  = 7.6, 2H, C11-CH), 4.66 (bs, 1H, NH), 3.17 - 3.12 (m, 2H, C5-CH<sub>2</sub>), 2.99 (t,  $J$  = 7.2 Hz, 2H, C2-CH<sub>2</sub>), 1.80 - 1.72 (m, 2H, C4-CH<sub>2</sub>), 1.60 - 1.52 (m, 2H, C3-CH<sub>2</sub>), 1.43 (s, 9H, *t*-Bu); **<sup>13</sup>C NMR** (100 MHz, CDCl<sub>3</sub>)  $\delta$ : 200.1 (C1), 156.1 (C6), 137.0 (C9), 133.1 (C12), 128.7 (C11), 128.1 (C10), 79.1 (C7), 40.3 (C5), 38.0 (C2), 29.7 (C3), 28.5 (C8), 21.3 (C4). *Data consistent with literature values.*<sup>82</sup>

### ***tert*-butyl(5-oxo-5-(*p*-methoxyphenyl)pentyl)carbamate**



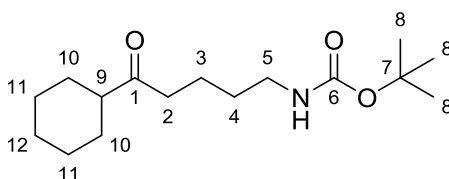
*N*-Boc- $\delta$ -valerolactam **84b** (1.61 g, 8.07 mmol) was reacted with *p*-methoxyphenylmagnesium bromide (0.5 M solution in THF, 22.6 mL, 11.3 mmol). Purification on silica (15% v/v ethyl acetate-cyclohexane + 0.1% triethylamine) gave **86c** (1.21 g, 49% yield) as a white solid. **<sup>1</sup>H NMR** (400 MHz, CDCl<sub>3</sub>)  $\delta$ : 7.90 - 7.87 (m, 2H, C10-CH), 6.89 - 6.86 (m, 2H, C11-CH), 4.73 (bs, 1H, NH), 3.81 (s, 3H, OMe), 3.15-3.07 (m, 2H, C5-CH<sub>2</sub>), 2.89 (t,  $J$  = 7.2 Hz, 2H, C2-CH<sub>2</sub>), 1.71 (p,  $J$  = 7.4 Hz, 2H, C4-CH<sub>2</sub>), 1.56-1.48 (p,  $J$  = 7.4 Hz, 2H, C3-CH<sub>2</sub>), 1.39 (s, 9H, *t*-Bu); **<sup>13</sup>C NMR** (100 MHz, CDCl<sub>3</sub>)  $\delta$ : 198.6 (C1), 163.4 (C6), 156.0 (C12), 130.2 (C9), 130.0 (C10), 113.7 (C11), 78.9 (C7), 55.4 (OMe), 40.2 (C5), 37.6 (C2), 29.6 (C3), 28.4 (C8), 21.4 (C4). *Data consistent with literature values.*<sup>82</sup>

### ***tert*-butyl(5-oxo-5-(*p*-fluorophenyl)pentyl)carbamate**



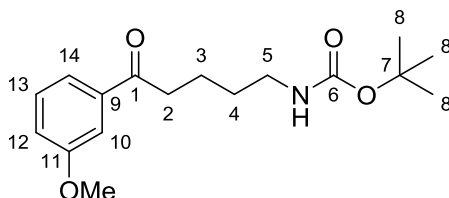
*N*-Boc- $\delta$ -valerolactam **84b** (1.10 g, 5.52 mmol) was reacted with *p*-fluorophenylmagnesium bromide (1 M solution in THF, 7.73 mL, 7.73 mmol). Purification on silica (15% v/v ethyl acetate-cyclohexane + 0.1% triethylamine) gave **86d** (1.07 g, 65% yield) as a white solid. **<sup>1</sup>H NMR** (400 MHz, CDCl<sub>3</sub>)  $\delta$ : 8.01 – 7.94 (m, 2H, C11-CH), 7.15 – 7.08 (m, 2H, C10-CH), 4.61 (bs, 1H, NH), 3.15 (t, *J* = 6.6 Hz, 2H, C5-CH<sub>2</sub>), 2.97 (t, *J* = 7.2 Hz, 2H, C2-CH<sub>2</sub>), 1.80 – 1.71 (m, 2H, C4-CH<sub>2</sub>), 1.61 – 1.52 (m, 2H, C3-CH<sub>2</sub>), 1.43 (s, 9H, *t*-Bu); **<sup>13</sup>C NMR** (100 MHz, CDCl<sub>3</sub>)  $\delta$ : 198.5 (C1), 165.8 (d, *J* = 256.1 Hz, C12), 156.2 (C6), 133.5 (d, *J* = 2.7 Hz, C9), 130.8 (d, *J* = 9.4 Hz, C10), 115.8 (d, *J* = 21.9 Hz, C11), 79.3 (C7), 40.3 (C5), 38.0 (C2), 29.8 (C3), 28.5 (C8), 21.3 (C4).

#### ***tert*-butyl(5-cyclohexyl-5-oxopentyl)carbamate**



*N*-Boc- $\delta$ -valerolactam **84b** (1.11 g, 5.57 mmol) was reacted with cyclohexylmagnesium chloride solution (2 M solution in diethyl ether, 3.90 mL, 7.80 mmol). Purification on silica (12.5% v/v ethyl acetate-cyclohexane + 0.1% triethylamine) gave **86e** (0.865 g, 55% yield) as a colourless oil. **<sup>1</sup>H NMR** (400 MHz, CDCl<sub>3</sub>)  $\delta$ : 4.59 (bs, 1H, NH), 3.12 – 3.04 (m, 2H, C5-CH<sub>2</sub>), 2.44 (t, *J* = 7.0 Hz, 2H, C2-CH<sub>2</sub>), 2.30 (tt, *J* = 11.0, 3.5 Hz, 1H, C9-CH), 1.83 – 1.71 (m, 4H, ), 1.68 – 1.60 (m, 1H), 1.60 – 1.49 (m, 2H, C3-CH<sub>2</sub>), 1.48 – 1.38 (m, 2H), 1.42 (s, 9H, *t*-Bu), 1.36 – 1.11 (m, 5H); **<sup>13</sup>C NMR** (100 MHz, CDCl<sub>3</sub>)  $\delta$ : 214.1 (C1), 156.1 (C6), 79.2 (C7), 51.0 (C9), 40.3 (C5), 40.1 (C2), 29.7 (C3), 28.6 (C10), 28.5 (C8), 26.0 (C12), 25.8 (C4), 20.7 (C11); **IR**,  $\nu_{\text{max}}(\text{neat})/\text{cm}^{-1}$ : 3383, 2931, 1704, 1685, 1515, 1363, 1272. *Data consistent with literature values.*<sup>82</sup>

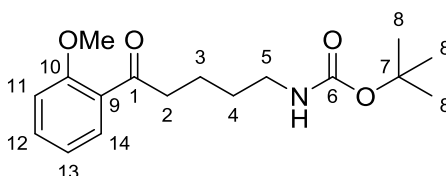
#### ***tert*-butyl(5-oxo-5-(*m*-methoxyphenyl)pentyl)carbamate**



*N*-Boc- $\delta$ -valerolactam **84b** (1.20 g, 6.02 mmol) was reacted with *m*-methoxyphenylmagnesium bromide (1 M solution in THF, 8.43 mL, 8.43 mmol). Purification on silica (15% v/v ethyl acetate-cyclohexane + 0.1% triethylamine) gave **86f** (1.21 g, 65% yield) as a white solid. **<sup>1</sup>H NMR** (400 MHz, CDCl<sub>3</sub>)  $\delta$ : 7.49 (d, *J* = 7.6 Hz, 1H, C14-CH), 7.43 (s, 1H, C10-CH), 7.32 (t, *J* = 7.9 Hz, 1H, C13-CH), 7.06 (d, *J* = 8.2 Hz, 1H, C12-CH), 4.72

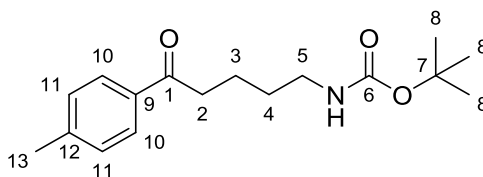
(bs, 1H, NH), 3.80 (s, 3H, OMe), 3.12 (m, 2H, C5-CH<sub>2</sub>), 2.94 (t,  $J = 7.1$  Hz, 2H, C2-CH<sub>2</sub>), 1.79 – 1.65 (m, 2H, C4-CH<sub>2</sub>), 1.60 – 1.45 (m, 2H, C3-CH<sub>2</sub>), 1.39 (s, 9H, *t*-Bu); <sup>13</sup>C NMR (100 MHz, CDCl<sub>3</sub>) δ: 199.9 (C1), 159.9 (C6), 156.1 (C9), 138.3 (C11), 129.6 (C13), 120.7 (C14), 119.4 (C12), 112.3 (C10), 79.1 (C7), 55.4 (OMe), 38.1 (C5), 29.7 (C2), 28.4 (C3), 26.9 (C8), 21.3 (C4). *Data consistent with literature values.*<sup>82</sup>

***tert*-butyl(5-oxo-5-(*o*-methoxyphenyl)pentyl)carbamate**



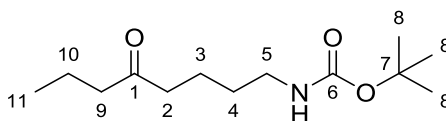
*N*-Boc- $\delta$ -valerolactam **84b** (1.20 g, 6.02 mmol) was reacted with *o*-methoxyphenylmagnesium bromide (1 M solution in THF, 6.62 mL, 6.63 mmol). Purification on silica (20% v/v ethyl acetate-cyclohexane + 0.1% triethylamine) gave **86g** (1.00 g, 54% yield) as pale yellow oil. <sup>1</sup>H NMR (400 MHz, CDCl<sub>3</sub>) δ: 7.63 (dd,  $J = 7.6, 1.8$  Hz, 1H, C14-CH), 7.43 (ddd,  $J = 8.4, 7.4, 1.8$  Hz, 1H, C12-CH), 6.97 (td,  $J = 7.5, 0.8$  Hz, 1H, C13-CH), 6.94 (d,  $J = 8.4$  Hz, 2H, C11-CH), 3.87 (s, 3H, OMe), 3.11 (t,  $J = 6.5$  Hz, 2H, C5-CH<sub>2</sub>), 2.97 (t,  $J = 7.2$  Hz, 2H, C2-CH<sub>2</sub>), 1.73 – 1.65 (m, 2H, C4-CH<sub>2</sub>), 1.56 – 1.48 (m, 2H, C3-CH<sub>2</sub>), 1.42 (s, 9H, *t*-Bu); <sup>13</sup>C NMR (100 MHz, CDCl<sub>3</sub>) δ: 202.7 (C1), 158.5 (C6), 156.1 (C9), 133.4 (C14), 130.2 (C12), 128.5 (C10), 120.7 (C11), 111.6 (C13), 79.1 (C7), 55.6 (OMe), 43.3 (C5), 29.7 (C2), 28.5 (C3), 27.0 (C8), 21.5 (C4). *Data consistent with literature values.*<sup>82</sup>

***tert*-butyl(5-oxo-5-(*p*-methoxyphenyl)pentyl)carbamate**



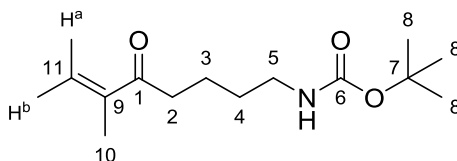
*N*-Boc- $\delta$ -valerolactam **84b** (1.09 g, 5.47 mmol) was reacted with *p*-tolylphenylmagnesium bromide (0.5 M solution in THF, 15.3 mL, 7.66 mmol). Purification on silica (15% v/v ethyl acetate-cyclohexane + 0.1% triethylamine) gave **86h** (516 mg, 32% yield) as a white solid. <sup>1</sup>H NMR (400 MHz, CDCl<sub>3</sub>) δ 7.88 - 7.83 (m, 2H, 2 x C10-CH), 7.28 – 7.22 (m, 2H, 2 x C11-CH), 4.61 (bs, 1H, NH), 3.19 – 3.12 (m, 2H, C5-CH<sub>2</sub>), 2.97 (t,  $J = 7.2$  Hz, 2H, C2-CH<sub>2</sub>), 2.41 (s, 3H, C13-CH<sub>3</sub>), 1.82 – 1.71 (m, 2H, C4-CH<sub>2</sub>), 1.62 – 1.50 (m, 2H, C3-CH<sub>2</sub>), 1.44 (s, 9H, *t*-Bu); <sup>13</sup>C NMR (100 MHz, CDCl<sub>3</sub>) δ: 199.8 (C1), 156.2 (C6), 143.9 (C9), 134.6 (C11), 129.4 (C12), 128.3 (C10), 79.3 (C7), 40.4 (C5), 38.0 (C13), 29.8 (C2), 28.6 (C8), 21.8 (C3), 21.5 (C4); HRMS C<sub>17</sub>H<sub>23</sub>O<sub>3</sub>N calculated [M<sup>+</sup>] 292.1912, found 314.1732 [M+Na]<sup>+</sup>.

### ***tert*-butyl(5-oxo-5-(*n*-propyl)pentyl)carbamate**



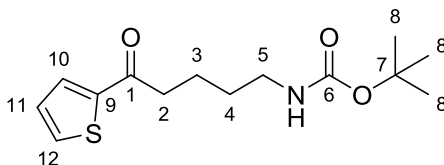
*N*-Boc- $\delta$ -valerolactam **84b** (2.21 g, 11.1 mmol) was reacted with *n*-propylmagnesium chloride (2 M solution in THF, 6.66 mL, 13.3 mmol). Purification on silica (12% v/v ethyl acetate-cyclohexane + 0.1% triethylamine) gave **86i** (1.82 g, 67% yield) as a colourless oil. **<sup>1</sup>H NMR** (400 MHz, CDCl<sub>3</sub>)  $\delta$ : 4.64 (bs, 1H, NH), 3.10-3.03 (m, 2H, C5-CH<sub>2</sub>), 2.38 (t,  $J$  = 7.2 Hz, 2H, C2-CH<sub>2</sub>), 2.33 (t,  $J$  = 7.3 Hz, 2H, C9-CH<sub>2</sub>), 1.60 – 1.50 (m, 4H, C3-CH<sub>2</sub> and C4-CH<sub>2</sub>), 1.47-1.38 (m, 2H, C10-CH<sub>2</sub>), 1.39 (s, 9H, *t*-Bu), 0.86 (t,  $J$  = 7.4 Hz, 3H, C11-CH<sub>3</sub>); **<sup>13</sup>C NMR** (100 MHz, CDCl<sub>3</sub>)  $\delta$ : 211.1 (C1), 156.1 (C6), 79.1 (C7), 44.8 (C9), 42.2 (C5), 40.2 (C2), 29.6 (C3), 28.5 (C8), 20.8 (C4), 17.4 (C10), 13.8 (C11); **HRMS** C<sub>13</sub>H<sub>23</sub>O<sub>3</sub>N [M<sup>+</sup>] calculated 244.1912, found 266.1732 [M+Na]<sup>+</sup>. *Data consistent with literature values.*<sup>130</sup>

### ***tert*-butyl(6-methyl-5-oxohept-6-en-1-yl)carbamate**



*N*-Boc- $\delta$ -valerolactam **84b** (1.25 g, 6.27 mmol) was reacted with isopropenylmagnesium bromide (0.5 M solution in THF, 14.4 mL, 7.22 mmol). Purification on silica (15% v/v ethyl acetate-cyclohexane + 0.1% triethylamine) gave **86j** (900 mg, 59% yield) as a pale yellow oil. **<sup>1</sup>H NMR** (400 MHz, CDCl<sub>3</sub>)  $\delta$  = 5.93 (s, 1H, C11-H<sup>a</sup>), 5.74 (s, 1H, C11-H<sup>b</sup>), 4.62 (bs, 1H, NH), 3.09 (t,  $J$  = 6.7, 2H, C5-CH<sub>2</sub>), 2.68 (t,  $J$  = 7.2, 2H, C2-CH<sub>2</sub>), 1.83 (s, 3H, C10-CH<sub>3</sub>), 1.65 – 1.56 (m, 2H, C4-CH<sub>2</sub>), 1.40 – 1.43 (m, 2H, C3-CH<sub>2</sub>), 1.40 (s, 9H, *t*-Bu); **<sup>13</sup>C NMR** (100 MHz, CDCl<sub>3</sub>)  $\delta$  = 202.1 (C1), 156.3 (C6), 144.7 (C9), 124.9 (C11), 79.4 (C7), 37.1 (C5), 29.0 (C2), 28.7 (C3), 21.7 (C4), 17.9 (C10); **IR**,  $\nu_{\text{max}}$ (neat)/cm<sup>-1</sup>: 3399, 2982, 1709, 1561, 1475, 1397; **HRMS** C<sub>13</sub>H<sub>23</sub>O<sub>3</sub>N calculated [M<sup>+</sup>] 242.1756, found 264.1576 [M+Na]<sup>+</sup>.

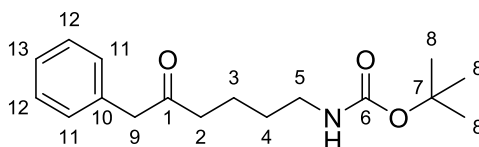
### ***tert*-butyl(5-oxo-5-(thiophen-2-yl)pentyl)carbamate**



*N*-Boc- $\delta$ -valerolactam **84b** (0.760 mg, 3.81 mmol) was reacted with 2-thienylmagnesium bromide (1 M solution in THF, 5.34 mL, 5.34 mmol). Purification on silica (12% v/v ethyl

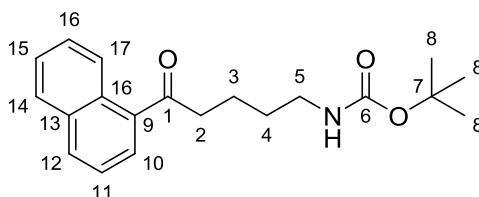
acetate-cyclohexane + 0.1% triethylamine) gave **86l** (465 mg, 43% yield) as a green oil. **<sup>1</sup>H NMR** (400 MHz, CDCl<sub>3</sub>) δ: 7.67 (dd, *J* = 3.8, 1.1 Hz, 1H, C10-CH), 7.58 (dd, *J* = 4.9, 1.1 Hz, 1H, C12-CH), 7.07 (dd, *J* = 4.9, 3.8 Hz, 1H, C11-CH), 4.72 (bs, 1H, NH), 3.11 (m, 2H, C5-CH<sub>2</sub>), 2.89 (t, *J* = 7.3 Hz, 2H, C2-CH<sub>2</sub>), 1.76 – 1.69 (m, 2H, C4-CH<sub>2</sub>), 1.56 – 1.48 (m, 2H, C3-CH<sub>2</sub>), 1.39 (s, 9H, *t*-Bu); **<sup>13</sup>C NMR** (100 MHz, CDCl<sub>3</sub>) δ: 193.0 (C1), 156.0 (C6), 144.3 (C9), 133.6 (C10), 131.9 (C12), 128.1 (C11), 79.0 (C7), 40.1 (C5), 38.7 (C2), 29.6 (C3), 28.4 (C8), 21.6 (C4). *Data consistent with literature values.*<sup>82</sup>

#### ***tert*-butyl(5-oxo-6-phenylhexyl)carbamate**



*N*-Boc- $\delta$ -valerolactam **84b** (1.20 g, 6.02 mmol) was reacted with benzylmagnesium chloride (2 M solution in THF, 3.92 mL, 7.83 mmol). Purification on silica (15% v/v ethyl acetate-cyclohexane + 0.1% triethylamine) gave **86m** (1.12 g, 63% yield) as colourless oil. **<sup>1</sup>H NMR** (400 MHz, CDCl<sub>3</sub>) δ: 7.34 – 7.30 (m, 2H, C11-CH), 7.28 – 7.25 (m, 1H, C13-CH), 7.20 – 7.17 (m, 2H, C12-CH), 4.56 (bs, 1H, NH), 3.67 (s, 2H, C9-CH<sub>2</sub>), 3.05 (m, 2H, C5-CH<sub>2</sub>), 2.47 (t, *J* = 7.2 Hz, 2H, C2-CH<sub>2</sub>), 1.59 – 1.52 (m, 2H, C4-CH<sub>2</sub>), 1.43 – 1.36 (m, 2H, C3-CH<sub>2</sub>), 1.42 (s, 9H, *t*-Bu); **<sup>13</sup>C NMR** (100 MHz, CDCl<sub>3</sub>) δ: 208.3 (C1), 156.1 (C6), 134.3 (C10), 129.5 (C11), 128.9 (C12), 127.1 (C13), 79.1 (C7), 50.3 (C9), 41.4 (C5), 40.2 (C2), 29.5 (C3), 28.5 (C8), 20.7 (C4); **IR**,  $\nu_{\text{max}}(\text{neat})/\text{cm}^{-1}$ : 3370, 2972, 2935, 1736, 1689, 1365, 1169, 1132.

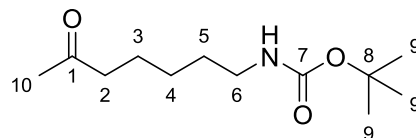
#### ***tert*-butyl(5-(naphthalene-1-yl)-5-oxopentyl)carbamate**



*N*-Boc- $\delta$ -valerolactam **84b** (1.19 g, 5.97 mmol) was reacted with (1-naphthyl)magnesium bromide (0.25 M slurry in THF, 29.8 mL, 7.47 mmol). Purification on silica (10% v/v ethyl acetate-cyclohexane + 0.1% triethylamine) gave **86n** (773 mg, 40% yield) as a yellow solid. **<sup>1</sup>H NMR** (400 MHz, CDCl<sub>3</sub>) δ: 8.53 (dd, *J* = 8.5, 0.6 Hz, 1H, ArH), 7.97 (d, *J* = 8.2 Hz, 1H, ArH), 7.88 – 7.83 (m, 2H, ArH), 7.59 – 7.47 (m, 3H, ArH), 3.62 (t, *J* = 7.3 Hz, 2H, C5-CH<sub>2</sub>), 3.08 (t, *J* = 7.4 Hz, 2H, C2-CH<sub>2</sub>), 1.84 – 1.76 (m, 2H, C4-CH<sub>2</sub>), 1.73 – 1.66 (m, 2H, C3-CH<sub>2</sub>), 1.49 (s, 9H, *t*-Bu); **<sup>13</sup>C NMR** (100 MHz, CDCl<sub>3</sub>) δ: 204.6 (C1), 152.8 (C6), 136.4 (ArC), 134.1 (ArC), 132.5 (ArC), 130.2 (ArC), 128.5 (ArC), 127.9 (ArC), 127.3 (ArC), 126.5

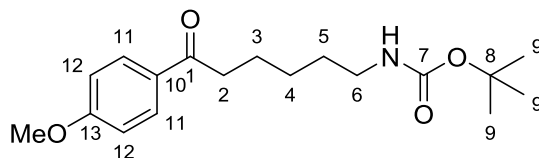
(ArC), 125.8 (ArC), 124.5 (ArC), 82.3 (C7), 46.2 (C5), 41.9 (C2), 28.8 (C8), 28.2 (C3), 22.0 (C4); **IR**,  $\nu_{\text{max}}(\text{neat})/\text{cm}^{-1}$ : 2971, 1736, 1683, 1437, 1333, 1171, 1131.

***tert*-butyl(6-oxo-6-methylhexyl)carbamate**



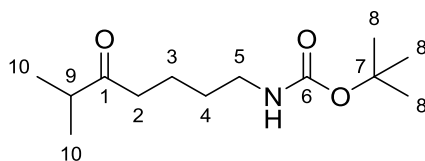
*N*-Boc- $\epsilon$ -caprolactam **84c** (1.81 g, 8.49 mmol) was reacted with methylmagnesium bromide (1.4 M solution in THF:toluene (1:3), 8.49 mL, 11.9 mmol). Purification on silica (15% v/v ethyl acetate-cyclohexane + 0.1% triethylamine) gave **87a** (700 mg, 36% yield) as a colourless oil. **<sup>1</sup>H NMR** (400 MHz, CDCl<sub>3</sub>)  $\delta$ : 4.68 (bs, 1H, NH), 2.99 (t,  $J$  = 7.0 Hz, 2H, C6-CH<sub>2</sub>), 2.33 (t,  $J$  = 7.4 Hz, 2H, C2-CH<sub>2</sub>), 2.02 (s, 3H, C10-CH<sub>3</sub>), 1.47 (dt,  $J$  = 15.1, 7.4 Hz, 2H, C5-CH<sub>2</sub>), 1.42-1.34 (m, 2H, C3-CH<sub>2</sub>), 1.33 (s, 9H, *t*-Bu), 1.26-1.14 (m, 2H, C4-CH<sub>2</sub>); **<sup>13</sup>C NMR** (100 MHz, CDCl<sub>3</sub>)  $\delta$ : 207.8 (C1), 154.9 (C7), 77.8 (C8), 63.4 (C10), 42.4 (C6), 39.3 (C2), 28.7 (C3), 27.3 (C5), 22.2 (C4); **IR**,  $\nu_{\text{max}}(\text{neat})/\text{cm}^{-1}$ : 3374, 2973, 2931, 2866, 1707, 1680, 1515, 1362, 1250, 1162, 1048, 997, 865, 781; **HRMS**: C<sub>12</sub>H<sub>23</sub>O<sub>3</sub>N, [M+Na]<sup>+</sup> found 252.1570.

***tert*-butyl(6-oxo-6-(*p*-methoxy)phenylhexyl)carbamate**



*N*-Boc- $\epsilon$ -caprolactam **84c** (1.45 g, 6.80 mmol) was reacted with (*p*-methoxyphenyl)magnesium bromide (0.5 M solution in THF, 19.0 mL, 9.52 mmol). Purification on silica (15% v/v ethyl acetate-cyclohexane + 0.1% triethylamine) gave **87c** (880 mg, 40% yield) as a white solid. **<sup>1</sup>H NMR** (400 MHz, CDCl<sub>3</sub>)  $\delta$ : 7.93 - 7.88 (m, 2H, C11-CH), 6.93 - 6.88 (m, 2H, C12-CH), 4.61 (bs, 1H, NH), 3.85 (s, 3H, OMe), 3.10 (t,  $J$  = 6.2 Hz, 2H, C6-CH<sub>2</sub>), 2.89 (t,  $J$  = 7.2 Hz, 2H, C2-CH<sub>2</sub>), 1.71 (p,  $J$  = 7.5 Hz, 2H, C5-CH<sub>2</sub>), 1.55 - 1.45 (m, 2H, C3-CH<sub>2</sub>), 1.41 (s, 9H, *t*-Bu), 1.40 - 1.32 (m, 2H, C4-CH<sub>2</sub>); **<sup>13</sup>C NMR** (100 MHz, CDCl<sub>3</sub>)  $\delta$ : 199.0 (C1), 163.4 (C7), 156.1 (C10), 130.4 (C11), 130.1 (C13), 113.8 (C12), 79.1 (C8), 55.5 (OMe), 38.1 (C6), 30.1 (C2), 28.5 (C3), 26.9 (C5), 24.2 (C4); **IR**,  $\nu_{\text{max}}(\text{neat})/\text{cm}^{-1}$ : 3377, 2982, 2934, 2866, 1701, 1664, 1597, 1511, 1455, 1445, 1250, 1170, 1045, 975, 829, 817; **HRMS** C<sub>18</sub>H<sub>27</sub>O<sub>4</sub>N [M+Na]<sup>+</sup> found 344.1930.

### 7.3.1.3 Preparation of *tert*-butyl(6-methyl-5-oxoheptyl)carbamate **86k**



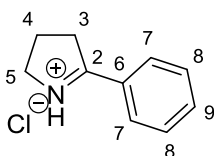
A round-bottom flask containing **86j** (312 mg, 1.29 mmol) was flushed with nitrogen gas. Under the flow of nitrogen, 10 mol% Pd/C was added. The flask was then evacuated and flushed with H<sub>2</sub> several times, before methanol (6.5 mL) was added. The stirring solution was then left to react under the H<sub>2</sub> atmosphere and monitored by TLC. Once consumption of starting material was confirmed, the mixture was filtered through a pad of Celite washed with MeOH in a sintered funnel under vacuum. The Celite was washed again with MeOH (2 x 10 mL), before the organic layers were collected and concentrated under vacuum with no further purification to yield **86k** (290 mg, 92% yield) as a colourless oil. **<sup>1</sup>H NMR** (400 MHz, CDCl<sub>3</sub>) δ: 4.59 (bs, 1H, NH), 3.09 (t, *J* = 6.6, 2H, C5-CH<sub>2</sub>), 2.57 (sept, *J* = 7.0 Hz, 1H, C9-CH), 2.46 (t, *J* = 7.1 Hz, 2H, C2-CH<sub>2</sub>), 1.61 – 1.53 (m, 2H, C4-CH<sub>2</sub>), 1.49 - 1.43 (m, 2H, C3-CH<sub>2</sub>), 1.42 (s, 9H, *t*-Bu), 1.07 (d, *J* = 7.0 Hz, 6H, C10-CH<sub>3</sub>); **<sup>13</sup>C NMR** (100 MHz, CDCl<sub>3</sub>) δ: 214.6 (C1), 156.0 (C6), 79.2 (C7), 41.0 (C9), 40.3 (C5), 39.8 (C2), 29.7 (C3), 28.5 (C4), 18.4 (C10); **IR**, *v*<sub>max</sub>(neat)/cm<sup>-1</sup>: 3361, 2970, 1692, 1515, 1364, 1269.

### 7.3.1.4 Synthesis of 2-substituted cyclic imine hydrochloride salts

*N*-Boc-protected aminoketones **85** - **87** were dissolved in TFA and stirred at room temperature for 4 h. The reaction mixture was then cooled to 0°C before addition of NaOH (20% in water) until pH 14. The aqueous phase was then extracted with CH<sub>2</sub>Cl<sub>2</sub> or diethyl ether (3 x 25 mL). The combined organic phases were dried over MgSO<sub>4</sub> and concentrated under vacuum to give the cyclic imine free base.

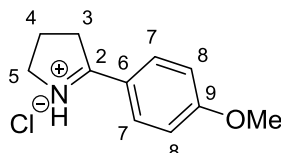
Without further purification, the imine was dissolved in diethyl ether (10-30 mL) and HCl (2 M solution in diethyl ether, 2 eq.) was added. The resulting hydrochloride salt was washed with ethyl acetate and dried under vacuum to give the final product.

### 2-phenyl-1-pyrrolinium chloride



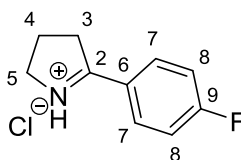
**85a** (680 mg, 2.58 mmol) was dissolved in TFA (4 mL). **1b** (330 mg, 71% yield) was obtained as an off-white solid. **<sup>1</sup>H NMR** (400 MHz, CD<sub>3</sub>OD) δ: 8.07 - 8.04 (m, 2H, C7-CH), 7.87-7.80 (tt, *J* = 7.6, 1.2 Hz, 1H, C9-CH), 7.72 - 7.67 (m, 2H, C8-CH), 4.25 (tt, *J* = 7.9, 2.1 Hz, 2H, C5-CH<sub>2</sub>), 3.65 (tt, *J* = 7.9, 2.1 Hz, 2H, C3-CH<sub>2</sub>), 2.45 (p, *J* = 7.9 Hz, 2H, C4-CH<sub>2</sub>); **<sup>13</sup>C NMR** (100 MHz, CD<sub>3</sub>OD) δ: 187.6 (C2), 137.6 (C6), 131.5 (C7), 130.9 (C8), 127.3 (C9), 54.9 (C5), 36.3 (C3), 20.9 (C4). *Data consistent with literature values.*<sup>131</sup>

### 2-(*p*-methoxyphenyl)-1-pyrrolinium chloride



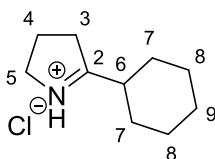
**85b** (720 mg, 2.45 mmol) was dissolved in TFA (4 mL). **1c** (401 mg, 77% yield) was obtained as a pale-pink solid. **<sup>1</sup>H NMR** (400 MHz, CD<sub>3</sub>OD) δ: 8.06 - 8.01 (m, 2H, C7-CH), 7.22 - 7.18 (m, 2H, C8-CH), 4.17 (tt, *J* = 7.8, 1.8 Hz, 2H, C5-CH<sub>2</sub>), 3.96 (s, 3H, OMe), 3.59 (tt, *J* = 7.8, 1.8 Hz, 2H, C3-CH<sub>2</sub>), 2.45 - 2.36 (m, 2H, C4-CH<sub>2</sub>); **<sup>13</sup>C NMR** (100 MHz, CD<sub>3</sub>OD) δ: 185.3 (C2), 168.0 (C6), 134.5 (C7), 119.4 (C9), 116.4 (C8), 56.7 (OMe), 54.2 (C5), 35.7 (C3), 21.1 (C4). *Data consistent with literature values.*<sup>132</sup>

### 2-(*p*-fluorophenyl)-1-pyrrolinium chloride



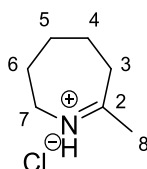
**85c** (1.18 g, 4.19 mmol) was dissolved in TFA (5 mL). **1d** (792 mg, 94% yield) was obtained as a white solid. **<sup>1</sup>H NMR** (400 MHz, CD<sub>3</sub>OD) δ: 8.26 - 8.17 (m, 2H, C8-CH), 7.48 - 7.42 (m, 2H, C7-CH), 4.32 - 4.24 (tt, *J* = 7.8, 2.0 Hz, 2H, C5-CH<sub>2</sub>), 3.69 (tt, *J* = 8.0, 2.0 Hz, 2H, C3-CH<sub>2</sub>), 2.50 - 2.41 (p, *J* = 8.0 Hz, 2H, C4-CH<sub>2</sub>); **<sup>13</sup>C NMR** (100 MHz, CD<sub>3</sub>OD) δ: 186.2 (C2), 168.8 (d, *J* = 260.3 Hz, C9), 135.0 (d, *J* = 10.3, C7), 124.0 (d, *J* = 3.1 Hz, C6), 118.2 (d, *J* = 23.5 Hz, C8), 55.0 (C5), 36.4 (C3), 21.0 (C4). *Data consistent with literature values.*<sup>132</sup>

## 2-cyclohexyl-1-pyrrolinium chloride



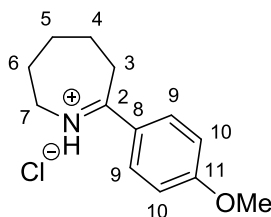
**85e** (700 mg, 2.60 mmol) was dissolved in TFA (2.5 mL). **1e** (422 mg, 87% yield) was obtained as a pale grey solid. **<sup>1</sup>H NMR** (400 MHz, CD<sub>3</sub>OD) δ: 4.06 (tdd, *J* = 7.8, 3.4, 2.1 Hz, 2H, C5-CH<sub>2</sub>), 3.19 (ddt, *J* = 8.2, 8.0, 2.1 Hz, 2H, C3-CH<sub>2</sub>), 2.88 – 2.78 (tt, *J* = 8.2, 2.1 Hz, 1H, C6-CH), 2.32 – 2.24 (m, 2H, C4-CH<sub>2</sub>), 2.04 – 1.97 (m, 2H), 1.91 – 1.84 (m, 2H), 1.80 – 1.73 (m, 1H), 1.52 – 1.36 (m, 4H), 1.35 – 1.23 (m, 1H); **<sup>13</sup>C NMR** (100 MHz, CD<sub>3</sub>OD) δ: 201.9 (C2), 54.6 (C5), 42.5 (C6), 36.6 (C3), 30.3 (C7), 26.3 (C8), 20.6 (C4); **HRMS** C<sub>10</sub>H<sub>18</sub>N calculated [M<sup>+</sup>] 153.1517, found 175.1337 [M+Na]<sup>+</sup>.

## 7-methyl-3,4,5,6-tetrahydro-2*H*-azepinium chloride



**87a** (640 mg, 2.79 mmol) was dissolved in TFA (2.5 mL). **3a** (320 mg, 78% yield) was obtained as a light-brown solid. **<sup>1</sup>H NMR** (400 MHz, CD<sub>3</sub>OD) δ: 3.68-3.62 (m, 2H, C7-CH<sub>2</sub>), 2.85 – 2.72 (m, 2H, C3-CH<sub>2</sub>), 2.42 (s, 3H, C8-CH<sub>3</sub>), 1.81 (ddd, *J* = 7.9, 7.3, 4.5 Hz, 2H, C6-CH<sub>2</sub>), 1.64 – 1.57 (m, 4H, C4-CH<sub>2</sub> and C5-CH<sub>2</sub>); **<sup>13</sup>C NMR** (100 MHz, CD<sub>3</sub>OD) δ: 199.4 (C2), 49.1 (C7), 36.3 (C8), 30.8 (C3), 27.2 (C6), 25.9 (C4), 22.4 (C5). *Data consistent with literature values.*<sup>133</sup>

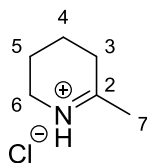
## 7-(*p*-methoxyphenyl)-3,4,5,6-tetrahydro-2*H*-azepinium chloride



**87c** (880 mg, 2.74 mmol) was dissolved in TFA (4 mL). **3c** (320 mg, 49% yield) was obtained as a white solid. **<sup>1</sup>H NMR** (400 MHz, CD<sub>3</sub>OD) δ: 8.00 – 7.96 (m, 2H, C9-CH<sub>2</sub>), 7.03 – 6.99 (m, 2H, C10-CH<sub>2</sub>), 3.87 (s, 3H, OMe), 3.03 (t, *J* = 7.0 Hz, 2H, C7-CH<sub>2</sub>), 2.94 (t, *J* = 7.7 Hz, 2H, C3-CH<sub>2</sub>), 1.80 – 1.65 (m, 4H, C4-CH<sub>2</sub> and C6-CH<sub>2</sub>), 1.51 – 1.42 (m, 2H, C5-CH<sub>2</sub>); **<sup>13</sup>C NMR** (100 MHz, CD<sub>3</sub>OD) δ: 201.0 (C2), 165.5 (C8), 131.5 (C11), 131.1 (C9),

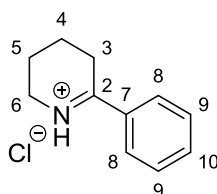
114.9 (C10), 56.1 (OMe), 40.6 (C7), 38.5 (C3), 28.5 (C4), 27.0 (C6), 24.9 (C5); **IR**,  $\nu_{\text{max}}(\text{neat})/\text{cm}^{-1}$  2945, 2925, 2785, 1594, 1267, 1197, 1018; **HRMS**  $\text{C}_{13}\text{H}_{18}\text{ON}$  [ $\text{M}^+$ ] found 204.1387.

### 2-methyl-1-piperideinium chloride



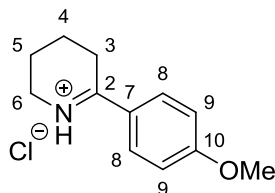
**86a** (1.02 g, 4.74 mmol) was dissolved in TFA (5 mL). **5a** (520 mg, 82% yield) was obtained as a light-brown solid.  **$^1\text{H NMR}$**  (400 MHz,  $\text{CD}_3\text{OD}$ )  $\delta$ : 3.68-3.62 (m, 2H, C6- $\text{CH}_2$ ), 2.85-2.79 (m, 2H (C3- $\text{CH}_2$ ), 2.41 (s, 3H, C7- $\text{CH}_3$ ), 2.02-1.80 (m, 4H, C4- $\text{CH}_2$  and C5- $\text{CH}_2$ );  **$^{13}\text{C NMR}$**  (100 MHz,  $\text{CD}_3\text{OD}$ )  $\delta$ : 191.8 (C2), 45.7 (C6), 32.1 (C7), 24.9 (C3), 20.1 (C5), 17.9 (C4).

### 2-phenyl-1-piperideinium chloride



**86b** (320 mg, 1.15 mmol) was dissolved in TFA (2.5 mL). **5b** (196 mg, 87% yield) was obtained as a white solid.  **$^1\text{H NMR}$**  (400 MHz,  $\text{CD}_3\text{OD}$ )  $\delta$ : 7.94 – 7.90 (m, 2H, C8- $\text{CH}$ ), 7.79 (tt,  $J = 7.5, 4.7, 1.1$  Hz, 1H, C10- $\text{CH}$ ), 7.69-7.63 (m, 2H, C9- $\text{CH}$ ), 3.91-3.83 (m, 2H, C6- $\text{CH}_2$ ), 3.32 – 3.29 (m, 2H, C3- $\text{CH}_2$ ), 2.06 – 1.99 (m, 4H, C4- $\text{CH}_2$  and C5- $\text{CH}_2$ );  **$^{13}\text{C NMR}$**  (100 MHz,  $\text{CD}_3\text{OD}$ )  $\delta$ : 185.1 (C2), 136.1 (C10), 133.1 (C9), 130.7 (C7), 129.1 (C8), 46.5 (C6), 29.8 (C3), 20.3 (C5), 18.2 (C4). *Data consistent with literature values.*<sup>134</sup>

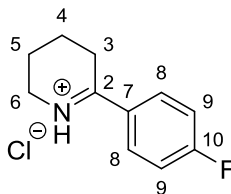
### 2-(*p*-methoxyphenyl)-1-piperideinium chloride



**86c** (1.04 g, 3.38 mmol) was dissolved in TFA (5 mL). **5c** (746 mg, 98% yield) was obtained as a pale-yellow solid.  **$^1\text{H NMR}$**  (400 MHz,  $\text{CD}_3\text{OD}$ )  $\delta$ : 7.96 – 7.91 (m, 2H, C8- $\text{CH}$ ), 7.20 – 7.15 (m, 2H, C9- $\text{CH}$ ), 3.93 (s, 3H, OMe), 3.82-3.77 (m, 2H, C6- $\text{CH}_2$ ), 3.31 – 3.26 (m, 2H, C3- $\text{CH}_2$ ), 2.03-1.98 (m, 4H, C4- $\text{CH}_2$  and C5- $\text{CH}_2$ );  **$^{13}\text{C NMR}$**  (100 MHz,  $\text{CD}_3\text{OD}$ )  $\delta$ : 182.2

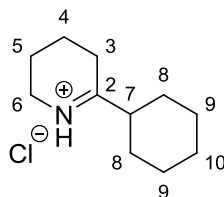
(C2), 167.0 (C7), 131.6 (C9), 124.6 (C10), 116.1 (C8), 56.5 (OMe), 46.1 (C6), 29.1 (C3), 20.6 (C5), 18.6 (C4).

### 2-(*p*-fluorophenyl)-1-piperideinium chloride



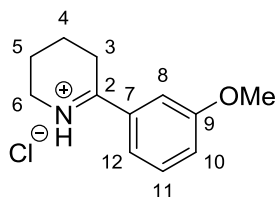
**86d** (986 mg, 3.34 mmol) was dissolved in TFA (4 mL). **5d** (513 mg, 72% yield) was obtained as a white solid. **<sup>1</sup>H NMR** (400 MHz, CD<sub>3</sub>OD) δ: δ 8.03 – 7.97 (m, 2H, C8-CH), 7.44 – 7.38 (m, 2H, C9-CH), 3.88 – 3.82 (m, 2H, C6-CH<sub>2</sub>), 3.32 – 3.30 (m, 2H, C3-CH<sub>2</sub>), 2.05 – 2.00 (m, 4H, C4-CH<sub>2</sub> and C5-CH<sub>2</sub>); **<sup>13</sup>C NMR** (100 MHz, CD<sub>3</sub>OD) δ: 183.6 (C2), 168.1 (d, *J* = 254.0 Hz, C10), 132.3 (d, *J* = 9.6 Hz, C8), 129.5 (d, *J* = 3.1 Hz, C7), 117.8 (d, *J* = 22.1 Hz, C9), 46.5 (C6), 29.2 (C3), 20.3 (C5), 18.2 (C4). *Data consistent with literature values.*<sup>135</sup>

### 2-cyclohexyl-1-piperideinium chloride



**86e** (668 mg, 2.36 mmol) was dissolved in TFA (3 mL). **5e** (423 mg, 90% yield) was obtained as brown crystals. **<sup>1</sup>H NMR** (400 MHz, CD<sub>3</sub>OD) δ: 3.69 – 3.63 (m, 2H, C6-CH<sub>2</sub>), 2.90 – 2.81 (m, 2H, C3-CH<sub>2</sub>), 2.68 – 2.59 (m, 1H, C7-CH), 1.97 – 1.82 (m, 8H), 1.79 – 1.73 (m, 1H), 1.54 – 1.23 (m, 5H); **<sup>13</sup>C NMR** (100 MHz, CD<sub>3</sub>OD) δ: 197.3 (C2), 48.5 (C7), 46.1 (C6), 30.4 (C8), 26.8(C3), 26.7 (C9), 26.5 (C10), 20.5 (C5), 18.0 (C4); **HRMS** C<sub>11</sub>H<sub>20</sub>N calculated [M<sup>+</sup>] 166.1596, found 166.1598 [M<sup>+</sup>].

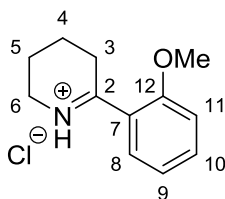
### 2-(*m*-methoxyphenyl)-1-piperideinium chloride



**86f** (1.00 g, 3.25 mmol) was dissolved in TFA (5 mL). **5f** (647 mg, 88% yield) was obtained as a brown solid. **<sup>1</sup>H NMR** (400 MHz, CD<sub>3</sub>OD) δ: 7.58 (dd, *J* = 1.8, 6.1, 2H, C8-CH and C12-

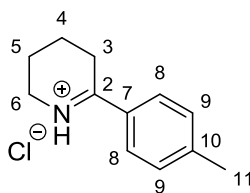
CH), 7.56 – 7.52 (m, 1H, C11-CH), 7.33 (dt,  $J = 2.2, 7.0$ , 1H, C10-CH), 3.91 (s, 3H, OMe), 3.90 - 3.87 (m, 2H, C6-CH<sub>2</sub>), 3.40 – 3.32 (m, 2H, C3-CH<sub>2</sub>), 2.09 – 1.99 (m, 4H, C4-CH<sub>2</sub> and C5-CH<sub>2</sub>); **<sup>13</sup>C NMR** (100 MHz, CD<sub>3</sub>OD)  $\delta$ : 184.2 (C2), 161.4 (C7), 134.1 (C9), 131.8 (C11), 122.2 (C12), 121.6 (C8), 113.8 (C10), 56.5 (OMe), 46.3 (C6), 29.9 (C3), 20.3 (C5), 18.4 (C4); **HRMS** C<sub>12</sub>H<sub>16</sub>N [M<sup>+</sup>] calculated 191.1310, found 213.1130 [M+Na]<sup>+</sup>. *Data consistent with literature values.*<sup>135</sup>

### 2-(*o*-methoxyphenyl)-1-piperideinium chloride



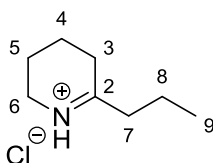
**86g** (950 mg, 3.09 mmol) was dissolved in TFA (4 mL). **5g** (590 mg, 85% yield) was obtained as an off-white solid. **<sup>1</sup>H NMR** (400 MHz, CD<sub>3</sub>OD)  $\delta$ : 7.84 (dd,  $J = 8.0, 1.6$  Hz, 1H, C8-CH), 7.74 (ddd,  $J = 8.5, 7.5, 1.6$  Hz, 1H, C10-CH), 7.33 (d,  $J = 8.5$  Hz, 1H, C11-CH), 7.23 – 7.19 (m, 1H, C9-CH), 4.05 (s, 3H, OMe), 3.91 - 3.86 (m, 2H, C6-CH<sub>2</sub>), 3.33 – 3.27 (m, 2H, C3-CH<sub>2</sub>), 2.04 – 1.99 (m, 4H, C4-CH<sub>2</sub> and C5-CH<sub>2</sub>); **<sup>13</sup>C NMR** (100 MHz, CD<sub>3</sub>OD)  $\delta$ : 182.3 (C2), 160.1 (C7), 137.9 (C8), 131.8 (C10), 122.6 (C11), 120.4 (C12), 113.8 (C9), 57.1 (OMe), 46.6 (C6), 30.3 (C3), 20.4 (C5), 18.5 (C4); **HRMS** C<sub>12</sub>H<sub>16</sub>N [M<sup>+</sup>] calculated 191.1310, found 213.1130 [M+Na]<sup>+</sup>. *Data consistent with literature values.*<sup>136</sup>

### 2-(*p*-tolyl)-1-piperideinium chloride



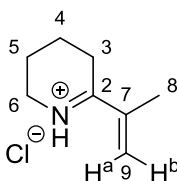
**86h** (470 mg, 1.61 mmol) was dissolved in TFA (3 mL). **5h** (315 mg, 93% yield) was obtained as an off-white solid. **<sup>1</sup>H NMR** (400 MHz, CD<sub>3</sub>OD)  $\delta$ : 7.84 - 7.80 (d,  $J = 8.5$  Hz, 2H, C8-CH), 7.50 - 7.46 (d,  $J = 8.0$  Hz, 2H, C9-CH), 3.86 - 3.80 (m, 2H, C6-CH<sub>2</sub>), 3.33 - 3.28 (m, 2H, C3-CH<sub>2</sub>), 2.48 (s, 3H, C11-CH<sub>3</sub>), 2.04 – 2.00 (m, 4H, C4-CH<sub>2</sub> and C5-CH<sub>2</sub>); **<sup>13</sup>C NMR** (100 MHz, CD<sub>3</sub>OD)  $\delta$ : 184.1 (C2), 148.1 (C7), 131.4 (C9), 130.2 (C10), 129.1 (C8), 46.3 (C6), 29.5 (C3), 21.7 (C11), 20.4 (C5), 18.4 (C4). *Data consistent with literature values.*<sup>136</sup>

## 2-(*n*-propyl)-1-piperideinium chloride



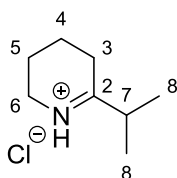
**86i** (1.81 g, 7.44 mmol) was dissolved in TFA (8 mL) and the freebase imine was extracted into diethyl ether (4 x 25 mL) before acidification HCl/diethyl ether without concentration. **5i** (1.12 g, 93% yield) was obtained as light brown crystals. **<sup>1</sup>H NMR** (400 MHz, CD<sub>3</sub>OD)  $\delta$ : 3.69 - 3.63 (m, 2H, C6-CH<sub>2</sub>), 2.84 (tt,  $J$  = 6.1, 2.2, 1.8 Hz, 2H, C3-CH<sub>2</sub>), 2.68 - 2.59 (tt,  $J$  = 7.9, 5.4, 1.1 Hz, 2H, C4-CH<sub>2</sub>), 1.96 - 1.82 (m, 4H, C5-CH<sub>2</sub> and C7-CH<sub>2</sub>), 1.72 (sxt,  $J$  = 7.4 Hz, 2H, C8-CH<sub>2</sub>), 1.03 (t,  $J$  = 7.4, 3H, C9-CH<sub>3</sub>); **<sup>13</sup>C NMR** (100 MHz, CD<sub>3</sub>OD)  $\delta$ : 194.4 (C2), 45.8 (C6), 41.0 (C7), 30.7 (C3), 20.3 (C5), 20.3 (C8), 17.9 (C4), 13.8 (C9); **HRMS** C<sub>8</sub>H<sub>16</sub>N calculated [M<sup>+</sup>] 126.1283, found 126.1281 [M<sup>+</sup>]. *Data consistent with literature values.*<sup>130</sup>

## 2-isopropenyl-1-piperideinium chloride



**86j** (550 mg, 2.28 mmol) was dissolved in TFA (3 mL). **5j** (321 mg, 88% yield) was obtained as a sticky brown solid. **<sup>1</sup>H NMR** (400 MHz, CD<sub>3</sub>OD)  $\delta$  = 6.27 (s, 1H, C9-H<sup>a</sup>), 6.05 (s, 1H, C9-H<sup>b</sup>), 3.78 - 3.74 (m, 2H, C6-CH<sub>2</sub>), 3.09 - 3.05 (m, 2H, C3-CH<sub>2</sub>), 2.11 (s, 3H C8-CH<sub>3</sub>), 1.98 - 1.88 (m, 4H, C4-CH<sub>2</sub> and C5-CH<sub>2</sub>); **<sup>13</sup>C NMR** (100 MHz, CD<sub>3</sub>OD)  $\delta$  = 183.5 (C2), 139.2 (C7), 131.8 (C9), 46.4 (C6), 27.7 (C3), 20.3 (C5), 18.1 (C5), 15.5 (C4); **IR**,  $\nu_{\text{max}}$ (neat)/cm<sup>-1</sup>: 3349, 2936, 2872, 1680, 1655, 1625, 1587, 1442; **HRMS** C<sub>8</sub>H<sub>14</sub>N calculated [M<sup>+</sup>] 124.1126, found 124.1122 [M<sup>+</sup>].

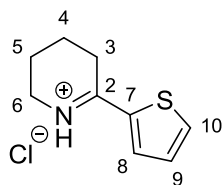
## 2-isopropyl-1-piperideinium chloride



**86k** (280 mg, 1.15 mmol) was dissolved in TFA (2.5 mL). **5k** (170 mg, 91% yield) was obtained as a yellow solid. **<sup>1</sup>H NMR** (400 MHz, CD<sub>3</sub>OD)  $\delta$  = 3.69 - 3.66 (m, 2H, C6-CH<sub>2</sub>), 2.94 (sept,  $J$  = 7.0 Hz, 1H, C7-CH), 2.88 - 2.84 (m, 2H, C3-CH<sub>2</sub>), 1.96 - 1.83 (m, 4H, C4-CH<sub>2</sub> and C5-CH<sub>2</sub>), 1.29 (d,  $J$  = 7.0 Hz, 6H, C8-CH<sub>3</sub>); **<sup>13</sup>C NMR** (100 MHz, CD<sub>3</sub>OD)  $\delta$  = 198.4

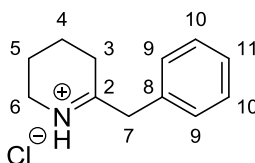
(C2), 46.0 (C6), 38.6 (C7), 28.2 (C3), 20.4 (C5), 19.7 (C4), 15.5 (C8); **HRMS** C<sub>8</sub>H<sub>16</sub>N calculated [M<sup>+</sup>] 126.1283, found 126.1280 [M<sup>+</sup>].

### 2-(thiophen-2-yl)-1-piperideinium chloride



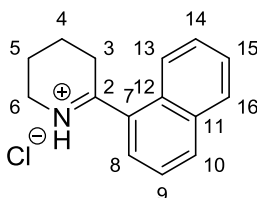
**86l** (436 mg, 1.54 mmol) was dissolved in TFA (2.5 mL). **5l** (280 mg, 90% yield) was obtained as a green solid. **<sup>1</sup>H NMR** (400 MHz, CD<sub>3</sub>OD) δ: 8.21 (dd, *J* = 5.0, 1.0 Hz, 1H, C8-CH), 8.16 (dd, *J* = 4.0, 1.0 Hz, 1H, C10-CH), 7.40 (dd, *J* = 5.0, 4.0 Hz, 1H, C9-CH), 3.81 – 3.76 (m, 2H, C6-CH<sub>2</sub>), 3.37 – 3.33 (m, 2H, C3-CH<sub>2</sub>), 2.04 – 1.97 (m, 4H, C4-CH<sub>2</sub> and C5-CH<sub>2</sub>); **<sup>13</sup>C NMR** (400 MHz, CD<sub>3</sub>OD) δ: 175.0 (C2), 139.0 (C7), 136.9 (C8), 135.4 (C10), 130.9 (C9), 46.0 (C6), 29.9 (C3), 20.6 (C5), 18.5 (C4).

### 2-benzyl-1-piperideinium chloride



**86m** (1.08 g, 3.71 mmol) was dissolved in TFA (5 mL). **5m** (620 mg, 80% yield) was obtained as a purple solid. **<sup>1</sup>H NMR** (400 MHz, CD<sub>3</sub>OD) δ: 7.44 – 7.36 (m, 5H, C9-CH, C10-CH and C11-CH), 4.07 (s, 2H, C7-CH<sub>2</sub>), 3.72 – 3.69 (m, 2H, C6-CH<sub>2</sub>), 2.79 – 2.76 (m, 2H, C3-CH<sub>2</sub>), 1.93 – 1.86 (m, 2H, C4-CH<sub>2</sub>), 1.84 – 1.78 (m, 2H, C5-CH<sub>2</sub>); **<sup>13</sup>C NMR** (100 MHz, CD<sub>3</sub>OD) δ: 192.5 (C2), 133.2 (C8), 130.8 (C9), 130.5 (C10), 129.5 (C11), 46.2 (C6), 44.8 (C7), 30.6 (C3), 20.3 (C5), 17.9 (C4).

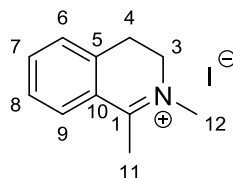
### 2-(1-naphthyl)-1-piperideinium chloride



**86n** (744 mg, 2.27 mmol) was dissolved in TFA (4 mL). **3n** (450 mg, 81% yield) was obtained as a yellow solid. **<sup>1</sup>H NMR** (400 MHz, CD<sub>3</sub>OD) δ: 8.21 – 8.19 (m, 1H, C8-CH), 8.08 – 8.05 (m, 1H, ArH), 7.99 – 7.96 (m, 1H, ArH), 7.81 (dd, *J* = 7.2, 0.8 Hz, 1H, ArH), 7.75 – 7.65 (m, 3H, ArH), 4.01 – 3.98 (m, 2H, C6-CH<sub>2</sub>), 3.39 – 3.29 (m, 2H, C3-CH<sub>2</sub>), 2.22 – 2.11

(m, 4H, C4-CH<sub>2</sub> and C5-CH<sub>2</sub>); <sup>13</sup>C NMR (100 MHz, CD<sub>3</sub>OD) δ: 189.1 (C2), 135.1 (C7), 134.2 (ArC), 132.2 (ArC), 130.2 (ArC), 130.1 (ArC), 129.7 (ArC), 128.4 (ArC), 127.7 (ArC), 126.1 (ArC), 124.6 (ArC), 46.7 (C6), 20.3 (C3), 18.3 (C5), 18.2 (C4).

### 7.3.1.5 Preparation of 1,2-dimethyl-3,4-dihydroisoquinolin-2-ium iodide **9a**



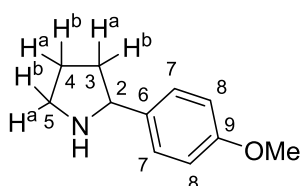
To a stirred solution of 1-methyl-3,4-dihydroisoquinoline hydrochloride **7a** (100 mg, 0.550 mmol) in acetonitrile (2 mL) was added methyl iodide (205 μL, 3.30 mmol). After the reaction had gone to completion, the precipitate was filtered and washed with acetone and left to dry in air to afford 1,2-dimethyl-3,4-dihydroisoquinolin-2-ium iodide **9a** (68 mg, 43% yield) as a bright yellow solid. <sup>1</sup>H NMR (400 MHz, CDCl<sub>3</sub>) δ: 7.88 (d, *J* = 8.1 Hz, 1H, C9-CH), 7.68 (td, *J* = 7.6, 1.1 Hz, 1H, C7-CH), 7.52 – 7.47 (m, 1H, C8-CH), 7.36 (d, *J* = 7.6 Hz, 1H, C6-CH), 4.20 (t, *J* = 7.6 Hz, 2H, C3-CH<sub>2</sub>), 3.98 (s, 3H, N-CH<sub>3</sub>), 3.39 (t, *J* = 7.6 Hz, 2H, C4-CH<sub>2</sub>), 3.01 (s, 3H, C11-CH<sub>3</sub>); <sup>13</sup>C NMR (100 MHz, CDCl<sub>3</sub>) δ: 176.1 (C1), 136.3 (C10), 136.2 (C5), 130.1 (C9), 128.3 (C7), 128.2 (C6), 127.3 (C8), 53.5 (C12), 47.2 (C11), 25.8 (C3), 20.7 (C4).

## 7.3.2 Synthesis of 2-substituted cyclic amines

### 7.3.2.1 Preparation of 2-substituted cyclic amines **2**, **4**, **6** and **10a**

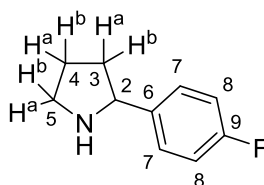
Cyclic imine hydrochloride salts **1**, **3**, **5** and **9** were dissolved in dH<sub>2</sub>O:MeOH (1:4) and stirred at room temperature. NaBH<sub>4</sub> (1 eq.) was added and the mixture was left overnight. The reaction was then quenched by adding 1 M HCl until pH 1 and left to stir for 30 minutes, before adding 10 M NaOH until pH 14. The aqueous phase was extracted with CH<sub>2</sub>Cl<sub>2</sub> (3 x 15mL). The combined organic layers were then dried over MgSO<sub>4</sub>, filtered and concentrated *in vacuo* to afford the freebase racemic cyclic amines.

### 2-(*p*-methoxy)phenylpyrrolidine



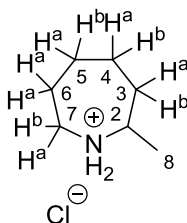
**1c** (20 mg, 0.0945 mmol) was dissolved in dH<sub>2</sub>O:MeOH (1:4, 5 mL) and was reduced by addition of NaBH<sub>4</sub> (3.57mg, 0.0945 mmol). Amine **2c** (18 mg, 89% yield) was isolated as light brown oil. **<sup>1</sup>H NMR** (400 MHz, CDCl<sub>3</sub>) δ: 7.30 – 7.26 (m, 2H, C7-CH), 6.88 – 6.84 (m, 2H, C8-CH), 4.05 (t, *J* = 7.8 Hz, 1H, C2-CH), 3.79 (s, 3H, OMe), 3.19 (ddd, *J* = 10.1, 7.8, 5.3 Hz, 1H, C5-H<sup>a</sup> or C5-H<sup>b</sup>), 3.07 (bs, 1H, NH), 2.98 (ddd, *J* = 10.1, 8.2, 6.8 Hz, 1H, C5-H<sup>a</sup> or C5-H<sup>b</sup>), 2.21 – 2.10 (m, 1H, C3-H<sup>a</sup> or C3-H<sup>b</sup>), 1.97 – 1.79 (m, 2H, C4-H<sup>a</sup> and C4-H<sup>b</sup>), 1.71 (ddd, *J* = 17.0, 12.3, 8.9 Hz, 1H, C3-H<sup>a</sup> or C3-H<sup>b</sup>); **<sup>13</sup>C NMR** (100 MHz, CDCl<sub>3</sub>) δ: 158.9 (C9), 135.0 (C7), 128.0 (C8), 114.0 (C6), 62.3 (C2), 55.4 (OMe), 46.5 (C5), 33.9 (C3), 25.4 (C4).

### 2-(*p*-fluoro)phenylpyrrolidine



**1d** (30 mg, 0.150 mmol) was dissolved in dH<sub>2</sub>O:MeOH (1:4, 5 mL) and was reduced by addition of NaBH<sub>4</sub> (5.7 mg, 0.150 mmol). Amine **2d** (27 mg, 89% yield) was isolated as pale yellow oil. **<sup>1</sup>H NMR** (400 MHz, CDCl<sub>3</sub>) δ: 7.35 – 7.29 (m, 2H, C8-H), 7.02 – 6.96 (m, 2H, C7-H), 4.08 (dd, *J* = 9.0 Hz, 1H, C2-CH), 3.38 (bs, 1H, NH), 3.23 (ddd, *J* = 10.6, 7.9, 6.0 Hz, 1H, C5-H<sup>a</sup> or C5-H<sup>b</sup>), 3.04 (ddd, *J* = 10.6, 8.6, 6.3 Hz, 1H, C5-H<sup>a</sup> or C5-H<sup>b</sup>), 2.22 – 2.11 (m, 1H, C3-H<sup>a</sup> or C3-H<sup>b</sup>), 1.98 – 1.72 (m, 2H, C4-H<sup>a</sup> and C4-H<sup>b</sup>), 1.69 – 1.55 (m, 1H, C3-H<sup>a</sup> or C3-H<sup>b</sup>); **<sup>13</sup>C NMR** (100 MHz, CDCl<sub>3</sub>) δ: 162.3 (d, *J* = 245.5 Hz, C9), 129.7 (d, *J* = 8.5 Hz, C7), 128.7 (d, *J* = 8.3 Hz, C6), 115.4 (d, *J* = 21.3 Hz, C8), 62.2 (C2), 46.4 (C5), 33.8 (C3), 25.1 (C4).

### 2-methylazepane

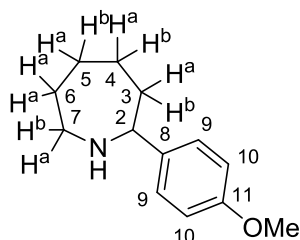


**3a** (20 mg, 0.135 mmol) was dissolved in dH<sub>2</sub>O:MeOH (1:4, 5 mL) and was reduced by addition of NaBH<sub>4</sub> (5.10 mg, 0.135 mmol). Amine 2-methylazepane (9 mg, 44% yield) was isolated as orange oil.

Without further purification, the freebase amine was dissolved into diethyl ether (5 mL) before HCl (2 M solution in diethyl ether, 59 μL, 0.19 mmol) was added. The hydrochloride

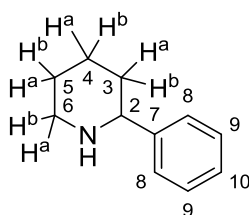
salt was washed with diethyl ether and dried under vacuum to give 2-methylazepane hydrochloride **4a** (10.1 mg, 84% yield) as a white powder. **<sup>1</sup>H NMR** (400 MHz, CD<sub>3</sub>OD) δ: 3.45 – 3.38 (m, 1H, C2-CH), 3.25 (ddd, *J* = 13.5, 6.6, 4.0 Hz, 1H, C7-CH<sup>a</sup> or C7-CH<sup>b</sup>), 3.18 – 3.12 (m, 1H, C7-CH<sup>a</sup> or C7-CH<sup>b</sup>), 2.02 – 1.60 (m; 8H; C3-CH<sub>2</sub>, C4-CH<sub>2</sub>, C5-CH<sub>2</sub> and C6-CH<sub>2</sub>), 1.34 (d, *J* = 6.7 Hz, 3H, C8-CH<sub>3</sub>); **<sup>13</sup>C NMR** (100 MHz, CD<sub>3</sub>OD) δ: 56.4 (C2), 46.3 (C7), 34.3 (C8), 27.4 (C3), 26.0 (C6), 25.6 (C4), 20.5 (C5).

### 7-(*p*-methoxyphenyl)azepane



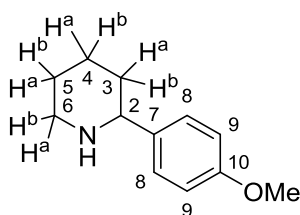
**3c** (30 mg, 0.125 mmol) was dissolved in dH<sub>2</sub>O:MeOH (1:4, 5 mL) and was reduced by addition of NaBH<sub>4</sub> (4.73 mg, 0.125 mmol). Amine **4c** (25 mg, 97% yield) was isolated as pale yellow oil. **<sup>1</sup>H NMR** (400 MHz, CDCl<sub>3</sub>) δ: 7.29 – 7.23 (m, 2H, C9-H), 6.86 – 6.82 (m, 2H, C10-H), 3.78 (s, 3H, OMe), 3.69 (dd, *J* = 10.1, 6.7 Hz, 1H, C2-CH), 3.12 (dt, *J* = 13.4, 4.9 Hz, 1H, C7-CH<sup>a</sup> or C7-CH<sup>b</sup>), 2.87 – 2.78 (m, 1H, C7-CH<sup>a</sup> or C7-CH<sup>b</sup>), 1.92 – 1.87 (m, 1H, C3-CH<sup>a</sup> or C3-CH<sup>b</sup>), 1.86 – 1.65 (m, 7H, C4-CH<sub>2</sub>, C5-CH<sub>2</sub> and C6-CH<sub>2</sub>), 1.65 – 1.53 (m, 1H, C7-CH<sup>a</sup> or C7-CH<sup>b</sup>); **<sup>13</sup>C NMR** (100 MHz, CDCl<sub>3</sub>) δ: 159.1 (C11), 137.2 (C9), 127.3 (C10), 113.9 (C8), 74.1 (C2), 55.5 (OMe), 40.4 (C7), 38.9 (C3), 30.2 (C6), 26.7 (C4), 25.6 (C5).

### 2-phenylpiperidine



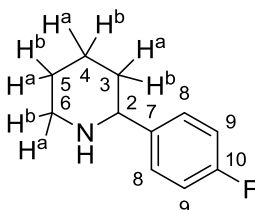
**5b** (50 mg, 0.256 mmol) was dissolved in dH<sub>2</sub>O:MeOH (1:4, 5 mL) and was reduced by addition of NaBH<sub>4</sub> (9.7 mg, 0.256 mmol). Amine **6b** (39.1 mg, 94% yield) was isolated as brown oil. **<sup>1</sup>H NMR** (400 MHz, CDCl<sub>3</sub>) δ: 7.39 – 7.29 (m, 4H, C8-CH and C9-CH), 7.26 – 7.21 (m, 1H, C10-CH), 3.59 (dd, *J* = 10.3, 2.5 Hz, 1H, C2-CH), 3.23 – 3.17 (m, 1H, C6-CH<sup>a</sup> or C6-CH<sup>b</sup>), 2.80 (td, *J* = 11.5, 2.9 Hz, 1H, C6-CH<sup>a</sup> or C6-CH<sup>b</sup>), 1.92 – 1.85 (m, 1H, C3-CH<sup>a</sup> or C3-CH<sup>b</sup>), 1.83 – 1.77 (m, 1H, C6-CH<sup>a</sup> or C6-CH<sup>b</sup>), 1.69 – 1.63 (m, 1H, C5-CH<sup>a</sup> or C5-CH<sup>b</sup>), 1.61 – 1.46 (m, 3H, C4-CH<sub>2</sub> and C5-CH<sup>a</sup> or C5-CH<sup>b</sup>); **<sup>13</sup>C NMR** (100 MHz, CDCl<sub>3</sub>) δ: 145.7 (C7), 128.5 (C8), 127.1 (C10), 126.8 (C9), 62.5 (C2), 47.9 (C6), 35.1 (C3), 26.0 (C5), 25.6 (C4).  
*Data consistent with literature values.*<sup>82</sup>

## 2-(*p*-methoxyphenyl)piperidine



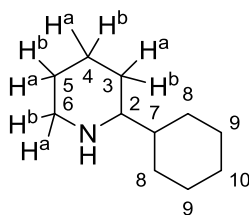
**5c** (30 mg, 0.133 mmol) was dissolved in dH<sub>2</sub>O:MeOH (1:4, 5 mL) and was reduced by addition of NaBH<sub>4</sub> (5.1 mg, 0.133 mmol). Amine **6c** (23 mg, 90% yield) was isolated as dark yellow oil. **<sup>1</sup>H NMR** (400 MHz, CDCl<sub>3</sub>) δ: 7.30 – 7.27 (m, 2H, C8-CH), 6.87 – 6.83 (m, 2H, C9-CH), 3.79 (s, 3H, OMe), 3.53 (dd, *J* = 10.4, 2.4 Hz, 1H, C2-CH), 3.20 – 3.14 (m, 1H, C6-CH<sup>a</sup> or C6-CH<sup>b</sup>), 2.78 (td, *J* = 11.5, 2.8 Hz, 1H, C6-CH<sup>a</sup> or C6-CH<sup>b</sup>), 2.07 (bs, 1H, NH), 1.90 – 1.84 (m, 1H, C3-CH<sup>a</sup> or C3-CH<sup>b</sup>), 1.79 – 1.72 (m, 1H, C3-CH<sup>a</sup> or C3-CH<sup>b</sup>), 1.68 – 1.61 (m, 1H, C5-CH<sup>a</sup> or C5-CH<sup>b</sup>), 1.60 – 1.40 (m, 3H, C4-CH<sup>a</sup>, C4-CH<sup>b</sup> and C5-CH<sup>a</sup> or C5-CH<sup>b</sup>); **<sup>13</sup>C NMR** (400 MHz, CDCl<sub>3</sub>) δ: 158.7 (C10), 137.8 (C8), 127.8 (C9), 113.8 (C7), 61.8 (C2), 55.4 (OMe), 48.0 (C6), 35.0 (C3), 25.9 (C5), 25.5 (C4). *Data consistent with literature values.*<sup>82</sup>

## 2-(*p*-fluorophenyl)piperidine



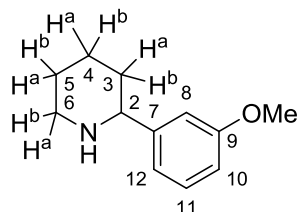
**5d** (30 mg, 0.140 mmol) was dissolved in dH<sub>2</sub>O:MeOH (1:4, 5 mL) and was reduced by addition of NaBH<sub>4</sub> (5.3 mg, 0.140 mmol). Amine **6d** (23 mg, 91% yield) was isolated as dark yellow oil. **<sup>1</sup>H NMR** (400 MHz, CDCl<sub>3</sub>) δ: 7.35 (dd *J* = 8.3, 5.4 Hz, 2H, C9-CH), 6.98 (t, *J* = 8.6 Hz, 2H, C8-CH), 4.86 (bs, 1H, NH), 3.62 (dd, *J* = 11.6, 1.8 Hz, 1H, C2-CH), 3.16 (d, *J* = 11.6 Hz, 1H, C6-CH<sup>a</sup> or C6-CH<sup>b</sup>), 2.77 (td, *J* = 11.6, 3.1 Hz, 1H, C6-CH<sup>a</sup> or C6-CH<sup>b</sup>), 1.94 – 1.85 (m, 1H, C3-CH<sup>a</sup> or C3-CH<sup>b</sup>), 1.82 – 1.74 (m, 1H, C3-CH<sup>a</sup> or C3-CH<sup>b</sup>), 1.70 – 1.40 (m, 4H, C4-CH<sup>a</sup>, C4-CH<sup>b</sup>, C5-CH<sup>a</sup> and C5-CH<sup>b</sup>); **<sup>13</sup>C NMR** (100 MHz, CDCl<sub>3</sub>) δ: 162.2 (d, *J* = 245.4 Hz, C10), 130.1 (d, *J* = 3.3 Hz, C7), 128.6 (d, *J* = 8.1 Hz, C8), 155.3 (d, *J* = 21.2 Hz, C9), 61.4 (C2), 47.3 (C6), 34.2 (C3), 29.8 (C5), 25.1 (C4).<sup>137</sup>

## 2-cyclohexylpiperidine



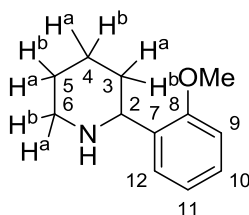
**5e** (30 mg, 0.149 mmol) dissolved in dH<sub>2</sub>O:MeOH (1:4, 5 mL) was reduced by addition of NaBH<sub>4</sub> (5.63 mg, 0.149 mmol). Amine **6e** (27 mg, 83% yield) was isolated as yellow oil. **<sup>1</sup>H NMR** (400 MHz, CDCl<sub>3</sub>) δ: 3.11 – 3.05 (m, 1H, C2-CH), 2.59 (td, *J* = 11.8, 2.8 Hz, 1H, C6-CH<sup>a</sup> or C6-CH<sup>b</sup>), 2.21 (ddd, *J* = 10.8, 6.2, 2.4 Hz, 1H, C6-CH<sup>a</sup> or C6-CH<sup>b</sup>), 1.82 – 1.60 (m, 8H, ), 1.60 – 1.52 (m, 1H), 1.43 – 1.03 (m, 8H), 1.02 – 0.90 (m, 2H); **<sup>13</sup>C NMR** (400 MHz, CDCl<sub>3</sub>) δ: 62.2, 47.7, 43.6, 29.9, 29.4, 29.4, 26.9, 26.8, 26.6, 26.6, 25.3. *Data consistent with literature values.*<sup>82</sup>

## 2-(*m*-methoxyphenyl)piperidine



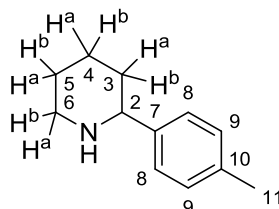
**5f** (30 mg, 0.133 mmol) was dissolved in dH<sub>2</sub>O:MeOH (1:4, 5 mL) and was reduced by addition of NaBH<sub>4</sub> (5.0 mg, 0.133 mmol). Amine **6f** (23 mg, 90% yield) was isolated as dark orange oil. **<sup>1</sup>H NMR** (400 MHz, CDCl<sub>3</sub>) δ: 7.22 (t, *J* = 8.1 Hz, 1H, C11-CH), 6.95 – 6.91 (m, 2H, C8-CH and C10-CH), 6.78 (ddd, *J* = 8.1, 2.5, 1.0 Hz, 1H, C12-CH), 3.80 (s, 3H, OMe), 3.58 – 3.53 (m, 1H, C2-CH), 3.21 – 3.15 (m, 1H, C6-CH<sup>a</sup> or C6-CH<sup>b</sup>), 2.80 (td, *J* = 11.5, 2.7 Hz, 1H, C6-CH<sup>a</sup> or C6-CH<sup>b</sup>), 1.98 (bs, 1H, NH), 1.91 – 1.83 (m, 1H, C3-CH<sup>a</sup> or C3-CH<sup>b</sup>), 1.82 – 1.73 (m, 1H, C3-CH<sup>a</sup> or C3-CH<sup>b</sup>), 1.68 – 1.61 (m, 1H, C5-CH<sup>a</sup> or C5-CH<sup>b</sup>), 1.60 – 1.42 (m, 3H, C4-CH<sup>a</sup>, C4-CH<sup>b</sup> and C5-CH<sup>a</sup> or C5-CH<sup>b</sup>); **<sup>13</sup>C NMR** (400 MHz, CDCl<sub>3</sub>) δ: 159.8 (C7), 147.3 (C9), 129.4 (C11), 119.1 (C10), 112.7 (C12), 112.0 (C8), 62.5 (OMe), 55.3 (C2), 47.9 (C6), 35.0 (C3), 25.9 (C5), 25.0 (C4). *Data consistent with literature values.*<sup>82</sup>

## 2-(*o*-methoxyphenyl)piperidine



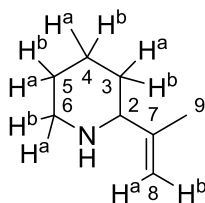
**5g** (30 mg, 0.133 mmol) was dissolved in dH<sub>2</sub>O:MeOH (1:4, 5 mL) and was reduced by addition of NaBH<sub>4</sub> (5.0 mg, 0.133 mmol). Amine **6g** (22 mg, 87% yield) was isolated as brown oil. **<sup>1</sup>H NMR** (400 MHz, CDCl<sub>3</sub>) δ: 7.43 (dd, *J* = 7.6, 1.6 Hz, 1H, C12-CH), 7.20 (ddd, *J* = 8.2, 7.6, 1.6 Hz, 1H, C10-CH), 6.94 (td, *J* = 7.6, 0.9 Hz, 1H (C11-CH), 6.85 (dd, *J* = 8.2, 0.9 Hz, 1H, C9-CH), 3.96 (dd, *J* = 10.4, 2.4 Hz, 1H, C2-CH), 3.83 (s, 3H, OMe), 3.18 (m, 1H, C6-CH<sup>a</sup> or C6-CH<sup>b</sup>), 2.82 (td, *J* = 11.6, 2.9 Hz, 1H, C6-CH<sup>a</sup> or C6-CH<sup>b</sup>), 1.94 – 1.79 (m, 3H, C3-CH<sup>a</sup>, C3-CH<sup>b</sup> and NH), 1.69 – 1.60 (m, 1H, C5-CH<sup>a</sup> or C5-CH<sup>b</sup>), 1.57 – 1.45 (m, 3H, C4-CH<sup>a</sup>, C4-CH<sup>b</sup> and C5-CH<sup>a</sup> or C5-CH<sup>b</sup>); **<sup>13</sup>C NMR** (100 MHz, CDCl<sub>3</sub>) δ: 156.6 (C8), 133.5 (C7), 127.7 (C12), 126.8 (C10), 120.8 (C9), 110.4 (C11), 55.4 (C2), 55.4 (OMe), 48.1 (C6), 33.0 (C3), 26.4 (C5), 25.7 (C4). *Data consistent with literature values.*<sup>82</sup>

### 2-(*p*-tolyl)piperidine



**5h** (30 mg, 0.143 mmol) was dissolved in dH<sub>2</sub>O:MeOH (1:4, 5 mL) and was reduced by addition of NaBH<sub>4</sub> (5.2 mg, 0.143 mmol). Amine **6h** (22 mg, 88% yield) was isolated as brown oil. **<sup>1</sup>H NMR** (400 MHz, CDCl<sub>3</sub>) δ: 7.26 (d, *J* = 7.8 Hz, 2H, C8-CH), 7.13 (d, *J* = 7.8 Hz, 2H, C9-CH), 3.59 – 3.52 (m, 1H, C2-CH), 3.22 – 3.15 (m, 1H, C6-CH<sup>a</sup> or C6-CH<sup>b</sup>), 2.79 (td, *J* = 11.5, 2.4 Hz, 1H, C6-CH<sup>a</sup> or C6-CH<sup>b</sup>), 2.33 (s, 3H, C11-CH<sub>3</sub>), 1.94 (bs, 1H, NH), 1.91 – 1.84 (m, 1H, C3-CH<sup>a</sup> or C3-CH<sup>b</sup>), 1.81 – 1.73 (m, 1H, C3-CH<sup>a</sup> or C3-CH<sup>b</sup>), 1.69 – 1.62 (m, 1H, C5-CH<sup>a</sup> or C5-CH<sup>b</sup>), 1.60 – 1.41 (m, 3H, C4-CH<sup>a</sup>, C4-CH<sup>b</sup> and C5-CH<sup>a</sup> or C5-CH<sup>b</sup>); **<sup>13</sup>C NMR** (100 MHz, CDCl<sub>3</sub>) δ: 142.5 (C7), 136.8 (C9), 129.2 (C10), 126.7 (C8), 62.2 (C2), 47.9 (C6), 35.0 (C3), 25.9 (C5), 25.6 (C4), 21.2 (C11).

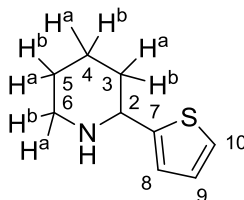
### 2-(*i*-propenyl)piperidine



**3j** (30 mg, 0.188 mmol) was dissolved in dH<sub>2</sub>O:MeOH (1:4, 5 mL) and was reduced by addition of NaBH<sub>4</sub> (7.1 mg, 0.188 mmol). The reaction was worked up as described previously and extracted into diethyl ether (3 x 10 mL). The organic phases were pooled together, dried over MgSO<sub>4</sub> and concentrated carefully *in vacuo* to yield 2-

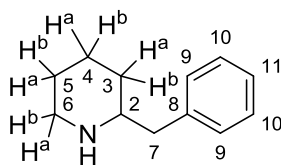
isopropenylpiperidine **6j** (18 mg, 75% yield) as dark yellow oil. **<sup>1</sup>H NMR** (400 MHz, CDCl<sub>3</sub>) δ: 4.88 (s, 1H, C8-H<sup>a</sup>), 4.75 (s, 1H, C8-H<sup>b</sup>), 3.15 – 3.05 (m, 1H, C2-CH), 2.95 (dd, *J* = 10.8, 1.8 Hz, 1H, C6-CH<sup>a</sup> or C6-CH<sup>b</sup>), 2.67 (td, *J* = 11.5, 2.9 Hz, 1H, C6-CH<sup>a</sup> or C6-CH<sup>b</sup>), 1.86 – 1.76 (m, 1H, C3-CH<sup>a</sup> or C3-CH<sup>b</sup>), 1.63 – 1.52 (m, 1H, C3-CH<sup>a</sup> or C3-CH<sup>b</sup>), 1.42 (s, 3H, C9-CH<sub>3</sub>), 1.42 – 1.24 (m, 4H, C4-CH<sup>a</sup>, C4-CH<sup>b</sup>, C5-CH<sup>a</sup> and C5-CH<sup>b</sup>); **<sup>13</sup>C NMR** (100 MHz, CDCl<sub>3</sub>) δ: 125.6 (C7), 109.4 (C8), 63.2 (C2), 47.6 (C6), 31.9 (C3), 30.4 (C9), 26.3 (C5), 25.3 (C4).

## 2-(thiophen-2-yl)piperidine



**5l** (30 mg, 0.149 mmol) was dissolved in dH<sub>2</sub>O:MeOH (1:4, 5 mL) and was reduced by addition of NaBH<sub>4</sub> (5.63 mg, 0.149 mmol). Amine **6l** (23 mg, 92% yield) was isolated as green oil. **<sup>1</sup>H NMR** (400 MHz, CDCl<sub>3</sub>) δ: 7.19 – 7.16 (m, 1H, C8-CH), 6.95 – 6.92 (m, 2H, C9-CH and C10-CH), 3.92 (dd, *J* = 10.3, 2.6 Hz, 1H, C2-CH), 3.20 – 3.14 (m, 1H, C6-CH<sup>a</sup> or C6-CH<sup>b</sup>), 2.79 (dt, *J* = 11.6, 3.0 Hz, 1H, C6-CH<sup>a</sup> or C6-CH<sup>b</sup>), 2.16 (bs, 1H, NH), 1.98 – 1.92 (m, 1H, C3-CH<sup>a</sup> or C3-CH<sup>b</sup>), 1.91 – 1.84 (m, 1H, C3-CH<sup>a</sup> or C3-CH<sup>b</sup>), 1.68 – 1.42 (m, 4H, C4-CH<sup>a</sup>, C4-CH<sup>b</sup>, C5-CH<sup>a</sup> or C5-CH<sup>b</sup>); **<sup>13</sup>C NMR** (100 MHz, CDCl<sub>3</sub>) δ: 149.6 (C7), 126.4 (C10), 123.7 (C8), 122.8 (C9), 57.3 (C2), 47.5 (C6), 35.8 (C3), 25.9 (C5), 25.0 (C4). *Data consistent with literature values.*<sup>82</sup>

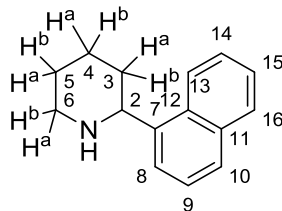
## 2-benzylpiperidine



**5m** (50 mg, 0.238 mmol) was dissolved in dH<sub>2</sub>O:MeOH (1:4, 5 mL) and was reduced by addition of NaBH<sub>4</sub> (9.0 mg, 0.238 mmol). Amine **6m** (38 mg, 91% yield) was isolated as brown oil. **<sup>1</sup>H NMR** (400 MHz, CDCl<sub>3</sub>) δ: 7.30 – 7.27 (m, 2H, C9-CH), 7.24 – 7.18 (m, 3H, C10-CH and C11-CH), 3.04 – 2.98 (m, 1H, C2-CH), 2.76 – 2.65 (m, 2H, C7-CH<sub>2</sub>), 2.64 – 2.57 (m, 1H, C6-CH<sup>a</sup> or C6-CH<sup>b</sup>), 2.53 (td, *J* = 11.8, 2.9 Hz, 1H, C6-CH<sup>a</sup> or C6-CH<sup>b</sup>), 2.07 (bs, 1H, NH), 1.83 – 1.73 (m, 1H, C3-CH<sup>a</sup> or C3-CH<sup>b</sup>), 1.73 – 1.64 (m, 1H, C3-CH<sup>a</sup> or C3-CH<sup>b</sup>), 1.62 – 1.54 (m, 1H, C5-CH<sup>a</sup> or C5-CH<sup>b</sup>), 1.46 (qt, *J* = 12.5, 3.9 Hz, 1H, C4-CH<sup>a</sup> or C4-CH<sup>b</sup>), 1.37 – 1.16 (m, 2H, C4-CH<sup>a</sup> or C4-CH<sup>b</sup> and C5-CH<sup>a</sup> or C5-CH<sup>b</sup>); **<sup>13</sup>C NMR** (100 MHz, CDCl<sub>3</sub>) δ:

139.2 (C8), 129.4 (C9), 128.6 (C10), 126.4 (C11), 58.4 (C2), 47.2 (C6), 43.8 (C7), 32.8 (C3), 26.1 (C5), 24.9 (C4).

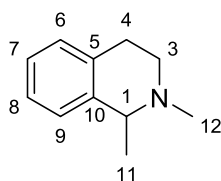
## 2-(1-naphthyl)piperidine



**5n** (50 mg, 0.204 mmol) was dissolved in dH<sub>2</sub>O:MeOH (1:4, 5 mL) and was reduced by addition of NaBH<sub>4</sub> (7.7 mg, 0.204 mmol). Amine **6n** (40 mg, 93% yield) was isolated as brown oil. **<sup>1</sup>H NMR** (400 MHz, CDCl<sub>3</sub>) δ: 8.15 (d, *J* = 8.4 Hz, 1H, ArH), 7.86 (dd, *J* = 8.1, 1.3 Hz, 1H, ArH), 7.77 – 7.70 (m, 2H, ArH), 7.55 – 7.43 (m, 4H, ArH), 4.47 – 4.38 (m, 1H, C2-CH), 3.33 – 3.26 (m, 1H, C6-CH<sup>a</sup> or C6-CH<sup>b</sup>), 3.09 – 2.95 (bs, 1H, NH), 2.94 (td, *J* = 11.2, 3.2 Hz, 1H, C6-CH<sup>a</sup> or C6-CH<sup>b</sup>), 2.08 – 1.99 (m, 1H, C3-CH<sup>a</sup> or C3-CH<sup>b</sup>), 1.99 – 1.91 (m, 1H, C3-CH<sup>a</sup> or C3-CH<sup>b</sup>), 1.79 – 1.58 (m, 4H, C4-CH<sup>a</sup>, C4-CH<sup>b</sup>, C5-CH<sup>a</sup> and C5-CH<sup>b</sup>); **<sup>13</sup>C NMR**, (100 MHz, CDCl<sub>3</sub>) δ: 140.6 (ArC), 134.0 (ArC), 130.9 (ArC), 129.1 (ArC), 127.6 (ArC), 126.0 (ArC), 125.9 (ArC), 125.5 (ArC), 123.1 (ArC), 123.0 (ArC), 57.8 (C2), 48.2 (C6), 34.1 (C3), 26.0 (C5), 25.7 (C4).

### 7.3.2.2 Preparation of 2-substituted bicyclic amine **10a**

#### 1,2-dimethyl-1,2,3,4-tetrahydroisoquinoline



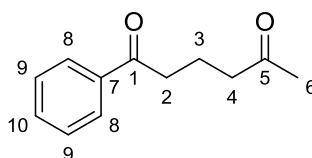
**9a** (30 mg, 0.104 mmol) was dissolved in dH<sub>2</sub>O:MeOH (1:4, 5 mL) and was reduced by addition of NaBH<sub>4</sub> (3.95 mg, 0.104 mmol). The reaction was quenched and then basified as previously described before being extracted into diethyl ether (3 x 15 mL). Subsequently, the organic layers were combined and dried over anhydrous magnesium sulphate. The solvent was then carefully removed on a rotary evaporator at 35°C and 300 mbar pressure to yield tertiary amine **10a** (15 mg, 89% yield) as brown oil. **<sup>1</sup>H NMR** (400 MHz, CDCl<sub>3</sub>) δ: 7.17 – 7.06 (m, 4H, C6-H, C7-H, C8-H and C9-H), 3.61 (q, *J* = 6.6 Hz, 1H C1-CH), 3.04 (ddd, *J* = 11.6, 6.3, 5.2 Hz, 1H, C3-CH<sup>a</sup> or C3-CH<sup>b</sup>), 2.95 – 2.79 (m, 2H, C4-CH<sub>2</sub>), 2.62 (ddd, *J* = 11.6, 7.2, 4.9 Hz, 1H, C3-CH<sup>a</sup> or C3-CH<sup>b</sup>), 2.49 (s, 3H, C11-CH<sub>3</sub>), 1.40 (d, *J* = 6.6 Hz,

3H, C10-CH<sub>3</sub>); <sup>13</sup>C NMR (100 MHz, CDCl<sub>3</sub>) δ: 140.0 (C10), 134.1 (C5), 128.8 (C9), 127.0 (C7), 125.9 (C6), 125.9 (C8), 59.2 (C12), 49.2 (C1), 43.2 (C11), 28.4 (C3), 19.8 (C4).

### 7.3.3 General procedure for the preparation of 1,5-diketones **11a** – **11d**

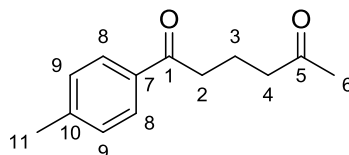
Under a nitrogen atmosphere, 3,4-dihydro-6-methyl-2H-pyran-2-one (1 eq.) was diluted in dry ether (4mL/mmol of pyran-2-one) before being cooled to -78°C. The Grignard reagent (1.1 eq.) was added drop wise and the mixture was stirred overnight at -78°C. The reaction was then warmed to room temperature and quenched by addition of 1 M HCl solution until pH 1-2. The mixture was then extracted with ethyl acetate (3 x 20 mL). The combined organic phases were dried over MgSO<sub>4</sub> and concentrated *in vacuo* to yield the crude product. Purification on silica gel afforded the desired product.

#### 1-phenylhexane-1,5-dione



Pyran-2-one (501 mg, 4.47 mmol) was reacted with phenylmagnesium bromide (1 M solution in THF, 4.92 mL, 4.92 mmol). Purification on silica (8% v/v ethyl acetate-cyclohexane) afforded the title compound **11a** (544 mg, 64% yield) as white crystals. <sup>1</sup>H NMR (400 MHz, CDCl<sub>3</sub>) δ: 7.98 – 7.94 (m, 2H, C8-H), 7.58 – 7.54 (m, 1H, C10-H), 7.49 – 7.44 (m, 2H, C9-H), 3.02 (t, *J* = 7.0 Hz, 2H, C2-CH<sub>2</sub>), 2.58 (t, *J* = 7.0 Hz, 2H, C4-CH<sub>2</sub>), 2.16 (s, 3H, C6-CH<sub>3</sub>), 2.02 (quin, *J* = 7.0 Hz, 2H, C3-CH<sub>2</sub>); <sup>13</sup>C NMR (100 MHz, CDCl<sub>3</sub>) δ: 208.5 (C5), 199.8 (C1), 136.8 (C7), 133.1 (C8), 128.6 (C10), 128.0 (C9), 42.6 (C4), 37.4 (C2), 30.0 (C6), 18.2 (C3). *Data consistent with literature values.*<sup>94</sup>

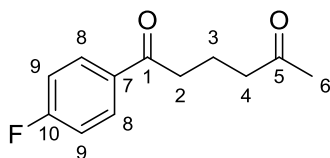
#### 1-(*p*-tolyl)hexane-1,5-dione



Pyran-2-one (501 mg, 4.47 mmol) was reacted with (*p*-tolyl)magnesium bromide (0.5 M solution in THF, 9.83 mL, 4.92 mmol). Purification on silica (8% v/v ethyl acetate-cyclohexane) afforded the title compound **11b** (428 mg, 47% yield) as a pale yellow solid. <sup>1</sup>H NMR (400 MHz, CDCl<sub>3</sub>) δ: 7.88 – 7.83 (m, 2H, C8-CH), 7.27 – 7.23 (m, 2H, C9-CH), 2.98 (t, *J* = 7.0 Hz, 2H, C2-CH<sub>2</sub>), 2.56 (t, *J* = 7.0 Hz, 2H, C4-CH<sub>2</sub>), 2.40 (s, 3H, C6-CH<sub>3</sub>), 2.15 (s,

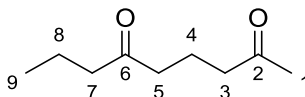
3H, C11-CH<sub>3</sub>), 2.00 (quin,  $J = 7.0$  Hz, 2H, C3-CH<sub>2</sub>); <sup>13</sup>C NMR (100 MHz, CDCl<sub>3</sub>) δ: 208.8 (C1), 199.6 (C5), 144.0 (C10), 134.5 (C7), 129.4 (C8), 128.3 (C9), 42.8 (C4), 37.4 (C2), 30.1 (C6), 21.8 (C11), 18.4 (C3). *Data consistent with literature values.*<sup>138</sup>

### 1-(4-fluorophenyl)hexane-1,5-dione



Pyran-2-one (1.1 g, 3.40 mmol) was reacted with (*p*-fluorophenyl)magnesium bromide (1 M solution in THF, 10.8 mL, 10.8 mmol). Purification on silica (15% v/v ethyl acetate-cyclohexane) afforded the title compound **11c** (640 mg, 31% yield) as an off-white solid. <sup>1</sup>H NMR (400 MHz, CDCl<sub>3</sub>) δ: 8.02 – 7.95 (m, 2H, C8-CH), 7.16 – 7.09 (m, 2H, C9-CH), 2.99 (t,  $J = 7.0$  Hz, 2H, C2-CH<sub>2</sub>), 2.57 (t,  $J = 7.0$  Hz, 2H, C4-CH<sub>2</sub>), 2.15 (s, 3H, C6-CH<sub>3</sub>), 2.00 (quin,  $J = 7.0$  Hz, 2H, C3-CH<sub>2</sub>); <sup>13</sup>C NMR (100 MHz, CDCl<sub>3</sub>) δ: 206.6 (C1), 198.3 (C5), 165.9 (d,  $J = 255.0$  Hz, C10), 133.3 (d,  $J = 3.0$  Hz, C7), 130.8 (d,  $J = 9.0$  Hz, C9), 115.8 (d,  $J = 22.0$  Hz, C8), 42.6 (C4), 37.5 (C2), 30.1 (C6), 18.3 (C3).

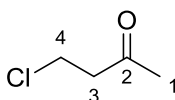
### Nonane-2,6-dione



Pyran-2-one (501 mg, 4.47 mmol) was reacted with (*n*-propyl)magnesium chloride (2 M solution in THF, 2.46 mL, 4.49 mmol). Purification on silica (10% v/v ethyl acetate-cyclohexane) afforded the title compound **11d** (560 mg, 80% yield) as pale yellow oil. <sup>1</sup>H NMR (400 MHz, CDCl<sub>3</sub>) δ: 2.45 (t,  $J = 7.0$  Hz, 2H, C5-H<sub>2</sub>), 2.41 (t,  $J = 7.0$  Hz, 2H, C3-H<sub>2</sub>), 2.35 (t,  $J = 7.4$  Hz, 2H, C7-H<sub>2</sub>), 2.11 (s, 3H, C1-H<sub>3</sub>), 1.81 (quin,  $J = 7.0$  Hz, 2H, C4-H<sub>2</sub>), 1.57 (sxt,  $J = 7.4$  Hz, 2H, C8-H<sub>2</sub>), 0.88 (t,  $J = 7.4$  Hz, 3H, C9-H<sub>3</sub>); <sup>13</sup>C NMR (100 MHz, CDCl<sub>3</sub>) δ: 210.8 (C6), 208.6 (C2), 44.8 (C7), 42.7 (C3), 41.6 (C5), 30.0 (C1), 17.8 (C4), 17.4 (C8), 13.8 (C9). *Data consistent with literature values.*<sup>94</sup>

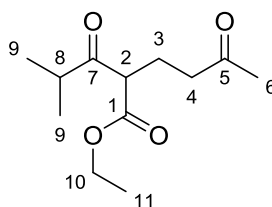
### 7.3.3 General procedure for the preparation of 1,5-diketone **11e**

#### 4-hydroxybutan-2-one



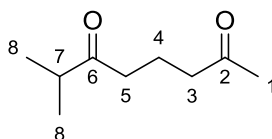
A drop of DMF was added to a stirring solution of 4-hydroxybutan-2-one (2.95 mL, 34.2 mmol) in CH<sub>2</sub>Cl<sub>2</sub> (15 mL). Thionyl chloride (1.05 x, 2.60 mL, 35.9 mmol) was then added to the reaction mixture, which was then allowed to stir overnight. The reaction was then quenched with sat. ammonium chloride solution, then the aqueous mixture was extracted with DCM (3 x 30 mL). The organic layers were pooled together, concentrated carefully *in vacuo* (400 mbar, 35C) before the crude was then flash filtered through a pad of silica. The organic was concentrated carefully *in vacuo* (400 mbar, 35C) to yield product (352 g, 97%) as a yellow liquid. **<sup>1</sup>H NMR** (400 MHz, CDCl<sub>3</sub>) δ: 3.72 (t, *J* = 6.5 Hz, 2H, C4-CH<sub>2</sub>), 2.90 (t, *J* = 6.5 Hz, 2H, C3-CH<sub>2</sub>), 2.19 (s, 3H, C1-CH<sub>3</sub>); **<sup>13</sup>C NMR** (100 MHz, CDCl<sub>3</sub>) δ: 205.3 (C2), 46.0 (C3), 38.3 (C4), 30.4 (C1). *Data consistent with literature values.*<sup>94</sup>

### Ethyl-2-isobutyryl-5-oxohexanoate



Ethyl isobutyrylacetate (1 mL, 6.20 mmol) was dissolved in dry THF (30 mL). <sup>t</sup>BuOK (1.1 x, 760 mg, 6.77 mmol) added in one portion and the reaction was allowed to stir for 10 min at 15°C., before 4-chlorobutan-2-one (660 mg, 6.20 mmol) added drop wise. The reaction was vigorously stirred until no starting material could be detected by TLC. The mixture was then poured onto saturated NH<sub>4</sub>Cl solution (50 mL) and then extracted with EtOAc (4 x 10 mL). The combined organic layers were then dried over MgSO<sub>4</sub>, filtered and concentrated *in vacuo*. The crude product was then subjected to column chromatography (15% EtOAc:cyclohexane) to yield the title compound (1.06 g, 75%) as an oil. **<sup>1</sup>H NMR** (400 MHz, CDCl<sub>3</sub>) δ: 4.15 (q, *J* = 7.0 Hz, 2H, C10-CH<sub>2</sub>), 3.70 (t, *J* = 7.0 Hz, 1H, C2-CH), 2.81 (sept, *J* = 7.0 Hz, 1H, C8-CH), 2.48 (t, *J* = 7.0 Hz, 2H, C4-CH<sub>2</sub>), 2.12 (s, 3H, C6-CH<sub>3</sub>), 2.06 (q, *J* = 7.0 Hz, 2H, C3-CH<sub>2</sub>), 1.24 (t, *J* = 7.0 Hz, 3H, C11-CH<sub>3</sub>), 1.10 (d, *J* = 7.0 Hz, 3H, C9-CH<sub>3</sub>), 1.09 (d, *J* = 7.0 Hz, 3H, C9-CH<sub>3</sub>); **<sup>13</sup>C NMR** (100 MHz, CDCl<sub>3</sub>) δ: 209.1 (C7), 207.8 (C5), 169.6 (C1), 61.5 (C10), 55.4 (C2), 40.8 (C4), 40.7 (C8), 30.1 (C6), 22.0 (C3), 18.4 (C9), 18.1 (C9), 14.2 (C11). *Data consistent with literature values.*<sup>94</sup>

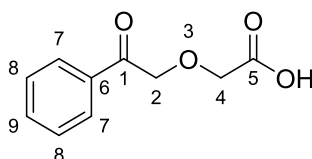
### 7-methyloctan-2,6-dione



Ethyl-2-isobutyryl-5-oxohexanoate (1.06 g, 4.65 mmol) was dissolved in wet DMSO (14 mL). NaCl (543 mg, 9.29 mmol) was added and the mixture was refluxed at 150°C for 24 h. Once the reaction had reached completion as judged by TLC, the mixture was cooled to room temperature and then diluted with saturated brine (40 mL), before it was extracted with EtOAc (4 x 20 mL). The organic layers were pooled together, dried over MgSO<sub>4</sub> and then concentrated *in vacuo*. The crude product was then subjected to flash column chromatography (silica, gradient 10% EtOAc to 15% EtOAc:cyclohexane) to yield the title compound (600 mg, 83%) as a yellow oil. **<sup>1</sup>H NMR** (400 MHz, CDCl<sub>3</sub>) δ: 2.56 (sept, *J* = 7.0 Hz, 1H, C7-CH), 2.47 (t, *J* = 7.0 Hz, 2H, C5-CH<sub>2</sub>), 2.45 (t, *J* = 7.0 Hz, 2H, C3-CH<sub>2</sub>), 2.12 (s, 3H, C1-CH<sub>3</sub>), 1.81 (pent, *J* = 7.0 Hz, 2H, C4-CH<sub>2</sub>), 1.06 (d, *J* = 7.0 Hz, 6H, C8-CH<sub>3</sub>); **<sup>13</sup>C NMR** (100 MHz, CDCl<sub>3</sub>) δ: 214.4 (C6), 208.7 (C2), 42.7 (C3), 40.9 (C7), 39.1 (C5), 30.0 (C1), 18.3 (C8), 17.8 (C4). *Data consistent with literature values.*<sup>94</sup>

### 7.3.5 Procedure for the preparation of ketoacids **17** and **20**

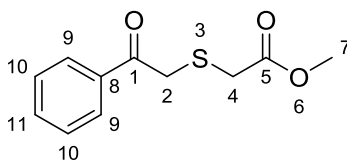
#### 7.3.5.1 2-(2-oxo-2-phenylethoxy)acetic acid



To a stirred solution of 1,4-dioxane-2,6-dione (1.0 g, 8.6 mmol) in benzene (17 mL) was added AlCl<sub>3</sub> (3.4 g, 26 mmol). The reaction mixture was heated to 60°C for 2 h and then refluxed for 1 h. The reaction mixture was then poured into a beaker containing conc. HCl (20 mL) and ice (20 g) and then stirred for 1 h. The mixture was then extracted with EtOAc (3 x 20 mL). The organic layers were pooled together, washed with brine (1 x 30 mL), dried over MgSO<sub>4</sub> and concentrated *in vacuo* to yield the crude product, which was then subjected to flash chromatography (silica gel, 25% v/v EtOAc-cyclohexane) to afford keto acid **17** (1.09 g, 65%), which was isolated as a brown solid. **<sup>1</sup>H NMR** (400 MHz, CDCl<sub>3</sub>) δ: 7.95 – 7.90 (m, 2H, C7-H), 7.69 – 7.61 (m, 1H, C9-H), 7.53 – 7.48 (m, 2H, C8-H), 5.02 (s, 2H, C4-CH<sub>2</sub>), 4.31 (s, 2H, C2-H<sub>2</sub>); **<sup>13</sup>C NMR** (100 MHz, CDCl<sub>3</sub>) δ: 197.1 (C5), 171.7 (C1), 134.7 (C6), 133.8 (C8), 129.2 (C7), 128.1 (C9), 75.0, (C4), 70.4 (C2).

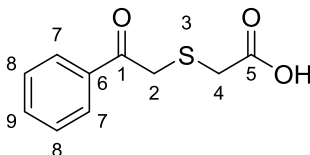
### 7.3.5.2 Preparation of 2-((2-oxo-2-phenylethyl)thio)acetic acid

#### Methyl 2-((2-oxo-2-phenylethyl)thio)acetate



To a flask under N<sub>2</sub> were added 2-bromoacetophenone (3.34 g, 16.8 mmol), methyl thioglycolate (1.5 mL, 16.8 mL) and anhydrous THF (22 mL). Oven-dried K<sub>2</sub>CO<sub>3</sub> (5 x, 11.6 g, 83.9 mmol) was added to the flask and the mixture was stirred for 24 h. The mixture was then filtered and the residue filter cake was washed with ethyl acetate (20 mL). The organic layers were pooled together and concentrated *in vacuo* to yield the crude product. The final product **88** was obtained by Kugelrohr distillation (180°C under high vacuum, 3.39 g, 90% yield) as clear oil. **<sup>1</sup>H NMR** (400 MHz, CDCl<sub>3</sub>) δ: 7.99 – 7.94 (m, 2H, C9-CH), 7.62 – 7.56 (m, 1H, C11-CH), 7.51 – 7.45 (m, 2H, C10-CH), 4.03 (s, 2H, C2-CH<sub>2</sub>), 3.73 (s, 3H, C7-CH<sub>3</sub>) 3.53 (s, 2H, C4-CH<sub>2</sub>); **<sup>13</sup>C NMR** (100 MHz, CDCl<sub>3</sub>) δ: 194.2 (C1), 170.5 (C5), 135.5 (C8), 133.7 (C11), 128.9 (C9), 128.8 (C10), 52.6 (C2), 37.9 (C4), 33.3 (C7).

#### 2-((2-oxo-2-phenylethyl)thio)acetic acid



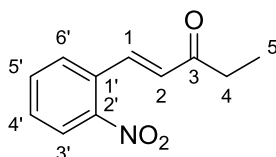
Methyl ester **88** (1.55g, 6.91 mmol) was dissolved in a flask containing 2 M NaOH (20 mL). The mixture was stirred for four hours before the pH was adjusted to pH 2 by addition of 1 M HCl. The mixture was extracted with ethyl acetate (3 x 15 mL). The organic phases were pooled together, dried over MgSO<sub>4</sub> and concentrated *in vacuo* to yield the ketoacid **20** (1.31 g, 90%) as a crystalline orange solid. **<sup>1</sup>H NMR** (400 MHz, CDCl<sub>3</sub>) δ: 7.95 – 7.90 (m, 2H, C7-CH), 7.63 – 7.57 (m, 1H, C9-CH), 7.51 – 7.46 (m, 2H, C8-CH), 4.06 (s, 2H, C4-CH<sub>2</sub>), 3.38 (s, 2H, C2-CH<sub>2</sub>); **<sup>13</sup>C NMR** (100 MHz, CDCl<sub>3</sub>) δ: 194.4 (C5), 175.6 (C1), 135.3 (C8), 133.9 (C9), 129.0 (C7), 128.8 (C8), 37.9 (C4), 33.4 (C2).

### 7.3.6 General procedure for the preparation of 2-substituted tetrahydroquinolines

#### 7.3.6.1 General procedure for the preparation of *o*-nitrophenylketones **89**

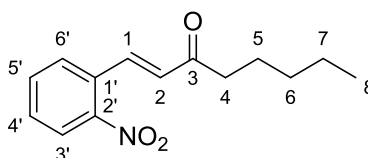
A three-neck round-bottom flask was charged with nitrobenzene (4.95 mmol), TBAC (10 mol %, 138 mg, 0.495 mmol) and the palladium catalyst Pd-118 [2 mol %, 64.5 mg, 0.990 mmol (Johnson-Matthey, UK)]. The flask was equipped with a thermometer and a water-cooled condenser. The system was then flushed with N<sub>2</sub> before sealing. DMAC (10 mL), Cy<sub>2</sub>NMe (1.59 mL, 7.43 mmol) and the alkene (12.4 mmol) were then added to the flask and the mixture was left to stir at 80°C for 24 h. The reaction mixture was then cooled to room temperature, before being diluted with MTBE (40 mL) and then filtered through Harborlite. The organic phase was then washed with dH<sub>2</sub>O (2 x 50 mL), dried over MgSO<sub>4</sub> and concentrated *in vacuo* to yield the crude product, which was then subjected to column chromatography using a Flashmaster system (silica gel in EtOAc/hexanes, 40 g column, gradient method) to yield the title compound.

#### **(E)-1-(2-nitrophenyl)pent-1-en-3-one**



Following the general Heck-coupling procedure, 2-nitrobenzene (1.00 g, 4.95 mmol) was reacted with 1-penten-3-one (2.5 x, 1.24 mL, 12.4 mmol) to yield the title compound **89b** (709 mg, 70% yield) as a yellow solid. **<sup>1</sup>H NMR** (400 MHz, CDCl<sub>3</sub>) δ: 8.08 – 8.03 (m, 1H, C3'-CH), 7.99 (d, *J* = 16.0 Hz, 1H, C1-CH), 7.69 – 7.62 (m, 2H, C5'-CH and C6'-CH), 7.59 – 7.51 (m, 1H, C4'-CH), 6.59 (d, *J* = 16.0 Hz, 1H, C2-CH), 2.75 (t, *J* = 7.5 Hz, 2H, C4-CH<sub>2</sub>), 1.18 (t, *J* = 7.5 Hz, 3H, C5-CH<sub>3</sub>); **<sup>13</sup>C NMR** (101 MHz, CDCl<sub>3</sub>) δ: 200.7 (C3), 148.5 (C2'), 137.9 (C1), 133.8 (C6'), 131.1 (C2), 130.4 (C4'), 129.2 (C5'), 125.2 (C3'), 33.5 (C4), 8.2 (C5). *Data consistent with literature values.*<sup>139</sup>

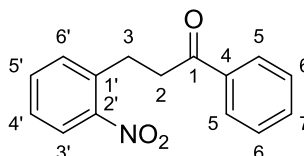
#### **(E)-1-(2-nitrophenyl)oct-1-en-3-one**



Following the general Heck-coupling procedure, 2-nitrobenzene (1.00 g, 4.95 mmol) was reacted with 1-octen-3-one (2.5 x, 1.84 mL, 12.4 mmol) to yield the title compound **89c** (604 mg, 49% yield) as a yellow solid. **<sup>1</sup>H NMR** (400 MHz, CDCl<sub>3</sub>) δ: 8.07 (dd, *J* = 8.5, 1.0 Hz, 1H, C3'-CH), 7.70 – 7.62 (m, 2H, C5'-CH and C6'-CH), 7.59 – 7.51 (m, 1H, C4'-CH),

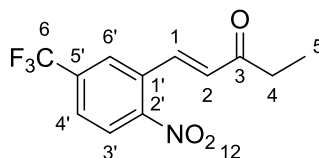
6.58 (d,  $J = 16.0$  Hz, 1H, C2-CH), 2.71 (t,  $J = 7.5$  Hz, 2H, C4-CH<sub>2</sub>), 1.75 – 1.64 (m, 2H, C5-CH<sub>2</sub>), 1.42 – 1.29 (m, 4H, C6-CH<sub>2</sub> and C7-CH<sub>2</sub>), 0.94 – 0.87 (m, 3H, C8-CH<sub>3</sub>); <sup>13</sup>C NMR (101 MHz, CDCl<sub>3</sub>) δ: 200.5 (C3), 148.5 (C2'), 138.0 (C1), 133.7 (C6'), 131.4 (C2), 131.1 (C1'), 130.4 (C4'), 129.2 (C5'), 125.1 (C3'), 40.3 (C4), 31.6 (C5), 24.0 (C6), 22.6 (C7), 14.1 (C8).

### 3-(2-nitrophenyl)-1-phenylpropan-1-one



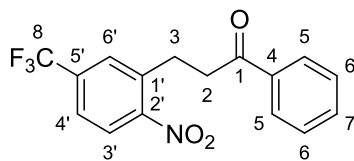
Following the general Heck-coupling procedure, 2-nitrobromobenzene (1.00 g, 4.95 mmol) was reacted with  $\alpha$ -vinylbenzyl alcohol (2.5 x, 1.63 mL, 12.4 mmol) to yield the title compound **89d** (602 mg, 48% yield) as a yellow solid. <sup>1</sup>H NMR (500 MHz, CDCl<sub>3</sub>) δ: 8.01 – 7.94 (m, 3H, C3'-CH and C5-CH), 7.59 – 7.52 (m, 2H, C5'-CH and C6'-CH), 7.50 – 7.43 (m, 3H, C4'-CH and C6-CH), 7.40 – 7.35 (m, 1H, C7-CH), 3.41 (ddd,  $J = 8.5, 2.0, 6.5$  Hz, 2H, C2-CH<sub>2</sub>), 3.34 (ddd,  $J = 8.5, 2.0, 6.5$  Hz, 2H, C3-CH<sub>2</sub>); <sup>13</sup>C NMR (100 MHz, CDCl<sub>3</sub>) δ: 198.5 (C1), 149.3 (C2'), 136.6 (C1'), 136.6 (C4), 133.3 (C6'), 132.6 (C4'), 128.7 (C5), 128.1 (C6), 127.5 (C5'), 124.9 (C3'), 39.5 (C2), 27.8 (C3).

### (E)-1-(2-nitro-5-(trifluoromethyl)phenyl)pent-1-en-3-one



Following the general Heck-coupling procedure, 4-bromo-3-nitrobenzotrifluoride (758  $\mu$ L, 4.95 mmol) was reacted with 1-penten-3-one (2.5 x, 1.24 mL, 12.4 mmol) to yield the title compound **89e** (847 mg, 63% yield) as white needle-like crystals. <sup>1</sup>H NMR (400 MHz, CDCl<sub>3</sub>) δ: 8.15 (d,  $J = 8.5$  Hz, 1H, C3'-CH), 7.94 (d,  $J = 16.0$  Hz, 1H, C1-CH), 7.93 – 7.88 (m, 1H, C6'-CH), 7.80 (dd,  $J = 8.5, 1.5$  Hz, 1H, C4'-CH), 6.68 (d,  $J = 16$  Hz, 1H, C2-CH), 2.76 (q,  $J = 7.5$  Hz, 2H, C4-CH<sub>2</sub>), 1.19 (t,  $J = 7.5$  Hz, 3H, C5-CH<sub>3</sub>); <sup>13</sup>C NMR (126 MHz, CDCl<sub>3</sub>) δ: 199.8 (C3), 150.2 (C2'), 135.7 (C1), 135.3 (q,  $J = 33.5$  Hz, C5'), 132.1 (C2), 131.8 (C1'), 127.1 (q,  $J = 3.5$  Hz, C4'), 126.4 (q,  $J = 3.5$  Hz, C6'), 125.7 (C3'), 122.6 (q,  $J = 273.0$  Hz, C6), 34.0 (C4), 7.9 (C5).

### 3-(2-nitro-5-(trifluoromethyl)phenyl)-1-phenylpropan-1-one

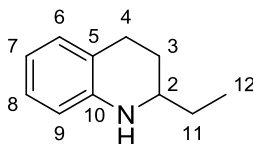


Following the general Heck-coupling procedure, 4-bromo-3-nitrobenzotrifluoride (758  $\mu\text{L}$ , 4.95 mmol) was reacted with  $\alpha$ -vinylbenzyl alcohol (2.5 x, 1.63 mL, 12.4 mmol) to yield the title compound **89f** (798 mg, 50% yield) as white needle-like crystals.  **$^1\text{H NMR}$**  (500 MHz,  $\text{CDCl}_3$ )  $\delta$ : 8.02 (d,  $J = 8.5$  Hz, 1H, C3'-CH), 7.96 (dd,  $J = 8.5, 1.0$  Hz, 2H, C5-CH), 7.79 (d,  $J = 1.0$  Hz, 1H, C6'-CH), 7.65 (dd,  $J = 8.5, 1.5$  Hz, 1H, C4'-CH), 7.58 (tt,  $J = 7.5, 1.5$  Hz, 1H, C7-CH), 7.47 (tt,  $J = 8.0, 1.5$  Hz, 2H, C6-CH), 3.43 (ddd,  $J = 8.5, 2.0, 6.5$  Hz, 2H, C2-CH<sub>2</sub>), 3.37 (ddd,  $J = 8.5, 2.0, 6.5$  Hz, 2H, C3-CH<sub>2</sub>);  **$^{13}\text{C NMR}$**  (126 MHz,  $\text{CDCl}_3$ )  $\delta$ : 197.8 (C1), 151.5 (C2'), 137.4 (C1'), 136.4 (C4), 134.6 (q,  $J = 33.5$  Hz, C5'), 133.4 (C7), 129.8 (q,  $J = 3.5$  Hz, C4'), 128.7 (C5), 128.1 (C6), 125.3 (C3'), 124.6 (q,  $J = 3.5$  Hz, C6'), 122.9 (q,  $J = 273.0$  Hz, C8), 39.1 (C2), 27.4 (C3).

#### 7.3.5.2 General procedure for the synthesis of 2-substituted-1,2,3,4-tetrahydroquinolines

A round-bottom flask was charged with *o*-nitrophenylketone **89**, Pd/C (10 mol%) and MeOH (10 mL). The mixture was then purged of air and left to stir and react under an  $\text{H}_2$  atmosphere overnight. Following completion of the reaction, the mixture was then filtered through a pad of Celite, dried over  $\text{MgSO}_4$  and concentrated *in vacuo* to yield to the tetrahydroquinoline product, which was subjected to column chromatography (silica gel, ethyl acetate/cyclohexane + 0.1% triethylamine) if further purification was required.

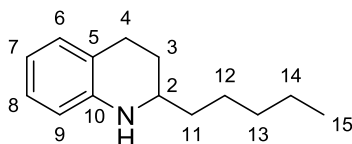
### 2-ethyl-1,2,3,4-tetrahydroquinoline



Following the general hydrogenation procedure, **89b** (600 mg, 2.93 mmol) was reduced with Pd/C (311 mg) to give the title compound (382 mg, 81%) as yellow oil.  **$^1\text{H NMR}$**  (400 MHz,  $\text{CDCl}_3$ )  $\delta$  6.97 (t,  $J = 7.5$  Hz, 1H, C8-CH), 6.96 (d,  $J = 7.5$  Hz, 1H, C6-CH), 6.61 (td,  $J = 7.5, 1.0$  Hz, 1H, C7-CH), 6.51 – 6.46 (m, 1H, C9-CH), 3.73 (bs, 1H, NH), 3.18 (dtd,  $J = 9.5, 6.5, 3.0$  Hz, 1H, C2-CH), 2.90 – 2.65 (m, 2H, C4-CH<sup>a</sup> and C4-CH<sup>b</sup>), 1.98 (ddd,  $J = 12.5, 3.0, 4.0$  Hz, 1H, C3-CH<sup>a</sup> or C3-CH<sup>b</sup>), 1.65 – 1.56 (m, 1H, C3-CH<sup>a</sup> or C3-CH<sup>b</sup>), 1.57 – 1.50 (m, 2H, C11-CH<sub>2</sub>), 1.00 (t,  $J = 7.5$  Hz, 3H, C12-CH<sub>3</sub>);  **$^{13}\text{C NMR}$**  (101 MHz,  $\text{CDCl}_3$ )  $\delta$ : 144.9

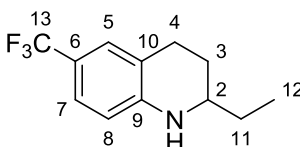
(C10), 129.4 (C6), 126.8 (C8), 121.5 (C5), 117.0 (C7), 114.1 (C9), 53.2 (C2), 29.5 (C11), 27.7 (C3), 26.5 (C4), 10.2 (C12). *Data consistent with literature values.*<sup>140</sup>

### 2-pentyl-1,2,3,4-tetrahydroquinoline



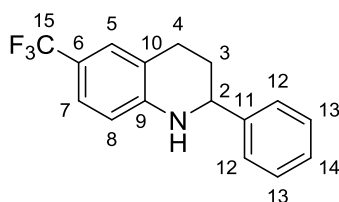
Following the general hydrogenation procedure, **89c** (550 mg, 2.22 mmol) was reduced with Pd/C (237 mg) to give the title compound (339 mg, 75%) as yellow oil. **<sup>1</sup>H NMR** (400 MHz, CDCl<sub>3</sub>) δ 6.99 – 6.92 (m, 1H, C8-CH), 6.95 (d, *J* = 7.5 Hz, 1H, C6-CH), 6.59 (td, *J* = 7.5, 1.0 Hz, 1H, C7-CH), 6.50 – 6.46 (m, 1H, C9-CH), 3.76 (bs, 1H, NH), 3.18 (dtd, *J* = 9.0, 6.0, 3.0 Hz, 1H, C2-CH), 2.86 – 2.68 (m, 2H, C4-CH<sup>a</sup> and C4-CH<sup>b</sup>), 2.00 – 1.92 (m, 1H, C3-CH<sup>a</sup> or C3-CH<sup>b</sup>), 1.66 – 1.53 (m, 1H, C3-CH<sup>a</sup> or C3-CH<sup>b</sup>), 1.57 – 1.25 (m, 9H, C11-CH<sub>2</sub>, C12-CH<sub>2</sub> and C13-CH<sub>2</sub>) 1.35 – 1.28 (m, 2H, C14-CH<sub>2</sub>), 0.91 (t, *J* = 7.0 Hz, 3H, C15-CH<sub>3</sub>); **<sup>13</sup>C NMR** (101 MHz, CDCl<sub>3</sub>) δ: 144.9 (C10), 129.4 (C6), 126.8 (C8), 121.5 (C7), 117.0 (C7), 114.2 (C9), 51.7 (C2), 36.8 (C11), 32.1 (C14), 28.3 (C3), 26.6 (C4), 25.5 (C12), 22.7 (C13), 14.2 (C15). *Data consistent with literature values.*<sup>140</sup>

### 2-ethyl-6-(trifluoromethyl)-1,2,3,4-tetrahydroquinoline



Following the general hydrogenation procedure, **89e** (800 mg, 2.93 mmol) was reduced with Pd/C (312 mg) to give the title compound (490 mg, 73%) as yellow oil. **<sup>1</sup>H NMR** (400 MHz, CDCl<sub>3</sub>) δ: 7.21 – 7.14 (m, 1H, C7-CH), 7.12 – 7.05 (m, 2H, C5-CH and C8-CH), 3.49 – 3.39 (m, 1H, C2-CH), 2.77 – 2.48 (m, 3H, C4-CH<sup>a</sup>, C4-CH<sup>b</sup> and C3-CH<sup>a</sup> or C3-CH<sup>b</sup>), 1.93 – 1.85 (m, 1H, C3-CH<sup>a</sup> or C3-CH<sup>b</sup>), 1.74 – 1.54 (m, 1H, C11-CH<sup>a</sup> or C11-CH<sup>b</sup>), 1.54 – 1.34 (m, 4H, C3-CH<sup>a</sup>, C3-CH<sup>b</sup> and C12-CH<sub>3</sub>); **<sup>13</sup>C NMR** (101 MHz, CDCl<sub>3</sub>) δ: 147.4 (C9), 126.3 (q, *J* = 4.0 Hz, C7), 125.3 (q, *J* = 271.0 Hz, C13), 124.1 (q, *J* = 4.0 Hz, C5), 120.74, 118.0 (q, *J* = 32.5 Hz, C6), , 114.8, 113.01, 77.48, 77.16, 76.84, 72.46, 52.98, 36.13, 30.70, 29.4 (C4), 26.9 (C3), 26.91, 26.2.

### 2-phenyl-6-(trifluoromethyl)-1,2,3,4-tetrahydroquinoline

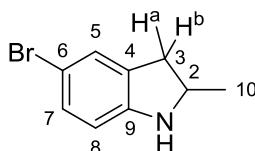


Following the general hydrogenation procedure, **89f** (700 mg, 2.17 mmol) was reduced with Pd/C (230 mg) to give the title compound (330 mg, 55 mmol) as a pale yellow solid. **<sup>1</sup>H NMR** (400 MHz, CDCl<sub>3</sub>) δ 6.99 – 6.92 (m, 1H, C8-CH), 6.95 (d, *J* = 7.5 Hz, 1H, C6-CH), 6.59 (td, *J* = 7.5, 1.0 Hz, 1H, C7-CH), 6.50 – 6.46 (m, 1H, C9-CH), 3.76 (bs, 1H, NH), 3.18 (dtd, *J* = 9.0, 6.0, 3.0 Hz, 1H, C2-CH), 2.86 – 2.68 (m, 2H, C4-CH<sup>a</sup> and C4-CH<sup>b</sup>), 2.00 – 1.92 (m, 1H, C3-CH<sup>a</sup> or C3-CH<sup>b</sup>), 1.66 – 1.53 (m, 1H, C3-CH<sup>a</sup> or C3-CH<sup>b</sup>), 1.57 – 1.25 (m, 9H, C11-CH<sub>2</sub>, C12-CH<sub>2</sub> and C13-CH<sub>2</sub>), 1.35 – 1.28 (m, 2H, C14-CH<sub>2</sub>), 0.91 (t, *J* = 7.0 Hz, 3H, C15-CH<sub>3</sub>); **<sup>13</sup>C NMR** (101 MHz, CDCl<sub>3</sub>) δ: 147.4 (C9), 144.2 (C11), 128.8 (C13), 127.8 (C14), 126.5 (C12), 126.4 (q, *J* = 3.5 Hz, C7), 125.8 (C10), 125.2 (q, *J* = 271.0 Hz, C15), 124.3 (q, *J* = 3.5 Hz, C5), 120.4 (C8), 118.6 (q, *J* = 32.5 Hz, C6), 56.1 (C2), 30.3 (C3), 26.0 (C4).

### 7.3.7 General procedure for the preparation of 2-substituted indolines

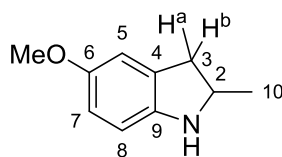
A three-necked round-bottom flask equipped with a reflux condenser and thermometer was charged with indole, ethanol, conc. HCl and tin. The mixture was stirred and refluxed for 6 h, after which the mixture was cooled to room temperature before being decanted from the tin into a beaker containing 20% KOH solution (30 mL). The resulting white solid and basic mixture was extracted with diethyl ether (3 x 30 mL). The organic phases were pooled, filtered through a pad of Celite, dried over MgSO<sub>4</sub> and concentrated *in vacuo* to yield the crude indoline product, which was then subjected to flash chromatography (silica gel, ethyl acetate/cyclohexane + 0.1% triethylamine) to yield the title product.

### 5-bromo-2-methylindoline



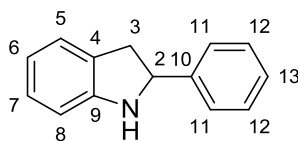
5-bromo-2-methylindole (1.64 g, 7.84 mmol), ethanol (9 mL), conc. HCl (6 mL) and tin (5 g, 42.1 mmol) were reacted. The crude product was isolated from the reaction and subjected to flash column chromatography (silica gel, 10% v/v ethyl acetate/cyclohexane + 0.1% triethylamine) to afford 5-bromo-2-methylindoline (1.21 g, 74%) as brown liquid. **<sup>1</sup>H NMR** (400 MHz, CDCl<sub>3</sub>) δ 7.17 - 7.14 (m, 1H, C5-CH), 7.11 – 7.07 (m, 1H, C7-CH), 6.45 (d, *J* = 8.0 Hz, 1H, C8-CH), 4.05 – 3.94 (m, 1H, C2-CH), 3.77 (bs, 1H, NH), 3.12 (d, *J* = 15.5, 8.5 Hz, 1H, C3-CH<sup>a</sup> or C3-CH<sup>b</sup>), 2.62 (dd, *J* = 15.5, 7.5 Hz, 1H, C3-CH<sup>a</sup> or C3-CH<sup>b</sup>), 1.27 (d, *J* = 6.0 Hz, 3H, C10-CH<sub>3</sub>); **<sup>13</sup>C NMR** (126 MHz, CDCl<sub>3</sub>) δ 150.1 (C9), 131.4 (C6), 129.9 (C4), 127.8 (C5), 110.4 (C7), 110.0 (C8), 55.8 (C2), 37.6 (C3), 22.3 (C10). *Data consistent with literature values.*<sup>141</sup>

## 5-methoxy-2-methylindoline



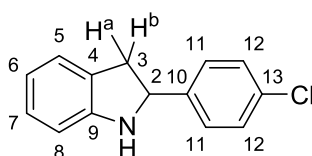
5-methoxy-2-methylindole (750 mg, 4.65 mmol), ethanol (5.5 mL), conc. HCl (3.8 mL) and tin (2.98 g, 25.1 mmol) were reacted. The crude product was isolated from the reaction to afford 5-methoxy-2-methylindoline (613 mg, 81%) as deep purple liquid. **<sup>1</sup>H NMR** (400 MHz, CDCl<sub>3</sub>) δ 6.74 – 6.70 (m, C5-CH), 6.59 (d, *J* = 8.5, 2.5 Hz, 1H, C7-CH), 6.54 (d, *J* = 8.5 Hz, 1H, C8-CH), 4.02 – 3.92 (m, 1H, C2-CH), 3.74 (s, 3H, OMe), 3.47 (bs, 1H, NH), 3.11 (dd, *J* = 15.5, 8.5 Hz, 1H, C3-CH<sup>a</sup> or C3-CH<sup>b</sup>), 2.62 (dd, *J* = 15.5, 8.5 Hz, 1H, C3-CH<sup>a</sup> or C3-CH<sup>b</sup>), 1.29 (d, *J* = 6.0 Hz, 3H, C10-CH<sub>3</sub>); **<sup>13</sup>C NMR** (126 MHz, CDCl<sub>3</sub>) δ 153.5 (C9), 144.9 (C6), 130.8 (C7), 112.2 (C5), 111.8 (C8), 109.9 (C4), 56.0 (OMe), 55.8 (C2), 38.4 (C3), 22.3 (C10). *Data consistent with literature values.*<sup>119</sup>

## 2-phenylindoline



2-phenylindole (1.5 g, 7.80 mmol), ethanol (9 mL), conc. HCl (6 mL) and tin (5 g, 42.1 mmol) were reacted. The crude product was isolated from the reaction and subjected to flash column chromatography (silica gel, 5% v/v ethyl acetate/cyclohexane + 0.1% triethylamine) to afford 2-phenylindoline (1.26 g, 83%) as a pale brown solid. **<sup>1</sup>H NMR** (400 MHz, CDCl<sub>3</sub>) δ: 7.49 – 7.43 (m, 2H), 7.41 – 7.34 (m, 2H, C11-CH), 7.34 – 7.27 (m, 1H), 7.15 – 7.08 (m, 2H), 6.78 (td, *J* = 7.5, 1.0 Hz, 1H, C6-CH), 6.71 (d, *J* = 7.5 Hz, 1H, C8-CH), 4.99 (t, *J* = 9.0 Hz, 1H, C2-CH) 4.18 (bs, 1H, NH), 3.48 (dd, *J* = 15.5, 9.0 Hz, 1H, C3-CH<sup>a</sup> or C3-CH<sup>b</sup>), 3.03 (dd, *J* = 15.5, 9.0 Hz, 1H, C3-CH<sup>a</sup> or C3-CH<sup>b</sup>); **<sup>13</sup>C NMR** (126 MHz, CDCl<sub>3</sub>) δ: 151.1 (C9), 144.8 (C4), 128.7 (C11), 128.2 (C10), 127.7 (C7), 127.5 (C5), 126.4 (C12), 124.7 (C13), 118.9 (C6), 108.9 (C8), 63.7 (C2), 39.7 (C3). *Data consistent with literature values.*<sup>142</sup>

## 2-(*p*-chlorophenyl)indoline



2-(4-chlorophenyl)indole (0.75 g, 3.29 mmol), ethanol (3.80 mL), conc. HCl (2.53 mL) and tin (2.11 g, 17.8 mmol) were reacted. The crude product was isolated from the reaction and subjected to flash column chromatography (silica gel, 3% v/v ethyl acetate/cyclohexane + 0.1% triethylamine) to afford 2-(4-chlorophenyl)indoline (642 mg, 85%) as a yellow solid. **<sup>1</sup>H NMR** (400 MHz, CDCl<sub>3</sub>) δ 7.40 – 7.34 (m, 2H, C12-CH), 7.34 – 7.28 (m, 2H, C11-CH), 7.12 – 7.06 (m, 2H, C5-CH), 6.76 (td, *J* = 7.5, 1.0 Hz, 1H, C7-H), 6.68 (d, *J* = 7.5 Hz, 1H, C5-CH), 4.54 (t, 3H, *J* = 9.0 Hz, 1H, C2-CH), 4.14 (bs, 1H, NH), 3.44 (dd, *J* = 15.5, 9.0 Hz, 1H, 3C-H<sup>a</sup> or 3C-H<sup>b</sup>), 2.93 (dd, *J* = 15.5, 9.0 Hz, 1H, 3C-CH<sup>a</sup> or 3C-CH<sup>b</sup>); **<sup>13</sup>C NMR** (126 MHz, CDCl<sub>3</sub>) δ 150.9 (C9), 143.3 (C4), 133.1 (C13), 128.8 (C11), 127.8 (C12), 127.7 (ArC), 124.7 (ArC), 119.1 (ArC), 109.0 (ArC), 63.0 (C2), 39.8 (C3). *Data consistent with literature values.*<sup>142</sup>

## 7.4 Growth and expression of biocatalysts

### 7.4.1 Amino acid sequences for proteins used in this report

#### 7.4.1.1 *Streptomyces* sp. GF3587 (*R*)-IRED<sup>143</sup>

```
ATGGGCGACAATCGTACGCCGGTCACGGTTATCGGTCTGGGTCTGATGGGTCAAGCACTGGCAG
CAGCATTCTGGAAGCAGGTCACACCACGACCGTGTGGAACCGTAGCGCGGGTAAAGCCGAACA
GCTGGTTTCTCAGGGTGCGGTTTCAGGCCGAACCCCGGCAGATGCTGTTGCAGCTTCAGAACTG
GTGGTTGTCTGCCTGTCGACCTATGATAACATGCATGACGTCATTGGTAGTCTGGGCGAATCCCT
GCGTGGTAAAGTCATCGTGAATCTGACGAGCGGTAGCTCTGATCAGGGTCGTGAAACCGCCGCA
TGGGCAGAAAAACAGGGTGTTGAATACCTGGACGGCGCAATTATGATCACGCCCGGGGTATTG
GCACGGAAACCGCAGTCCTGTTTTATGCTGGTACCCAGTCTGTGTTGAAAAATACGAACCGGCT
CTGAAACTGCTGGGCGGTGGCACGACCTATCTGGGTACCGATCATGGCATGCCGGCCCTGTACG
ACGTGTCACTGCTGGGTCTGATGTGGGGCAGCTGAACTCGTTTCTGCATGGCGTGGCAGTGGT
TGAAACCGCGGGTGTGGCGCCAGCAATTTCTGCCGTGGGCACACATGTGGCTGGAAGCTATT
AAAATGTTACCGCGGATTATGCAGCTCAAATCGATGCGGGTGACGGCAAATCCCGGCAAATGA
CGCTACGCTGGAAACCCACCTGGCGGCCCTGAAACATCTGGTTCACGAATCAGAAGCGCTGGGCA
TTGATGCCGAACTGCCGAAATACAGTGAAGCGCTGATGGAACGCGTGATCTCCAGGGTCACGCT
AAAAACAGCTATGCGGCAGTCCTGAAAGCCTTCCGTAAACCGTCCGAATAA
```

#### 7.4.1.2 *Streptomyces* sp. GF3546 (*S*)-IRED<sup>78</sup>

```
ATGAGCAAACAGTCAGTTACGGTGATTGGTCTGGGTCCGATGGGTCAAGCGATGGTCAATACCTTT
CTGGATAATGGTCACGAAGTGACCGTGTGGAACCGTACGGCGTCAAAGCAGAAGCTCTGGTGGCG
CGCGGCGCAGTTCTGGCACCGACCGTCGAAGATGCTCTGAGCGCGAATGAACTGATTGTTCTGTCT
```

CTGACCGATTATGACGCCGTGTACGCAATCCTGGAACCGGTTACGGGCTCACTGTCGGGTAAAGTG  
ATTGCAAACCTGAGCTCTGATACCCCGACAAAGCGCGTGAAGCGGCCAAATGGGCAGCTAAACAT  
GGTGCGAAACATCTGACCGGCGGTGTGCAGGTTCCGCCGCCGCTGATCGGCAAACCGGAAAGTTCC  
ACCTATTACTCCGGTCCGAAAGATGTTTTTGACGCCATGAAGATACCCTGAAAGTCCTGACGAACG  
CCGATTATCGTGGTGAAGATGCAGGTCTGGCCGAATGTATTACCAGGCGCAAATGACCATTTTCT  
GGACCACGATGCTGAGCTATTACCAGACGCTGGCTCTGGGCCAAGCGAATGGTGTAGTGCTAAAG  
AACTGCTGCCGTATGCCACCATGATGACGTCCATGATGCCGATTTTCTGGAAGTGTATGCTCAGCA  
CGTCGATTCTGCGGACTATCCGGGTGATGTGGACCGTCTGGCGATGGGCGCAGCTTCAGTCGATCA  
CGTGCTGCATACCCACCAAGATGCGGGTGTAGCACCGTCTGCCGGCCGAGTGGCCGAAATCTT  
CAAAGCCGGTATGGAAAAGGCTTTGCTGAAAATTCGTTCTCCTCTCTGATTGAAGTCCTGAAAAA  
CCGGCAGTGTA

#### 7.4.1.3 *Amycolatopsis orientalis* Ao-IRED<sup>144</sup>

ATGACCGACCAGAACCTGCCGGTACCCTGGCGGGTCTGGGCCCGATGGGCTCCGCTCTGGCGGC  
TGACTGCTGGACCGTGGTCACGACGTTACTGTTTGAACCGCTCTCCGGGCAAAGCAGCACCGCT  
GGTGGCTAAAGGTGCGCGTCAGGCGGACGACATCGTTGACGCGGTTAGCGCGTCCCGCCTGCTGG  
TTGTGTGCCTGGCGGACTACGATGCGCTGTATAGCGCACTGGGTCCGGCTCGTGAAGCGCTGCGT  
GGTCGTGTTGTTGTTAACCTGAACTCTGGCACCCCGAAAGAAGCGAACGAAGCTCTGCGTTGGGC  
GAGCGTCACGGTACTGGTTACCTGGACGGTGCATCATGGTTCCGCCGGCAATGGTTGGTCACCCA  
GGCTCTGTTTTCTGACTCTGGCTCTGCTGAAGTTTTCGAAGAATACAAAGAAACCTGGCTGGCC  
TGGGCGACCCGGTTCACCTGGGTAAGCGGGCCTGGCAGTTCTGTACAACACCGCGCTGCTGT  
CTATGATGTACAGCTCTATGAACGGTTTTCTGCATGCTGCGGCACTGGTGGGTTCTGCAGGTGTT  
CGGCTGCGGAGTTCACCAAACCTGGCTGTTGACTGGTTTTCTGCCGGCTGTGATCGGTCAGATCATCA  
AAGCGGAAGCGCCGACCATCGACGAAGGCGTTTATCCGGGCGATGCGGGTCTCTGGAAATGAACG  
TGACTACTCTGAAACACATCATCGGCACCTCTCAGGAACAGGGTGTGATACCGAAATCCCGGTGC  
GTAACAAAGAGCTGCTGGATCGTGAGTTGCAGCGGGTTTCGGCGAATCTTCTTACTATTCTGTTA  
TCGAACTGTGGCGTTAA

#### 7.4.1.4 *Mycobacterium marinum* CAR (MCAR)<sup>95</sup>

ATGAGCCCGATTACCCGTGAAGAACGTCTGGAACGTCGTATTCAGGATCTGTATGCGAACGATCCG  
CAGTTCGCAGCAGCCAAACCGGCGACCGGATTACCGCGGCGATTGAACGTCCGGGTCTGCCGCTG  
CCGAGATCATCGAAACGGTGTGACCGGCTATGCGGATCGTCCGGCACTGGCACAACGTAGCGTG  
GAATTTGTGACCGATGCGGGCACCGGTCATAACCACCTGCGTCTGCTGCCGATTTTGAACCAATT  
AGCTATGGCGAACTGTGGGATCGTATTAGCGCGCTGGCCGATGTTCTGAGCACCGAACAGACCGTG  
AAACCGGGCGATCGTGTGTGCCTGCTGGGCTTTAACAGCGTGGATTATGCGACCATTGATATGACC

CTGGCACGTCTGGGTGCTGTCGCTGTCCCGCTGCAGACCTCTGCTGCGATTACCCAGCTGCAGCCG  
ATTGTGGCGGAAACCCAGCCGACCATGATTGCGGCGAGCGTGGATGCCCTGGCCGATGCGACCGA  
ACTGGCACTGAGTGGTCAAACGGCTACGCGTGTGCTGGTGTGGATCATCATCGTCAGGTGGATGC  
GCATCGTGCGGCGGTTGAAAGCGCGCGTGAACGTCTGGCCGGTAGCGCGGTGGTTGAAACCCTGG  
CCGAAAGCGATTGCGCGTGGTATGTGCCGCGTGGTGCAGCGCGGGTAGCGCACCCGGGACCGAT  
GTGAGCGATGATAGCCTGGCCCTGCTGATTTATACCTCTGGTAGTACGGGTGCGCCGAAAGGCGCC  
ATGTATCCGCGTCGTAACGTGGCGACCTTTTGGCGTAAACGTACCTGGTTTGAAGGCGGCTATGAA  
CCGAGCATTACCCTGAACTTTATGCCGATGAGCCATGTGATGGGCCGTGAGATTCTGTATGGCACC  
CTGTGCAACGGCGGCACCCGCTATTTTGTGGCGAAAAGCGATCTGAGCACCTGTTTGAAGATCTG  
GCCCTGGTGCCTCCGACCGAACTGACCTTCGTCCCGCGTGTGGGATATGGTGTTCGATGAATTT  
CAGAGCGAAGTGGATCGTCGTCTGGTGGATGGCGCGGATCGTGTTGCGCTGGAAGCGCAGGTGAA  
AGCGGAAATTCGTAACGATGTGCTGGGCGGTCGTTATACCTCTGCTCTGACGGGTTCTGCTCCGAT  
TAGCGATGAAATGAAAGCGTGGGTGGAAGAACTGCTGGATATGCATCTGGTGGAAAGGCTATGGCA  
GCACCGAAGCGGGCATGATTCTGATTGATGGCGCGATTTCGTTCGTCGCGCGGTGCTGGATTATAAC  
TGGTGGATGTTCCGGATCTGGGCTATTTTCTGACCGATCGTCCGCATCCGCGTGGCGAACTGCTGG  
TGAAAACCGATAGCCTGTTTCCGGGCTATTATCAGCGTGCAGGAAAGTACCAGCGGATGTGTTTATG  
CGGATGGCTTTTATCGCACCCGGCGATATTATGGCGGAAAGTGGGCCCCGGAACAGTTTGTGTATCTGG  
ATCGTCGTAACAACGTGCTGAAACTGAGCCAGGGCGAATTTGTTACCGTGAGCAAACCTGGAAGCGG  
TGTTTGGCGATAGCCCCTGGTGCCTCAGATTTATATTTATGGCAACAGCGCGCTGCGTATCTGC  
TGGCCGTGATTGTGCCGACCCAGGAAGCGCTGGACGCGGTCCCGGTTGAAGAACTGAAAGCGCGT  
CTGGGTGACTCTCTGCAGGAAGTGGCGAAAAGCGCGGGTCTGCAGAGCTATGAAATCCGCGCGA  
TTTTATTATCGAAACCACCCCGTGGACCCTGGAAAACGGCCTGCTGACGGGTATTCGTAACCTGGC  
CCGTCCGAGCTGAAAAACATTATGGTGAACCTGCTGGAACAAATTTATACCGATCTGGCCACGG  
CCAGGCGGATGAACTGCGTAGCCTGCGTCAGAGCGGTGCGGATGCGCCGGTGTGGTGACCGTTT  
GTCGTGCGGCTGCAGCTCTGCTGGGTGGTAGCGCGAGCGATGTGCAGCCGGATGCGCATTTTACC  
GATCTGGGTGGTGTAGCCTGAGCGCCCTGAGCTTTACCAACCTGCTGCATGAAATCTTTGATATT  
GAAGTGCCGGTGGGCGTGATTGTGAGCCCGGCGAACGATCTGCAGGCGCTGGCCGATTATGTGGA  
AGCGGCGCGTAAACCGGGTAGCAGCCGTCCGACCTTTGCGAGCGTGCATGGCGCGAGCAACGGCC  
AGGTGACCGAAGTGCATGCGGGCGATCTGAGCCTGGATAAATTTATTGATGCGGGCACCCCTGGCCG  
AAGCCCCGCGTCTGCCGGCTGCAAATACCCAGGTGCGTACCGTGCTGCTGACCGGTGCGACCGGCT  
TTCTGGGCCGTTACCTGGCCCTGGAATGGCTGGAACGTATGGATCTGGTTGATGGCAAACCTGATTT  
GCCTGGTGCCTGCCAAAAGCGATACCGAAGCGCGTGCAGCGTCTGGATAAAACCTTTGATAGCGGCG  
ATCCGGAACCTGCTGGCCATTATCGTGCCTGGCCGGCGATCATCTGGAAGTGTGGCCGGTGATA  
AAGGCGAAGCGGATCTGGGCCTGGATCGTCAGACCTGGCAACGCCTGGCAGATACCGTGGATCTGA  
TTGTTGACCCGGCTGCCCTGGTGAATCATGTGCTGCCGTATAGCCAGCTGTTTGGCCCGAATGCGC  
TGGGCACCGCTGAACTGCTGCGCCTGGCTCTGACCAGCAAAATTAACCGTATAGCTACACCAGCA  
CCATTGGCGTGGCGGATCAGATTCCGCCGAGCGGTTTACCGAAGATGCGGATATTTCGTGTGATTA  
GCGCGACCCGTGCGGTGGATGATAGCTATGCGAACGGCTATAGCAACAGCAAATGGGCGGGTGAA

GTGCTGCTGCGTGAAGCGCATGATCTGTGCGGTCTGCCGGTGGCGGTGTTTCGTTGCGATATGATC  
CTGGCAGACACGACCTGGGCGGGTCAGCTGAACGTGCCGGATATGTTTACCCGTATGATTCTGTCT  
CTGGCAGCTACGGGTATCGCACCGGGTAGCTTTTATGAACTGGCCGCGGATGGTGCGCGTCAGCGT  
GCGCATTATGATGGCCTGCCGGTGAATTTATTGCGGAAGCGATTAGCACCTGGGCGCGCAGAGC  
CAGGATGGCTTTCATACCTATCATGTGATGAATCCGTATGATGATGGCATTGGCCTGGATGAATTT  
GTGGATTGGCTGAACGAAAGCGGCTGCCGATTCAGCGTATTGCGGATTATGGCGATTGGCTGCAG  
CGTTTTGAAACCGCGCTGCGCGCTCTGCCGGATCGTCAGCGTCATAGCAGCCTGCTGCCGCTGCTG  
CATAACTATCGTCAGCCGGAACGTCCGGTGCCTGGTAGCATTGCGCCGACCGATCGCTTTCGTGCG  
GCCGTGCAGGAAGCGAAAATTGGCCCGGATAAAGATATCCGCATGTGGGTGCGCCGATTATTGTG  
AAATATGTGAGCGATCTGCGCCTGCTGGGCCTGCTGTAA

#### 7.4.1.5 Bs Sfp<sup>95</sup>

ATGGGCAAGATTTACGGAATTTATATGGACCGCCCGCTTTCACAGGAAGAAAATGAACGGTTCATG  
TCTTTCATATCACCTGAAAAACGGGAGAAATGCCGGAGATTTTATCATAAAGAAGATGCTCACCGCA  
CCCTGCTGGGAGATGTGCTCGTTCGCTCAGTCATAAGCAGGCAGTATCAGTTGGACAAATCCGATA  
TCCGCTTTAGCACGCAGGAATACGGGAAGCCGTGCATCCCTGATCTTCTGACGCCATTTCAATAT  
TTCTCACTCTGGCCGCTGGGTCAATTTGCGCGTTTGATTCACAGCCGATCGGCATAGATATCGAAAA  
ACGAAACCGATCAGCCTTGAGATCGCCAAGCGCTTCTTTGCAAAAACAGAGTACAGCGACCTTTTAG  
CAAAAGACAAGGACGAGCAGACAGACTATTTTTATCATCTATGGTCAATGAAAGAAAGCTTTATCAA  
ACAGGAAGGCAAAGGCTTATCGCTTCCGCTTGATTCCTTTTCAGTGCGCCTGCATCAGGACGGACA  
AGTATCCATTGAGCTTCCGGACAGCCATCCCCATGCTATATCAAACGTATGAGGTGATCCCCGGC  
TACAAAATGGCTGTATGCGCCGCACACCCTGATTTCCCTGAGGATATCACAATGGTCTCGTACGAAG  
AGCTTTTATAA

#### 7.4.1.6 6-HDNO E350L/E352D<sup>105</sup>

#### 7.4.1.7 CHAO<sup>110</sup>

TGTCGTAGCCGTGAGGCAGCACGTAGCAAACGTGAAGAAAGCGCACTGACCCATCTGAATACCTAT  
GAAAGCGTTACCCCTGATCCGGATGTTGATGTTATTATCATTGGTGCAGGTATTAGCCGTAGCGCA  
GCAGCAAAAGCACTGCATGATCAGGGTGCAAGCGTTCTGGTTGTTGAAGCAAATGATCGTATTGGT  
GGTCGTACCTGGACCGAACAAGAGGGTGACCCGGTGGTCCGATTGATTATGGTGGTATGTTTATT  
GGTGAAACCCATACCCACCTGATTGAACTGGGCACCAGCCTGGGTCTGAAAATGACCCCGAGCGGT  
AAACCGGGTGTGATACCTATATTGTTGCAGGTAATGTTCTGCGTGACCCGGATGATCAGCTGGAC  
CCGAATCTGCCGTTTGTCCGGAATTTCTGAGCAGCCTGAAAGCCCTGGATGAACTGGCAGATAGC

GTTGGTTGGGATCAGCCGTGGGCAAGCCCGAATGCAGCAGCACTGGATAGCAAAAACCGTTGCAACC  
TGGCTGGCAGAAACCATTGAAAGCGAAGAAGTTCGTCTGCATACCGTTATTGTGAATTTAGC  
CTGGGTGCAGATCCGTATGAAGTTAGCCTGCTGTATTGGGCATATTATGTTAGCGAATGTGAAGGC  
ATTCAGAGCCTGTTTGGCACCCGTGATGGTGCACAGTGGGCATGGTGGTTTGGTGGTGCAGCACA  
GGTTAGCTGGCGTATTGCAGATGCAATTGGTCGTGATAAATTTCTGCTGGAATGGCCTGTTGATCG  
CATTGAACATGATGAAAGCGGTGTTACCCTGTTTAGCGGTCAGCGTAGCCTGCGTGCCCCTCATAT  
TGTTATTGCAATGAGTCCGCTGGCAGCAAATCAGATTGTTTTGAACCGGCACTGCCGACCAGCCG  
TGCACAGCTGCAAGCACGTGCACCGATGGGTGTTATTACAAAGTTCAGGCACGTTATCCGAGCAG  
CTTTTGGGTTGAACAGGGTTATAGCGGTGCACTGCTGGATACCGAAGATGTTGGTGTTCCTGCT  
GGATGGCACCAAACCGACCGATACCCTGGCAACCCTGATTGGTTTTATTGGCGGTAGCAATTATGA  
TCGTTGGGCAGCACATACACCGCAAGAACGTGAACGTGCATTTCTGGATCTGCTGGTTAAAGCATT  
TGGTCCGCAGGCAGCCGATCCGAGCTATTTTACGAAACCGATTGGACCCAGCAAGAATGGGCAAA  
AGGTGGTCCGGTTACCTATATGCCTCCGGGTGTTCTGGCAAATTTTGGTGCAGCCCTGCGTGATCC  
GGTTGGTAAAGTTCATTTTGCAGGCACCGAAGCAAGCTTTTCAAGTGGTTCAGGTTATATGGAAGGTGG  
TGTTGCTGCAGGTCAGAAAGCAGCAGCAGCCATTGCAGAAGAAGTGGAACTGCCGAAATAAAGG  
TGCACTGGTT

#### 7.4.2 Growth and expression of imine reductases

##### 7.4.2.1 Procedure for the growth and expression of (*R*)/(*S*)-IREDs

For expression of the IRED biocatalyst genes, chemically-competent *E. coli* BL21 (DE3) cells (New England Biolabs, MA, USA) were transformed with plasmid vector pET-28a containing the gene for the (*R*)-IRED from *Streptomyces* sp. GF3587/(*S*)-IRED from *Streptomyces* sp. GF3546. Transformations were carried out by mixing 1  $\mu$ L – 2  $\mu$ L plasmid DNA in chemically-competent cells (50  $\mu$ L) on ice, leaving on ice for 20 min before subjecting the mixture to heat-shock treatment (42°C, 45 s). The cells were then incubated in LB-Broth Miller or SOC medium (500  $\mu$ L) for 1 h at 37°C, 250 rpm. Transformants were selected following overnight growth on LB-agar plates containing appropriate selective agents (30  $\mu$ g/mL kanamycin).

Single colonies were picked to initiate 10 mL overnight cultures of LB-Broth Miller containing 30  $\mu$ g/mL kanamycin in 50 mL Falcon tubes. These overnight cultures were grown for 16 h at 37°C, 250 rpm, before being inoculated into 500 mL of LB-Broth Miller (1:100 dilution) supplemented with 30  $\mu$ g/mL kanamycin in a 2 L baffled flask. The cells were grown in a shaking incubator at 37°C, 250 rpm to OD<sub>600nm</sub> 0.6 - 0.8. Subsequently, protein expression was induced by addition of IPTG (0.2 mM final concentration) and the cells were grown at 20°C, 250 rpm for 16 h. For higher cell growth densities, where larger amounts of biocatalyst were required eg. for preparative-scale biotransformations, TB medium was used as the cell growth medium in 2 L baffled flasks. The same procedure was

followed, with the exception of 50 µg/mL kanamycin working concentration, due to the increased kanamycin resistance conferred to cells by the high phosphate buffered medium.

The cells were then harvested by centrifugation (4°C, 6000 rpm, 20 min) and washed with 100 mM, pH 7.0 sodium phosphate buffer, before being harvested again by centrifugation (4°C, 4000 rpm, 20 min). The cells were then ready to use in biotransformation reactions or be lysed for protein isolation.

#### 7.4.2.2 Procedure for the growth and expression of *Ao*-IRED

For the production of cells containing the *Ao*-IRED from *Amycolatopsis orientalis*, the procedure outlined in Section 7.4.2.1 was followed, using a pET-28a vector containing the gene for the *Ao*-IRED. 2 x YT medium was used for cell culturing in a 2 L baffled flask at 30°C, 250 rpm for 16 h.

#### 7.4.3 Growth and expression of CHAO

The gene for CHAO variant T198FL199SM226F was codon-optimised for expression in *E. coli* and synthesised by GeneArt (Thermo Fisher Scientific, MA, USA). Sub-cloning of the gene into the vector pET-16b (which contains a His<sub>10</sub>-tag to all facile isolation of the protein, see Figure 103) using NdeI/BamHI restriction sites was carried out using restriction enzymes (New England Biolabs, MA, USA) and completed according to the manufacturer's instructions.

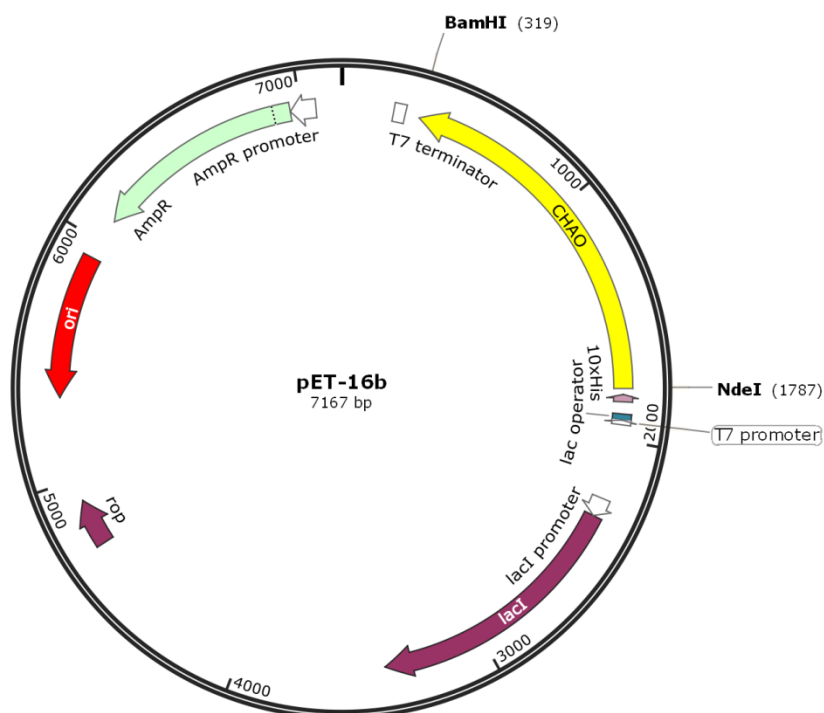


**Figure 103:** pET-16b plasmid map displaying location of CHAO gene between restriction sites BamHI and NdeI.

*E. coli* BL21 (DE3) cells (New England Biolabs, MA, USA) were transformed with the pET-16b vector harbouring the CHAO gene. Transformants were selected by growth on LB agar plates containing 100 µg/mL ampicillin. Single colonies were picked to initiate 10 mL overnight cultures of LB-Broth Miller containing 100 µg/mL ampicillin in 50 mL Falcon tubes. These overnight cultures were grown for 16 h at 37°C, 250 rpm, before being inoculated into 500 mL of auto-induction medium (1:100 dilution) supplemented with 100 µg/mL ampicillin in a 2 L baffled flask. The cells were grown in a shaking incubator at 25°C, 250 rpm for 48 h. The cells were then harvested by centrifugation (4°C, 6000 rpm, 20 min) and washed with 100 mM pH 7.8 potassium phosphate, before being harvested again by centrifugation (4°C, 4000 rpm, 20 min). The harvested cells were then ready to use in biotransformation reactions.

#### 7.4.4 Growth and expression of 6-HDNO

For the growth and expression of 6-HDNO whole-cell biocatalysts, the same procedure outlined for CHAO was followed, using *E. coli* BL21 (DE3) cells harbouring the plasmid vector pET-16b containing the gene for 6-HDNO. Expression of the gene was carried out at 26°C, 200 rpm for 48 h in 2 L baffled flasks.

#### 7.4.5 Growth and expression of MAO-N D5, D9 and D11

For the growth and expression of MAON whole-cell biocatalysts, the same procedure outlined for CHAO was followed, using *E. coli* C43 (DE3) cells (Lucigen) harbouring the plasmid vector pET-16b containing the gene for MAO-N variant D5/D9/D11. Expression of the gene was carried out at 25°C, 150 rpm for 72 h in 2 L baffled flasks containing MAO-N auto-induction medium (see Section 7.2.1.2).

#### 7.4.6 Growth and expression of MCAR

For the growth and expression of MCAR whole-cell biocatalysts, the same procedure outlined for CHAO was followed, using *E. coli* BL21 (DE3) cells harbouring the plasmid vectors pET-21 containing the gene for *Mycobacterium marinum* CAR and pCDF vector containing the phosphopantetheinyl transferase (Sfp) gene from a *Bacillus subtilis* strain. Expression was carried out at 20°C, 250 rpm for 48 h in 2 L baffled flasks in auto-induction medium.

### 7.5 Biotransformation conditions

#### 7.5.1 Procedure for imine reductase biotransformations

##### 7.5.1.1 General procedure for imine reductase biotransformations

Reactions were carried out in 2 mL Eppendorf tubes with a total reaction volume of 500  $\mu$ L at 30°C, 250 rpm. The *E. coli* cells expressing (*R*)-imine reductase were resuspended in 100 mM, pH 7.0 sodium phosphate buffer to a final OD<sub>600nm</sub> of 30. To aid cofactor regeneration, glucose was added to a final concentration of 50 mM. Substrate stock solutions (250 mM) were prepared by dissolving the imine hydrochloride salts in dH<sub>2</sub>O or DMF if freebase. 10  $\mu$ L of the substrate stock solution was added to the biotransformation reaction mixture to give a final substrate concentration of 5mM. Samples were taken after 24 h, basified to pH 12.0 – 14.0 with 10 M sodium hydroxide and extracted into ethyl acetate or MTBE (1 mL), followed by analysis of the organic extracts by normal phase chiral HPLC or chiral GC-FID. Conversions and *ee* based on HPLC/GC-FID analysis of imine and amine peaks. Whole-cell biotransformations using cells harbouring empty pET-28a vector were taken as negative controls for each compound tested.

#### 7.5.1.2 Procedure for the preparative-scale biotransformation of imine **5i** with the (*R*)-IRED

The biotransformation was carried out according to the general procedure (see Section 7.5.1.1). 2-*n*-propyl-1-piperidine hydrochloride (25 mM) was added from a 250 mM stock solution of the substrate **5i** (1.00 g, 6.12 mmol) dissolved in dH<sub>2</sub>O. The reaction was carried out in a 1L baffled flask in a shaking incubator at 30°C, 250 rpm. After 24 h the pH of the biotransformation was adjusted to pH 12.0 by addition of 10 M sodium hydroxide and the aqueous phase was extracted with diethyl ether four times. The organic phases were pooled together, dried over anhydrous MgSO<sub>4</sub> and then acidified by addition of 2M HCl/diethyl ether solution (6.19 mL, 12.4 mmol). The excess diethyl ether was carefully decanted from the product which was subsequently left to air-dry, yielding (*R*)-coniine hydrochloride (898 mg, 90% yield) as pale brown needle-shaped crystals.

#### 7.5.1.3 Time-point assay for (*R*)-IRED catalysed reduction of dihydroisoquinoline **7a**

To assess if any change in product *ee* from whole-cell biotransformations occurred over time, a time-point assay was used where the (*R*)-IRED whole-cell biotransformation of 1-methyl-3,4-dihydroisoquinoline **7a** was monitored at regular intervals. The same biotransformation protocol as previously described (see Section 7.5.1.1) was followed, with the exception of a cell resuspension at a final OD<sub>600</sub> = 3.

### 7.5.2 General procedure for carboxylic acid reductase, ω-transaminase and imine reductase cascade biotransformations

#### 7.5.2.1 General procedure for ATA/IRED cascade biotransformations

Analytical-scale reactions were carried out in 2 mL Eppendorf tubes with a total reaction volume of 500 μL. Preparative-scale reactions were carried out in non-baffled conical flasks with a total reaction volume to suit the amount of substrate to be converted. Substrate stock solutions (250 mM) were prepared by dissolving the diketones in DMSO. Each biotransformation contained 5 mM substrate, 2.5 mg/mL ATA-113 or ATA-117, 1 mg/mL GDH, 0.5 mg/mL LDH, 250 mM D/L-alanine, 100 mM glucose, 1.5 mM, NAD<sup>+</sup> and 1 mM PLP in 100 mM pH 7.0 sodium phosphate buffer and 1% v/v DMSO (from addition of substrate as a solution in DMSO). The reaction mixture was incubated at 30°C, 250 rpm for 24 h to facilitate full conversion of the starting diketone by the transaminase, before addition of 200 mg/mL IRED wet whole cells and a further 24 h incubation time. The pH of the reactions was then adjusted to pH 12.0 with 10 M sodium hydroxide and extracted with ethyl acetate (1 mL for analytical-scale reactions) or diethyl ether (for the preparation of **13d** – see

Section 7.5.4.2), followed by analysis of the organic phase by GC-FID or GC-MS. Conversions was based on GC-FID analysis of diketone, imine and amine peaks.

#### 7.5.2.2 General procedure for carboxylic acid reductase/ $\omega$ -transaminase/imine reductase cascade biotransformations

Analytical-scale reactions were carried out in 2 mL Eppendorf tubes with a total reaction volume of 500  $\mu$ L. Preparative-scale reactions were carried out in non-baffled conical flasks with a total reaction volume to suit the amount of substrate to be converted. Substrate stock solutions (250 mM) were prepared by dissolving the ketoacids in DMSO. Each biotransformation contained 5 mM substrate, 2.5 mg/mL ATA-113 or ATA-117, 75 mg/mL CAR wet whole-cells, 1 mg/mL GDH, 0.5 mg/mL LDH, 250 mM D/L-alanine, 100 mM glucose, 1.5 mM, NAD<sup>+</sup> and 1 mM PLP in 500 mM pH 7.0 sodium phosphate buffer and 1% v/v DMSO (from addition of substrate as a solution in DMSO). The reaction mixture was incubated at 30°C, 250 rpm for 24 h. The pH of the reactions was then adjusted to pH 12.0 with 10 M sodium hydroxide and extracted with ethyl acetate (1 mL for analytical-scale reactions). The layers were separated and the organic phase was taken for analysis by GC-FID or GC-MS. In order to ensure that full conversion of the starting diketone was accomplished by the CAR enzyme, the pH of the aqueous phase remaining from the biotransformation extraction was acidified to pH 2 by addition of conc. HCl. The aqueous phase was then extracted with MTBE (1 mL), followed by analysis of the organic phase by HPLC.

#### 7.5.3 Procedure for amine oxidase-catalysed chemo-enzymatic redox biotransformations

##### 7.5.3.1 General procedure for amine oxidase/imine reductase redox biotransformations

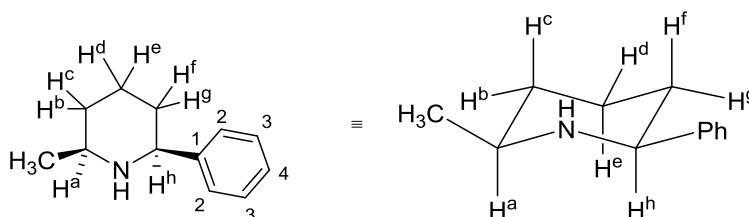
Analytical-scale reactions were carried out in 2 mL Eppendorf tubes with a total reaction volume of 500  $\mu$ L. Preparative-scale reactions were carried out in non-baffled conical flasks with a total reaction volume to suit the amount of substrate to be converted. Substrate stock solutions (250 mM) were prepared by dissolving the racemic cyclic amine in DMSO or freebase imine in dH<sub>2</sub>O. Each biotransformation contained 5 mM substrate, 50 mg/mL CHAO/6-HDNO/MAO-N D9 wet whole-cells, 50 mg/mL (*R*)-IRED/(*S*)-IRED/*A<sub>o</sub>*-IRED wet whole-cells, 10 mM glucose and 1 M pH 7.4 potassium phosphate buffer. Reactions were carried out at 30 °C, 250 rpm for 24 hours. The pH of the reactions was then adjusted to pH 12.0 with 10 M sodium hydroxide and extracted with MTBE (1 mL for analytical-scale reactions) followed by analysis by HPLC. Conversions and *ee* based on HPLC analysis of imine and amine peaks as well as other product peaks.

### 7.5.3.2 General procedure for amine oxidase-ammonia borane redox biotransformations

Analytical-scale reactions were carried out in 2 mL Eppendorf tubes with a total reaction volume of 500  $\mu$ L. Preparative-scale reactions were carried out in non-baffled conical flasks with a total reaction volume to suit the amount of substrate to be converted. Substrate stock solutions (250 mM) were prepared by dissolving the racemic amine in DMSO or freebase imine in dH<sub>2</sub>O. Each biotransformation contained 5 mM substrate, 50 mg/mL CHAO/6-HDNO/MAO-N D9 wet whole-cells, NH<sub>3</sub>BH<sub>3</sub> complex (as specified, typically 50 mM final concentration used) and 1 M pH 7.4 potassium phosphate buffer. Reactions were carried out at 30 °C, 250 rpm for 24 hours. The pH of the reactions was then adjusted to pH 12.0 with 10 M sodium hydroxide and extracted with MTBE (1 mL for analytical-scale reactions) followed by analysis by HPLC. Conversions and *ee* based on HPLC analysis of imine and amine peaks as well as other product peaks.

### 7.5.4 Procedures for preparative-scale biotransformations

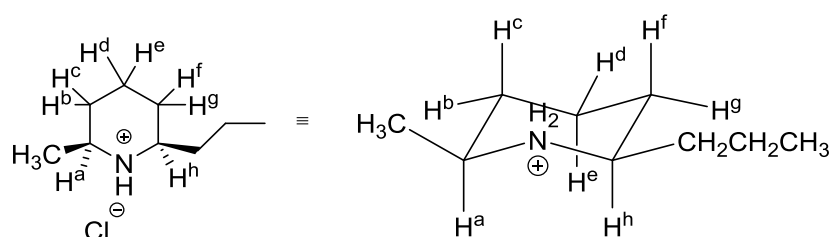
#### 7.5.4.1 Procedure for the preparation of (2*S*,6*S*)-2-methyl-6-phenylpiperidine, (2*S*,6*S*)-**13a**



A non-baffled conical flask was charged with the hydrochloride salt of (*S*)-**12a** (60 mg, 0.286 mmol), (*R*)-IRED whole-cells (11.4 g), 50 mM glucose and the mixture was made up to 57 mL with 100 mM pH 7.0 sodium phosphate buffer. The reaction mixture was incubated at 30°C, 250 rpm for 24 h and the biotransformation was monitored by GCMS. The pH of the reaction mixture was then adjusted to pH 12.0 by addition of 10 M sodium hydroxide and the aqueous mixture was extracted with ethyl acetate (3 x 60 mL). The organic phases were combined, dried over MgSO<sub>4</sub> and concentrated under reduced pressure to yield (2*S*,6*S*)-**13a** (46 mg, 0.262 mmol, 92%, *de* >98%) as pale yellow oil. **<sup>1</sup>H NMR** (400 MHz, CDCl<sub>3</sub>)  $\delta$ : 7.33 – 7.27 (m, 2H, C2-CH), 7.27 – 7.21 (m, 2H, C3-CH), 7.19 – 7.13 (m, 1H, C4-CH), 3.58 (dd, *J* = 10.5, 2.5 Hz, 1H, H<sup>h</sup>), 2.73 (dq, *J* = 11.0, 6.5, 2.5 Hz, 1H, H<sup>a</sup>), 1.84 (m, 1H, H<sup>e</sup>), 1.72 – 1.65 (m, 1H, H<sup>g</sup>), 1.64 – 1.54 (m, 2H, NH and H<sup>b</sup>), 1.50 – 1.32 (m, 2H, H<sup>d</sup> and H<sup>f</sup>), 1.14 – 1.04 (m, 1H, H<sup>c</sup>), 1.04 (d, *J* = 6.5, 3H, CH<sub>3</sub>); **<sup>13</sup>C NMR** (100 MHz, CDCl<sub>3</sub>)  $\delta$ : 145.7 (C1), 128.5 (C3), 127.1 (C4), 126.9 (C2), 62.6 (CH<sup>h</sup>), 53.2 (CH<sup>a</sup>), 34.4 (CH<sup>f</sup>), 34.0 (CH<sup>b</sup>), 25.5 (CH<sup>e</sup>), 23.2 (CH<sub>3</sub>); [ $\alpha$ ]<sub>D</sub><sup>23</sup> = –40.0 (*c* = 1.0, CHCl<sub>3</sub>) [Lit. ref. [ $\alpha$ ]<sub>D</sub><sup>20</sup> = –35.6 (*c* = 1.38, CHCl<sub>3</sub>).<sup>145</sup> Spectroscopic data is consistent with literature values.<sup>145</sup>

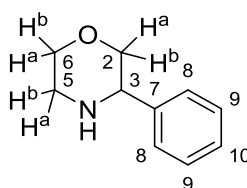
Formation of the *cis*-diastereomer of **13a** was confirmed by the large coupling constant  $J^c = 11.0$  Hz, which equates to a diaxial proton-proton coupling according to the Karplus equation, therefore indicative of the equatorial orientation of the methyl substituent on C2. NOESY analysis also showed correlation between H<sup>a</sup> and H<sup>h</sup>.

#### 7.5.4.2 Procedure for the preparation of (2*S*,6*R*)-2-methyl-6-propylpiperidine hydrochloride, (-)-dihydropinidine hydrochloride, (2*S*,6*R*)-**13d**.HCl



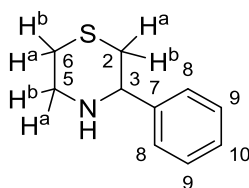
Nonane-2,6-dione, **11d** (50 mg, 0.320 mmol from a 1 M stock solution in DMSO), was subjected to the general procedure for the TA-IRED cascade with ATA-113 and (*R*)-IRED (see Section 7.5.2). The pH of the reaction mixture was then adjusted to pH 12.0 with 10 M sodium hydroxide. The aqueous mixture was then extracted with diethyl ether (3 x 60 mL). The organic phases were combined and dried over MgSO<sub>4</sub>, before addition of 2 M HCl/diethyl ether solution (1 mL). The excess diethyl ether was carefully decanted and the remaining liquid was allowed to dry in air to yield amine (2*S*, 6*R*)-**13d** (51 mg, 0.298 mmol, 90%, *de* >98%, *ee* >98%) as a white solid. <sup>1</sup>H NMR (400 MHz, CD<sub>3</sub>OD) δ 3.25 – 3.14 (m, 1H, H<sup>a</sup>), 3.13 – 3.02 (m, 1H, H<sup>h</sup>), 2.01 (d, *J* = 14.0 Hz, 1H, H<sup>g</sup>), 1.96 – 1.83 (m, 2H, H<sup>b</sup> and H<sup>d</sup>), 1.78 – 1.65 (m, 1H, CH<sub>2</sub>CH<sub>2</sub>CH<sub>3</sub>), 1.65 – 1.52 (m, 2H, CH<sub>2</sub>CH<sub>2</sub>CH<sub>3</sub> and H<sup>e</sup>), 1.51 – 1.28 (m, 4H, CH<sub>2</sub>CH<sub>2</sub>CH<sub>3</sub>, H<sup>c</sup> and H<sup>f</sup>) 1.35 (d, *J* = 6.5 Hz, 3H, CH<sub>3</sub>), 0.98 (t, *J* = 7.5 Hz, 3H, CH<sub>2</sub>CH<sub>2</sub>CH<sub>3</sub>); <sup>13</sup>C NMR (100 MHz, CD<sub>3</sub>OD) δ 58.7 (CH<sup>h</sup>), 54.9 (CH<sup>a</sup>), 36.9 (CH<sub>2</sub>CH<sub>2</sub>CH<sub>3</sub>), 31.6 (CH<sup>b</sup>), 29.0 (CH<sup>f</sup>), 23.5 (CH<sup>d</sup>), 19.6 (CH<sub>3</sub>), 19.5 (CH<sub>2</sub>CH<sub>2</sub>CH<sub>3</sub>), 14.1 (CH<sub>2</sub>CH<sub>2</sub>CH<sub>3</sub>); [ $\alpha$ ]<sub>D</sub><sup>23</sup> = –40.0 (*c* = 1.0, EtOH) [Lit. ref. [ $\alpha$ ]<sub>D</sub><sup>20</sup> = –12.2 (*c* = 0.5, EtOH)].<sup>102</sup> Spectroscopic data is consistent with literature values.<sup>102</sup>

#### 7.5.4.3 Procedure for the preparation of (*R*)-3-phenylmorpholine (*R*)-**19**



Ketoacid **17** (50 mg, 0.257 mmol from a 1 M stock solution in DMSO) was subjected to the general CAR-TA-IRED cascade (see Section 7.5.2.2 for details of the procedure). The pH of the reaction mixture was then adjusted to pH 12.0 with 10 M sodium hydroxide. The aqueous mixture was then extracted with ethyl acetate (3 x 20 mL). The organic phases were combined, dried over MgSO<sub>4</sub> and concentrated *in vacuo* to yield the crude product, which was subjected to flash chromatography (silica gel, 10% v/v methanol-ethyl acetate + 0.1% triethylamine) to produce amine (3*R*)-**19** (24 mg, 60%) as an off-white solid. **<sup>1</sup>H NMR** (400 MHz, CDCl<sub>3</sub>) δ: 7.42 – 7.37 (m, 2H, C8-CH), 7.37 – 7.30 (m, 2H, C9-CH), 7.30 – 7.26 (m, 1H, C10-CH), 3.97 – 3.89 (m, 1H, C3-CH), 3.91 – 3.83 (m, 1H, C5-CH<sup>a</sup> or C5-CH<sup>b</sup>), 3.85 – 3.78 (m, 1H, C2-CH<sup>a</sup> or C2-CH<sup>b</sup>), 3.66 (td, *J* = 11.5, 2.5 Hz, 1H, C5-CH<sup>a</sup> or C5-CH<sup>b</sup>), 3.40 (dd, *J* = 11.0, 10.5 Hz, 1H, C2-CH<sup>a</sup> or C2-CH<sup>b</sup>), 3.14 (td, *J* = 11.5, 3.0 Hz, 1H, C6-CH<sup>a</sup> or C6-CH<sup>b</sup>), 3.04 – 2.98 (m, 1H, C6-CH<sup>a</sup> or C6-CH<sup>b</sup>), 2.00 (bs, 1H, NH); **<sup>13</sup>C NMR** (100 MHz, CDCl<sub>3</sub>) δ: 140.6 (C7), 128.7 (C9), 127.9 (C10), 127.3 (C8), 73.8 (C2), 67.4 (C5), 60.7 (C3), 46.7 (C6). *Spectroscopic data is consistent with that of an authentic chemical standard.*

#### 7.5.4.4 Procedure for the preparation of (*R*)-3-phenylthiomorpholine (*R*)-**22**



Ketoacid **20** (50 mg, 0.238 mmol from a 1 M stock solution in DMSO) was subjected to the general CAR-TA-IRED cascade (see Section 7.5.2.2 for details of the procedure). The pH of the reaction mixture was then adjusted to pH 12.0 with 10 M sodium hydroxide. The aqueous mixture was then extracted with ethyl acetate (3 x 20 mL). The organic phases were combined, dried over MgSO<sub>4</sub> and concentrated *in vacuo* to yield amine (3*R*)-**22** (30 mg, 72%) as an off-white solid. **<sup>1</sup>H NMR** (400 MHz, CDCl<sub>3</sub>) δ: 7.31 – 7.23 (m, 4H, C8-CH and C9-CH), 7.23 – 7.17 (m, 1H, C10-CH), 3.86 (dd, *J* = 10.5, 2.0 Hz, 1H, C3-CH), 3.39 (td, *J* = 12.0, 3.0 Hz, 1H, C5-CH<sup>a</sup> or C5-CH<sup>b</sup>), 3.11 (td, *J* = 12.0, 2.5 Hz, 1H, C5-CH<sup>a</sup> or C5-CH<sup>b</sup>), 2.85 (ddd, *J* = 13.0, 3.0, 12.0 Hz, 1H, C6-CH<sup>a</sup> or C6-CH<sup>b</sup>), 2.78 (dd, *J* = 13.0, 10.5 Hz, 1H, C2-CH<sup>a</sup> or C2-CH<sup>b</sup>), 2.45 – 2.39 (m, 1H, C2-CH<sup>a</sup> or C2-CH<sup>b</sup>), 2.40 – 2.33 (m, 1H, C6-CH<sup>a</sup> or C6-CH<sup>b</sup>), 1.79 (bs, 1H, NH); **<sup>13</sup>C NMR** (100 MHz, CDCl<sub>3</sub>) δ: 144.4 (C7), 128.8 (C9), 127.9 (C10), 126.7 (C8), 63.2 (C3), 49.3 (C5), 35.0 (C2), 27.6 (C6). *Spectroscopic data is consistent with that of an authentic chemical standard.*

## 7.6 Protocols for the purification of the (*R*)-IRED and glucose dehydrogenase (GDH-II)

### 7.6.1 Protocol for HisTag purification of (*R*)-IRED and GDH-II

The cell pellet from 500 mL culture was disrupted by ultrasonication in sodium phosphate buffer (100 mM, pH 7.0). Crude extract was then loaded onto a 5 mL HisTrap column. Purification was achieved manually or automated using an AKTA Pure system (GE Healthcare, Uppsala, Sweden), using de-gassed buffers. These consisted of the loading buffer, 100 mM pH 7.0 sodium phosphate buffer containing NaCl (300 mM) and an elution buffer of 100 mM pH 7.0 sodium phosphate containing NaCl (300 mM) and imidazole (300 mM). The column was initially washed with 5 column volumes of loading buffer containing 10% elution buffer, followed by a second column wash phase using 5 column volumes of loading buffer containing 20% elution buffer. The protein was then eluted with 10 column volumes of 100% elution buffer, where 100% elution buffer was reached over 5 column volumes. 1 mL fractions were collected during the elution phase. SDS\_PAGE analysis confirmed presence of the (*R*)-IRED in fractions, which were pooled together.

HisTag purification of GDH-II was achieved in the same manner.

### 7.6.2 Gel filtration of isolated (*R*)-IRED protein and de-salting of GDH-II

Purification and of the isolated (*R*)-IRED was achieved automated using an AKTA Pure system equipped with a preparative gel filtration column. The concentrated protein sample was loaded onto the column and then washed with 0.3 column volumes of de-gassed 100 mM pH 7.0 sodium phosphate buffer with 100 mM NaCl (100 mM), before elution using one column volume of the same buffer. 3 mL fractions containing (*R*)-IRED (confirmed by SDS\_PAGE analysis) were pooled together to yield pure protein solution. Removal of salt was achieved by buffer exchange on a PD-10 desalting column (GE Healthcare).

For the removal of imidazole, the HisTag purified GDH-II was run through a PD-10 desalting column (GE Healthcare, Uppsala, Sweden) with 100 mM pH 7.0 sodium phosphate buffer. It should be noted that although the GDH-II enzyme has a molecular weight of ~28 kDa, on SDS-PAGE the protein tends to run slower to ~36 kDa.

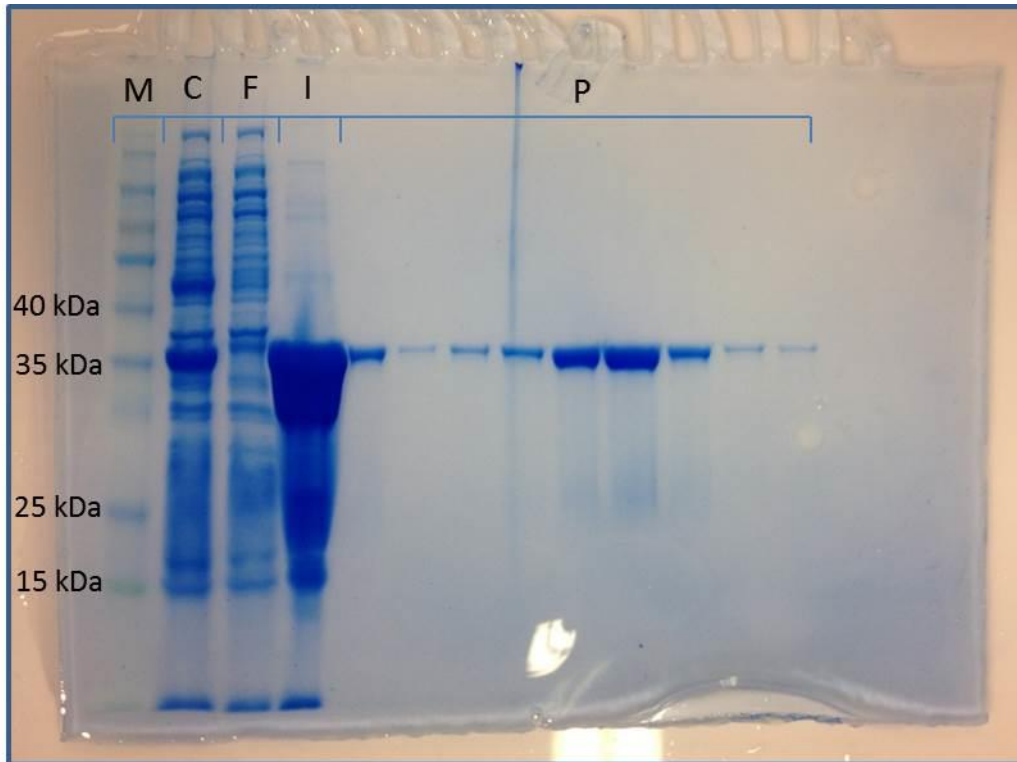


**Figure 104:** SDS-PAGE analysis for the purification of recombinant (*R*)-IRED protein (M = protein marker, C = crude extract, F = flow-through of crude extract during column loading, I = protein solution post HisTag purification, P = samples of isolated (*R*)-IRED post gel filtration).

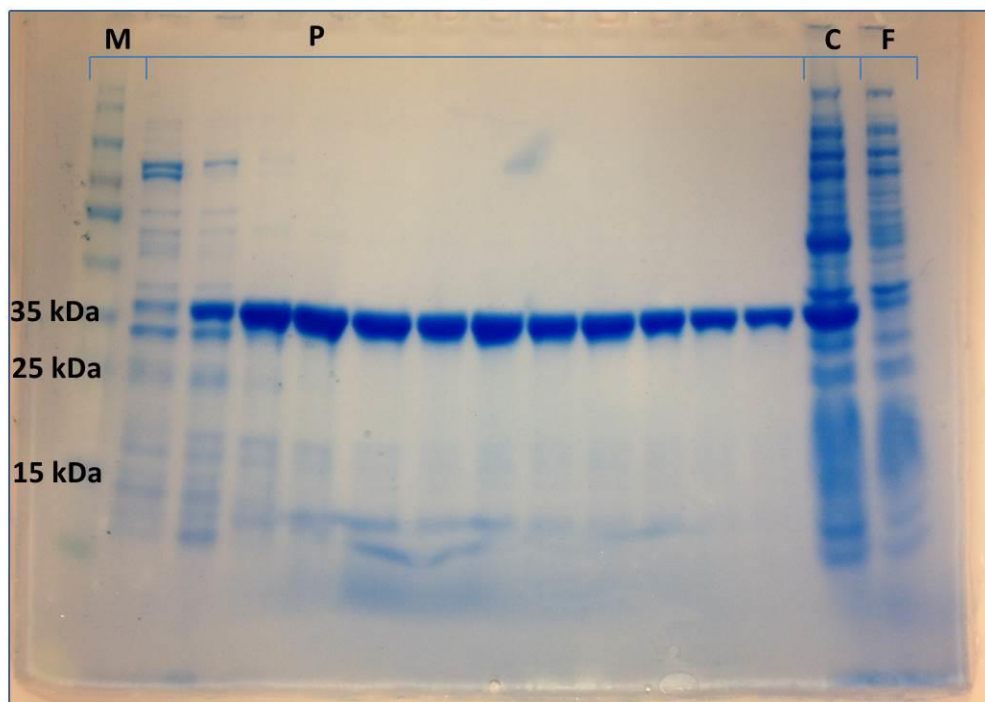


**Figure 105:** SDS-PAGE analysis for the purification of recombinant GDH-II protein (M = protein marker, C = crude extract, F = flow-through of crude extract during column loading, P = fractions of GDH-II enzyme post HisTag purification). Only GDH-II fractions from lane 4 onwards of the product elution were collected.

**Table 26:** Total yield of wet cells and isolated protein from 500 mL culture broth

Enzyme	Wet cells from 500 mL culture <sup>[a]</sup>	Isolated protein <sup>[b]</sup>
	g	mg
( <i>R</i> )-IRED	2.75	18.2
GDH-II	2.82	16.7

[a] Cell harvested from overnight growth in 500 mL LB media [b] Amount of protein isolated following purification of the cell pellets

## 7.7 Isolated enzyme biotransformations with the (*R*)-IRED

### 7.7.1 General procedure for pure enzyme biotransformations

Analytical-scale biotransformations with the isolated (*R*)-IRED protein were carried out following the general imine reductase biotransformation protocol (see Section 7.5.1.1), using isolated (*R*)-IRED protein in sodium phosphate buffer to a final concentration of 1000 µg/mL, NADPH (1.7 µL from a 150 mM stock solution) and isolated glucose dehydrogenase enzyme (GDH-II) in sodium phosphate buffer was added to a final concentration of 1000 µg/mL for cofactor recycling.

**Table 27:** Results of isolated (*R*)-IRED biotransformations with GDH-II cofactor recycling system

Substrate	<i>wt</i> ( <i>R</i> )-IRED	
	Conversion <sup>[a]</sup> %	<i>ee</i> %
<b>5c</b>	>98	>98
<b>5e</b>	>98	71
<b>5i</b>	>98	98
<b>5j</b>	>98	91
<b>7a</b>	>98	47

[a] Conversion recorded after 24 h

### 7.7.2 Procedure for the continuous flow biotransformation of 2-(*n*-propyl)-1-piperidine.HCl **5i** with purified (*R*)-IRED enzyme

Each Freactor unit of approximately 2 mL internal volume, equipped with a cross-shaped magnetic stirrer bar, was linked in series to produce a system of approximately 10 mL total volume. The first Freactor unit, equipped with two inlet feeds, was connected to two peristaltic pumps. The last Freactor unit was equipped with a single outlet line. The reaction system was initially flushed with dH<sub>2</sub>O and purged of air bubbles. The system was then flushed with 100 mM pH 7.0 sodium phosphate buffer (10 x system volume). The peristaltic pumps were set to equal flow rates and the residence time (19 min 20 s) was assumed to be equal to the time taken to collect 10 mL (1 x system volume) from the reactor.

Inlet 1 was connected to an enzyme feed solution, consisting of purified (*R*)-IRED protein (2 mg/mL) and CDX-901 (2 mg/mL) dissolved in 100 mM pH 7.0 sodium phosphate buffer. Inlet 2 was connected to a reagent feed solution, consisting of substrate **5i** (100 mM), NADPH (10 mM) and glucose (100 mM) dissolved in 100 mM pH 7.0 sodium phosphate buffer. The reaction was conducted at room temperature (20°C measured using a thermometer). The reaction was started by turning on both pumps simultaneously, with a flow rate of 0.518 ml/min at the outlet. The outflow was collected in 2 mL Eppendorf tubes containing a 10 M NaOH reaction quench. Samples were collected over 4 min intervals. Steady-state equilibrium for the reaction was reached after 3 – 4 system volumes had passed through the reactor. The reaction was stopped after 60 mL total volume had been passed through the system. 1 mL aliquots of the samples were extracted with MTBE (500 µL). The samples were dried over MgSO<sub>4</sub> prior to analysis by GC-FID and GC-MS.

Equivalent batch reactions were conducted by placing the enzyme feed solution (500 µL) and the reagent feed solution (500 µL) into 2 mL Eppendorf tubes, which were then incubated at 20°C, 250 rpm. The batch reactions were quenched after 1 h and 2 h time-points by adjusting the pH of the reaction mixture to pH 12.0 and then subsequently extracted and analysed in the same fashion as the continuous-flow reaction samples.

### 7.8 Spectrophotometric assay for the determination of kinetic constants with (*R*)-imine reductase

Kinetic parameters for substrates were determined using the isolated enzyme on a Tecan spectrophotometer/plate reader, by monitoring the decrease of NADPH at 370 nm ( $\epsilon = 2.216 \text{ mM}^{-1} \text{ cm}^{-1}$ ) at 30°C. On a microtiter plate, reaction mixtures (200 µL) contained sodium phosphate buffer (100 mM, pH 7.00), 10-50 µg of pure enzyme, 600 - 750 µM

NADPH, 1% (v/v) dimethylsulfoxide (except for substrate **5I**, where 2% (v/v) dimethylsulfoxide was used) and imine substrate.

The determination of kinetic constants for 2-cyclohexyl-1-piperidine **5e** was carried out on an Agilent Cary Series 300 UV/Vis spectrophotometer in 1 mL plastic cuvettes. The reaction volume (1000  $\mu$ L) contained 100 mM pH 7.0 sodium phosphate buffer and enzyme as above, 450  $\mu$ M NADPH, 1% (v/v) dimethylsulfoxide and 2-cyclohexyl-1-piperidine.

The reaction was started by adding the enzyme to the mixture. One unit of imine reductase is defined as the amount of protein that oxidizes 1  $\mu$ mol NADPH per minute. Kinetic parameters were deduced by non-linear regression analysis based on Michaelis–Menten kinetics using the program QtiPlot. Due to the high absorbance of several substrates tested at 340 nm, all activities were measured at 370 nm.

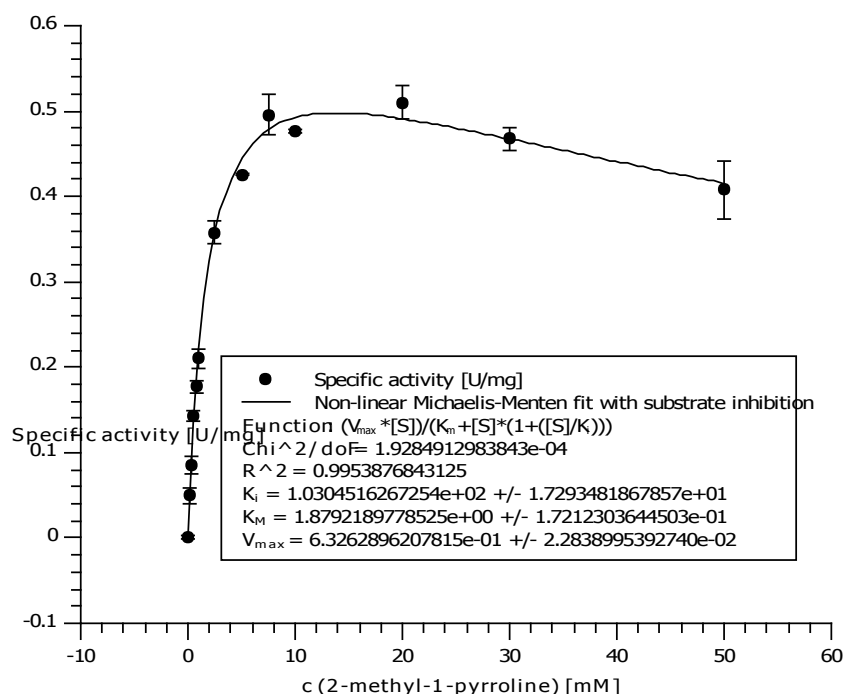


**Figure 106:** Determination of kinetic constants for (*R*)-IREd for substrate 2-methyl-1-pyrroline **1a**. Measurements were taken in triplicates and error bars indicate the standard deviation. Due to substrate inhibition, the adapted equation for uncompetitive inhibition was used for fitting:  $v = (V_{\max} \times [S]) / (K_m + [S] \times (1 + ([S]/K_i)))$  with  $[S]$  being the substrate concentration and  $K_i$  the uncompetitive inhibition constant.  $K_i$  was determined to be  $103 \pm 17.2$  mM.

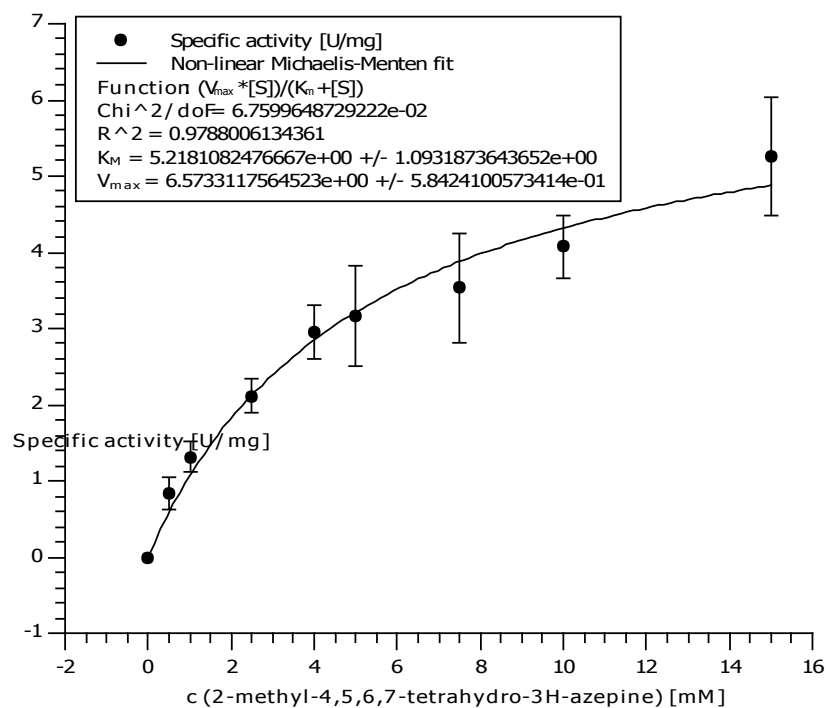


**Figure 107:** Determination of kinetic constants for (*R*)-IRED for substrate 2-methyl-4,5,6,7-tetrahydro-3*H*-azepine **3a**. Measurements were taken in triplicates and error bars indicate the standard deviation.

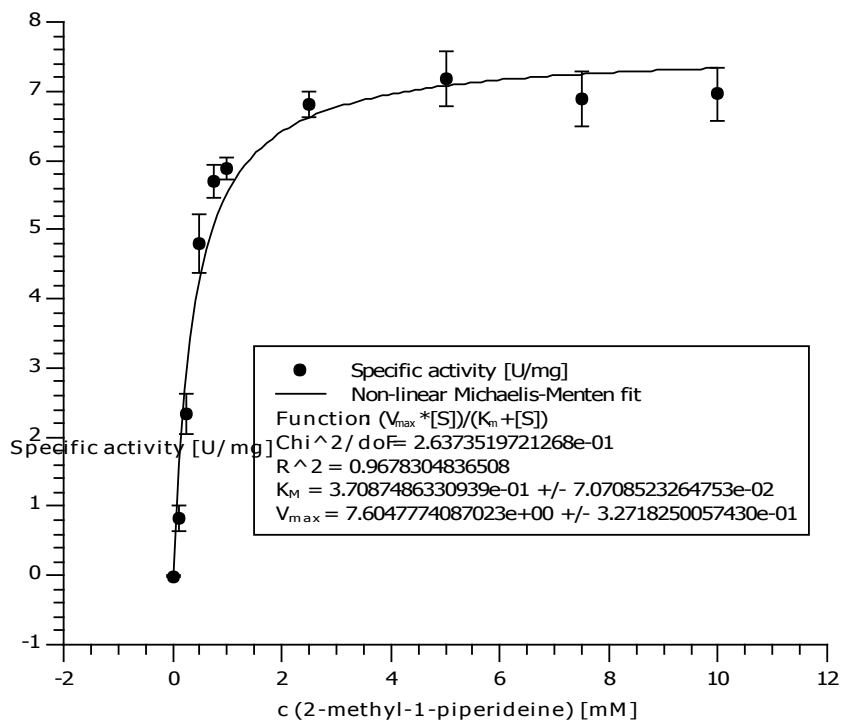


**Figure 108:** Determination of kinetic constants for (*R*)-IRED for substrate 2-methyl-1-piperidine **5a**. Measurements were taken in triplicates and error bars indicate the standard deviation.

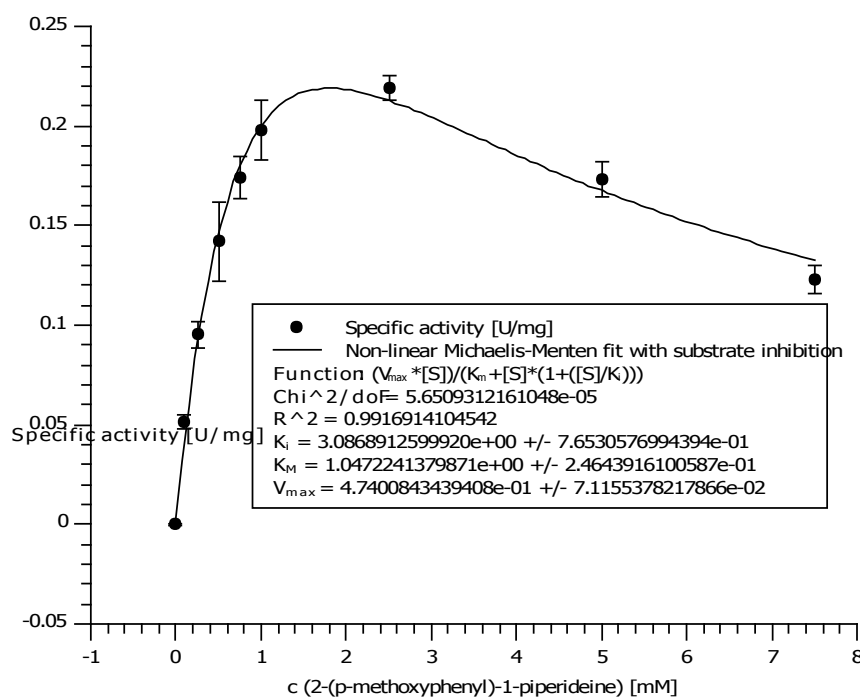


**Figure 109:** Determination of kinetic constants for (*R*)-IRED for substrate 2-(*p*-methoxyphenyl)-1-piperidine **5c**. Measurements were taken in triplicates and error bars indicate the standard deviation. Due to substrate inhibition, the adapted equation for uncompetitive inhibition was used for fitting:  $v = (V_{max} \times [S]) / (K_m + [S] \times (1 + ([S]/K_i)))$  with  $[S]$  being the substrate concentration and  $K_i$  the uncompetitive inhibition constant.  $K_i$  was determined to be  $3.09 \pm 0.765$  mM.

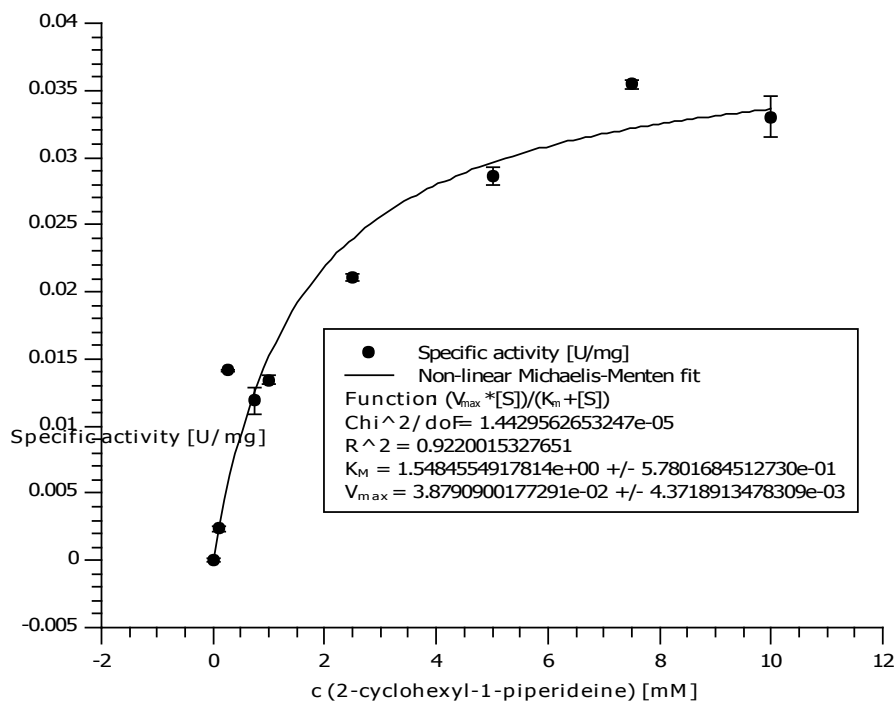


**Figure 110:** Determination of kinetic constants for (*R*)-IRED for substrate 2-cyclohexyl-1-piperidine **5e**. Measurements were taken in triplicates and error bars indicate the standard deviation.

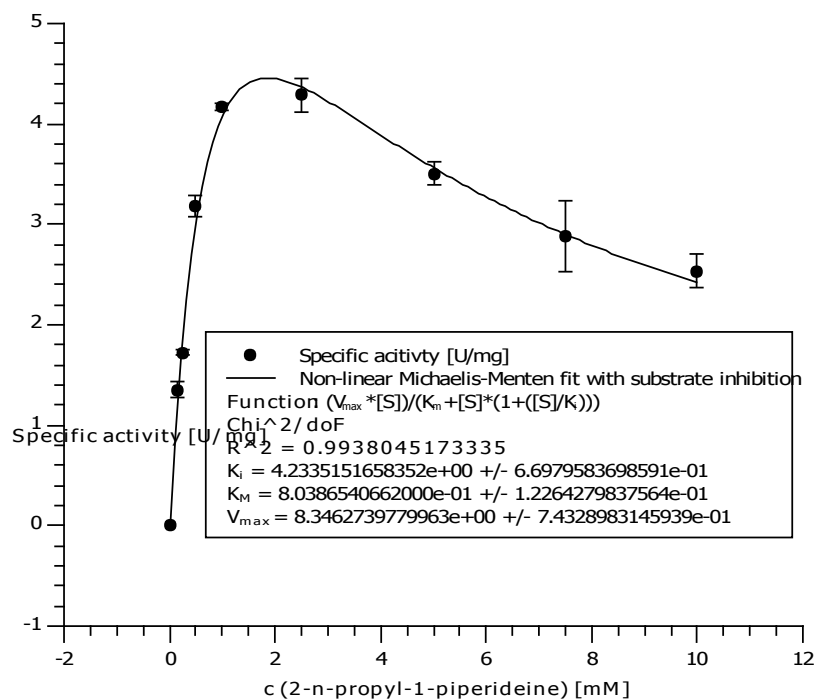


**Figure 111:** Determination of kinetic constants for (*R*)-IRED for substrate 2-(*n*-propyl)-1-piperidine **5i**. Measurements were taken in triplicates and error bars indicate the standard deviation. Due to substrate inhibition, the adapted equation for uncompetitive inhibition was used for fitting:  $v = (V_{max} \times [S]) / (K_m + [S] \times (1 + ([S] / K_i)))$  with  $[S]$  being the substrate concentration and  $K_i$  the uncompetitive inhibition constant.  $K_i$  was determined to be  $4.23 \pm 0.670$  mM.

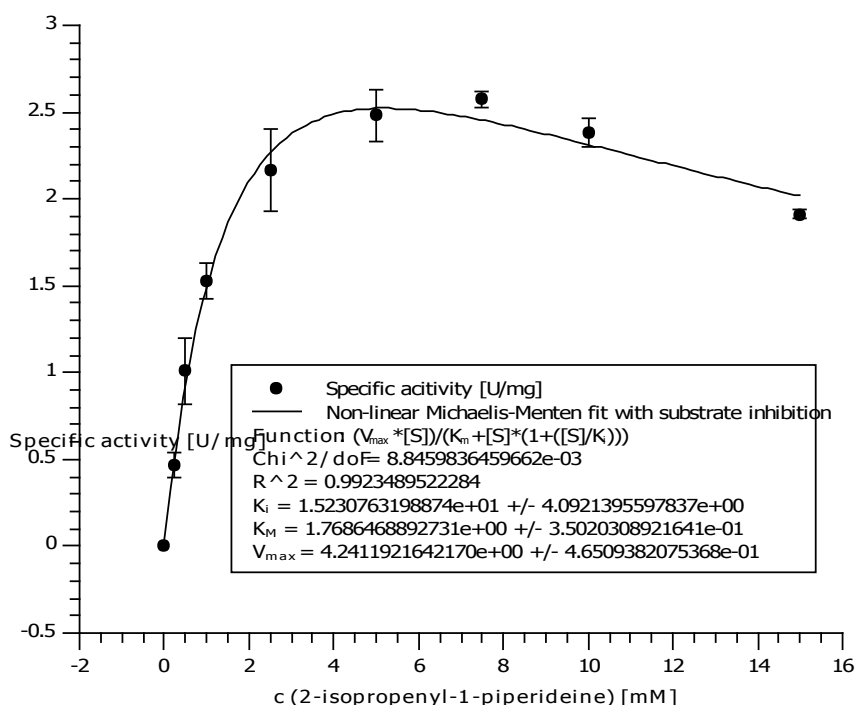


**Figure 112:** Determination of kinetic constants for (*R*)-IRED for substrate 2-isopropenyl-1-piperidine **5j**. Measurements were taken in triplicates and error bars indicate the standard deviation. Due to substrate inhibition, the adapted equation for uncompetitive inhibition was used for fitting:  $v = (V_{max} \times [S]) / (K_m + [S] \times (1 + ([S] / K_i)))$  with  $[S]$  being the substrate concentration and  $K_i$  the uncompetitive inhibition constant.  $K_i$  was determined to be  $15.2 \pm 4.09$  mM.

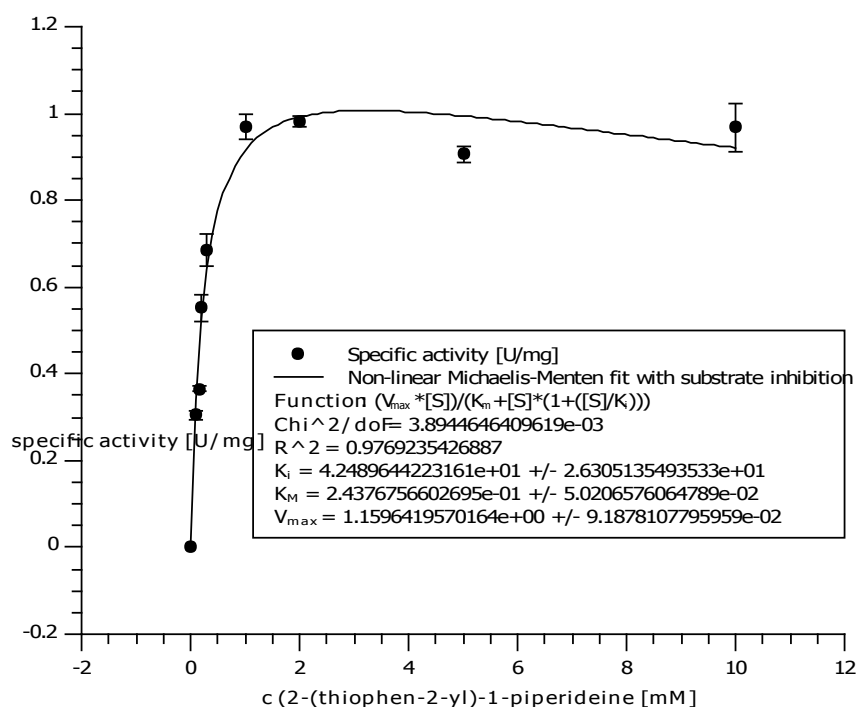


**Figure 113:** Determination of kinetic constants for (*R*)-IRED for substrate 2-(thiophen-2-yl)-1-piperidine **5n**. Measurements were taken in triplicates and error bars indicate the standard deviation. Due to substrate inhibition, the adapted equation for uncompetitive inhibition was used for fitting:  $v = (V_{max} \times [S]) / (K_m + [S] \times (1 + ([S] / K_i)))$  with  $[S]$  being the substrate concentration and  $K_i$  the uncompetitive inhibition constant.  $K_i$  was determined to be  $42.5 \pm 26.3$  mM.

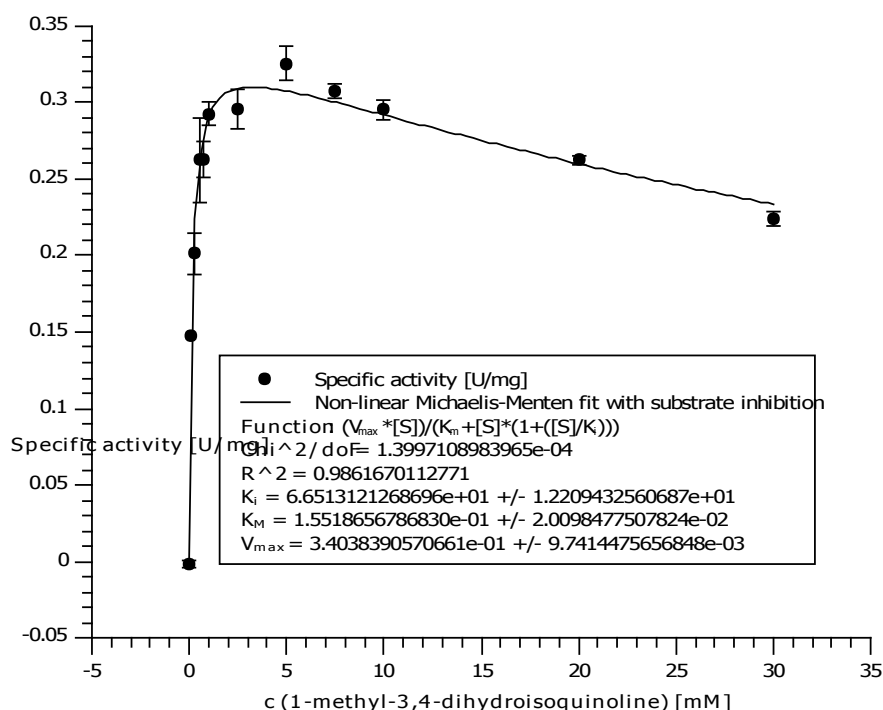


**Figure 114:** Determination of kinetic constants for (*R*)-IRED for substrate 1-methyl-3,4-dihydroisoquinoline **7a**. Measurements were taken in triplicates and error bars indicate the standard deviation. Due to substrate inhibition, the adapted equation for uncompetitive inhibition was used for fitting:  $v = (V_{max} \times [S]) / (K_m + [S] \times (1 + ([S] / K_i)))$  with  $[S]$  being the substrate concentration and  $K_i$  the uncompetitive inhibition constant.  $K_i$  was determined to be  $66.5 \pm 12.2$  mM.

## 7.9 Mutagenesis of the (*R*)-IRED and general biotransformation procedure using (*R*)-IRED D172A and (*R*)-IRED D172L variants

### 7.9.1. Mutagenesis of wild-type (*R*)-IRED to produce mutants D172A and D172L

Residue Asp172 was mutated to Ala172 and Leu172 by site-directed mutagenesis following the QuikChange protocol (Agilent, Santa Clara, CA, USA). Complimentary forward and reverse direction synthetic primers were designed and ordered as follows:

**Table 28:** Oligonucleotide primers used for site-directed mutagenesis

( <i>R</i> )-IRED mutation position	Direction	Base sequence for primers
D172L	Forward	5'-ggccctgtacctggtgcactgct-3'
	Reverse	5'-agcagtgacaccaggtacagggcc-3'
D172A	Forward	5'-ggccctgtacgccgtgcactgct-3'
	Reverse	5'-agcagtgacacggcgtacagggcc-3'

The following temperature sequence was used in the thermocycler for the PCR reaction:

- 95°C denaturation for 1 min, then
- 95°C denaturation for 50 s, then 60°C annealing for 50 s, then 68°C extension for 8 min (18 cycles)
- 68°C final extension for 7 min then 4°C final hold

The PCR product was then subjected to a Dpn1 digest using the following thermocycler sequence:

- 37°C incubation for 1 h, then 80°C denaturation for 20 min, then
- 4°C final hold

The product was then cloned in *E. coli* XL1 Blue supercompetent cells and the plasmid was sequenced to confirm successful mutagenesis. These mutants were transformed and expressed in *E. coli* BL21 as previously described for the wild-type (*R*)-IRED gene. The mutants were then purified by HisTag Ni<sup>2+</sup> affinity chromatography following the same procedure as previously described, before the isolated proteins were used in biotransformations.

## 7.9.2 General procedure for pure enzyme biotransformations with (*R*)-IRED mutants

Analytical-scale biotransformations with the isolated (*R*)-IRED protein were carried out following the general imine reductase biotransformation protocol (see Section 7.5.1.1), using 500 µg/mL (*R*)-IRED variant protein in sodium phosphate buffer to a final concentration of 500 µg/mL, NADPH (17 µL from a 150 mM stock solution) and 5 mM substrate (10 µL from a 250 mM stock solution).

## 7.10 Methods and conditions used for biotransformation analysis

### 7.10.1 Chiral HPLC

#### 7.10.1.1 Chiral HPLC analysis conditions for 2-substituted cyclic imines

The 2-substituted cyclic imine compounds were analyzed by normal phase chiral HPLC using isocratic methods of varying mixtures of the running solvents *n*-hexane/isopropanol, with 0.1% diethylamine as additive using the following columns:

Daicel CHIRALPAK®IA 250 mm × 4.6 mm, 5 µm

Daicel CHIRALPAK®IC 250 mm × 4.6 mm, 5 µm

Daicel CHIRALPAK®IE 250 mm × 4.6 mm, 5 µm

The flow rate was set to 1 mL min<sup>-1</sup> and analytes were detected by the U.V. detector at a wavelength of 265 nm.

Due to the variation of UV response of the imine versus the corresponding amine, the relative response was corrected using an experimentally-determined relative response factor. These values were determined from the ratio of the slopes of standard curves plotted for varying concentrations of both the imine and amine at a UV detection wavelength of 265 nm.

**Table 29:** Columns and methods used to analyse biotransformation results of imine compounds **1**, **3**, **5**, **7** and **9**

Compound	Column	<i>n</i> -hexane/IPA/ diethylamine running solvent ratio	Relative response factor ( $A_{\text{imine}}/A_{\text{amine}}$ )	Imine retention time/ min	Amine retention time/ min	
					T <sup>1</sup>	T <sup>2</sup>
<b>1b</b>	CHIRALPAK ®IC	90:10:0.1	25.3	9.41	7.5 ( <i>R</i> )	8.1 ( <i>S</i> )

<b>1c</b>	CHIRALPAK ®IE	90:10:0.1	36.8	16.9	13.0 ( <i>R</i> )	14.3 ( <i>S</i> )
<b>1d</b>	CHIRALPAK ®IA	98:2:0.1	4.68	9.4	10.5 ( <i>R</i> )	11.4 ( <i>S</i> )
<b>3c</b> <sup>[a]</sup>	CHIRALPAK ®IC	90:10:0.1	21.4	17.8	7.5	10.5
<b>5c</b>	CHIRALPAK ®IC	90:10:0.1	19.1	16.1	8.9 ( <i>R</i> )	12.9 ( <i>S</i> )
<b>5d</b>	CHIRALPAK ®IC	98:2:0.1	2.53	8.3	5.4 ( <i>R</i> )	5.8 ( <i>S</i> )
<b>5f</b>	CHIRALPAK ®IC	90:10:0.1	1.64	14.7	9.2 ( <i>R</i> )	10.3 ( <i>S</i> )
<b>5g</b>	CHIRALPAK ®IC	95:5:0.1	1.29	27.5	9.5 ( <i>S</i> )	11.0 ( <i>R</i> )
<b>5h</b>	CHIRALPAK ®IC	90:10:0.1	21.7	9.87	6.4 ( <i>R</i> )	7.5 ( <i>S</i> )
<b>5n</b> <sup>[a]</sup>	CHIRALPAK ®IA	95:5:0.1	1.31	10.15	5.78	8.07
<b>7a</b>	CHIRALPAK ®IC	90:10:0.1	9.10	18.2	10.4 ( <i>S</i> )	11.4 ( <i>R</i> )
<b>9</b>	CHIRALPAK ®IC	90:10:0.1	9.10	5.2		6.6

[a] Absolute configuration undetermined

#### 7.10.1.2 Chiral HPLC analysis conditions for 2-substituted tetrahydroquinolines

The 2-substituted tetrahydroquinoline compounds were analyzed by normal phase chiral HPLC using isocratic methods of varying mixtures of the running solvents *n*-hexane/isopropanol, with 0.1% diethylamine as additive using the following columns:

Daicel CHIRALCEL®OJ-H 250 mm × 4.6 mm, 5 μm

The flow rate was set to 1 mL min<sup>-1</sup> and analytes were detected by the U.V. detector at a wavelength of 254 nm.

The *ee* of the amine following deracemisation was calculated based on the peak areas of the two enantiomers of the amine.

**Table 30:** Columns and methods used to analyse biotransformation results of 2-substituted tetrahydroquinoline compounds **23**

Compound	Column	<i>n</i> -hexane/IPA/ diethylamine running solvent ratio	Quinoline <b>25</b> retention time/ min	Amine retention time/ min	
				T <sup>1</sup>	T <sup>2</sup>
<b>23a</b>	CHIRALCEL® OJ-H	90:10:0.1	8.3	13.5 ( <i>R</i> )	14.9 ( <i>S</i> )
<b>23b</b>	CHIRALCEL® OJ-H	95:5:0.1	8.4	14.5 ( <i>R</i> )	16.2 ( <i>S</i> )
<b>23c</b>	CHIRALCEL® OJ-H	90:10:0.1	15.2	14.1 ( <i>R</i> )	15.2 ( <i>S</i> )
<b>23d</b>	CHIRALCEL® OJ-H	90:10:0.1	16.1	8.9 ( <i>R</i> )	12.9 ( <i>S</i> )
<b>23e</b>	CHIRALCEL® OJ-H	95:5:0.1	8.3	9.3 ( <i>R</i> )	10.3 ( <i>S</i> )
<b>23f</b>	CHIRALCEL® OJ-H	90:10:0.1	-	23.5 ( <i>R</i> )	27.3 ( <i>S</i> )
<b>23g</b>	CHIRALCEL® OJ-H	90:10:0.1	-	14.0 ( <i>S</i> )	15.2 ( <i>R</i> )

[a] Absolute configuration undetermined

#### 7.10.1.3 Chiral HPLC analysis conditions for 2-substituted indolines

The 2-substituted indoline compounds were analyzed by normal phase chiral HPLC using isocratic methods of varying mixtures of the running solvents *n*-hexane/isopropanol, with 0.1% diethylamine as additive using the following column:

Daicel CHIRALCEL®OD-H 250 mm × 4.6 mm, 5 μm

The flow rate was set to 1 mL min<sup>-1</sup> and analytes were detected by the U.V. detector at a wavelength of 254 nm.

The *ee* of the amine following deracemisation was calculated based on the peak areas of the two enantiomers of the amine.

**Table 31:** Columns and methods used to analyse biotransformation results of the 2-substituted indoline compounds **26**

Compound	Column	<i>n</i> -hexane/IPA/ diethylamine running solvent ratio	Indole <b>28</b> retention time/ min	Amine retention time/ min	
				T <sup>1</sup>	T <sup>2</sup>
<b>26a</b>	CHIRALCEL® OD-H	90:10:0.1	12.2	7.2 ( <i>R</i> )	7.8 ( <i>S</i> )
<b>26b</b>	CHIRALCEL® OD-H	80:20:0.1	13.3	5.4 ( <i>R</i> )	8.1 ( <i>S</i> )
<b>26c</b>	CHIRALCEL® OD-H	80:20:0.1	8.8	6.2 ( <i>R</i> )	10.9 ( <i>S</i> )
<b>26d</b>	CHIRALCEL® OD-H	80:20:0.1	7.6	12.0 ( <i>R</i> )	21.2 ( <i>S</i> )
<b>26e</b>	CHIRALCEL® OD-H	80:20:0.1	6.2	10.6 ( <i>R</i> )	29.2 ( <i>S</i> )

[a] Absolute configuration undetermined

#### 7.10.2 Chiral GC-FID analysis

##### 7.10.2.1 Chiral GC-FID analysis conditions for 2-substituted cyclic imines and amines

Samples were derivatised using an excess of triethylamine (2 eq.) and acetic anhydride (1 eq.) if run on the CP-ChiraSil-DEX CB column, or an excess of trifluoroacetic anhydride if run on the  $\beta$ -DEX 325 column.

It should be noted that derivatisation of the unreacted imine substrate leads to *N*-acetylation of the imine, which most likely undergoes tautomerisation to give the resulting enaminate. GC-MS analysis (recorded on a Hewlett Packard HP 6890 equipped with an HP-1MS column, an HP 5973 Mass Selective Detector and an ATLAS GL FOCUS sampling robot) confirms the presence of this side-product (eg. derivatised imine **5i** GC-MS  $m/z$  167 [M<sup>+</sup>]), which also has a different retention time on GC-FID chromatograms compared to the underderivatised imine substrate.

**Table 32:** Methods used to analyse biotransformation results of imine compounds **1**, **3**, **5** and **9a** and for amines **19** and **22** on CP-ChiraSil-DEX CB column

Compound	Injector temp.	Helium flow/ mL min <sup>-1</sup>	Oven temp.	Detector temp.	Imine retention time/ min	Amine retention time/ min	
						T <sup>1</sup>	T <sup>2</sup>
<b>1a</b>	200	1.2	90°C - 160°C, 0.5°C min <sup>-1</sup> , hold 160°C for 10 minutes	250	27.52	32.11 ( <i>R</i> )	32.72 ( <i>S</i> )
<b>3a</b>	200°C	1.2	90°C - 160°C, 1°C min <sup>-1</sup> then 10°C min <sup>-1</sup> to 200°C	250°C	61.34	35.85 ( <i>S</i> )	36.15 ( <i>R</i> )
<b>5a</b>	200°C	1.5	50°C - 200°C, 10°C min <sup>-1</sup>	250°C	10.70	10.84 ( <i>R</i> )	10.94 ( <i>S</i> )
<b>5b</b>	200°C	1.2	90°C - 200°C, 4°C min <sup>-1</sup>	250°C	18.11	24.78 ( <i>S</i> )	25.05 ( <i>R</i> )
<b>5e</b> <sup>[a]</sup>	220°C	1.5	120°C - 180°C, 1°C min <sup>-1</sup>	250°C	35.53	37.11	37.13
<b>5i</b>	200°C	1.2	90°C - 200°C, 4°C min <sup>-1</sup>	250°C	14.92	15.57 ( <i>S</i> )	15.81 ( <i>R</i> )
<b>5j</b>	200°C	1.2	90°C - 160°C, 2°C min <sup>-1</sup>	250°C	6.71	24.74 ( <i>S</i> )	25.23 ( <i>R</i> )
<b>5k</b>	200°C	1.2	90°C - 160°C, 2°C min <sup>-1</sup>	250°C	7.95	23.79 <sup>[b]</sup>	
<b>5l</b> <sup>[a]</sup>	200°C	1.2	90°C - 200°C, 4°C min <sup>-1</sup>	250°C	18.91	24.82	25.06
<b>5m</b>	200°C	1.2	90°C - 200°C, 4°C min <sup>-1</sup> , hold 200°C for 10 min	250°C	25.59	27.02 ( <i>R</i> )	27.24 ( <i>S</i> )
<b>9a</b>	200°C	1.2	90°C - 200°C, 4°C min <sup>-1</sup>	250°C	16.19	12.79 ( <i>R</i> )	13.22 ( <i>S</i> )
<b>19</b>	200°C	0.7	90°C - 150°C, 10°C min <sup>-1</sup>	250°C	-	30.8 ( <i>R</i> )	31.1 ( <i>S</i> )
<b>22</b>	200°C	1.2	90°C - 200°C, 3°C min <sup>-1</sup>	250°C	-	37.7 ( <i>R</i> )	38.0 ( <i>S</i> )

[a] Absolute configuration undetermined [b] Unable to separate enantiomers of the racemic amine standard **6k** on this column, see Table 33.

**Table 33:** Methods used to analyse biotransformation results of imine compounds **1**, **3**, **5** and **7** on the  $\beta$ -DEX 325 column

Compound	Injector temp.	Helium flow/ mL min <sup>-1</sup>	Oven temp.	Detector temp.	Imine retention time/ min	Amine retention time/ min	
						T <sup>1</sup>	T <sup>2</sup>
<b>1e</b>	250°C	1.7	115°C isothermal	250°C	17.10	48.60 (S)	50.08 (R)
<b>5k</b>	200°C	1.3	90°C - 115°C, 1°C min <sup>-1</sup>	250°C	16.50	19.40 (S)	19.61 (R)

For substrates **5j** and **5k**, the retention time for the peak of the derivatised imine on the GC-FID chromatograms overlaps with the peaks of by-products from the derivatisation process, therefore to calculate conversions in these cases the samples were run without additional derivatisation on the CP-ChiraSil-DEX CB column. For substrate **5m**, as the biotransformation did not go to completion after 24 h, conversion was calculated from the underivatised sample.

**Table 34:** Methods used to analyse conversions from biotransformations of imine compounds **5j**, **5k** and **5m** on CP-ChiraSil-DEX CB column, using underivatised samples

Compound	Injector temp.	Helium flow/ mL min <sup>-1</sup>	Oven temp.	Detector temp.	Imine retention time/ min	Amine retention time/ min
<b>5j</b>	200°C	1.2	90°C - 160°C, 2°C min <sup>-1</sup>	250°C	8.17	7.06
<b>5k</b>	200°C	1.2	90°C - 160°C, 2°C min <sup>-1</sup>	250°C	6.56	6.87
<b>5m</b>	200°C	1.2	90°C - 200°C, 4°C min <sup>-1</sup> , hold 200°C for 10 min	250°C	17.60	16.94

7.10.2.2 Chiral GC-FID analysis conditions for 2,5-disubstituted pyrrolidine and 2,6-disubstituted piperidines

Samples were extracted with base for analysis of conversion of the diketone and disubstituted imine using the CP-ChiraSil-DEX CB column.

**Table 35:** Methods used to analyse biotransformation results of diketones **11a** – **11d** on CP-ChiraSil-DEX CB column

Compound	Injector temp.	Helium flow/ mL min <sup>-1</sup>	Oven temp.	Detector temp.	Diketone time/ min	Imine retention time/ min T <sup>1</sup>	T <sup>2</sup>
<b>11a</b>	250	1.7	130°C hold for 12 min, then 130°C - 200°C, 15°C min <sup>-1</sup> , hold 200°C for 5 minutes	275°C	16.32, 17.21	13.83( <i>R</i> )	14.01( <i>S</i> )
<b>11b</b>	250	1.7	130°C hold for 12 min, then 130°C - 200°C, 15°C min <sup>-1</sup> , hold 200°C for 5 minutes	275°C	17.48, 18.54	15.55( <i>R</i> )	15.71( <i>S</i> )
<b>11c</b>	220°C	1.5	100°C hold for 3 min, then 100°C - 160°C, 40°C min <sup>-1</sup> , hold for 20 min	250°C	20.06	8.41( <i>R</i> )	8.54( <i>S</i> )
<b>11d</b>	250°C	1.1	80°C hold for 2 min, then 80°C - 140°C, 1.5°C min <sup>-1</sup> , hold for 3 min, then 140°C - 200°C, 4°C min <sup>-1</sup> , hold for 2 min	250°C	22.61, 26.26, 30.29	12.98( <i>R</i> )	13.25( <i>S</i> )
<b>14</b>	220°C	1.7	100°C hold for 3 min, then 100°C - 160°C, 40°C min <sup>-1</sup> , hold for 20 min	250°C	9.27	6.48( <i>R</i> )	6.52( <i>S</i> )

Chemical standards of disubstituted piperidines **13a** – **13d** and **16** were prepared from the corresponding diketones by following the general procedure outlined in Section 7.5.2.1 on an analytical scale and effecting the transaminase step only, to produce the corresponding disubstituted imines. Following extraction with ethyl acetate, the solvent was allowed to evaporate before each sample was redissolved in dH<sub>2</sub>O:MeOH (1:4, 50 μL). A small spatula

of NaBH<sub>4</sub> was added to each sample, which was then left to react for three hours. The reaction was subsequently quenched by acidification with 1 M HCl (50 µL) before the pH was readjusted to pH 12 by addition of 1 M NaOH (100 µL). The reaction mixture was extracted with ethyl acetate (500 µL) and the organic phase was separated, dried over MgSO<sub>4</sub> and transferred to a sample vial for analysis. The diastereomers were assigned based on the preference observed for formation of the 1,3-diequatorial product. For analysis of the *de* of the amine, samples were derivatised using an excess of triethylamine (2 eq.) and acetic anhydride (1 eq.) and run on the CP-ChiraSil-DEX CB column.

**Table 36:** Methods used to analyse biotransformation results of di-substituted piperidines **13a** – **13d** and **16** on CP-ChiraSil-DEX CB column

Compound	Injector temp.	Helium flow/ mL min <sup>-1</sup>	Oven temp.	Detector temp.	Amine retention time/ min			
					T <sup>1</sup>	T <sup>2</sup>	T <sup>3</sup>	T <sup>4</sup>
<b>13a</b>	250	1.7	130°C hold for 12 min, then 130°C - 200°C, 15°C min <sup>-1</sup> , hold 200°C for 5 minutes	275	18.17 <i>2S,6S</i>	18.51 <i>2S,6R</i>	18.04 <i>2R,6S</i>	18.23 <i>2R,6R</i>
<b>13b</b>	250	1.7	130°C hold for 12 min, then 130°C - 200°C, 15°C min <sup>-1</sup> , hold 200°C for 5 minutes	275	19.50 <i>2S,6R</i>	19.66 <i>2S,6S</i>	19.40 <i>2R,6S</i>	19.71 <i>2R,6R</i>
<b>13c</b>	220°C	1.5	100°C hold for 3 min, then 100°C - 160°C, 40°C min <sup>-1</sup> , hold for 20 min	250°C	21.90 <i>2S,6S</i>	22.55 <i>2S,6R</i>	21.35 <i>2R,6S</i>	22.54 <i>2R,6R</i>
<b>13d</b>	250°C	1.1	80°C hold for 2 min, then 80°C - 140°C, 1.5°C min <sup>-1</sup> , hold for 3 min, then 140°C - 200°C, 4°C min <sup>-1</sup> , hold for 2 min	250°C	41.99 <i>2S,6R</i>	42.96 <i>2S,6S</i>	39.95 <i>2R,6S</i>	40.76 <i>2R,6R</i>
<b>16</b>	220°C	1.7	100°C hold for 3 min, then 100°C - 160°C, 40°C min <sup>-1</sup> , hold for 20 min	250°C	13.07 <i>2S,5S</i>	14.02 <i>2S,5R</i>	13.10 <i>2R,5R</i>	13.68 <i>2R,5S</i>

### 7.11 Determination of the absolute configuration of piperidines **6a** – **6m**

For pyrrolidine products **2a** – **2e**, azepanes **6a** and **6c**, tetrahydroisoquinolines **8a** and **10a** the absolute configuration of the biotransformation products was determined by comparison of the biotransformation HPLC/GC-FID chromatograms with the chromatograms of samples of known configuration. For piperidines **6a** – **6m**, the absolute configuration of the products obtained from preparative-scale biotransformations of the corresponding imine substrates **5a** – **5m** with the (*R*)-IRED was determined by comparison of the measured specific rotation values to reported literature values for the same compounds.

**Table 37:** Comparison of experimentally-determined and known literature reference  $[\alpha]_D^{25}$  values for determination of absolute configuration of product piperidines **6a** – **6m**

Amine product	Absolute configuration	$[\alpha]_D^{25}$ / degcm <sup>3</sup> g <sup>-1</sup> dm <sup>-1</sup>	Literature $[\alpha]_D$ / degcm <sup>3</sup> g <sup>-1</sup> dm <sup>-1</sup>	Reference
<b>6a</b>	( <i>R</i> )	-4.7° (c= 0.90, EtOH)	( <i>R</i> ) = -9.4° [c=0.95, EtOH]	[146]
<b>6b</b>	( <i>S</i> )	-15.5° (c=0.5, CHCl <sub>3</sub> )	( <i>S</i> ) = -63.8° [c=0.50, CHCl <sub>3</sub> ]	[147]
<b>6c</b>	( <i>S</i> )	-23.4° (c =0.5, MeOH)	( <i>S</i> ) = -21.1° [c=0.54, MeOH]	[148]
<b>6d</b>	( <i>S</i> )	-28.3 (c=1.0, CHCl <sub>3</sub> )	-	_[c]
<b>6e</b>	_[b]	-1.3 (c=0.5, CHCl <sub>3</sub> )	-	_[c]
<b>6f</b> <sup>[a]</sup>	( <i>S</i> )	-11.0° (c=0.26, CH <sub>2</sub> Cl <sub>2</sub> )	( <i>S</i> ).HCl = -24.6° (c=0.26, CH <sub>2</sub> Cl <sub>2</sub> )	[149]
<b>6g</b>	( <i>S</i> )	-48.0° (c=0.5, CHCl <sub>3</sub> )	-	_[c]
<b>6h</b>	( <i>S</i> )	-26.4° (c=0.4, CHCl <sub>3</sub> )	( <i>R</i> ) = +36.7° (c=0.4, CHCl <sub>3</sub> )	[150]
<b>6i</b> <sup>[a, d]</sup>	( <i>R</i> )	-11.0° (c=1.0, CH <sub>2</sub> Cl <sub>2</sub> )	( <i>S</i> ) = +19.8° (c=0.5, CH <sub>2</sub> Cl <sub>2</sub> )	[149]
<b>6j</b>	( <i>S</i> )	- 8.0° (c=1.0, CHCl <sub>3</sub> )	-	_[c]
<b>6k</b>	( <i>S</i> )	-6.3 (c=1.0, CHCl <sub>3</sub> )	( <i>R</i> ) = +7.5 (c=0.5, CHCl <sub>3</sub> )	[151]
<b>6l</b>	_[b]	-26.5 (c=1.0, CHCl <sub>3</sub> )	-	_[c]
<b>6m</b>	( <i>S</i> )	+1.59° (c=1.0, Et <sub>2</sub> O)	( <i>S</i> ) = +0.5° (c=5.60, Et <sub>2</sub> O)	[152]

[a] Isolated and measured as the HCl salt [b] Absolute configuration undetermined [c] No reported  $[\alpha]_D$  value for configuration found in literature

For the determination of the absolute configuration of the product obtained from the biotransformation of **5j**, the double-bond of the product amine was chemocatalytically hydrogenated using Pd/C catalyst under a hydrogen atmosphere (using the same protocol as the hydrogenation of **86j** – see Section 7.3.1.3). The hydrogenation product was then run on chiral GC-FID and the chromatogram compared to that of the biotransformation product of imine **5k** [(*S*)-2-isopropylpiperidine, Figure 115]. As both peaks have the same retention time, it can be assumed that the (*S*)-enantiomer is formed in the biotransformation of **5j**.

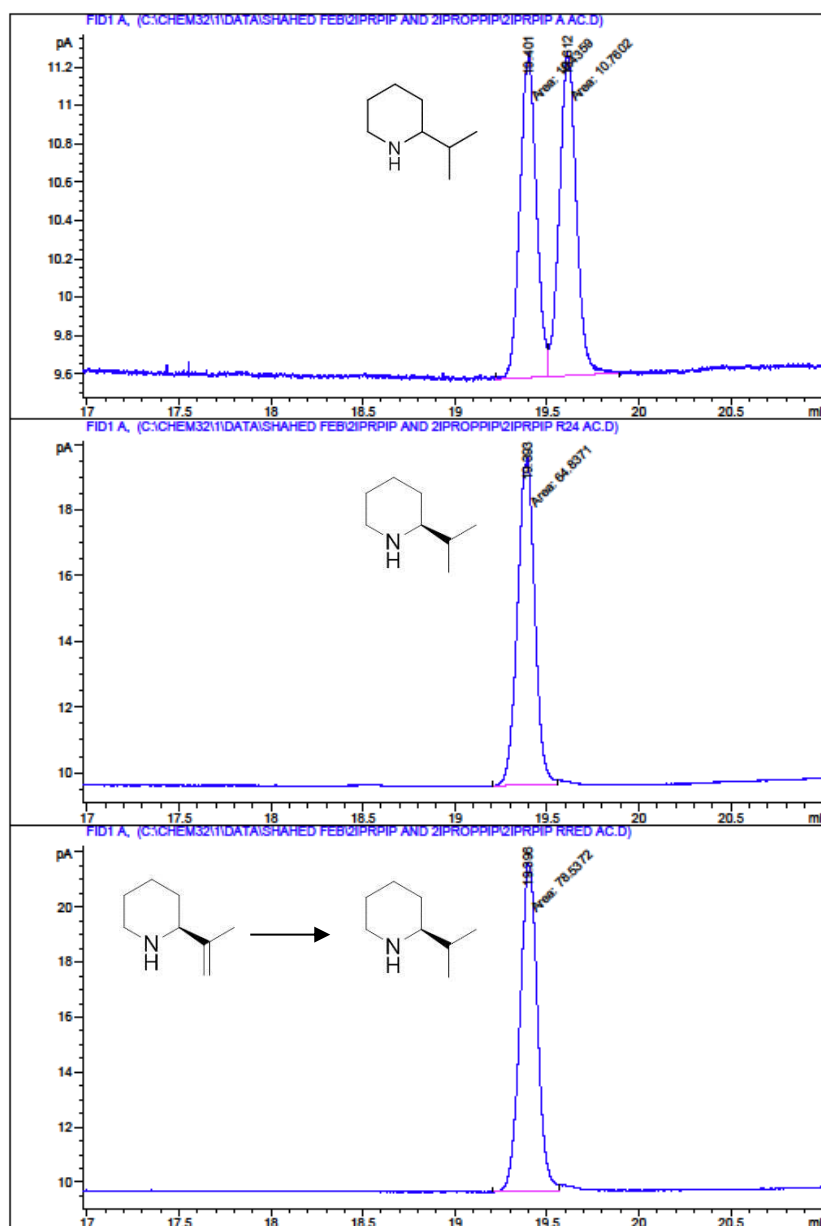


**Figure 115:** GC-FID chromatograms showing standard of the racemic amine 2-isopropylpiperidine **6k** (top), product (*S*)-2-isopropylpiperidine **6k** (middle) isolated from the (*R*)-IRED biotransformation of imine **5k**, followed by the compound produced via the chemical reduction of product 2-isopropenylpiperidine **6j** isolated from the biotransformation of 2-isopropenyl-1-piperidine **5j** by the (*R*)-IRED (bottom).

## Chapter 8: References

- (1) Grond, S.; Sablotzki, A. *Clin. Pharmacokinet.* **2004**, *43* (13), 879.
- (2) Eriksson, T.; Bjorkman, S.; Roth, B.; Fyge, A.; Hoglund, P. *Chirality* **1995**, *7* (1), 44.
- (3) *Chirality* **1992**, *4*, 338.
- (4) Welsch, M. E.; Snyder, S. A.; Stockwell, B. R. *Curr. Opin. Chem. Biol.* **2010**, *14* (3), 347.
- (5) Flack, H. D. *Acta Crystallogr. Sect. A Found. Crystallogr.* **2009**, *65* (5), 371.
- (6) Fujima, Y.; Ikunaka, M.; Inoue, T.; Matsumoto, J. *Org. Process Res. Dev.* **2006**, *10* (5), 905.
- (7) Breuer, M.; Ditrich, K.; Habicher, T.; Hauer, B.; Keßeler, M.; Stürmer, R.; Zelinski, T. *Angew. Chemie - Int. Ed.* **2004**, *43* (7), 788.
- (8) Binanzer, M.; Hsieh, S. Y.; Bode, J. W. *J. Am. Chem. Soc.* **2011**, *133* (49), 19698.
- (9) Kreituss, I.; Murakami, Y.; Binanzer, M.; Bode, J. W. *Angew. Chemie - Int. Ed.* **2012**, *51* (42), 10660.
- (10) Knowles, W. S. *Acc. Chem. Res.* **1983**, *16* (3), 106.
- (11) Xu, L.; Wu, X.; Jiao, J. In *Science of Synthesis: Stereoselective Synthesis 2: Stereoselective Reactions of Carbonyl and Imino Groups*; Molander, G. A., Ed.; Georg Thieme Verlag, 2011; pp 251–310.
- (12) Blaser, H. U.; Spindler, F. *Top. Catal.* **1997**, *4*, 275.
- (13) Blaser, H. U.; Buser, H. P.; Häusel, R.; Jalett, H. P.; Spindler, F. *J. Organomet. Chem.* **2001**, *621* (1-2), 34.
- (14) Han, Z.; Wang, Z.; Zhang, X.; Ding, K. *Angew. Chemie - Int. Ed.* **2009**, *48* (29), 5345.
- (15) Burk, M. J.; Feaster, J. E. *J. Am. Chem. Soc.* **1992**, *114* (15), 6266.
- (16) Willoughby, C. a.; Buchwald, S. L. *J. Am. Chem. Soc.* **1994**, *116* (I), 8952.
- (17) Li, C.; Xiao, J. *J. Am. Chem. Soc.* **2008**, *130* (40), 13208.
- (18) Uematsu, N.; Fujii, A.; Hashiguchi, S.; Ikariya, T.; Noyori, R. *J. Am. Chem. Soc.* **1996**, *118* (20), 4916.
- (19) Shimizu, M.; Kamei, M.; Fujisawa, T. *Tetrahedron Lett.* **1995**, *36* (47), 8607.
- (20) Bornscheuer, U. T.; Huisman, G. W.; Kazlauskas, R. J.; Lutz, S.; Moore, J. C.; Robins, K. *Nature* **2012**, *485* (7397), 185.
- (21) Turner, N. J. *Nat. Chem. Biol.* **2009**, *5* (8), 567.
- (22) Turner, N. J.; O'Reilly, E. *Nat. Chem. Biol.* **2013**, *9* (5), 285.
- (23) Gotor-Fernández, V.; Brieva, R.; Gotor, V. *J. Mol. Catal. B Enzym.* **2006**, *40* (3-4), 111.
- (24) Dürrenberger, M.; Heinisch, T.; Wilson, Y. M.; Rossel, T.; Nogueira, E.; Knörr, L.;

- Mutschler, A.; Kersten, K.; Zimbron, M. J.; Pierron, J.; Schirmer, T.; Ward, T. R. *Angew. Chemie - Int. Ed.* **2011**, *50* (13), 3026.
- (25) Schwizer, F.; Köhler, V.; Dürrenberger, M.; Knörr, L.; Ward, T. R. *ACS Catal.* **2013**, *3*, 1752.
- (26) Benkovic, S. J.; Hammes-Schiffer, S. *Science (80-. )*. **2003**, *301* (5637), 1196.
- (27) Filman, D. J.; Bolin, J. T.; Matthews, D. A.; Kraut, J. *J. Biol. Chem.* **1982**, *257* (22), 13663.
- (28) Hallen, A.; Jamie, J. F.; Cooper, A. J. L. *Neurochem Res.* **2014**, *39* (3), 527.
- (29) Li, W.; Khullar, A.; Chou, S.; Sacramo, A.; Gerratana, B. *Appl. Environ. Microbiol.* **2009**, *75* (9), 2869.
- (30) Li, W.; Chou, S.; Khullar, A.; Gerratana, B. *Appl. Environ. Microbiol.* **2009**, *75* (9), 2958.
- (31) Meister, A.; Radhakrishnan, A. N.; Buckley, D. *J. Biol. Chem.* **1957**, *229* (2), 789.
- (32) Muramatsu, H.; Mihara, H.; Kakutani, R.; Yasuda, M.; Ueda, M.; Kurihara, T.; Esaki, N. *J. Biol. Chem.* **2005**, *280* (7), 5329.
- (33) Vaijayanthi, T.; Chadha, A. *Tetrahedron Asymmetry* **2008**, *19* (1), 93.
- (34) Chimni, S. S.; Singh, R. J. *World J. Microbiol. Biotechnol.* **1998**, *14* (2), 247.
- (35) Espinoza-Moraga, M.; Petta, T.; Vasquez-Vasquez, M.; Laurie, V. F.; Moraes, L. A. B.; Santos, L. S. *Tetrahedron Asymmetry* **2010**, *21* (16), 1988.
- (36) Mirabal-Gallardo, Y.; Soriano, M. D. P. C.; Santos, L. S. *Tetrahedron Asymmetry* **2013**, *24* (8), 440.
- (37) Mitsukura, K.; Suzuki, M.; Tada, K.; Yoshida, T.; Nagasawa, T. *Org. Biomol. Chem.* **2010**, *8* (20), 4533.
- (38) Mitsukura, K.; Suzuki, M.; Shinoda, S.; Kuramoto, T.; Yoshida, T.; Nagasawa, T. *Biosci. Biotechnol. Biochem.* **2011**, *75* (9), 1778.
- (39) [www.uniprot.org](http://www.uniprot.org).
- (40) Myronovskyi, M.; Tokovenko, B.; Manderscheid, N.; Petzke, L.; Luzhetskyy, A. *J. Biotechnol.* **2013**, *168* (1), 117.
- (41) Mitsukura, K.; Kuramoto, T.; Yoshida, T.; Kimoto, N.; Yamamoto, H.; Nagasawa, T. *Appl. Microbiol. Biotechnol.* **2013**, *97* (18), 8079.
- (42) Li, H.; Luan, Z. J.; Zheng, G. W.; Xu, J. H. *Adv. Synth. Catal.* **2015**, *357* (8), 1692.
- (43) Li, H.; Zhang, G.-X.; Li, L.-M.; Ou, Y.-S.; Wang, M.-Y.; Li, C.-X.; Zheng, G.-W.; Xu, J.-H. *ChemCatChem* **2016**, *200237*, n/a.
- (44) Rodríguez-Mata, M.; Frank, A.; Wells, E.; Leipold, F.; Turner, N. J.; Hart, S.; Turkenburg, J. P.; Grogan, G. *ChemBioChem* **2013**, *14* (11), 1372.
- (45) Gand, M.; Müller, H.; Wardenga, R.; Höhne, M. *J. Mol. Catal. B Enzym.* **2014**, *110*, 126.
- (46) Huber, T.; Schneider, L.; Präg, A.; Gerhardt, S.; Einsle, O.; Müller, M. *ChemCatChem* **2014**, *6* (8), 2248.

- (47) Scheller, P. N.; Fademrecht, S.; Hofelzer, S.; Pleiss, J.; Leipold, F.; Turner, N. J.; Nestl, B. M.; Hauer, B. *Chembiochem* **2014**, *15*(15), 2201.
- (48) Scheller, P. N.; Lenz, M.; Hammer, S. C.; Hauer, B.; Nestl, B. M. *ChemCatChem* **2015**, *7*(20), 3239.
- (49) <https://ired.biocatnet.de/>
- (50) Fademrecht, S.; Scheller, P. N.; Nestl, B. M.; Hauer, B.; Pleiss, J. *Proteins Struct. Funct. Bioinforma.* **2016**, *84*(5), 600.
- (51) Wetzl, D.; Berrera, M.; Sandon, N.; Fishlock, D.; Ebeling, M.; Müller, M.; Hanlon, S.; Wirz, B.; Iding, H. *ChemBioChem* **2015**, *16*(12), 1749.
- (52) Schrittwieser, J. H.; Velikogne, S.; Kroutil, W. *Adv. Synth. Catal.* **2015**.
- (53) Grogan, G.; Turner, N. J. *Chem. - A Eur. J.* **2015**, 1900.
- (54) Gamenara, D.; de Maria, P. *Org. Biomol. Chem.* **2014**, *12*(19), 2989.
- (55) F. Leipold, S. Hussain, S.P. France, N. J. T. In *Science of Synthesis: Biocatalysis in Organic Synthesis 2*; K. Faber, W. D. Fessner, N. J. T., Ed.; Georg Thieme Verlag: Stuttgart, 2015; pp 359–382.
- (56) Napora-Wijata, K.; Strohmeier, G. A.; Winkler, M. *Biotechnol. J.* **2014**, *9*(6), 822.
- (57) Venkitasubramanian, P.; Daniels, L.; Rosazza, J. P. N. *J. Biol. Chem.* **2007**, *282*(1), 478.
- (58) Akhtar, M. K.; Turner, N. J.; Jones, P. R. *Proc. Natl. Acad. Sci. U. S. A.* **2013**, *110*(1), 87.
- (59) Li, T.; Rosazza, J. P. N. *Appl. Environ. Microbiol.* **2000**, *66*(2), 684.
- (60) Koszelewski, D.; Clay, D.; Rozzell, D.; Kroutil, W. *European J. Org. Chem.* **2009**, No. 14, 2289.
- (61) Simon, R. C.; Richter, N.; Busto, E.; Kroutil, W. *ACS Catal.* **2014**, *4*(1), 129.
- (62) Koszelewski, D.; Lavandera, I.; Clay, D.; Guebitz, G. M.; Rozzell, D.; Kroutil, W. *Angew. Chemie - Int. Ed.* **2008**, *47*(48), 9337.
- (63) Richter, N.; Farnberger, J. E.; Pressnitz, D.; Lechner, H.; Zepeck, F.; Kroutil, W. *Green Chem.* **2015**, *17*(5), 2952.
- (64) Savile, C. K.; Janey, J. M.; Mundorff, E. C.; Moore, J. C.; Tam, S.; Jarvis, W. R.; Colbeck, J. C.; Krebber, A.; Fleitz, F. J.; Brands, J.; Devine, P. N.; Huisman, G. W.; Hughes, G. J. *Science (80-. )*. **2010**, *329*(5989), 305.
- (65) Slabu, I.; Galman, J. L.; Weise, N. J.; Lloyd, R. C.; Turner, N. J. *ChemCatChem* **2016**, *8*(6), 1038.
- (66) Lovelock, S. L.; Lloyd, R. C.; Turner, N. J. *Angew. Chemie - Int. Ed.* **2014**, *53*(18), 4652.
- (67) Weise, N. J.; Parmeggiani, F.; Ahmed, S. T.; Turner, N. J. *J. Am. Chem. Soc.* **2015**, *137*(40), 12977.
- (68) Turner, N. J. *Curr. Opin. Chem. Biol.* **2011**, *15*(2), 234.
- (69) DeLange, B.; Hyett, D. J.; Maas, P. J. D.; Mink, D.; van Assema, F. B. J.; Sereinig,

- N.; de Vries, A. H. M.; de Vries, J. G. *ChemCatChem* **2011**, *3*(2), 289.
- (70) Abrahamson, M. J.; Vázquez-Figueroa, E.; Woodall, N. B.; Moore, J. C.; Bommarius, A. S. *Angew. Chemie - Int. Ed.* **2012**, *51*(16), 3969.
- (71) Lackner, A. D.; Samant, A. V.; Toste, F. D. *J. Am. Chem. Soc.* **2013**, *135*(38), 14090.
- (72) Ji, Y.; Shi, L.; Chen, M.; Feng, G.; Zhou, Y. *J. Am. Chem. Soc.* **2015**, *137*(33), 10496.
- (73) Ghislieri, D.; Green, A. P.; Pontini, M.; Willies, S. C.; Rowles, I.; Frank, A.; Grogan, G.; Turner, N. J. *J. Am. Chem. Soc.* **2013**, *135*(29), 10863.
- (74) Ghislieri, D.; Houghton, D.; Green, A. P.; Willies, S. C.; Turner, N. J. *ACS Catal.* **2013**, *3*(12), 2869.
- (75) Li, T.; Liang, J.; Ambrogelly, A.; Brennan, T.; Gloor, G.; Huisman, G.; Lalonde, J.; Lekhal, A.; Mijts, B.; Muley, S.; Newman, L.; Tobin, M.; Wong, G.; Zaks, A.; Zhang, X. *J. Am. Chem. Soc.* **2012**, *134*(14), 6467.
- (76) Znabet, A.; Polak, M. M.; Janssen, E.; de Kanter, F. J. J.; Turner, N. J.; Orru, R. V. a; Ruijter, E. *Chem. Commun. (Camb).* **2010**, *46*(42), 7918.
- (77) Cowart, M.; Pratt, J. K.; Stewart, A. O.; Bennani, Y. L.; Esbenshade, T. A.; Hancock, A. A. *Bioorganic Med. Chem. Lett.* **2004**, *14*(3), 689.
- (78) Leipold, F.; Hussain, S.; Ghislieri, D.; Turner, N. J. *ChemCatChem* **2013**, *5*(12), 3505.
- (79) Mitsukura, K.; Suzuki, M.; Shinoda, S.; Kuramoto, T.; Yoshida, T.; Nagasawa, T. *Biosci. Biotechnol. Biochem.* **2011**, *75*(9), 1778.
- (80) Bates, R. W.; Sa-Ei, K. *Tetrahedron* **2002**, *58*(30), 5957.
- (81) Ren, H.; Wulff, W. D. *Org. Lett.* **2013**, *15*(2), 242.
- (82) Williams, G. D.; Pike, R. A.; Wade, C. E.; Wills, M. *Org. Lett.* **2003**, *5*(22), 4227.
- (83) Walton, A. Z.; Stewart, J. D. *Biotechnol. Prog.* **2004**, *20*(2), 403.
- (84) Nagao, T.; Mitamura, T.; Wang, X. H. U. I.; Negoro, S. **1992**, *174*(15), 5013.
- (85) Heath, R. S.; Pontini, M.; Hussain, S.; Turner, N. J. *ChemCatChem* **2016**, *8*(1), 117.
- (86) Köhler, V.; Wilson, Y. M.; Dürrenberger, M.; Ghislieri, D.; Churakova, E.; Quinto, T.; Knörr, L.; Häussinger, D.; Hollmann, F.; Turner, N. J.; Ward, T. R. *Nat. Chem.* **2013**, *5*, 93.
- (87) Man, H.; Wells, E.; Hussain, S.; Leipold, F.; Hart, S.; Turkenburg, J. P.; Turner, N. J.; Grogan, G. *ChemBioChem* **2015**, *16*(7), 1052.
- (88) Scheller, P. N.; Nestl, B. M. *Appl. Microbiol. Biotechnol.* **2016**, *100*(24), 10509.
- (89) Matzel, P.; Gand, M.; Höhne, M. *Green Chem.* **2017**, 385.
- (90) Muschiol, J.; Peters, C.; Oberleitner, N.; Mihovilovic, M. D.; Bornscheuer, U. T.; Rudroff, F. *Chem. Commun.* **2015**, *51*(27), 5798.
- (91) Oberleitner, N.; Peters, C.; Muschiol, J.; Kadow, M.; Saß, S.; Bayer, T.; Schaaf, P.; Iqbal, N.; Rudroff, F.; Mihovilovic, M. D.; Bornscheuer, U. T. *ChemCatChem* **2013**, *5*

- (12), 3524.
- (92) Skalden, L.; Peters, C.; Dickerhoff, J.; Nobili, A.; Joosten, H. J.; Weisz, K.; Höhne, M.; Bornscheuer, U. T. *ChemBioChem* **2015**, *16* (7), 1041.
- (93) O'Reilly, E.; Iglesias, C.; Ghislieri, D.; Hopwood, J.; Galman, J. L.; Lloyd, R. C.; Turner, N. J. *Angew. Chemie - Int. Ed.* **2014**, *53* (9), 2447.
- (94) Simon, R. C.; Grischek, B.; Zepeck, F.; Steinreiber, A.; Belaj, F.; Kroutil, W. *Angew. Chemie - Int. Ed.* **2012**, *51* (27), 6713.
- (95) France, S. P.; Hussain, S.; Hill, A. M.; Hepworth, L. J.; Howard, R. M.; Mulholland, K. R.; Flitsch, S. L.; Turner, N. J. *ACS Catal.* **2016**.
- (96) Eriksson, C.; Sjödin, K.; Schlyter, F.; Högberg, H. E. *Tetrahedron Asymmetry* **2006**, *17* (7), 1074.
- (97) Daloz, D.; Braekman, J. C.; Pasteels, J. M. *Chemoecology* **1994**, *5-6* (3-4), 173.
- (98) Maruoka, K.; Yamamoto, H.; Maruoka, K. *Angew. Chem. Int. Ed.* **1983**, *55* (11), 668.
- (99) Maruoka, K.; Miyazaki, T.; Ando, M.; Matsumura, Y.; Sakane, S.; Hattori, K.; Yamamoto, H. *J. Am. Chem. Soc.* **1983**, *105* (9), 2831.
- (100) Mazzocchi, P. H.; Pople, J. A.; Jeffrey, A.; Wipff, G.; Caramella, P.; Houk, N. *J. Am. Chem. Soc. Commun.* **1981**, *103* (9), 2438.
- (101) Cieplak, A. S. *J. Am. Chem. Soc.* **1981**, *103* (1), 4540.
- (102) Simon, R. C.; Zepeck, F.; Kroutil, W. *Chem. - A Eur. J.* **2013**, *19* (8), 2859.
- (103) Stults, J. S.; Varie, D. L.; Wilde, R. G.; Wittenberger, S. *J. Org. Chem.* **1986**, No. 10, 1556.
- (104) Lamm, A. S.; Venkitasubramanian, P.; Rosazza, J. P. N. In *Science of Synthesis: Biocatalysis in Organic Synthesis 2*; K. Faber, W. D. Fessner, N. J. T., Ed.; Georg Thieme Verlag: Stuttgart, 2015; p 672.
- (105) Heath, R. S.; Pontini, M.; Bechi, B.; Turner, N. J. *ChemCatChem* **2014**, *6* (4), 996.
- (106) Yasukawa, K.; Nakano, S.; Asano, Y. *Angew. Chemie - Int. Ed.* **2014**, *53* (17), 4517.
- (107) Iwaki, H.; Shimizu, M.; Tokuyama, T. *Appl. Environ. Microbiol.* **1999**, *65* (5), 2232.
- (108) Dunsmore, C. J.; Carr, R.; Fleming, T.; Turner, N. J. *J. Am. Chem. Soc.* **2006**, *128* (7), 2224.
- (109) Leisch, H.; Grosse, S.; Iwaki, H.; Hasegawa, Y.; Lau, P. C. K. **2012**, *45*, 39.
- (110) Li, G.; Ren, J.; Yao, P.; Duan, Y.; Zhang, H.; Wu, Q.; Feng, J.; Lau, P. C. K.; Zhu, D. *ACS Catal.* **2014**, *4*, 903.
- (111) Murray, P. M.; Bower, J. F.; Cox, D. K.; Galbraith, E. K.; Parker, J. S.; Sweeney, J. B. *Org. Process Res. Dev.* **2013**, *17* (3), 397.
- (112) Conway, B.; Grady, F. O.; Wall, M. D. *Synlett* **2006**, *7*, 1043.
- (113) Horn, J.; Marsden, S. P.; Nelson, A.; House, D.; Weingarten, G. G. *Org. Lett.* **2008**, *10* (18), 4417.

- (114) Studier, F. W. *Protein Expr. Purif.* **2005**, *41* (1), 207.
- (115) Theeraladanon, C.; Arisawa, M.; Nakagawa, M.; Nishida, A. *Tetrahedron Asymmetry* **2005**, *16* (4), 827.
- (116) Temperini, C.; Cecchi, A.; Scozzafava, A.; Supuran, C. T. *J. Med. Chem.* **2009**, *52* (2), 322.
- (117) Gotor-Fernández, V.; Fernández-Torres, P.; Gotor, V. *Tetrahedron Asymmetry* **2006**, *17* (17), 2558.
- (118) Saito, K.; Akiyama, T. *Angew. Chemie Int. Ed.* **2016**, n/a.
- (119) Saito, K.; Shibata, Y.; Yamanaka, M.; Akiyama, T. *J. Am. Chem. Soc.* **2013**, *135* (32), 11740.
- (120) Poehlauer, P.; Manley, J.; Broxterman, R.; Gregertsen, B.; Ridemark, M. *Org. Process Res. Dev.* **2012**, *16* (10), 1586.
- (121) Heider, P. L.; Born, S. C.; Basak, S.; Benyahia, B.; Lakerveld, R.; Zhang, H.; Hogan, R.; Buchbinder, L.; Wolfe, A.; Mascia, S.; Evans, J. M. B.; Jamison, T. F.; Jensen, K. F. *Org. Process Res. Dev.* **2014**, *18* (3), 402.
- (122) Porta, R.; Benaglia, M.; Puglisi, A. *Org. Process Res. Dev.* **2015**, *20*, 2.
- (123) Pastre, J. C.; Browne, D. L.; Ley, S. V. *Chem. Soc. Rev.* **2013**, *42* (23), 8849.
- (124) de Oliveira Lopes, R.; de Miranda, A. S.; Reichart, B.; Glasnov, T.; Kappe, C. O.; Simon, R. C.; Kroutil, W.; Miranda, L. S. M.; Leal, I. C. R.; de Souza, R. O. M. a. *J. Mol. Catal. B Enzym.* **2014**, *104*, 101.
- (125) Andrade, L. H.; Kroutil, W.; Jamison, T. F. *Org. Lett.* **2014**, *16* (23), 6092.
- (126) Lücke, D.; Dalton, T.; Ley, S. V.; Wilson, Z. E. *Chem. - A Eur. J.* **2016**, *22*, 4206.
- (127) Tidwell, W. D.; Rushforth, S. R.; Reveal, J. L.; An, A.; Blum, M. S.; Fales, H. M. *Science (80- )*. **1970**, *168* (8), 840.
- (128) Wilkinson, T. J.; Stehle, N. W.; Beak, P. *Org. Lett.* **2000**, *2* (2), 155.
- (129) Posner, G. H.; Cho, C. G.; Green, J. V.; Zhang, Y.; Talalay, P. *J. Med. Chem.* **1994**, *37* (1), 170.
- (130) Abdel-Kader, M. S.; Bahler, B. D.; Malone, S.; Werkhoven, M. C. M.; Van Troon, F.; David; Wisse, J. H.; Bursuker, I.; Neddermann, K. M.; Mamber, S. W.; Kingston, D. G. I. *J. Nat. Prod.* **1998**, *61* (10), 1202.
- (131) L. Sorgi, K.; A. Maryanoff, C.; F. McComsey, D.; E. Maryanoff, B. *Org. Synth. Collect.* **1998**, *75* (September), 215.
- (132) Chang, M.; Li, W.; Hou, G.; Zhang, X. *Adv. Synth. Catal.* **2010**, *352* (18), 3121.
- (133) Vaultiera, M.; Benaliv, A.; Guerin, A.; Carboni, B. *J. Chem. Soc. Perkin Trans. 1* **1993**, No. 9, 1061.
- (134) Nenajdenko, V. G.; Gulevich, A. V.; Balenkova, E. S. *Tetrahedron* **2006**, *62* (25), 5922.
- (135) Koldobskii, A. B.; Vakhmistrov, V. E.; Solodova, E. V.; Shilova, O. S.; Kalinin, V. N. *Dokl. Chem.* **2002**, *387* (1-3), 289.

- (136) Shirai, N.; Sumiya, F.; Sato, Y.; Hori, M. *J. Org. Chem.* **1989**, *54* (4), 836.
- (137) Cochrane, E. J.; Leonori, D.; Hassall, L. A.; Coldham, I. *Chem. Commun.* **2014**, *50* (69), 9910.
- (138) Li, L. Z.; Xiao, B.; Guo, Q. X.; Xue, S. *Tetrahedron* **2006**, *62* (33), 7762.
- (139) Burckhalter, J. H.; Johnson, S. H. *J. Am. Chem. Soc.* **1951**, *73* (10), 4835.
- (140) Saito, K.; Miyashita, H.; Akiyama, T. *Chem. Commun.* **2015**, *51* (93), 16648.
- (141) Núñez-Rico, J. L.; Fernández-Pérez, H.; Vidal-Ferran, A. *Green Chem.* **2014**, *16* (3), 1153.
- (142) Hou, X. L.; Zheng, B. H. *Org. Lett.* **2009**, *11* (8), 1789.
- (143) Hussain, S.; Leipold, F.; Man, H.; Wells, E.; France, S. P.; Mulholland, K. R.; Grogan, G.; Turner, N. J. *ChemCatChem* **2015**, *7* (4), 579.
- (144) Aleku, G. A.; Man, H.; France, S. P.; Leipold, F.; Hussain, S.; Toca-Gonzalez, L.; Marchington, R.; Hart, S.; Turkenburg, J. P.; Grogan, G.; Turner, N. J. *ACS Catal.* **2016**, *6* (6), 3880.
- (145) Poerwono, H.; Higashiyama, K.; Yamauchi, T.; Kubo, H.; Ohmiya, S.; Takahashi, H. *Tetrahedron* **1998**, *54*, 13955.
- (146) P. C. Walchli, G. Mukherjeemuller, C. H. Eugster, *Helv. Chim. Acta*, **1978**, *61*, 921-928.
- (147) M. Amat, O. Bassas, N. Llor, M. Canto, M. Perez, E. Molins, J. Bosch, *Chem. Eur. J.* **2006**, *12*, 7872-7881.
- (148) R. Kammler, K. Polborn, K. T. Wanner, *Tetrahedron* **2003**, *59*, 3359-3368.
- (149) L. V. Adriaenssens, C. A. Austin, M. Gibson, D. Smith, R. C. Hartley, *Eur. r. Org. Chem.* **2006**, 4998-5001.
- (150) J. E. D. Martins, M. A. C. Redondo, M. Wills, *Tetrahedron-Asymmetry* **2010**, *21*, 2258-2264.
- (151) A. J. Burke, S. G. Davies, A. C. Garner, T. D. McCarthy, P. M. Roberts, A. D. Smith, H. Rodriguez-Solla, R. J. Vickers, *Org. Biomol. Chem.* **2004**, *2*, 1387-1394.
- (152) A. I. Meyers, D. A. Dickman, T. R. Bailey, *J. Am. Chem. Soc.* **1985**, *107*, 7974-7978.